UNIVERSITY OF OKLAHOMA

GRADUATE COLLEGE

SURFACE CHARACTERIZATION AND TRIBOLOGY IN FLAT LAPPING OF METALS

A DISSERTATION

SUBMITTED TO THE GRADUATE FACULTY

in partial fulfillment of the requirements for the

Degree of

DOCTOR OF PHILOSOPHY

By

CASMIR I. AGBARAJI
Norman, Oklahoma
2008

SURFACE CHARACTERIZATION AND TRIBOLOGY IN FLAT LAPPING OF METALS

A DISSERTATION APPROVED FOR THE
SCHOOL OF INDUSTRIAL ENGINEERING

BY

Dr. Shivakumar Raman, Chair

Dr. Theodore B. Trafalis

Dr. Floyd H. Grant

Dr. Chandra S. Rai

Dr. Thomas L. Landers

ACKNOWLEDGMENTS

First and foremost, my thanks go to the chairman of my committee, Dr. Shivakumar Raman, who helped me achieve my childhood dream. Also, I would like to acknowledge the invaluable contribution of other members of my committee: Dr. Theodore B. Trafalis, Dr. Floyd H. Grant, Dr. Chandra S. Rai, and Dr. Thomas L. Landers. I am greatly indebted to Brent Dustman of EATON Corporation, for giving me a plant tour of EATON Lapping Department in Shawnee, Oklahoma, which broadened my scope of knowledge in lapping operation. I am grateful to Gerard Pardeilhan of the Precision Optics Equipment, Strasbaugh, for his help and time when I struggled with the lapping machine.

My special thanks are extended to Dr. P. Larson of the Samuel Roberts Noble Electron Microscopy Laboratory, University of Oklahoma, for his help in the scanning of my samples with a scanning electron microscope. I would like to express my sincere gratitude to Dr. M.C. Altan of the School of Aerospace and Mechanical Engineering, University of Oklahoma, for allowing me use of his viscometer. I am very thankful to the School of Industrial Engineering, University of Oklahoma, for awarding me a scholar fellowship, which supported me through this long journey. Also, my special thanks go to the Department of Industrial Engineering staff, Amy Piper, Cheryl Carney, and Jean Shingledecker for their assistance in my work.

I would like to express my appreciation to other students in the School of Industrial Engineering, and all my friends at the University of Oklahoma, who contributed in one way or the other to make my stay in Norman very memorable. In addition, I would like to thank my nephew, Chuka, and my nieces, Ije and Chioma for their invaluable support. Finally, I must acknowledge the moral support and love from my parents, my elder brother, Vincent Agbaraji, M.D., my younger brother, Canice, my sister, Olivia and her husband, Linus. It was a rough road, but you supported me along the way. Thank you.

TABLE OF CONTENTS

Page

LIST OF TABLES

Table **Page**

LIST OF FIGURES

Figure **Page**

ABSTRACT

Lapping is a loose abrasive process employed to remove very small quantities of materials leading to a good surface finish. This research makes several investigations on the lapping process, both qualitative and quantitative. Lapping has been in existence for several decades and yet remains more of an art rather than a science. The principal objective is to create a scientific basis to the study of lapping common metals with common abrasives. The important goals are to study friction, material removal rate, roughness, surface characterization, redox chemistry, burn, and microvoids during flat lapping of aluminum 2024, 304 stainless steel, and 1018 steel. The effects of different abrasives: garnet, silicon carbide, and white aluminum oxide were studied experimentally while lapping aluminum 2024, 304 stainless steel, and 1018 steel.

In addition, the area of lapped parts, unfinished zones, and scratched zones were determined using image analysis. Although the aim of lapping is to improve surface finish, sometimes parts are rejected after lapping because of burn, friction, incomplete lapping, scratches, microvoids, and wear. Scratches may be caused by excessive load, low supply of abrasive slurry, or high friction and burn may be caused by excessive load. Uneven distribution of load occurs when the lapping table is not flat, but rather concave or convex in shape. The factors that cause burn, scratches, and incomplete lapping should be minimized.

A new method is proposed for calculation of frictional force during lapping using the current consumed in the process. The effects of different abrasives on material removal rate and surface finish on three different types of work materials were evaluated quantitatively. It was found that silicon carbide and white aluminum oxide abrasives

removed more material per minute than garnet. Furthermore, from geometric and Energy Dispersive Spectroscopy (EDS) analysis obtained using a Scanning Electron Microscope (SEM), it was confirmed that some abrasives became embedded into the lapped metal substrates. No burn was observed on the lapped samples. Scratches and unfinished lapped parts were observed primarily in 304 stainless steel. There were little or no scratches found on lapped Al 2024 and 1018 steel.

Based on the net cell reaction potentials using the Nernst equation, the possible reactions during the lapping process are reactions between magnesium and its hydroxides and white aluminum oxide abrasive. Also, SiO_2 from SiC abrasives oxidized Al, Mn, Mg, and Ti in Al 2024 as well as Mn in 304 stainless steel, and Al and Mn in 1018 steel. Analysis of Variance (ANOVA) was performed using Statistical Analysis Software (SAS^{TM} 9.1) in order to determine the effects of each variable. ANOVA results revealed that the main effects of abrasive types, size of abrasives, and type of work material had statistically significant influence on material removal rate and surface finish**.**

CHAPTER 1

INTRODUCTION

Lapping can be defined as a low-velocity and low-pressure finishing operation in which small amounts of material are removed from the workpiece (usually flat, cylindrical or curved surfaces) by means of loose abrasive grains (Lynah and Hoffman, 1989; Davis, 1994). This finishing operation method was first applied in ancient times when grinding and polishing precious metals.

1.1 Types of Lapping

The lapping process can be classified as single-sided lapping or double-sided lapping. If only one side of the work material is lapped against the lapping plate, the process is regarded as a single-sided lapping operation. In contrast, if the workpiece is positioned between two parallel lapping plates (lap), and the abrasive slurry is made to complete the lapping operation on both sides of the work material simultaneously, then this is called double-sided lapping. According to Subramanian (1994), some of the advantages of double-sided lapping over single-sided lapping include: time savings, higher quantities of production, reduction of internal stresses, lower heat generation, and better efficiencies.

1.2 Functions of Lapping

Lynah and Hoffman (1989); Davis (1994) enumerated the features and functions of lapping. Lapping is a low-velocity, low-pressure abrading technique, in which one or more of the following objectives are accomplished:

- Form accuracy (i.e., flatness in the case of flat objects and sphericity of round objects);
- Surface finishing (i.e., damaged and subsurface layers are removed during the lapping process);
- Correcting minor imperfections;
- Making close fit or alignment between mating work surfaces;
- Elongating wear life, reducing risk of seizure and noise, and maximizing the percentage bearing area since hills and valleys on the surface of workpiece are minimized;
- Reducing the possibility of re-hardened and de-carburized areas on hardened or heat treated components since less heat is generated in lapping than other finishing operations;
- Achieving extreme parallelism; and
- Eliminating stresses in the workpiece.

Lapping does not require the use of chucks or other holding/clamping devices. Therefore, form tolerance (circularity, cylindricity, flatness, straightness, and sphericity), orientation tolerance (angularity, parallelism, and perpendicularity), and size tolerance are improved.

1.3 Applications of Lapping

Lapping operations can be applied to materials that require high dimensional accuracy and fine surface finishing, including: crankshafts, cutting tools and dies, cylinders, gears, industrial ceramics (e.g., heat exchangers), magnetic memory disks, optical component fabrication (i.e., glass and lenses), piston rings, precision components (such as gage blocks and micrometers), and valves.

1.4 Problem Definition

Although the aim of lapping is to improve surface finish, sometimes parts are rejected after lapping because of burn, friction, incomplete lapping, scratches, microvoids, and wear. Scratches can be due to excessive load, low supply of abrasive slurry or high friction. Incomplete lapping can be caused when there is an uneven distribution of load. Uneven distribution of load occurs when the lapping table is not flat, but rather either concave or convex in shape. Therefore, the factors that cause burn, scratches, and incomplete lapping should be minimized.

In a competitive market, there is a need to produce metal components with good surface finish, integrity, and dimensional accuracy. During a lapping operation, friction, roughness, and wear affect dimensional accuracy, life span of parts, and material removal rate. In other words, friction force and wear of the work material increase during the course of a lapping operation. Friction is produced between the lapping plate and workpiece by an application of lapping pressure. During the course of lapping operation, the actual area of contact increases because of an improvement in surface finish. As a result of an increase in the actual area of contact, friction increases, thereby leading to an

increase in power consumption. Also, an increase in friction increases the wear rate of two or more surfaces in contact. Although the effect of friction in lapping is observed at the microscopic level, this can lead to failure of the lapped surfaces over a period of time. Furthermore, toxic chemicals may also result during the course of lapping.

1.5 Research Objective and Methodology

This research makes several investigations on the lapping process, both qualitative and quantitative. The principal objective is to create a scientific basis for the study of lapping common metals with common abrasives. Lapping has been in existence for several decades and yet remains more of an art rather than a science. The important goals are to study friction, material removal rate, roughness, surface characterization, redox chemistry, burn, and microvoids during flat lapping of aluminum 2024, 304 stainless steel, and 1018 steel. In addition, the area of lapped parts, unfinished zones, and scratched zones must determined. This research proposes two methods (motor constant model and temperature model) for determining frictional force during lapping. In addition, the effects of different abrasives on material removal rate and surface finish on three different types of work materials were evaluated.

The most efficient abrasive for achieving a high material removal rate (MRR) or lapping rate while machining a good surface finish was determined. An optimum lapping pressure that gives a high MRR without causing breakage of the work material or affecting the dimensional accuracy was established. Also, a suitable lapping speed and lapping time was determined. Furthermore, wear tracks left on the workpiece as result of abrasive grains in the lapping process were investigated**.** In order to avoid producing

toxic chemicals, redox chemistry was investigated before any lapping operation. Fundamentally, benefits and effects of the lapping process are studied, shedding light on the scientific basis that transforms lapping from art to engineering.

In order to determine the effects of each variable, an Analysis of Variance (ANOVA) was performed using Statistical Analysis Software (SAS^{TM} 9.1). Based on the results obtained from ANOVA, the main effects of abrasive types, size of abrasives, and type of work material had statistically significant influence on material rate and surface finish. Also, Finite Element Analysis (FEA) was performed in order to determine the distribution of the displacement, strain, and stress when a normal load of 24.9 N (5.6 lbf) was applied on the sample.

Chapter 2 discusses the principle of tribology. The literature review is presented in Chapter 3 and Chapter 4 explains the methodology used in the research. In Chapter 5, background information on the materials is provided. Image analysis of the materials used is provided in Chapter 6. The results and analysis are discussed in Chapter 7. Finally, contributions, conclusions, and recommendations are presented in Chapter 8.

CHAPTER 2

PRINCIPLES OF TRIBOLOGY

In this chapter, the concepts of tribology (friction, lubrication, and wear) are explained. The mechanisms of friction, laws of friction, types of friction, and detrimental and beneficial effects of friction are highlighted. Also, types of wear and lubrication are discussed.

Tribology is the study of mechanisms of friction, lubrication, and wear of surfaces that are in a relative motion. The term was originally derived from a Greek word: tribos, meaning rubbing. The function of many mechanical systems depends on factors such as friction, lubrication, and wear. It is necessary to take an adequate precaution in designing of mechanical systems to avoid the inconvenience that emanate from friction and wear of mechanical components.

According to Suh (1986), tribology deals with science and technology of interfaces between two or more bodies that are in a relative motion. The nature and impacts of the interactions that take place at the interface determines the extent of friction and wear behavior of the materials. In a tribological process, the following interactions are observed:

- forces are generated and transmitted between the surfaces in contact;
- energy is consumed;
- physical and chemical properties of the materials are changed (i.e., density, melting point, specific heat, thermal expansion, thermal conductivity, electrical properties, optical properties, corrosion, and oxidation);

- surface topography of the material is altered; and
- loose abrasive wear particles are generated.

2.1 Friction

Friction force is defined as the resisting force, which is tangential to the interface or common boundary between two bodies, when one body moves relative to another body, under the application of an external force (Blau et al., 1992; Hersey**,** 1966). In other words, friction is a force that resists the rolling or sliding of two objects that are initially at rest or moving.

2.1.1 Mechanism of Friction

The two common theories used in explaining friction are: adhesion theory (two clean and dry surfaces in contact with each other at only a fraction of their apparent contact area, irrespective of their smoothness), and abrasion theory (asperity from a hard surface penetrates through a softer work material). According to Szeri (1998), friction in metals occurs from three different mechanisms, namely: adhesion, plowing, and asperity deformation. In other words, the coefficient of friction is the sum of adhesion component (f_a), plowing component (f_p), and deformation component (f_d). Alternative classification of friction into macroscopic and microscopic mechanisms was proposed by Larsen-Basse (1992).

Macroscopic Mechanisms

The factors that fall into this category include nature of the surface involved in friction, materials, environment, application conditions, characteristics of the apparatus, that is, vibration, and clamping of the samples.

Microscopic mechanisms

The microscopic mechanisms that contribute to friction are: adhesion interactions, plowing interactions, asperities deformations (mechanical interaction of surface asperities), deformation, or fracture of surface layers such as oxides, and interference, and local plastic deformation.

- **Adhesion Interactions**

One cause of friction in metals is the force of attraction, (i.e., adhesion). This adhesion occurs between the contact regions of the surfaces, and these appear irregular in shape when viewed under a microscope. The irregularities appear as hills (peaks) and valleys when a load is applied between two surfaces in contact. The peaks adhere, or weld to each other, and/or interlock with the valleys in the opposing surfaces as depicted in Figure 1. Therefore, friction force arises from shearing the adhesion and/or weld, which are formed at the actual area of contact between the asperities.

- **Plowing (Ploughing) Interactions**

The frictional force results from plowing of harder metals through the surface of softer materials. Plowing can also be defined as displacing of materials from a groove to the sides. In other words, formation of grooves (ridges) is due to the plastic deformation of a softer material by a harder material when two surfaces which are in a relative motion.

- **Asperity Deformations**

This usually involves mechanical interaction of surface asperities. Asperity deformation is the factor that is responsible for static coefficient of friction (Suh, 1986).

- **Interference and Local Plastic Deformation**

Interference and local plastic deformation are caused by third bodies. For example, accumulated wear particles trapped between two or more moving surfaces leads to friction.

- **Deformation or Fracture of Surface Layers**

Deformation or fracture of surface layers such as oxides can cause friction.

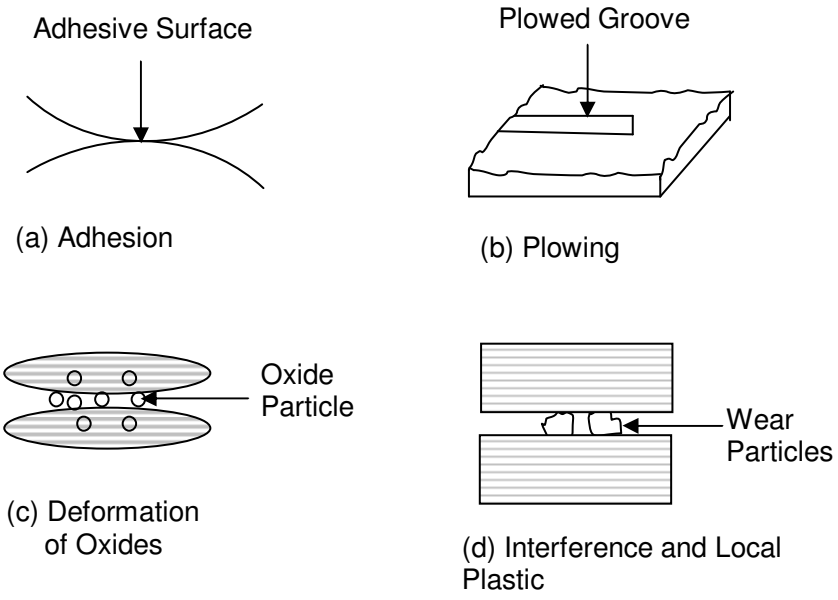

Figure 1. Microscopic Mechanism of Friction (Larsen-Basse, 1992).

2.1.2 Laws of Friction

The pioneering work in tribology was done by Amontons' (1699) and Coulomb (1785). More (1972); Fuller (1984); Szeri (1998) cited Amontons' and Coulomb's laws of friction, which have been stated as follows:

(1) Frictional force is directly proportional to the applied load (Amontons' 1st law,

1699).

(2) Frictional force is independent of apparent area of contact (Amontons' 2nd law, 1699).

(3) Kinetic friction is independent of sliding velocity (Coulomb's law, 1785).

(4) Static friction is higher than kinetic friction.

(5) Friction depends on the nature of the sliding surface.

The first two laws of friction were deduced by da Vinci (1519), and discussed by Amontons (1699), but Coulomb (1785) proved these laws experimentally. These laws are generally applied to dry friction and are still applicable to many engineering problems.

Moore (1972) stated that friction force is a function of sliding velocity, properties of work material, contact area, and surface finish of the wokpiece. Coulomb's law of friction is described mathematically in Equation (1). The friction force and coefficient of friction are independent of apparent area of contact since the actual area of contact is less than the apparent area of contact as shown in Figure 2. Friction force is higher in smooth surfaces because of larger area of contact.

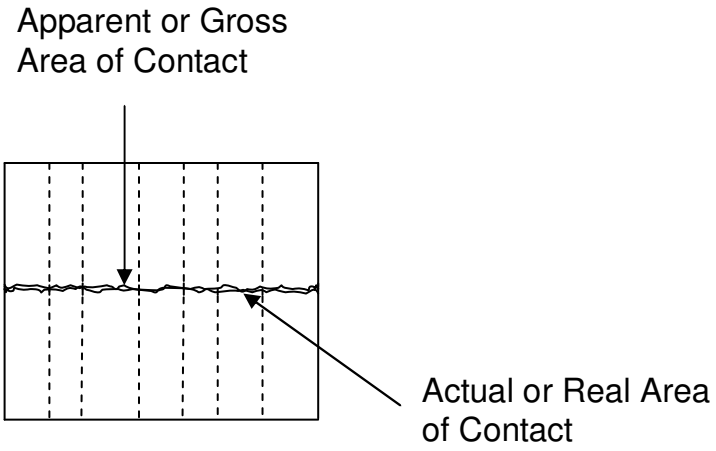

Figure 2. Apparent Area - Actual Area of Contact.

Actual or real or true area of contact < Apparent or gross area of contact for a rough surface.

The coefficient of friction, μ, is the ratio of F/N or slope from the plot of frictional force, F, and normal (contact) load or, N. The coefficient of friction is a function of the work materials and the type of manufacturing processes, according to (Kalpakjian, and Schmid, 2006). The coefficient of friction varies from 0.03 in a cold working operation to 0.7 for a hot working operation. Also, the coefficient of friction varies from 0.5 to 2 for machining operations, when only sliding is considered

$$F = \mu N \,, \tag{1}$$

where

F: frictional force

μ : coefficient of dynamic friction (depends on nature of two sliding surfaces and type of work material)

N: normal force or contact load. .

The coefficient of friction, μ, is always greater than zero, that is, $\mu = \frac{F}{N} > 0$. Also, the coefficient of friction is usually less than one for most materials, and it is dimensionless. The factors that affect friction force include:

- Contact area
- Deformation effects
- Molecular adhesion
- Properties of materials
- Sliding velocity
- Surface finish

2.1.3 Types of Friction

Friction can classified into five categories, namely - fluid friction, kinetic friction, rolling friction, sliding friction, and static friction.

- Fluid friction (viscous friction)

This occurs in a case where an object is in contact with a fluid such as a liquid or gas. If a force is applied to either the object or the fluid, then a friction force will resist the motion. If the viscosity of the fluid or thickness of the fluid is high, there may be no movement because of static friction. In other words, fluid friction is the force that resists the flow of liquids (Groshart, 1989). There are other forms of fluid friction such as boundary friction and mixed film friction that describe forces of friction under extreme pressure. In this situation, the lubricant is forced into very thin molecular layers, and the solid surfaces greatly influence the movement of the layers.

- Kinetic friction

If the normal force, N, is greater than the frictional force, F, then object will move. Therefore, the friction is considered to be kinetic friction. Figure 3 illustrates the kinetic friction force as well as sliding friction force of an object in motion.

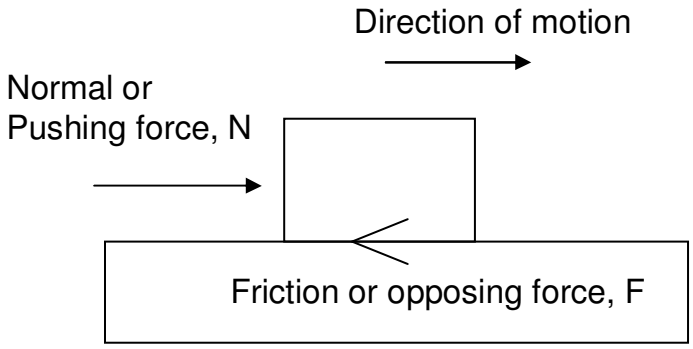

$N > \mathrm{F} \rightarrow$ Kinetic friction (moving friction)

$N < \mathrm{F} \rightarrow$ Static friction (no motion)

Figure 3. Normal Force versus Friction Force.

- Rolling friction

Rolling friction is the force that resists rolling of an object. Normally, it is easier to roll objects than to slide them. If a ball or wheel is in contact with a solid object, and a force is applied, then it starts to roll because of friction at the point of contact with the other surface. This is regarded as the onset rolling friction for the wheel. As soon as the ball or the wheel starts to roll, there is a resistive force that slows down the outer surface, which is considered as rolling frictional force. Rolling friction occurs when one or both of the contacting bodies are round in shape. Normally, the magnitude of rolling friction

is less than that of sliding friction. This is because a wheel can roll to some extent before slowing and stopping.

Rabinowicz (1966) enumerated laws of rolling friction, and these include:

- Rolling friction force is directly proportional to the applied load. As would be expected, for small loads, where deformation at the point of contact is elastic, frictional force varies as a low power of the load. For heavy loads, where deformation at the point of contact is plastic deformation, frictional force increases with high power of the load.
- Rolling friction is inversely proportional to the radius of the work material.
- Frictional force is higher for smoother surfaces than for rough surfaces since the actual area of contact for smoother surfaces is greater than that of rough surfaces.
- Static frictional force is higher than that of kinetic frictional force.
- Kinetic frictional force depends on rolling velocity. Generally, the kinetic frictional force increases with rolling velocity, but it drops off when the rolling velocity reaches a maximum level.
- Rolling friction is usually associated with a small degree of slip or sliding friction.
- The sliding velocity is normally $\leq$ 10% of the overall rolling velocity. This small percentage of slip velocity causes the major portion of total resistance to rolling.

➢ Sliding friction

When a force is applied to slide one object against the other, then sliding frictional force resists the motion of the object. In other words, sliding friction is a force that hinders the relative motion of two bodies that slide against each other in a dry

situation. The wear rate of dry friction is very high. The relationship between the normal force, N, and frictional force, F, will determine if the object will slide or not.

- Static friction

  If the frictional force, F, is greater than the normal force, N, then there will be no motion. Hence, the objects remain static with respect to each other. This implies that the static friction that keeps the object in place is greater than the kinetic friction. If the object starts to move, the static friction decreases. Initially, it may be very difficult to move an object, but once it starts to move, it becomes easier to push.

2.1.4 Detrimental Effects of Friction

In cases where friction is undesirable, it is recommended that friction be decreased, although friction is not completely eliminated. Fuller (1984); Hersey (1966); Rabinowicz (1966); Szeri (1998); Vogelpohl (1951) enumerated the detrimental effects of friction as well as the benefits of friction. The determination of frictional force in manufacturing operation is very important because of its detrimental effects. The demerits of friction are as follows:

- A large amount of productive capacity is devoted in replacing mechanical systems that are rendered useless by wear or seizure of machine components. Wear is usually associated with friction, which reduces the effective life of machines and its parts.
- Friction restricts freedom of movement at the interface, and this slows down the flow of metalworking processes.
- More than 6% of the Gross National Product (GNP) is wasted as a result of high friction and wear.

- Friction uses up or wastes an enormous amount of energy generated by mankind. Vogelpohl (1951) estimated that one third to one half of the world's energy is expended by friction. There is loss of power due to work done against friction. Frictional force creates difficulty for in starting machine under load, thereby causing power loss.
- In automobile, about 30% of engine power is consumed in order to overcome frictional forces in moving parts (Hersey, 1966; Szeri, 1998).
- Frictional forces lead to an increase in temperature, and consequently surface damage. Friction converts useful kinetic energy to heat, thereby decreasing the efficiency of the machine.
- Time is wasted in trying to overcome friction
- Friction reduces the efficiency and working life of machines, especially in moving parts.

2.1.5 Beneficial Effects of Friction

However, not all frictional forces are undesirable. In situations where friction is desirable, it is recommended that friction be maintained at sufficiently high level. In some instances where frictional forces are beneficial include: brakes, metal-rolling, clamping of workpieces on machines, friction welding, or holding of drill bits in chucks in order to avoid slippage. If the friction provided by the brakes of an automobile is too low, it will not stop the car rapidly enough. On the other hand, if friction is too high, it will give the passengers an uncomfortable sudden movement in a forward direction. High friction between automobiles tires and railroad helps in coming to a quick stop.

2.1.6 Reduction of Friction

Dry friction could be reduced by introducing rollers for sliding contact, improved design, suitable contacting materials, or by using lubricants. Improved tribology will increase potential savings in manufacturing.

2.1.7 Friction in Lapping

The friction in lapping can be regarded as a three-body friction because the abrasive grains, specimen, and the lapping plate are in a relative motion during a lapping operation. The friction between the abrasive particles and the sample causes scratches or voids on the specimen. In addition, the friction between the lapping plate, specimen, and the abrasive particles causes abrasive wear and fatigue wear on the lapping plate after a period of time. The wear on the lapping plate causes the plate to change either to a concave or convex shape. Therefore, the shape of the table has to be determined before each lapping operation with a straight edge, and the effect has to be corrected before lapping.

Friction in lapping can be regarded as a function of (contact area, properties of material, rotating friction, sticking friction, and surface finish). In the sticking friction, some abrasives become embedded in the workpiece, and the velocity is assumed to be zero in this case since there is no relative movement between the abrasives grains and the work material. Thus, it is a two-body friction between the work material and with some embedded abrasives in the lapping plate. Figure 4 illustrates two-body and three-body friction in lapping. The abrasives in a lapping operation may roll, slide, or become embedded in the lapping plate. The abrasives that become embedded are involved in sliding friction, while the loose abrasive grains are involved in rolling friction.

Therefore, rolling friction and sliding friction (slip friction) may all be present during lapping. Normally, rolling friction is associated with a small degree of slip or sliding friction. The shape and properties of abrasive grains, including the composition of the lapping plate will determine whether one type of friction or all these types of friction will occur at a particular point in time.

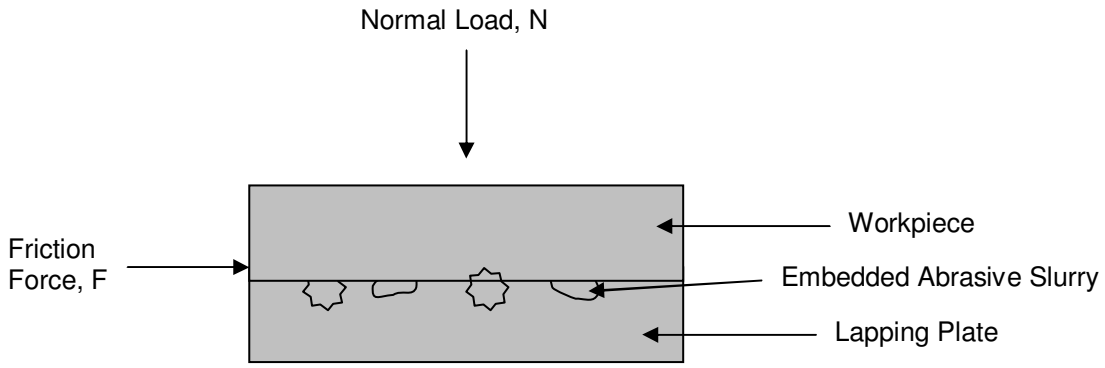

(a) Two-body Friction

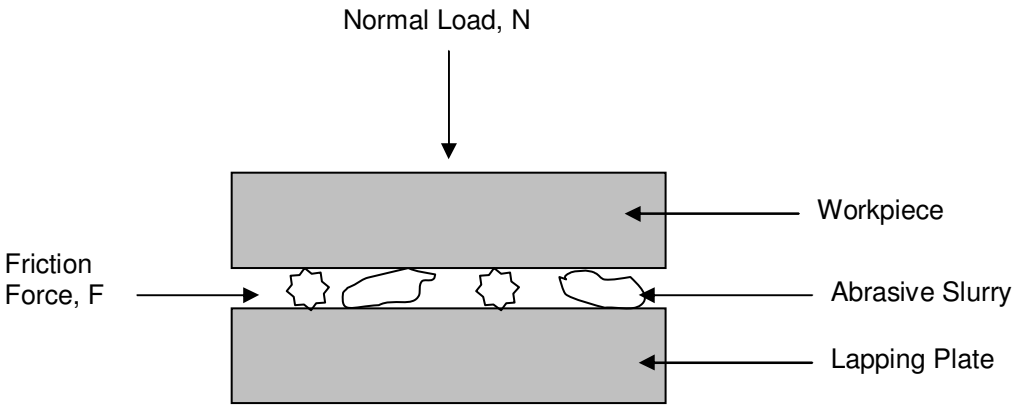

(b) Three-body Friction

Figure 4. Friction in Lapping.

2.2 Surface Texture

According to Bhushan (2002), surface texture is a repetitive or random deviation from a flat or normal surface. Every surface has its own unique characteristics, which is known as surface texture. Surface texture includes: flaws or defects, lays, roughness, and waviness. A pictorial display of a surface texture is shown in Figure 5.

- Flaws or Defects

  Flaws or defects are random, unexpected, or unintentional irregularities (interruptions) in the surface textures. Examples of flaws include: scratches, cracks, holes, depressions, grooves (ridges), tears, or inclusions.

- Lay or Directionality

  Lay or directionality is the direction of the predominant surface pattern, which is visible to the naked eye. It is determined by the production method.

- Roughness (nano-roughness and micro-roughness)

Nano-roughness and micro-roughness are formed due to fluctuations in the surface of short wavelengths. Surface roughness is normally characterized by hills (asperities or peaks or local maxima), and valleys (local minima). Surface roughness is defined as fine irregularities (asperities or undulations) in the surface texture of the workpiece that occurs on a small scale during production processes, and can be measured using a surface profilometer (Cotell, Sprague, and Smidt, 1994). It is expressed in terms of height, width, and distance along the surface of a sample.

Surface roughness increases friction force and tool wear, especially in moving parts, hence adequate care has to be taken in order to reduce asperities on the surfaces of manufactured parts. Also, surface roughness, which is reported as the arithmetic roughness average of the absolute values, $R_{a,}$ in micrometers and in root-mean-square

average, R_q, are represented in Equations (2) and (3), respectively (Kalpakjian and Schmid, 2001).

$$R_a = \frac{|a| + |b| + |c| + |d| + |e| + |f| + ...}{n}, \tag{2}$$

$$R_q = \sqrt{\left(\frac{a^2 + b^2 + c^2 + d^2 + e^2 + f^2 + ...}{n} \right)}, \tag{3}$$

where

a, b, c, d, e, and f are absolute ordinates values

n: number of observations

Ra: arithmetic roughness average

R_q: root-mean-square average.

Grain structures are also affected during a lapping operation, that is, scratches and microvoids are created on the surface of the work material due to the type of abrasive particles used for lapping. Metals used in lapping operations consist of polycrystal structures, that is, many crystal structures, which are randomly oriented. Hence, it is necessary to investigate the impact of abrasives materials on the grain structure of the workpiece.

- Waviness (macro-roughness)

A surface irregularity or recurrent deviation of longer wavelengths is referred to as waviness or macro-roughness. According to Kalpakjian and Schmid (2006),

waviness is usually described in form of space between adjacent crests of the waves, i.e., waviness width, and the height between the crests and the valleys of the waves (waviness

height). Waviness can result from factors such as machine deflection, workpiece deflection, vibration, chatter, heat treatment, or warping.

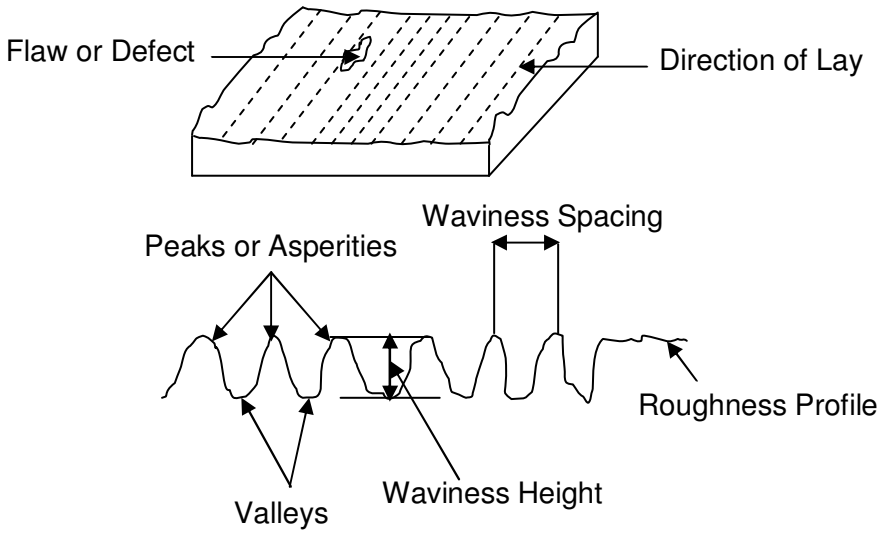

Figure 5. Diagram of a Surface Texture (Bhushan, 2002).

2.2.1 Surface Finish and Surface Integrity

Surface finish refers to geometric (topographic) feature of the produced surface, whereas surface integrity includes chemical and mechanical properties such as corrosion resistance, fatigue strength, and service life, which are determined by the kind of surface produced. Kalpakjian and Schmid (2001) enumerated factors that affect surface integrity as:

- Temperature produced during a processing operation
- Residual stresses

Stresses are that remain within the work material after it has been worked upon and all the external forces were removed.

- Metallurgical or phase transformation
- Surface plastic deformation

Plasticity is one of the properties of a metal that permits it to be extensively deformed without fracture. Spitler et al. (2003) classified plasticity into two categories, namely: ductility and malleability. Ductility permits the metal to be stretched or drawn without fracture or rupture, while malleability allows the material to be hammered or rolled without rupture.

- Tearing
- Cracking

According to Chandrasekar and Kotini (1990), the surface finish of products obtained from lapping is normally flatter than those from polished surfaces. The abrasive slurry is applied between the workpiece and a fitting surface known as a lapping plate.

2.3 Wear

Wear is the progressive removal of material from the surface of the workpiece because of relative motion at the interface of the work material and the contacting surface (Kalpakjian and Schmid, 2001; Szeri, 1998; Tylczak, 1992). In other words, wear can be defined as a damage or loss of material from the surface of workpiece by means of some mechanical actions. Wear changes the shape of the tools, size and quality of the product produced. Wear occurs due to dynamic friction, whereas friction results from molecular attraction between two or more bodies that are in physical contact with each other (Groshart, 1989). The higher the surface irregularities between two bodies, the less intimate contact they will have, hence less molecular attraction and less friction**.** The

shape of abrasive grains determines the shape of the groove that is produced during a lapping operation. According to Tylczak (1992), less wear is observed if the work material is abraded by round particles, rather than sharp abrasive grains. As would be expected, the rate of loss of material is directly proportional to the toughness of the abrasive particles.

2.3.1 Types of Wear

According to Schey (1983), wear can be classified into seven main categories namely: abrasive wear (two-body-wear or three-body wear), adhesive wear, attrition wear, chemical wear (corrosive or oxidation wear), erosion, fatigue wear (impact wear), and fretting wear. In most cases, these types of wear could occur simultaneously in each scenario (Garzino-Demo and Lama, 1994). Furthermore, they concluded that some external factors such as changes in the degree of humidity and temperature of the environment, chemically active contaminants, and interaction between the surface and the fluids, significantly influence the wear of two sliding surfaces. In addition, mechanical stresses and oxidation influence the mechanisms of wear.

2.3.2 Abrasive Wear (Two-body Wear and Three-body Wear)

When asperities of a rough, hard surface, or hard particles slide on a softer surface, it often results in damage of the interface due to plastic deformation or fracture and this phenomenon is known as abrasive wear (Bhushan, 2002). This is the removal of material either by a hard, rough surface, which slides against another surface, and this is known as two-body wear (Schey, 1983). In ductile materials such as metals and alloys, hard asperities or hard particles results in plastic flow of softer work materials. There are two types of abrasive wear mechanisms, namely: two-body abrasive wear and three-body

abrasion. In two-body abrasive wear, the harder surface slides on the softer material and damage the interface. For the three-body wear, the harder surface is a third body such as abrasive grains. Three-body wear occurs in some finishing operations such as abrasive grinding and lapping as shown in Figure 4. If hard particles or hard protuberances are forced to move along a solid surface, this causes an abrasive wear. A three-body wear, occurs when a particle is placed between two surfaces. Kang and Hadfield (2005) reported that the material removal mechanism in grinding, lapping and polishing of ceramics were associated with a two-body or three-body wear.

In general, lapping can be classified as a three-body wear because the abrasive grains act like indenters, which slide and roll between the lapping plate and the work material. The authors also believed that the amount of load applied to abrasive grains, sliding speed of the abrasive grains, and the presence of chemical reactants influence each wear mechanisms. This type of phenomenon is known as abrasive wear. Removal of material from a workpiece due to plastic deformation occurs in three different ways during abrasion (Bhushan, 2002). These include plowing, wedge formation, and cutting as illustrated in Figure 6.

(i) Plowing (Ridge Formation)

During plowing or ridge formation process, material is displaced from a groove to the side without removal of material. Plowing leads to a series of grooves because of plastic flow of softer materials to the sides.

(ii) Wedge Formation

Wedge formation is a type of abrasive wear, which occurs when the tip of an abrasive plows a groove, and then develops a wedge on its front. Generally, wedge

formation occurs when the ratio of shear strength of the interface relative to the shear strength of the bulk material is high, normally in the magnitude of 0.5 to 1. When this happens, only some portion of the material displaced from the groove is displaced to the sides, while the remaining material develops as wedge in front.

(iii) Cutting

Cutting form of abrasive wear occurs when an abrasive tip with a large attack angle plows a grove, and then removes the material in the form of discontinuous chips or ribbon-shaped debris, which is similar to those that are produced during a metal cutting operation. Generally, cutting is a form of abrasive wear, which results in significant removal of material.

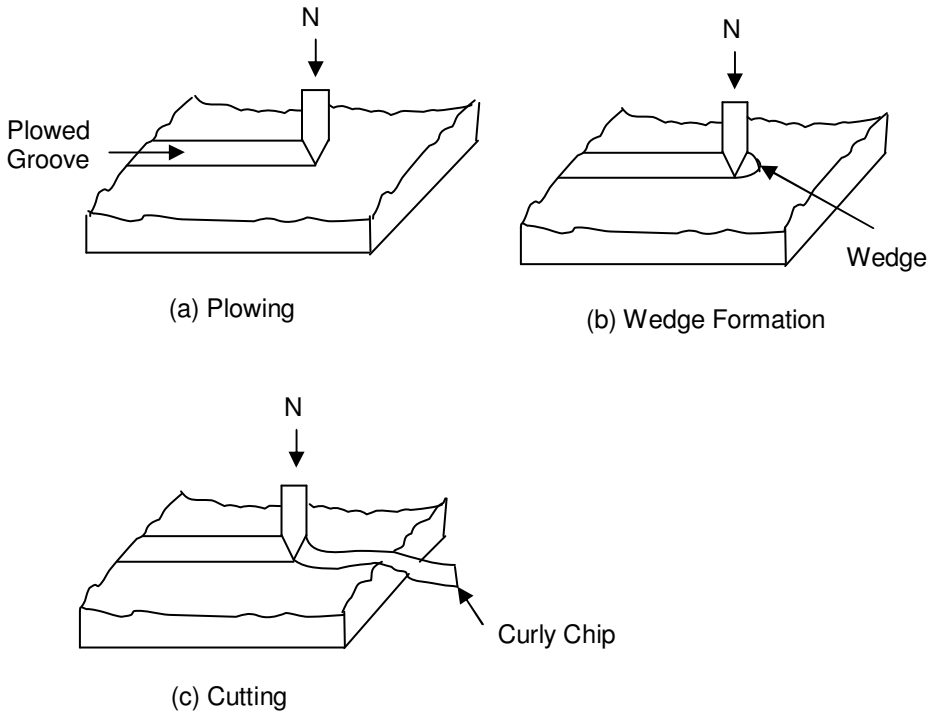

Figure 6. Modes of Abrasives Wear (Bhushan, 2002).

Schey (1983); Tylczak (1992) stated that the wear volume is directly proportional to normal load and distance of sliding, but inversely proportional to hardness of material as expressed in Equation (7). According to Tylczak (1992), the maximum volume wear during an abrasive cutting is given in Equations (4) to (7).

$$W = A * d, \tag{4}$$

$$A = k_1 * p, \tag{5}$$

$$p = k_2 * \left(\frac{N}{H} \right), \tag{6}$$

Substituting Equations (5) and (6) into (4), Archard equation for abrasive wear is obtained (Archard, 1953). Also, the author defined the degree of penetration as depth of penetration divided by the area of contact.

$$W = k_3 \frac{N * d}{H}, \tag{7}$$

Archard equation for abrasive wear.

where

W: volume of material removed (in^3)

A: cross-sectional area of the groove

P: depth of penetration

N: load

d: distance slid

H: hardness of material

k_1, k_2, and k_3: constants which depend on shape of the abrasive grain, plowing

and cutting.

2.3.3 Adhesive Wear

If two solid surfaces are brought in contact, adhesion or bonding takes place across the interface, hence a finite amount of force is referred to as adhesive force, which is the force required to pull the surface apart (Bhushan, 2002). When a load is applied to a work material, shearing can take place, and this causes an adhesive wear. In other words, adhesive wear is caused by localized bond between two surfaces that are in contact, therefore, this leads to transfer of material between the two surfaces or loss of materials from either of the surface. Figure 7 depicts adhesive force and normal compressive force. On the other hand, cohesion force is the atomic bonding forces that occur within the material. Factors such as strain hardening at the asperity contact, diffusion, mutual solid solubility, make the adhesive bonds stronger than the base metals.

Therefore, during sliding, wear fragment occurs in the softer component. This wear fragment is usually attached to the harder component, which is later detached during rubbing at the interface, leading to adhesive wear or sliding wear (Kalpakjian and Schmid, 2001). Adhesive wear can be reduced using harder workpiece, materials that do not form strong adhesive bonds, less oxidizing materials, and applying hard coatings on the materials. As represented in Equation (8), the ratio of normal tensile force (adhesive force) needed for separation of the two surfaces to the normal compressive force is known as coefficient of adhesion**.**

$$\mu_a = \frac{F_a}{N}, \tag{8}$$

where

μ_a : coefficient of adhesion

F_a : adhesive force or normal tensile force

N : normal compressive force.

Adhesion is observed in both solid-solid contact, and in two solids interposed with liquid or thin films. In most cases, surface contaminants, thin films, and lubricants reduce adhesion between two or more solid surfaces. Strong adhesion is desirable if bonding is required between two surfaces. However, in many engineering applications such as rotating and sliding machines, adhesion is undesirable.

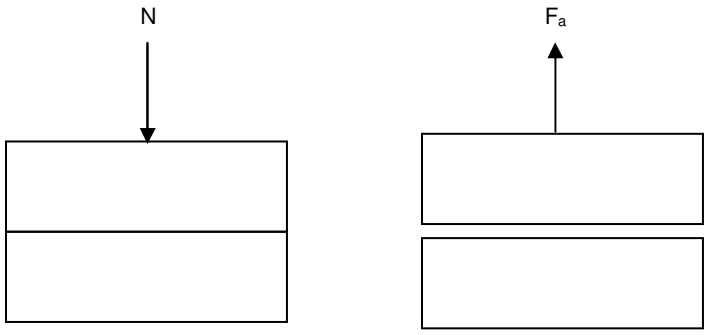

Figure 7. Adhesion Force.

2.3.4 Attrition Wear

This type of wear is caused by gradual wearing of material due to friction. Attrition wear involves both chemical and physical interactions of the abrasive grain and the workpiece. If the abrasive grain and the work material are chemically inert, the attrition wear will be low. Aluminum oxide and cubic boron nitride are chemically inert

to iron and steel, hence they are suitable abrasives for lapping of steel. Contrarily, silicon carbide can dissolve in iron; therefore it is not an adequate abrasive for lapping of steel.

2.3.5 Chemical Wear (Corrosive Wear or Oxidation Wear)

Kalpakjian and Schmid (2001) reported that corrosive wear occurs as a result of chemical or electrochemical reactions between the workpiece and the environment. The medium in which corrosive wear occurs includes: water, oxygen, chemicals, atmospheric hydrogen sulfide, and sulfur dioxide. Selection of material that will resist environmental attack and reduction in operating temperature will lessen the impact of chemical wear.

2.3.6 Erosion Wear

Erosion wear is caused by mechanical interaction between the surface of a work material and some fluids. Also, erosion wear occurs when loose abrasive grains abrade the surface of the work material.

2.3.7 Fatigue (Impact Wear)

Fatigue wear, which is also known as impact wear, surface fatigue, or surface-fracture wear, is normally caused by cyclic loading of the work material (Kalpakjian and Schmid, 2001). Abrasive grains are brittle materials, their fracture characteristics is very important during lapping. According to Schey (1983), subsequent loading and unloading cause microcrack, usually below the surface and this microcrack propagates to fatigue wear.

2.3.8 Fretting Wear

Fretting wear occurs due to small amplitude of oscillatory motion between two solid surfaces that are in contact. In other words, when two solid surfaces are exposed to small reciprocal movements, fretting wear is initiated.

2.4 Lubrication

Lubrication is used to reduce or present wear, thereby lowering friction.

2.4.1 Types of Lubrication

Lubrication can be classified into three types, namely: boundary lubrication, fluid-film lubrication, and solid lubrication (Fuller, 1984; Szeri, 1998).

2.4.2 Boundary Lubrication

If the speed is reduced or the load is increased, then the surfaces will not be in intimate solid contact, rather are separated by one or more molecular layers of the lubricant. This condition is known as boundary lubrication. At low speeds or high loads, the lubricant film becomes thinner than some of the asperities. When these asperities are covered by molecular layers of lubricant, there will be no welding or adhesion of lubricant to the rubbing surfaces. Lubrication depends on strong adhesion of the lubricant to the rubbing surfaces. Boundary lubrication usually occurs during starting and stopping of machines.

2.4.3 Fluid-film Lubrication

Fluid film that separates sliding surfaces results in fluid-film lubrication. This can be introduced intentionally, as oil is the main bearings of automobile. It could be introduced unintentionally, as in the case of water between automobile tire and a wet pavement.

Hryniewicz et al. (2001a) studied the application of Reynolds lubrication theory fluid flow in grinding. To simplify the analysis, a smooth grinding wheel was used in their study. In related study, Hryniewicz et al. (2001b) applied Reynolds classical

lubrication theory to fluid flow in a rough grinding wheel. They authors derived an expression for determination of film thickness as shown in Equations (9) and (10).

$$h(x) = h(g) + r - \sqrt{r^2 - x^2}, x_l \le x \le x_r, \tag{9}$$

$$h(s) = \delta_2^{\max} + \delta_1^{\min}, \tag{10}$$

where

$h(x)$: nominal film thickness

$h(g)$: minimum nominal gap size

r : radius of wheel

x_l, x_r : boundaries of fluid film in x-direction

$h(s)$: minimum gap size at spark-out position

$\delta_2^{\max}$: maximum wheel roughness height

$\delta_1^{\min}$: minimum workpiece roughness height (negative).

The minimum gap size, $h_{(g)}$, equals the minimum gap size at the spark-out position, $h_{(s)}$. At this point, where $h_{(g)}$, equals $h_{(s)}$, is the closest to the actual grinding of the workpiece. They authors assumed that the point of maximum height of the surface of the wheel corresponded to the minimum height on the work material since the work material surface was generated by abrasive particles on the surface of the wheel.

2.4.4 Solid Lubrication

Some solids such as graphite, molybdenum disulfide (MoS_2), and Teflon are used as lubricants when conventional lubricants do not have enough resistance to load or extreme temperatures.

The section on friction, wear, and lubrication serve as a basis for various tribological investigations undertaken in this research. Although not explicitly stated elsewhere in this research, much investigation was done to verify the basis of tribology in this research.

CHAPTER 3

LITERATURE REVIEW

This chapter provides a background on different abrasive machining processes, hardness tests, and types of work materials used in a lapping operation, frictional forces, and types of wear mechanisms. Section 3.1 presents different types of abrasive machining processes. Section 3.2 discusses different types of abrasives, while section 3.3 describes methods of hardness tests that could be used to determine the hardness of the abrasives and the work materials. Lapping of ceramics, lapping of glass, and lapping of metals are discussed in sections 3.4 through 3.6, respectively. In section 3.7, frictional force models are described. The type of finishing operation employed depends on the following factors:

- Amount of material to be removed from the work material
- Capability of the process
- Cost
- Time
- Shape and size of the workpiece

Le and Peterson (1999) reported that many precision manufacturing companies make use of lapping operation to achieve desired tolerance and surface quality requirements. According to statistics compiled by manufacturers, lapped plug gages and gage blocks have longer life span than those that are not lapped (Player, 1930). In order to achieve a very low cost lapping operation, factors such as adequate machine, sample

preparation, abrasives, lapping speed, lapping time, and pressure had to be evaluated before lapping (Tweedy, 1928).

3.1 Abrasive Machining Techniques

According to Schey (1987), abrasive machining refers to a process in which metal is removed by hard, angular abrasive grains or grits that could be bonded or loose, which form a tool of a particular geometry. If high dimensional accuracy and fine surface are required in production of a part, abrasive machine processes such as buffing, grinding, honing, lapping, polishing, ultrasonic machining and wire brushing are normally used. A comparison of types of abrasive machining processes and surface finish is presented in Table 1. The functions and applications of lapping operation are discussed in Chapter 1. After machining, materials are first ground, lapped, and finally polished, and this sequence is very important in order to obtain a very fine surface finish.

3.1.1 Buffing

In this technique, very fine abrasives are used on soft disks that are made of cloth or hide. Buffing is done after polishing in order to obtain a very finer surface quality. The major difference between buffing and polishing is that finer abrasives are used for buffing, unlike in polishing. Buffing is usually accomplished by making the workpiece to come in contact with a revolving cloth or buffing wheel, which is charged with a suitable abrasive compound. Also, buffing produces smooth and reflective shiny surfaces for both decorative and functional purposes.

3.1.2 Grinding

In this process, individual abrasive grains bonded on grinding wheels or abrasive belts are used for removal of chips. Bonded abrasives in form of grinding wheel are good for high material removal rates, unlike single abrasive that removes a small amount of material at a time. The common types of bond in bonded abrasives are: vitrified (glasslike), resinoid, rubber, and metal bonds.

3.1.3 Honing

It is predominantly used for fine surface finishing of holes. In other words, honing can be defined as a low-speed abrasive process that is used to produce high dimensional accuracy, and fine surface finish inside cylindrical surfaces (Cotell, Sprague, and Smidt, 1994). The honing tool comprises a set of aluminum oxide or silicon carbide bonded abrasives, usually referred to as stones. The stones are mounted on cylindrical rod, which rotates in a hole with an application of radial force.

3.1.4 Polishing

This is an abrasive machining technique that results in production of a smooth and shiny surface. It is done after lapping as illustrated in Figure 8. Normally, polishing is used to remove or smoothen grinding lines, scratches, pits, mold marks, parting lines, tool marks, stretcher strains, and surface defects that could severely affect appearance or performance of a produced part (Cotell, Sprague, and Smidt, 1994). It is a fine abrasive removal process, and involves smoothening and smearing work material surface due to frictional heating. Polishing is done with bonded abrasive wheel or belt. Polishing wheels or belts are usually driven at high speeds. Also, polishing improves the edge and surface of the work material for both decorative and functional purposes.

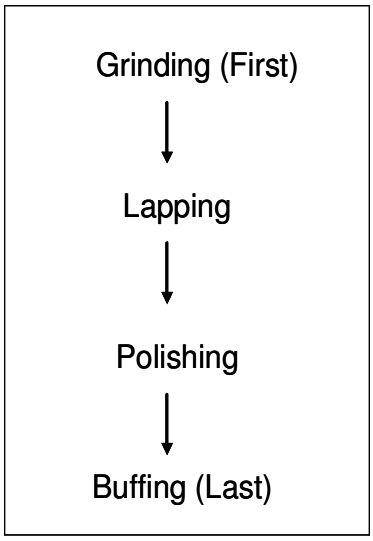

Figure 8. Lapping Precedence.

3.1.5 Ultrasonic Machining and Rotary Ultrasonic Machining

In ultrasonic machining (UM), some materials are removed from the workpiece by microchipping and erosion using fine abrasive grains in a slurry form. The tip of the tool vibrates at a frequency of 20 KHz, which in turn, imparts a high velocity abrasive grain between the tool and the work material (Kalpakjian and Schmid, 2001). This technique is usually applied to hard, brittle, and nonmetallic materials. Conversely, in a rotary ultrasonic machining (RUM), the loose abrasive slurry is replaced with metal-bonded diamond abrasives.

3.1.6 Wire Brushing

This produces fine surface texture. According to Kalpakjian and Schmid (2001), the work material is placed against a circular wire brush, which rotates at high speeds (1750 rpm for large wheels, and 3500 for small wheels).

Table 1. Comparison of Different Abrasive Machining Processes.

Abrasive Machining	Nature of Abrasive	Liquid vehicle	Surface Finish	Stock Removal	Velocity
Buffing	Loose abrasive	Slurry	Improves	Low	Low
Grinding	Bonded	-	Improves	High	High
Honing	Embedded	-	Improves	Low	Low
Lapping	Loose abrasive	Slurry	Improves	Low	Low
Polishing	Bonded	-	Improves	Low	High
Rotary Ultrasonic machining	Metal bonded	-	Improves	High	High
Ultrasonic machining	Loose abrasive	Water slurry	Improves	High	High
Wire brushing	Embedded	-	Improves	Low	High

3.2 Abrasives

An abrasive is defined as a small nonmetallic particle of an irregular shape, with sharp edges that could remove tiny amounts of material or chips from the workpiece through a cutting process, thereby a achieving a very fine surface finish and dimensional accuracy (Kalpakjian and Schmid, 2001). The grit number is used to define the grain size, and this depends on the sieve size. If the grit number is large, this means that the grain size is small. For instance, a grit number of 100 will be very coarse, whereas a grit number of 900 will have a fine grain size as shown in Table 2.

3.2.1 Properties of Good Abrasives

Schey (1987) described certain number of requirements that have to be fulfilled by abrasive particles in order obtain good surface finish; good surface integrity, and the desired material removal rate. Qualities of good abrasives include:

- Abrasives with high hardness at both room and elevated temperatures would resist abrasive wear due to hard particles.

- Abrasives that have low adhesion to the work material help in reducing formation of build-up edge (BUE), decrease re-deposition of ground debris on the workpiece, and aid in removal particles from a bonded structure.
- Also, abrasives with good chemical stability usually resist wear and corrosion from oxygen and cutting fluids.
- Abrasives should have sharp cutting edges in order to achieve the desired material removal rate.

Table 2. Abrasive Grain Sizes (United States Products CO., 2006).

Grit or Mesh Number	Grain Size (inches)	Grain Size (μm)
100	0.0068	173
120	0.0056	142
150	0.0048	122
180	0.0034	86
220	0.0026	66
240	0.00248	63
280	0.00175	44
320	0.00128	32
400	0.00090	23
500	0.0065	16
600	0.00033	8
900	0.00024	6

Conversion Factors

One micron (μ) = 0.001 millimeter

One micron (μm) = 0.000039 inch

One inch = 25, 641.0256 μm

One microinch = 0.000001 inch

One micrometer = 0.000001 m

3.2.2 Types of Abrasives

- **Natural Abrasive Grains**

Some abrasive such as emery (coarse rock of corundum and magnetite), corundum (alumina), quartz (silica), garnet (vitreous silicate mineral), diamond (pure carbon crystallized in octahedrons), and other softer materials that occur in nature. Natural abrasives contain some impurities, and give unreliable results (Kalpakjian and Schmid, 2001). Therefore, synthetic abrasives are preferred over natural abrasives.

- **Synthetic Abrasive Grains**

Artificial abrasives that are used in manufacturing processes include: diamond, silicon carbide, boron carbide, cubic boron nitride, aluminum oxide, and various aluminas. The aluminas are divided into two categories, namely: fused aluminas and unfused aluminas. Fused aluminas are produced from high electric furnace temperatures that produce hard crystals.

On the contrary, unfused alumina abrasives are produced from lower temperatures and chemical additives. Also, unfused alumina abrasives have soft crystalline structure. The abrasive grains used in lapping and other abrasive machining techniques are random geometry multipoint operations because the abrasive particles are irregular in shape, and are randomly distributed between the work material and the lapping plate. A brief description of properties and applications of some abrasives are stated below.

- **Fused Aluminum Oxide (Al_2O_3) or Alundum**

Fused alumina has a hardness number of 9 on Mohs hardness scale. It is suitable for lapping of high tensile materials, rough lapping operation, hardened gears, and ball

bearings grooves. Fused aluminum oxide is not suitable for fine finishing or precision lapping (United States Products CO., 2006).

- **White Fused Aluminum Oxide (Al_2O_3)**

Fused white aluminum oxide abrasives are very friable crystals, and have a hardness value of 9 on Mohs hardness scale. It is good in lapping of stainless steel, chrome plate, beryllium, and ferrite, with hardness below 62 to 63 on Rockwell hardness scale. The lapping pressure causes the friable crystals to keep fragmenting into smaller pieces that perform the finish operation, hence low finish roughness values.

- **Unfused Alumina (Al_2O_3)**

Unfused aluminas are produced either in hydrate or calcined form (high temperature treatment). The hydrate alumina is soft and used for polishing. Calcined aluminas which are produced by heat treatment are recommended for lapping and polishing of harder metals with Rockwell hardness values, ranging from 45 to 63. Unfused alumina abrasives particles have platey shape, which allows more pressure to be distributed over a larger surface area than fused alumina abrasive grains

- **Corundum (Al_2O_3)**

Corundum is a hard crystallized alumina, and it sometimes contains iron, magnesium or silica. It occurs in gem varieties such as ruby and sapphire, and in a common black, brown, or blue form. This is a one of the natural abrasives. It has a hardness value of 9 on Mohs hardness scale. It has a softer crystalline structure than silicon carbide or aluminum oxide. It breaks frequently, and is suitable for lapping of medium hard components with hardness values, ranging from 35 to 45 on Rockwell hardness scale. A medium polish or reflective finish is obtained using corundum.

- **Cubic boron nitride (cBN)**

It is commonly known as Borazon^{TM} cBN. Cubic boron nitride is a synthetic abrasive that has hardness value close to that of diamond as provided in Table 3. CBN is well suited for lapping of ferrous metals since it does not carbonize with iron, unlike diamond abrasives. CBN is good in lapping of materials such as 52100 steel (bearing steel), cast iron, die steel, tool steel, stellite (i.e, cobalt-base alloy with chromium and other metals), super alloys (i.e., temperature-resistant alloys of nickel, cobalt or iron), and ceramics.

- **Diamond (C)**

Diamond abrasive is found in nature and can also be produced artificially. It is extremely hard, highly refractive crystalline form of carbon, which is usually colorless. It is used as a gemstone and in abrasives, cutting tools, etc. Diamond is the hardest and sharpest known substance, Mohs hardness number of 10 (United States Products CO., 2006). Due to these qualities, synthetic diamond abrasive particles are being used widely in industrial applications**.** It is very suitable for lapping of tungsten carbide and other hard materials. Diamond abrasives should not be used in softer substances in order to avoid embedding of materials.

- **Garnet (Mg, Mn, Fe)$_3$Al$_2$Si$_3$O$_{12}$ and Ca$_3$(Cr, Al, Fe)$_2$Si$_3$O$_{12}$**

This is a natural abrasive with a rocky crystalline structure, and has hardness values of 8 to 9 on Mohs hardness scale. Garnet is a common aluminum or calcium silicate mineral that occur in two isomeric series namely: (Mg, Mn, Fe)$_3$Al$_2$Si$_3$O$_{12}$ and Ca$_3$(Cr, Al, Fe)$_2$Si$_3$O$_{12}$. It is usually crystallized and often embedded in igneous and metamorphic rocks. Garnet is used as precious stones as well as abrasives. Its color

ranges from red, brown, black, green, yellow, or white. Garnet does not become embedded in lapped parts, therefore it is widely used in lapping of cast iron, brass (alloy of copper and zinc), bronze (alloy of copper and tin), and aluminum. Lapping with garnet abrasive grains results in a medium polishing quality.

- **Norbide or Boron carbide (B_4C)**

Boron carbide is black, crystalline, extremely hard, water-insoluble, used mainly as a moderator in nuclear reactors as well an abrasive and a refractory. Norbide is a fused abrasive with hardness value of 9.7 on Mohs hardness scale. Its structure is hexagonal and is not easily crumbled. It is used for special lapping operation.

- **Silicon Carbide (SiC) or Crystolon**

Silicon carbide is a bluish-black crystalline compound, and it is one of the hardest known substances. This is a fused crystalline abrasive, and has a hardness value of 9.5 on Mohs hardness scale. It is used both as an abrasive and a heat-refractory material and in single crystals as semiconductors, especially where high-temperature applications are required. It is well suited for rough lapping, forged gears or hardened gears, valves, and general maintenance where polish is not required. Fast cutting with good crystal fragmentation results from lapping of either high or low tensile strength materials with silicon carbide. Materials lapped with silicon carbide usually have a gray or frosty surface finish. Acheson (1891) developed silicon carbide, and this can be synthesized by reacting silicon oxide with carbon as shown below.

$$SiO_2 + 3C \rightarrow SiC + 2CO$$

Apart from hardness of abrasive, friability, which is the ability of the grains to fracture into smaller fragments, is a very important factor in lapping operation.

Abrasives with high friability have low strength and low fracture resistance such abrasives fracture is easier than those with low friability. Aluminum oxide abrasive has lower friability than silicon carbide abrasive; therefore it has less tendencies to fracture than silicon carbide. In selection of abrasives, wear resistance abrasive as well as mechanical properties such as hardness and toughness have to be taken into consideration.

3.3 Hardness Tests

Kalpakjian and Schmid (2001) defined hardness as a resistance to permanent indentation, which depends on the applied load, and the shape of the indenter. Hardness gives a general ideal about the strength of materials, and the extent to which a material resists to scratching and wear. The resistance to indentation depends on the shape of the indenter and the load applied (Kalpakjian and Schmid, 2006). Alternatively, Spitler, Lantrip, Nee, and Smith (2003) defined hardness as a resistance to penetration or ability of a material to withstand abrasion.

Hardness is not the only factor that determines resistance to wear or abrasion, also the alloy content of elements affect resistance to wear or abrasion. Aluminum oxide and silicon carbide are referred to as conventional abrasives, whereas cubic boron nitride and diamond are regarded as super abrasives because they are very hard materials. Kalpakjian and Schmid (2001) reported eight different methods that could be used for testing of hardness of materials, and these techniques are discussed below. Vickers and Knoop hardness tests are good techniques for testing of ceramic materials, whereas Brinell and Rockwell tests are good methods for testing of metals.

- Brinell test

The Brinell hardness number is usually represented by HB or BHN and it is defined as the ratio of applied load to the curved surface area of indentation. In this technique, a steel or tungsten carbide ball is pressed against the surface to be tested, with an application of the recommended load. A load of 500 kg to 3000 kg is recommended in order to obtain an accurate measurement, and the load is normally applied for 10 to 15 seconds for iron and steel, and for about 30 second for other metals. As would be expected, it is observed that soft materials have large impressions, while hard materials result in small impressions.

- Durometer

Durometer is used to test the hardness of elastomers (rubbers and plastics). The indenter is pressed against the surface to be tested; a constant load is usually applied. If the work material is hard, then the penetration will be smaller. In other words, hardness is inversely proportional to penetration. The hardness number in this technique ranges from zero to 100.

- Hot hardness

Hot hardness is very good indicator for performance of a metal or an alloy for high-temperature and high-strength applications. Hot hardness at higher temperatures is very important, for example, the use of cutting tools in machining, and the use of dies in hot-working and casting operations. If conventional hardness test are modified, then they could be performed at elevated temperatures. It can provide some information about change in deformation mechanisms of metals at elevated temperatures. For instance, the indenter and the work material could be enclosed in an electric furnace.

- Knoop test

This is a microhardness indentation test because light loads applied to a diamond indenting tool, and the resulting dimensions of indentation are measured. It is used in measuring the hardness of grains and components of metal alloys. The hardness number is represented by HK or KHN, which is the ratio of applied load to the area of indentation. The applied load ranges from 25 g to 5 kg, while the indentation size ranges from 0.01 mm to 0. 1 mm. Table 3 provides the Knoop hardness number and Mohs hardness number for various industrial abrasive grains.

Table 3. Knoop Hardness Number and Mohs Hardness Number of Abrasives (Kalpakjian and Schmid, 2001).

Abrasives	**Knoop Hardness (HK) (kg/sq. mm)**	**Mohs Hardness Number**
Garnet $(Mg, Mn, Fe)_3Al_2Si_3O_{12}$ and $Ca_3(Cr, Al, Fe)_2Si_3O_{12}$	1360	8-9
Aluminum oxide (Al_2O_3) or alundum	2000-3000	9
Silicon Carbide (SiC) or crystolon	2100-3000	9.5
Boron carbide (B_4C) or norbide	2900-3580	9.7
Cubic boron nitride (cBN)	4000-5000	9.9
Diamond (C)	7000-8000	10

- Mohs test

The Mohs hardness scale ranges from 1 to 10, with scale of 1 for the softest material (talcum powder), and scale of 10 for the hardest known material, that is, diamond. This test is based on the capability of one material to scratch another material. The Mohs hardness scale values for various abrasives are presented in Table 3, and the values correlate well with the Knoop hardness number as shown in Table 3.

- Rockwell test

In this process, the depth of penetration is measured instead of the diameter of the indentation. During the course of the experiment, the indenter is pressed onto the surface of the test material with a small load, and then followed by a major load. The hardness is measured as the difference in depths of penetration of the test material.

- Scleroscope

In scleroscope test, a diamond-tipped indenter enclosed in a glass tube is dropped from a given height onto surface of the material to be tested. If the rebound of the indenter is high, this implies that the material is hard, and vice versa. The height of the rebound is measured on a graduated scale, and harder materials result in higher rebound.

- Vickers test

A pyramid-shaped diamond indenter is used for Vickers hardness test. The load applied ranges from 1 kg to 120 kg, and it is applied for 10 to 15 seconds. A microscope is used to measure the two diagonals of indentation left in the surface of material. Then Vickers hardness is calculated by dividing the load by the area of indentation. Regardless of the amount of load applied, Vickers test results in the same hardness number. It is good in testing materials with a wide range of hardness. Vickers hardness number is represented with HV or DPH.

3.4 Lapping of Ceramics

Davis (1974) investigated the influences of different lapping plates on various types of work materials during flat lapping using natural diamond abrasives, and synthetic diamond abrasives. The four types of lapping plates used in the experiment

were: fine grained cast iron, coarse grained cast iron, mild steel and copper, while four types of workpieces included: alumina ceramic, steel, synthetic sapphire, and tungsten carbide. The author concluded that the best surface finish was obtained with a copper lapping plate in lapping of a synthetic sapphire workpiece. However, it was observed that the copper lapping plate had a very good initial material removing rate (MRR), that is, the quantity of material removed per unit time, but this decreased after sometime because the abrasives either broke down or became embedded in the copper lapping plate. The steel work materials were easier to lap than the sapphire workpieces, but the steel had the worst surface finish.

Additionally, the highest stock removal rate was obtained with a fine-grained cast iron lapping plate when lapping a high alumina ceramic work material. From this experiment, the author confirmed that the harder the lapping plate, the higher the MRR On the contrary, the softer the lapping plate, the better the surface finish. Also, Davis (1974) established that natural diamond abrasive was superior over the synthetic diamond abrasive. This performance, the author attributed to the fact that, synthetic diamond abrasives contained some impurities and inclusions, which caused them to break down more often that the more perfect natural diamond abrasive grains. This was in contrast to the findings of (Kalpakjian and Schmid, 2001).

Chen, Sakai, and Inasaki (1991) studied the lapping of advanced ceramics. According to their findings, increase in lapping pressure and lapping speed were directly proportional to material removal rate. Also, they found that lapping pressure did not have a great impact on surface roughness. Furthermore, softer lapping plate resulted in reduced surface roughness; however, the material removal rate was decreased. In

addition, Chen, Sakai, and Inasaki (1991) established that larger abrasive grains yielded higher material removal rate, although surface roughness was increased. This was in agreement with the findings of (Davis, 1974).

Guha and Chatterjee (1980) reported the effect of lapping and polishing on the strength of alumina ceramic. There has been an increase in the demand of sintered alumina ceramic substrates in micro-electronic industries, especially in integrated circuit application. Alumina substrates are suitable in micro-electronic industries because of their negligible thermal conductivity, high compressive strength, and adequate surface finish. A high compressive strength of 2×10^4 psi and a surface finish of 1 x 10-3 or 4 x 10^{-7} for thick film, and thin film deposition respectively, are required for sintered alumina ceramic substrates.

To achieve the desired surface finish, sintered alumina substrates require lapping and polishing. However, Guha and Chatterjee (1980) found that lapping and polishing of alumina ceramic substrates generated some surface defects, which caused a decrease in compressive strength. In their study, diamond and silicon carbide abrasives were used, while the abrasive grain sizes, ranged from 1 to 300 microns. The compressive strength of sintered alumina ceramic substrates decreased from 1.85×10^4 to 1.37×10^4 psi when polished and lapped with 1 and 300 microns abrasive grains of diamond and silicon carbides, respectively. Finally, they concluded that for a good sintered alumina ceramic that has an ideal microstructure, the ultimate strength might not be affected by some surface defects initiated by lapping and polishing.

In a related study conducted by Chandrasekar and Kotini (1990), the influence of abrasive particles on residual stresses during lapping of ferrite and alumina was

examined. Four types of abrasive grains used in their study included magnesium oxide (softest), silica, aluminum oxide, and diamond (hardest). Due to material removal mechanism, lapping and polishing caused surface damage to ceramic material in form of cracking and dislocations. Therefore, this damage gave rise to residual stresses, because of difference in permanent deformation between the deformed and undeformed layers.

This induced residual stresses significantly affected the strength, hardness, alteration in the near-surface permeability, electrical conductivity, thermal conductivity, and refractive index of the ceramic workpiece. They concluded that softer abrasive particle caused smaller residual stresses, and improved surface finish of the work material. This was in agreement with the study of (Chen, Sakai, and Inasaki, 1991). However, the material removal rate was decreased. Also, smaller grit sizes produced smaller residual stresses with an improvement in surface finish. Furthermore, they found that increased lapping pressure was directly proportional to residual stresses.

Kang and Hadfield (2005) evaluated the material removal mechanisms during lapping of two types of HIPed silicon nitride (Si_3N_4) bearing ball blanks, with various hardness and toughness. Silicon nitride has good chemical, mechanical and physical properties such as corrosion resistance, high elastic modulus, high toughness, high hardness, low density, and temperature resistance. These properties make silicon nitride suitable for rolling element in precision ball bearings, although high cost of production, including finishing operation such as lapping prevent their extensive application.

They conducted the experiment with an eccentric lapping plate, and the independent variables manipulated in their study included: loads, speeds, and lubricants. The authors found that lapping load had the most significant effect on material removal

rate. This was in agreement with the work of (Chen, Sakai, and Inasaki, 1991). At a load of 43N/ball, the highest material removal rate was obtained. However, at very high lapping loads of 78 and 107N/ball, MRR was reduced, while surface and subsurface damage increased.

In addition, material removal rate increased at lapping speeds, ranging from 8.5 to 169 revolution per minute. Furthermore, different lapping fluids influenced material removal rate at lower lapping loads, but their effect was not significant at higher lapping loads. However, at high lapping speeds of 270 and 500 rpm, there was no significant increase in material removal rate. This implied that optimum lapping conditions need to be determined in order to achieve the desired accuracy. Material removal rate of silicon nitride during lapping operation was dominated by mechanical mechanisms. Also, Kang and Hadfield (2005) established that the material removal rate of bearing ball blanks (type 1), with higher hardness and lower toughness was 3 to 4 times greater than bearing ball blanks (type 2) with lower hardness and higher toughness.

3.5 Lapping of Glass

Buijs and Houten (1993a) determined a three-body abrasion model by rolling and indenting abrasive grains for lapping of glass materials. In their study, the following factors were analyzed: lateral fracture, influence of material parameters such as Young's modulus, hardness, and toughness on material removal rate and surface roughness in lapping of glass. Two types of abrasive (aluminum oxide and silicon carbide) were used. The lapping slurry was in a ratio of 1:5 by weight of abrasive particles and water.

After polishing, the samples were lapped for 40 minutes, and the MRR was determined by weighing every 4 minutes. It was established that MRR was constant with time. Surface roughness of lapped work materials were determined using a Talysurf instrument, with a tip radius of 2.5 μm, step size of 2 μm, measured length of 6.4 mm and cut-off length digital filter of 800 μm. They concluded that lapping of glass was a three-body abrasion process, which could be described by a lateral fracture, originating from Vickers' indentation experiment. As would be expected, the authors found that MRR during lapping of glass materials was directly proportional to the amount of load applied.

In a related study, Buijs and Houten (1993b) extended their experiment of three-body abrasion of brittle materials during a lapping operation. According to their findings, MRR is directly proportional to lapping pressure and relative velocity. Their model showed that MRR, surface roughness, and damage penetration were functions of materials and experimental parameters. They predicted the relative abrasion of workpiece with consideration of mechanical properties of the material. Also, the authors believed that surface roughness and damage penetration are independent of the amount of load applied, and the relative velocity. In addition, they derived an expression which showed that the load particle depended on abrasive grain size, and the hardness of the lapping plate. Buijs and Houten (1993b) also concluded that load per particle is proportional to the square of the abrasive grain size.

Chang, Hashimura, and Dornfeld (2000) evaluated the material removal mechanisms in lapping of soda lime glass work material using a copper lapping plate. A 3.45 Newton force was applied, and alumina abrasive grain sizes of 3 μm were mixed with water in a weight ratio of 1:6. Also, the authors investigated the concepts of two-

body abrasion versus three-body abrasion, and ductile versus brittle machining processes. They reported that the abrasive grain particles suspended in the lapping slurry were able to roll and rotate between the work material and the lapping. Any indentation left by this kind of process is known as a three-body abrasive wear. This was in agreement with Buijs and Houten (1993a) definition of a three-body abrasive wear. Contrarily, the abrasive grains became embedded in the lapping plate: an abrasive/work material interaction such as in the case of fixed abrasive machining processes was formed, and authors referred to this as a two-body abrasion.

In addition, Chang, Hashimura, and Dornfeld (2000) described the expressions used in MRR for two-body abrasion and three-body abrasion in the case of brittle materials such as glass as expressed in Equations (11) and (12), respectively. According to the authors, MRR associated with generation of lateral crack was referred to as brittle machining process.

$$\frac{dQ}{dt} = 2ch\frac{dL}{dt}, \tag{11}$$

(Two-body abrasion mode for brittle materials)

$$\frac{dQ}{dt} = \pi c^2 h\frac{2V}{\pi D}, \tag{12}$$

(Three-body abrasion mode for brittle machining)

where

Q: volumetric removal rate (in^3/min)

c: length of lateral crack

h: depth of lateral crack

L: length of groove

V: relative velocity of lapping plate and workpiece

$\frac{2V}{\pi D}$: abrasive grain rotation factor

D: mean diameter abrasive grain particle.

3.6 Lapping of Metals

Knight and Case (1915) studied the effects of various abrasives, laps, and lubricants when lapping hardened steel specimens. The types of lubricants used in their experiment were: lard oil, machine oil, kerosene, gasoline, alcohol, turpentine, and soda water. In addition, they used emery (impure corundum), alundum (fused alumina), corundum (Al_2O_3), and carborundum (SiC) as abrasives.

The objectives of their study were: determination of efficiency of various abrasive particles, performance of different lubricants, determination of MRR of different laps (cast iron, soft steel, and copper), determination of wear of different laps, effects of pressure on MRR, and efficiency of wet and dry cutting. Wet cutting had surplus oil and abrasive grains on the surface of the lapping machine, while in dry cutting method the surface of the lap was moistened with kerosene or gasoline. The objective of keeping the surface moistened with kerosene or gasoline was to avoid the building up of small spot of steel on the surface of the lap.

Knight and Case (1915) concluded that initial rate of cutting using different abrasive was not significant; carborundum had the highest cutting rate for all the abrasive grains used in the experiment. However, caborundum wore the lap twice faster than

other abrasives, whereas alundum wore the lapping plate about one and a half times faster than emery abrasive particles. The authors found that cast iron lap had the least wear resistance, followed by steel lapping plate, and lastly, copper lap was most prone to wear by the abrasive grains. However, copper and steel laps had higher MRR than cast iron lapping plate. As would be expected, the rate of wear was inversely proportional to hardness of the material, while MRR was directly proportional to lapping pressure.

Additionally, they found that gasoline and kerosene were best lubricants for cast iron lapping plate, while lad oil and machine oil acted as best lubricants for copper and steel laps. Furthermore, turpentine worked better with carborundum abrasives, while soda water performed better than alcohol and turpentine. In general, for all lapping plates and all abrasives used in the study, MRR was faster with lad oil than with machine oil. Finally, they concluded that wet lapping was about 1.2 to 6 folds faster than dry lapping, and this depended on the component of the laps and procedure of charging.

Ichida and Kishi (1985) studied the influence of abrasive particle, hardness, and lapping pressure on material removal rate; and surface roughness during lapping of high-carbon high-vanadium steel. High-carbon high-vanadium steel is one of the materials that is hard to machine by abrasives machining techniques because it contains vanadium carbide which is harder than some abrasive grains such as garnet, magnesium oxide, and aluminum oxide. They found that the MRR with green silicon carbide (GC) abrasive particles was three to four folds higher than those of white calcined alumina (WCA) abrasive grains. The authors attributed this trend to the hardness disparities between the abrasive grains, and the work materials. The Vickers hardness number (HV) of GC abrasive grains ranged from 2600 to 3200, whereas that of WCA abrasive particles

ranged from 2100 to 2300. Additionally, the Vickers hardness number for vanadium carbide (an alloy of steel) ranged from 2800 to 2900.

Based on this hardness differences, it was difficult for WCA abrasive grains, which is softer than vanadium carbide to lap high-carbon high-vanadium steel. Furthermore, the authors concluded that lapping pressure was proportional to MRR for both lapping with GC abrasive particles, and WCA abrasive grains. This was in agreement with the study of (Chen, Sakai, and Inasaki, 1991). In addition, there was a sharp increase in MRR at the onset of lapping, followed by a steady increase with MRR with time.

Finally, the mean surface roughness value obtained from lapping with WCA abrasive particles was two to be three times higher than those of GC abrasive grains. The authors attributed this to the fact that vanadium carbide projected easily from the matrix structure, hence it was difficult to obtain a good surface finish from lapping with WCA abrasive grains, unlike in the case of lapping with GC abrasive grains that were harder than vanadium carbide.

Eugene (1947) examined the lapping of rectangular and cylindrical steel specimens using chromic oxide (Cr_2O_3), kaolin or China clay ($Al_2O_3.2SiO_3.2H_2O$), alumina (Al_2O_3), and calcined ferrous oxalate ($F_2(C_2O_4)_3$ as abrasives. The factors manipulated in his study included: lapping pressure, lapping speed, lapping time, abrasives, hardness of the metal, and laps.

Different kinds of laps investigated were: aluminum, cast iron, copper, lead, soft steel, and tin. As a control measure, fluid supplied to the lap was controlled throughout the course of the experiment, and the concentration of the abrasives was 200 grams per

liter of lapping fluid. To determine the amount of abrasion, the sample was weighed before and after the test, and this is represented mathematically in Equation (13).

$$A = \frac{w}{svt}, \tag{13}$$

where

A: amount of abrasion

w: weight loss of specimen (μm)

s: cross sectional area (meters)

v: lapping speed (rpm)

t: time of test (minutes).

It was found that under different types of load tested, material removal rate or abrasion was directly proportional to lapping time. The author also established that the lapping speed and lapping pressure had a significant influence on the MRR. Furthermore, the author found that the hardness of the sample was inversely proportional to MRR. In addition, it was concluded that MRR of laps such as cast iron, copper, and mild steel increased with time of the test. There was no permanent embedding of the abrasive particles during the use of cast iron, copper, and mild steel lapping plate, unlike in the case of soft metals such as aluminum, lead, and tin. The embedding of abrasive grains in the lapping plate is a function of hardness, and the amount of pressure exerted the workpiece and the lapping plate. On the other hand, some laps such as aluminum, lead, and tin did not show any significant increment on MRR with duration of the test.

Additionally, the author reported that the wear of laps depended on the composition of the material. He determined that under the same test condition, cast iron

lap wore 1.28 times less than the lapped specimen, while tin lap wore 4.06 folds less than the lapped sample. In addition, Eugene (1947) derived a relationship between the material removal rate (abrasion) and lapping speed as expressed in Equation (14).

$$MRR = b + aV \,, \tag{14}$$

where

MRR: material removal rate (in/min)

V: speed

a: characteristic constant for the pressure

b: characteristic constant for the test conditions, nature of abrasives, lapping fluid concentration of the abrasives in the fluid, and the lap.

Allan and Sutherland (1962) investigated the effects of lapping speed and pressure during lapping of brass, steel, and aluminum. The authors termed the abrasion of the lapping plate (lap) as wear, while the abrasion of the work material was regarded a material or stock removal. They both believed that copper lapping plates wore about 2.5 times faster than cast iron laps, whereas steel lapping plate wore about two-thirds of cast iron laps. Allan and Sutherland (1962) cited a mathematical relationship between MRR and lapping speed of the plate developed by Eugene (1947), as represented in Equation (10). Also, they cited the relationship between MRR, and relative velocity (between the work material and the lapping plate) described by Eugene (1947), as shown in Equation (10).

Furthermore, Chang, Hashimura, and Dornfeld (2000) derived expressions used in MRR for two-body abrasion, and three-body abrasion in the case of ductile materials, that

is, metals as given in Equations (15) and (16), respectively. The authors referred to MRR associated with plastic deformation as ductile machining process.

$$\frac{dQ}{dt} = kWd_w \frac{dL}{dt}, \tag{15}$$

(Two-body abrasion for ductile machining)

$$\frac{dQ}{dt} = \frac{2\pi}{3} d_w R^2 \frac{2V}{\pi D}, \tag{16}$$

(Three-body abrasion for ductile materials)

where

Q: volumetric removal rate (in^3/min)

k: material fracture toughness

W: width of groove

d_w: depth of abrasive penetration

L: length of groove

t: time

R^2: radius

V: relative velocity of lapping plate and workpiece

$\frac{2V}{\pi D}$: abrasive grain rotation factor

D: mean diameter abrasive grain particle.

Le and Peterson (1999) examined the material removal rate during lapping of nickel-zinc ferrite. This is an important alloy because it is used in production of magnetic heads for electronic storage industries. In their study, copper lapping plate, and diamond

abrasives mixed with ethylene glycol, and distilled water was used a liquid vehicle. According to the authors, MRR changed with time, but pressure and relative velocity were held constant. The authors cited Preston equation that showed the relationship between MRR with time as shown in Equation (17), (Preston, 1927).

$$MRR = CP\frac{ds}{dt}, \tag{17}$$

where

C: Preston constant, which accounts for relative hardness of abrasive, work material, and the density of the abrasive grains on the lapping plate

P: lapping pressure

$\frac{ds}{dt}$: relative velocity of the work material and the lap.

Furthermore, the authors developed a mathematical model for damage rate of diamond abrasive grains, and the re-embedding rate diamond abrasives particles as shown in Equation 18. Based on Equation (18), if RDD > DRD, MRR increased and vice versa. The authors concluded that the abrasive grains were irregular in size and shape, and were randomly distributed between the work material and the lapping plate; hence MRR was regarded as a random variable, and was constantly changing with time.

$$(MRR)_{average} = (MRR)_{theoretical}\,[1+\{RDD-DRD\}* t], \tag{18}$$

where

$(MRR)_{average}$: average MRR at lapping time

$(MRR)_{theoretical}$: theoretical MRR after charging

RDD: Re-embedding rate of diamond abrasives

DRD: damage rate of diamond particles

t: lapping time.

Modeling and simulation of lapping processes based on grain size sensitivity was investigated by Dai et al. (2006). The authors believed that the grain size sensitivity defines the relative change in depth of cutting, which is based on the size of the abrasive grains. During a lapping operation, the grain size sensitivity is used to evaluate the probability of scratches occurring. If the grain size sensitivity of the machine is low, it implies that the probability of scratching to occur should also be relatively minimal. Grain size sensitivity can be expressed in Equation (19), according to Dai et al. (2006).

$$\text{Grain size sensitivity} = \frac{h_i - h_j}{D_i - D_j} = \frac{1}{1+\sqrt{\frac{\sigma_w}{\sigma_p}}}, \tag{19}$$

where

h_i and h_j: average depth penetrated on the work material by different grains

D_i: and D_j: size of different grains

σ_w: yield strength of the workpiece

σ_p: yield strength of the lapping plate.

Letner and Synder (1953) studied the stress distribution in grinding and lapping of manganese oil hardening tool. The experiment was conducted through sectioning of stressed surface layers, and changes in curvature of the sample using an optical interferometer. Three identical samples were lapped simultaneously on a 12-inch-

diameter cast iron lapping plate, at a speed of 72 rpm using aluminum oxide abrasive. The average lapping pressure was 0.07 psi, and all samples were given four 10-minute runs. Afterwards, one or 2-hour runs were given to all the samples. They both believed that residual stresses caused by lapping or grinding had influence on both the service of the tool, and the finished parts. Curvature and weight measurements were determined before the test, and after each run. The thickness of the metal removed was measured with a micrometer.

To determine the residual distribution in the lapped surfaces, the equilibrium curvatures of removed thin and uniform layers from the surface of the metal was measured with an optical interferometer. Then the principal stresses in the layers of the sample were computed. The authors found that the residual stress induced by lapping operation was in the form of biaxial compression. Also, they believed that nominal stress was not a good indicator for true stress in both lapping and grinding. Furthermore, Letner and Synder (1953) concluded that residual stress induced by lapping had a high compressive value at the plastically deformed region, which was 0.0002 to 0.0003 inch. However, this compressive value dropped to a negligible value at lower boundary in both lapping and grinding.

Belyaev (1984) evaluated the effects microcutting process during lapping of sealing surfaces using steel, and bronze for a case study. The samples were in cylinder form, with an outer diameter of 80 mm, inner diameter of 62 mm, and 25 mm in length. Prior to lapping, the surfaces work materials were tuned on a lathe and a surface finish of 8-10 μm was obtained. It was observed that swarf (fractured abrasive grains and metallic chips) were generated from an intense microcutting of the sample and the lap, which

accumulated in the slurry, and this made the slurry more viscous. White aluminum oxide with M20 grit size was used as abrasive grains. The authors established that removal of the swarf from the layer of the slurry, led to the loss of the abrasive grains required for lapping.

Also, material removal rate (MRR) was determined as a function of time at a lapping pressure of 0.5 Mpa, and lapping speed of 32 m/minute. Due to the accumulation of swarf in the slurry as lapping progressed, it was found that the MRR at the end of lapping operation was about 2.2 folds less than the MRR at the beginning of lapping process. The generation of fine chips changed the viscosity of the slurry, and loss of adhesion property of the slurry. Therefore, the lapping operation and microcutting conditions were hindered. In order to remedy this situation, an increase in pressure was required for achieving a required surface finish; otherwise this could lead to seizure of the lap and the surface. According to Trent and Wright (2000), seizure is defined as a condition in which the relative motion between two sliding surfaces stops or interlocks. In other words, seizure occurs, when there is an insufficient force to shear the metal at the seizure phase.

Dong et al. (2003) modeled the velocity and trajectory of relative velocity of a zone of a work material during surface lapping. According to their findings, the velocity profile and the trajectory can be used in determining the kinematic adjustment parameters of the machines. These adjustments made it possible to obtain uniform wear of the work material during a lapping process.

3.7 Frictional Force Models

Garzino-Demo and Lama (1994) evaluated the effects of friction and wear of coated and uncoated stainless steel; and of coated and uncoated aluminum. Three types of surface finishing such as grinding, lapping, and polishing were applied to the stainless steel. Afterwards, some silica antiwear coatings were used on the stainless steel disks, while aluminum nitride (AlN) antiwear coatings were applied to the aluminum. The authors observed that the smoothness and dynamic friction coefficients of lapped and polished surfaces were higher than those of the ground surfaces. Also, the wear tracks found on the lapped and polished surfaces were higher than those found on ground surfaces.

They concluded that smoother surface increased adhesion between two surfaces. This implied that an adhesive force had to be applied to the weight, hence causing abrasive wear, which eventually led to an increase in frictional force. For the case of stainless coated with SiO_2, the dynamic friction coefficient was lower. This was attributed to the fact that SiO_2 is brittle, and the tip of asperities disintegrated instead of deforming, therefore the effective contact area was smaller than those of metals after plastic deformation.

In another study conducted by et al. (1999), friction and wear of wood ceramics was studied using oil and water as lubricants in a sliding contact environment. They used non-additive turbine oil and distilled water as lubricant. The lubricant was delivered to the frictional interface at a flow rate of 23 cm^3/minute, with an aid of a micro-tube pump. As a control variable, the lubricant temperature was maintained at a rate of $30 \pm 3^{o} C$. The sliding velocity was varied between 1 to 19 m/sec, while the force was varied from

98 to 294 Newton. During the course of the experiment, a torque was pressed gently against the rotating ring at a load of 200 N/min. The friction torque was measured with a torque meter. Akagaki et al. (1999) determined the coefficient of friction, and specific wear volume using Equations (20) and 21, respectively.

$$\mu = \frac{\Delta T}{P * R}, \tag{20}$$

$$W_s = \frac{\Delta V}{P * S}, \tag{21}$$

where

μ : coefficient of friction

ΔT : frictional torque (Nm)

P : load (N)

R : radius of the ring (mm)

W_s : specific wear rate (mm^3/Nm)

ΔV : wear volume (mm^3)

S : sliding distance (m).

In the case of oil lubricated contacts, the authors found that irrespective of sliding velocity, the coefficient of friction, and specific wear rate of wood ceramics were small and almost constant. Also, when the load was increased in the oil lubrication, the coefficient of friction and the specific wear rate of wood ceramics decreased. This is due to the fact that the coefficient of friction is the ratio of frictional force to normal load. In the second scenario when water was used as a lubricant, it was found that the coefficient

of friction and the specific wear rate of wood ceramics were small and almost constant until up to a sliding velocity of 12 meters/second.

After a sliding velocity of 12m/sec, the friction and wear rate increased under water lubrication. In the case of dry friction, there was a linear increase in the coefficient of friction, and this depended on the sliding velocity. The coefficient of friction reached up to 1.2 at a sliding velocity of 10m/sec.

Lubricants alter the tribological properties of materials; hence Reynolds in the 1880's introduced the theory of fluid-film lubrication, which is still valid until date. Reynold's steady state equation is represented in Equation (22).

$$F\alpha\frac{v\eta}{D}, \tag{22}$$

where

F: frictional force

v: sliding velocity

η: fluid viscosity

D: thickness of the lubricant (abrasive grain size).

Jiandong et al. (1998) examined theoretical moment between pressure head and pressure disc during lapping. During a lapping process, the pressure head was stationary, but the pressure disc rotated with the work material. According to their findings, the friction moment between the pressure head and pressure disc prevented the work material from rotating, thereby affecting the accuracy of machining. Also, they reported that moment of friction is directly proportional to coefficient of friction. As would be

expected, as coefficient of friction increased, the friction resistant moment increased as well, and it will be difficult for the work material to rotate.

The authors further suggested that pressure head and pressure disc should be made with materials with low coefficient of friction. Although an increase in lapping pressure increased the efficiency of lapping, it restricted the rotation of the work material. However, as the lapping pressure increased, friction resistant moment also increased. Based on the result obtained from resultant moment, the factors that affect the moment were determined, and this helped to increase the accuracy of lapping. The major factor that prevented the work material from rotating was the friction resistant moment of pressure head that acted on the pressure disc.

Ashkerov (1992) investigated the role of frictional forces in grinding, and polishing processes in lapping machines. The author reported that during constant loading and increasing speed, the width of clearance increased, while frictional force was reduced. He found that an increase in load resulted to a decrease in clearance width, and an increase in frictional force. Therefore, in order to return the tool to cutting zone, it was necessary to decrease the speed or increase the load as shown in Equation (23).

$$h = \frac{kv}{p}, \tag{23}$$

where

h: clearance width

k: viscosity coefficient

v: speed

p: pressure.

Ashkerov's (1992) findings indicated that during grinding, vertical vibrations in the grinding tool, along with increasing speed, decreased frictional forces. The author concluded that the amplitudes of normal vibrations that occurred during grinding and polishing were due to impact interactions of the abrasive grains of the tool with the microscopic profile of the workpiece. These vibrations, affected the stability of motion of the tool, and also determined the rate of decrease in frictional forces when the speed was increased.

Schmitz et al. (2005) enumerated the difficulties associated with measurement of coefficient of friction. According to the authors, the factors that contributed errors in measurement of coefficient of friction included: calibration of the force transducers, misalignment of the transducer axes with the tribometer axes, and uncertainties in recording of data from the measurement of the voltage. Baleri et al. (2003) studied frictional force phenomenon in stick-slip vibration system between two concentric circular discs in rotational contact with multiple point loads. In order to obtain a good contact between the two surfaces, the surfaces of the discs were lapped with a 1500-grit paper. A tachometer was used to measure the speed of the disc. The forces used varied from 22.5 N to 225 N. According to the findings of the authors, an increase in normal led to an increase in frictional torque. Also, this increased the beam deflection, hence leading to an increase in the amplitude of stick period as well.

From further investigation conducted by Baleri et al. (2003), it was observed that increasing both the rotational speed of the disc, and the stiffness of the spring, caused a decrease in the amplitude stick-slip vibration. Based on the experimental results obtained, single loading was more susceptible to cause stick-slip vibration with greater

amplitude of stick-slip vibration than the two-point or four-point loading. It was also observed that both simulated and experimental results decreased with sliding speed in the low velocity range. Again, as the rotational velocity was decreased, the tangential force also increased.

Blau (1981) evaluated the unlubricated friction, and wear break-in behavior of a dual-phase steel, that is, martensite and austensite. If two surfaces that are unworn slide against each other, then mechanical, thermal, chemical, and microstructural changes take place at the contact interface. In order to investigate the effect of surface finish on frictional break-in, steel DP 80 was reground by wet hand grinding using silicon carbide abrasive of 240, 320, 400, and 600 grit sizes. For a purpose of comparison, 1015 steel was also tested. The authors find that argon environments resulted in lower wear track width for steel DP 80 than air environments at similar test lengths.

Again, it was observed that diamond-polished 1015 steel had wider tracks in air than in argon. Further observations showed that steel DP 80 in air with silicon carbide finish had lower track widths than 1015 steel in air, however, the slope of a least squares line indicated a higher rate track width increase than that of 1015 steel or steel DP 80 in argon. The authors observed rapid changes in friction and wear during the early period of sliding. Also, it was established that the friction of steel DP 80 tested in air was lower for diamond polished surfaces than for surfaces polished with 600 grit silicon carbide cloth. A Power law relationship between the track width and the number of strokes (number of sliding cycles for 1015 steel and steel DP 80) is given in Equation (24).

$$W = AN^{m}, \tag{24}$$

where

W: average track width

A and m are empirical constants, m is the track widening rate

N: number of strokes.

CHAPTER 4

METHODOLOGY

Chapter 4 presents the methodology for performing the experiment. Section 4.1 describes the specifications of the experimental setup. Section 4.2 presents the factors manipulated in the experiment, dependent measures, and control variables. A brief description of sample tolerance is explained in section 4.3. The precautions taken in order to ensure accurate results are presented in section 4.4. In section 4.5, the test procedure used in performing the experiment is discussed. Section 4.6 presents the observations made during the course of the experiment. Finally, quality control procedures used in lapping operations are provided in section 4.7.

4.1 Equipment

A ring lapper manufactured by Strasbaugh with model number 6BK-DC was used to conduct the experiment. Table 4 provides the specification of the equipment.

Table 4. Specifications of Equipment (Strasbaugh, 1999).

Specifications		
Model 6BK-DC	English	metric
Table O.D.	16.00 in.	40.64 cm
Table I.D.	5.00 in.	12.7 cm
Table Annular Width	5.50 in.	13.97 cm
Work Rings	3	3
Work Ring I.D.	5.00 in.	12. 7 cm
Work Ring O.D.	6.62 in.	16.82 cm
Work Ring Offset Range	0.5 in.	1. 27 cm
Table Motor	3/4 HP	3/4 HP
Table Torque (at 10 rpm)	600 in-lbs	2670 N
Table Load Rating	1000 lbs	454 Kg
Table Speed Range	0-100 rpm	
Electrical	110V/220V, 60 Hz, (10 Amps)	
Width	28 in.	71.12 cm
Height	48 in.	121.92 cm
Net Weight	330 lbs	149.69 kg

4.1.1 Maintaining Wheel Flatness

The conditioning provides an offset adjustment in order to maintain the flatness of the lapping plate. A straight edge is used to determine if the lapping plate is concave, convex, or trough. If any of these three conditions exist, then the conditioning rings were adjusted as illustrated in Figure 9. Normally, the contour of the work material is the mirror image of the lapping plate. In other words, a concave lapping plate produces a convex part, and vice versa (EATON Corporation, 1977). If the table is flat, no corrective action is required.

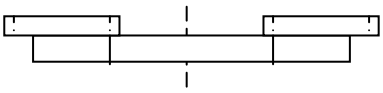

(a) Flat late, no corrective action is required.

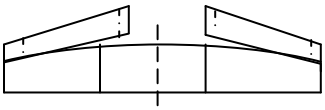

(b) Convex plate, adjust 1, 2, or all rings inward.

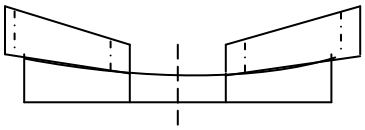

(c) Concave plate, adjust 1, 2 or all rings outward.

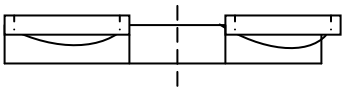

(d) Trough Plate, adjust 1 ring inward, 1 ring outward out, or the ring is set at maximum ring oscillation if the machine has oscillating rings.

Figure 9. Maintaining Flatness of Lapping Plate (Strasbaugh, 1999).

4.1.2 Lapping Machine Materials

The lapping plate used in conducting the experiment is made of gray cast iron with hardness of 97 on the Rockwell B scale. It is fine grade Class 20 cast iron. Class 20 specifies a minimum tensile strength of 20, 000 psi. Subramanian (1994) reported that cast iron is the most commonly used material for making laps because it has close-grain microstructure, is nonporous, and has no other imperfections that can affect the lapping process. A machine charged with abrasives is known as a lap. Apart from cast iron, other materials that can be used for making lap include: copper, leather or cloth (Kalpakjian and Schmid, 2006). The close-grain has the ability of gripping the abrasive grain, and makes them roll efficiently, thereby providing a stronghold for the abrasive particles, so that they can lap the work material efficiently.

The abrasive grains can either be embedded in the lap or may be circulated through loose abrasive slurry. Also, lapping machines can be made from steel-alloy, which is hardened to 60 hot rolled coils (HRC). It has been observed that this brand of steel-alloy prevents embedding of the rolling abrasive grains, therefore achieving an adequate abrading of the workpiece.

4.1.3 Lapping Vehicle Fluids

According to Subramanian (1994), the most commonly used lapping vehicle fluid is water-based vehicle. Oil is rarely used as a lapping vehicle fluid because it penetrates into the pores of some work materials, and it is expensive. Additionally, oil is regarded as a hazardous material, and it is difficult and expensive to dispose; hence water-based vehicle is often a preferred choice. In order to prevent rusting of machine components, inhibitors are usually added to water-based vehicles.

A major disadvantage of water-based fluid is that the abrasives settle faster at the bottom of the liquid vehicle than the oil-based vehicle. In order to avoid settling of the abrasives, suspension agents are sometimes added to lapping vehicle fluids. Allan and Sutherland (1962) enumerated the major functions of the vehicle as**:**

- serves as **c**arrier for abrasive grains, and deposits them to work very efficiently;
- lubricates the surface in order to reduce friction during cutting action;
- carries away the abraded materials (fine chips) removed from the workpiece and spent abrasives; and
- acts as a coolant by carrying away heat generated from the lapping process.

4.2 Design of Experiment

4.2.1 Independent Variables or Allowed-to-vary Factors

According to Montgomery (2001), independent variables are the factors that the experimenter would like to vary or manipulate during the course of the experiment. The factors to be manipulated in the study are:

- Abrasive grains (garnet, silicon carbide, and white aluminum oxide)
- Abrasive grain size (23 µm and 8 µm)
- Workpiece (aluminum 2024, 304 stainless steel, and 1018 steel)

There are three independent variables at three and two levels. Therefore, the number of treatment combinations is 3 x 2 x 3 (i.e., eighteen treatment combinations as presented in Table 5).

Table 5. Experimental Layout.

Material	Abrasives					
	Garnet		SiC		White Al_2O_3	
	23 µm	8 µm	23 µm	8 µm	23 µm	8 µm
Aluminum 2024						
304 Stainless Steel						
1018 Steel						

Aluminum 2024 (Al)	304 Stainless Steel (SST)	1018 Steel	Time (min)	Speed (rpm)
Al_1 + Garnet Al_2 + Garnet	SST_1 + Garnet SST_2 + Garnet	$Steel_1$ + Garnet $Steel_2$ + Garnet	45	85
Al_3 + SiC Al_4 + SiC	SST_3 + SiC SST_4 + SiC	$Steel_3$ + SiC $Steel_4$ + SiC	45	85
Al_5 + White Al_2O_3 Al_6 + White Al_2O_3	SST_5 + White Al_2O_3 SST_6 + White Al_2O_3	$Steel_5$ + White Al_2O_3 $Steel_6$ White Al_2O_3	45	85

4.2.2 Dependent Measures or Response Variables

Dependent variables are the variables that the experimenter would like to measure in the experiment. The response measures include:

- Flatness

According to Spitler, Lantrip, Nee, and Smith (2003), flatness is defined as a condition when all the elements of a surface lie in the same plane. In other words, flatness tolerance indicates a tolerance zone that is bounded by two parallel planes in which the whole surface must lie.

- Surface characterization using images from Scanning Electron Microscope (SEM) micrographs
- Flow rate of abrasive slurry (18 ml/minute)
- Frictional force (lbf)
- Lapping force (lbf)

Scratching pattern and microvoids are created on the workpiece due to the type of abrasives used during lapping. The extent of plastic deformation on the metals determines the occurrence of microstructure. Other measures include:

- Material removal rate (MRR) or lapping rate (inch/minute) or (g/minute)
- Power consumed in lapping (hp or Kw)
- Surface roughness (µm) - measured using a profilometer

Factorial Design

The dependent measures used for statistical analysis were material (MRR) and surface roughness and the independent measures were abrasives types (garnet, SiC, and white Al_2O_3), with two grain sizes (23 µm and 8 µm)**,** and the workpiece. The statistical model used to analyze the data was a 3 x 2 x 3 factorial design as represented in Equation (25). This implies eighteen treatment combinations.

$$Y_{ijkn} = \mu + A_i + S_j + W_k + (AS)_{ij} + (SW)_{jk} + (AW)_{ik} + (ASW)_{ijk} + \epsilon_{ijkn} \quad (25)$$

where

Y_{ijk}: ijk observation of the dependent measure

µ: overall mean

A_i: effect of ith abrasive type, i = 1, 2, and 3 (garnet, SiC, and white Al_2O_3)

S_j: effect of jth abrasive size within the ith level of abrasive type, j = 1, 2 (23 µm vs. 8 µm)

W_k: is the effect of kth workpiece type, k = 1, 2 and 3 (Al 2024, 304 stainless steel and 1018 steel)

$(AS)_{ik}$: interaction between abrasive type and abrasive size

$(SW)_{jk}$: abrasive size x work material interaction

$(AW)_{ik}$: interaction between abrasive type and workpiece

$(ASW)_{ijk}$: abrasive type, abrasive size, and workpiece interaction

ϵ_{ijkn}: random error component

n: number of replicates (2).

4.2.3 Control Variables or Held-constant Factors

Control variables are the factors that could exert some effects on the responses or measures. These factors are not of interest, therefore are maintained at one particular level (Montgomery, 2001). As control variables, the lapping time was maintained at 45 minutes, and lapping speed was held constant at 85 revolutions per minute throughout the course of the experiment. In addition, all experiments were conducted at room temperature. The same abrasive grain sizes were used for garnet, silicon carbide, and white aluminum oxide. The abrasive flow rate was maintained constant at 18 milliliter/minute. Also, a lapping pressure of 12.3 KPa (1.8 psi) was used for each experimental run.

4.3 Sample Tolerance

According to Giesecke et al. (2003), the geometric tolerance) is the total amount of variation that is allowed for a particular dimension. In other words, tolerance is the difference between the upper and lower limit for a specific dimension, as per ANSI/ASME Y14.5M-1994. Standard geometric forms include planes, cylinders, cones, squares, rectangles, polygons, etc. In theory, geometric forms are perfect, but in practice, they are not. Since it is impossible to produce perfect forms, it is essential to specify the amount of variation that is permitted for proper functioning of parts.

Geometric tolerance specifies either the diameter or the width of a tolerance zone within which a surface or an axis of a cylinder or a hole have to lie in order for the part to meet the required accuracy for proper functioning, and fitting of mating surfaces.

Tolerance can be divided into four main categories, namely size tolerance, form tolerance (circularity, cylindricity, flatness, straightness, and sphericity), orientation tolerance (angularity, parallelism, and perpendicularity), and location tolerance (coaxiality, concentricity, and position). The samples used for the experiment were aluminum 2024, 304 stainless steel, and 1018 steel specimens in form of disks (solid cylinder), with outer diameters of 2.000 ± 0.003 inches cut from a metal bar, and the thickness was 0.125 ± 0.003 inch. The work materials were turned on a lathe until an initial surface finish of 0.003 inch was obtained. Also, the sample was ground and deburred to improve the flatness before lapping. Figure 10 illustrates the work material used for the study.

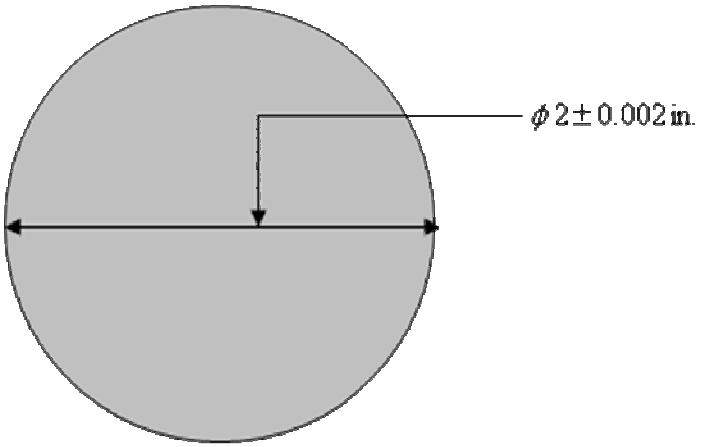

Figure 10. Specimen.

4.4 Precautions

It is necessary to take adequate measure to achieve good results after a lapping operation. Actions that were taken to avoid risks and to ensure good results include the following steps:

- For initial lapping, larger abrasive grain size (23 µm) was used to remove as much material as possible. Then for final lapping, smaller grain size (8 µm) was used to achieve a better finishing.
- To achieve a high material removal, the hardness of the abrasive grains was higher than the work materials.
- The lapping plate was charged (i.e., the machine was run with some abrasive slurry, without the work material for about 5 minutes).
- Degreaser was used to clean the lap and the workpiece after each lapping operation. Subsequently, 95% ethanol l was used to clean the lapping plate, and the workpiece after each lapping operation to avoid damaging the surface of the work material.
- Soft tissue paper (lint-free wipes) was used in the degreasing and alcohol cleaning process, to avoid scratching the sample, which could affect the quality of the final product.
- After each lapping operation, the lapping plate (lap) was cleaned before another lapping operation was executed.
- The slurry pump was flushed with distilled water after using a particular abrasive to avoid mixture of abrasives in different runs.
- SEM analysis was done in about 1 to 2 days after lapping.

- Distilled or deionized water was used as a lapping fluid in mixing the abrasives as well as for cleaning the lapping machine after each run since ordinary tap water might contain more impurities, which could affect the results obtained from lapping**.**
- Also, the sample was ground to improve the flatness before lapping.
- A gage block was used to determine if the lapping plate is concave or convex (i.e., the flatness of the lapping plate before lapping). Then an appropriate remedy was implemented.
- Same portion of the specimen was scanned with an SEM before and after lapping, in order to determine if the abrasives created voids on the sample.

4.5 Test Procedure

The work materials used for the study were aluminum 2024, 304 stainless 1018 cold rolled steel, with diameter of 2.000 ± 0.003 inches, and thickness of 0.125 ± 0.003 inch. Three samples were lapped at each run in order to have a balanced weight on the specimens. The abrasive particles were mixed with distilled water in a weight ratio of 1:5 (i.e., 180 grams of abrasives mixed with 900 grams of distilled water). Also, the flow rate of the abrasive slurry was maintained constant at 18 milliliter/minute. The weighing scale used was manufactured by American Scientific model type SP 120, with a resolution of $1x10^{-4}\,g$. Equation (26) represents the slurry concentration used in conducting the experiment, and this is defined as the ratio of the weight of abrasives to the weight of the liquid used in mixing the slurry.

$$\text{Slurry concentration} = \frac{\textit{Weight of abrasives}}{\text{Weight of distilled water}} = \frac{180\,\text{g}}{900\,\text{g}} = \frac{1}{5} = 0.2 \qquad (26)$$

The hardness of the work materials aluminum 2024, 304 stainless steel, and 1018 steel were determined using Rockwell hardness tester. In this process, the depth of penetration was measured instead of the diameter of the indentation. The term microhardness refers to static indentation performed with loads less than or equal to 1 kg such as Knoop hardness test. Aluminum 2024 is softer than 304 stainless steel and 1018 steel, with hardness value of 58 on Rockwell B scale. Conversely, 304 stainless and 1018 steel are harder than aluminum 2024, with hardness values of 91 and 92, respectively on Rockwell B.

The objective of the indentation made on the specimens was to scan the same location with the profilometer and SEM before and after lapping. A Nikon optical microscope was used to magnify the size of the indentation (5x) to determine the diameter of the indentation. The diameter of the indentation was 0.75 mm (750 μm) and a load of 978.6 N (220 lb) was applied for the hardness test. The temperature of the lapping plate was recorded with Fluke^{TM} thermocouple (model 53/54 II) and was found to be 78°F (25.5°C).

A cast iron single-sided lapping machine was charged with abrasives for 5 minutes (i.e, the lapping plate was run without the work material for 5 minutes), in order to have some abrasives on the lapping plate before the actual lapping began. After charging, additional abrasive slurry was supplied to the surface of lapping plate at 18 ml/minute in the actual lapping operation. The 14-inch-diameter (0.3 m) lapping machine was rotated at a speed of 85 rpm. Then the samples were placed in a lapping

ring, and they rotated freely inside a circular ring (conditioning ring) as depicted in Figure 11. A lapping pressure of 12.3 KPa (1.8 psi) was applied to the work material during the course of lapping and the normal load equivalent was 24.9 N (5.6 lbf).

The slurry was stirred intermittently to prevent the abrasive particle from settling at the bottom of the vehicle compartment. Three types of abrasives used in the experiment were garnet, silicon carbide (SiC), and white aluminum oxide (Al_2O_3). For initial lapping, larger abrasive grain grit size of 400 (23 µm) was used to remove as much material as possible. Finally, smaller grains (i.e., 600 sieve size or 8 µm) were used in order to achieve a better surface finish. For identification purposes, each workpiece was numbered on the periphery, and one-sided lapping operation was carried out.

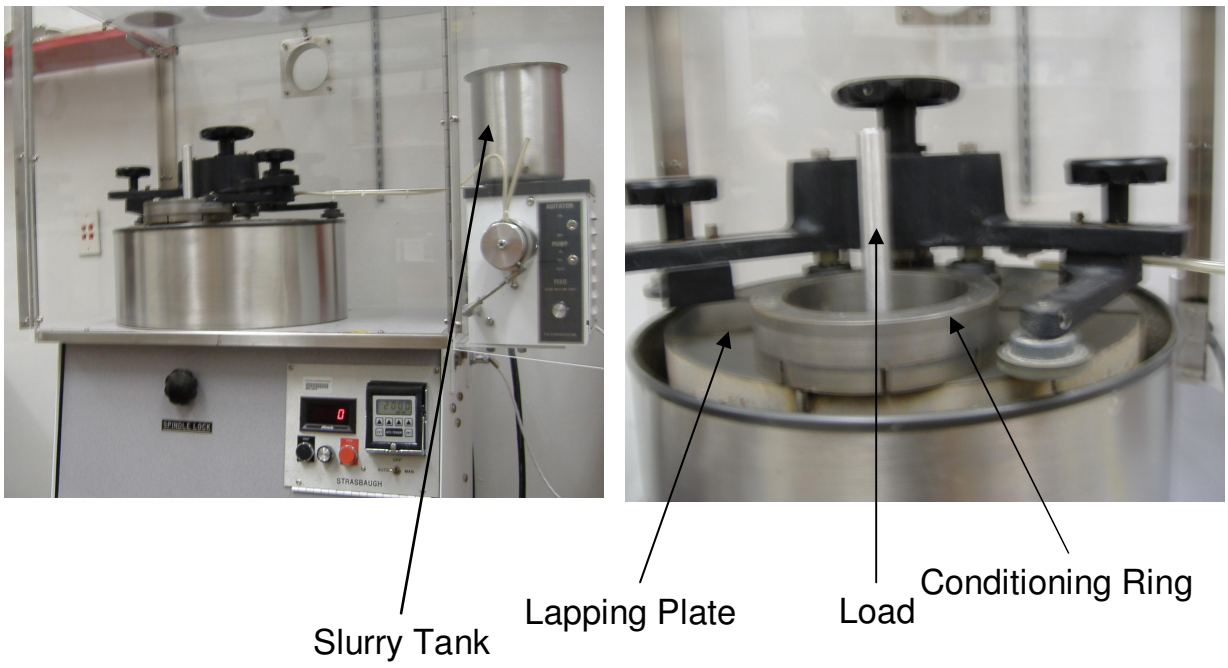

Figure 11. Experimental Setup - Strasbaugh.

4.5.1 Data Collection

A ring lapper manufactured by Strasbaugh (model number 6BK-DC), operating at 3/4 horsepower at full load which corresponds to 8 amperes, was used for the experiment. In order to balance the load, three work materials were lapped in a single run. Torque is the ability of the rotating element to overcome turning resistance. The lapping machine was run first for twenty minutes without data collection (warm-up). In order to determine the frictional torque, the machine was run dry for twenty minutes (without the workpiece and lapping ring), and lapping force and the current consumed were recorded. Fluke 45 Dual Display Mutimeter manufactured by Fluke Electronic Corporation was used to record the current as illustrated in Figure 12. Also, Flukeview™ software produced by Davis Inotek Instruments, LLC was used in recording the current every second. The measurement was gathered off 120 volt mains.

Figure 12. Fluke 45 Dual Display Multimeter.

Afterwards, the work materials and the lapping load were placed on the lapping machine. Again, ten minutes was allowed for steady state to be accomplished. Finally, the actual data for wet run was collected for twenty minutes. Figure 13 depicts the data collection procedure. Finally, the lapping machine was run wet for twenty minutes (i.e., with the

abrasive slurry, lapping ring, and sample). The difference between the dry and wet run was used to evaluate the frictional torque.

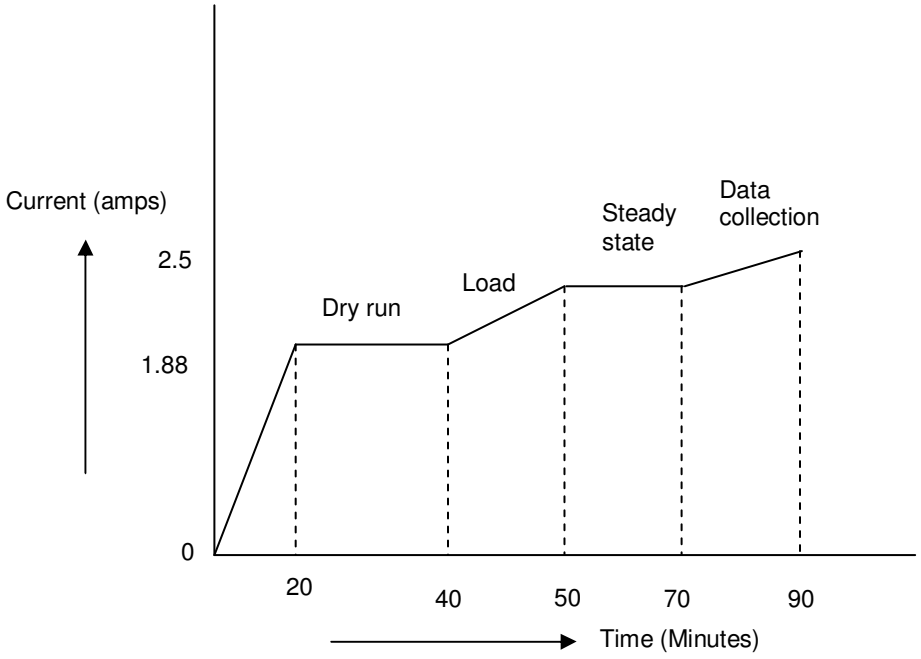

Figure 13. Data Collection Scheme.

Each workpiece was weighed before and after lapping using a precision weighing scale to determine the material removal rate in gram per minute. In addition, the initial thickness of each sample was determined with a digital micrometer. The difference between the initial and final thickness was used to obtain the material removal rate in inch/minute.

4.5.2 Profilometry

Profilometry is a technique in which a diamond stylus (probe) comes in contact with a piece of sample, and measures the surface topography or the physical surface

variation as a function of position. As delineated in Figure 14, Mitutoyo™ surftest 211 profilometer with a resolution of 0.01 μm was used to determine the surface roughness before and after lapping. The radius of the stylus used was 2.5 µm. A contact force of 1.1 x 10^{-4} N was used for each run of the experiment. An indentation was made on each sample using a Rockwell hardness tester, and this was done to scan the same location before and after lapping. Table 6 presents the profilometry parameters used for the experiment. Also, the mean roughness values were determined as presented in Tables 15 through 17 and 21 to 23 in Chapter 7.

Figure 14. Mitutoyo Surftest 211 Profilometer.

Table 6. Profilometry Parameters.

Profilometer Parameters	Values
Number of scans, n	5
Resolution	0.01 μm
Stylus force	1.1 x 10^{-4} N
Stylus tip diameter	5 μm
Time	5 sec

In order to characterize the wear pattern on the workpiece, Scanning Electron Microscope (SEM) images were used to study the wear pattern (i.e., surface structure, fracture patterns, and scratches of the work material before and after lapping process). The

SEM used in scanning the specimens was manufactured by Carl Zeiss MicroImaging GmbH (model number DSM 960 A) as illustrated in Figure 15. The SEM consists of a gun assembly, which produces a primary electron beam; electromagnetic lenses and aperture, which focus the primary electron beam on the specimen; a vacuum system that allows the passage of electron beam through the column without interference of air molecules; a specimen stage; signal detection and display components, which permit the observation and photography of an enlarged image of the sample.

Two different images were scanned taken from each sample at different locations and angles. The images were scanned at 0˚ (left hand side) and 6˚ (right hand side) near an indent. Rockwell hardness tester was used to make an indent on the samples in order to scan the same location before after lapping.

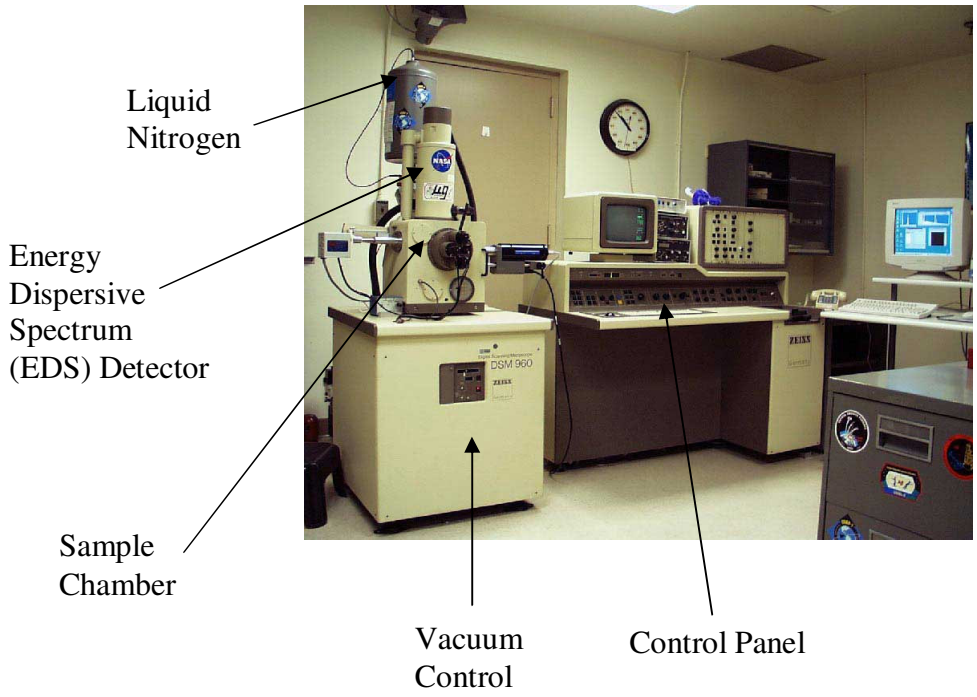

Figure 15. Scanning Electron Microscope - Carl Zeiss DSM 960 A.

The SEM images of the specimen were scanned at 500 and 1000 magnification using excitation energy of 15 kilovolts. The magnification of DSM 960 A ranges from 10x to 300,000x. Backscattering detector was used to compare the contrast between the secondary images and backscattered images from SEM analysis. This comparison helped to confirm the presence or absence of voids in the lapped specimen. If there are no voids, the secondary images and backscattered images will have similar SEM signals as discussed in Chapter 5.

Additionally, Energy Dispersive Spectrometer (EDS) analysis was used to determine the material composition of the work material before and after lapping as discussed in Chapter 5. Initial SEM analyses are shown in Appendix A. EDS was done to confirm if lapping process had affected the alloying element initially present in the

work material after the workpiece had been lapped. In order to determine the chemical composition of the abrasives, an EDS analysis was carried out on the abrasives as shown in Figures 17 and 18 in Chapter 5. After each run, the sample was removed from the lapping plate, cleaned with distilled water and 95% ethanol using soft tissue paper (lint-free wipes). Finally, each sample was reweighed, and the final weight finish was determined. The experiment was repeated under different experimental conditions in order to determine the influence of different abrasives and workpieces on MRR and roughness during lapping of AL 2024, 304 stainless, and 1018 steel.

Speedfam (1970) determined that normal free abrasive machining pressures are in the range of 3 psi. Therefore, the force required for one sample is given in Equation (27). Depending on the number of samples in the lapping ring, the surface area is multiplied by the number of samples in each lapping ring in order to determine the total surface area and the lapping force.

$$\text{Lapping force} = 3 \text{ psi} * \text{Surface area of sample}$$

$$\text{Lapping force} = \left[3 \text{ psi} * \left(\pi * r^2\right)\right] \text{lbf}, \tag{27}$$

where

r: radius of the specimen = 1 inch.

4. 6 Observations

During the course of the experiment, the following observations were made.

- The abrasive particles were worn and disintegrated into smaller sizes during lapping.

- Also, the lapping plate was worn during lapping.
- The worn or fractured particles from the abrasive grains and the metals were mixed up with the lapping fluid, thereby changing the viscosity of the lapping fluid, hence a reduction in MRR.
- Some voids (microns in size) were observed on the specimens after lapping (Figure 24d in Chapter 6). Some wear tracks or scratches were found on the sample, and may be attributed to the abrasives.
- After lapping, the color of the lapped surface changed from gray to black, due to the presence of carbon (graphite) from the lapping plate. This black coloration coating on the work material acts as lubricant.

4.7 Quality Control - Burn Test

According to American National Standards Institute (ANSI), a procedure for inspection of surface of ground or lapped part has been developed in order to detect damage due to burn. Burn is grinding or lapping damage that results due to an application of an excess force on the workpiece. Grinding or lapping burn can be detected on hardened steel by etching (acid treatment) of the ground or lapped surface. The solutions used for etching include:

Solution 1: Mineral spirit or its equivalent

Solution 2: Methanol (CH_3OH)

Solution 3: 5% by volume of concentrated nitric acid (HNO_3) in methanol

Solution 4: 5% by volume of concentrated hydrochloric acid (HCl) in methanol

Solution 5: Rinse with water and neutralize in alkaline solution

Etching Procedure:

The part is cleaned and then immersed in solution 1, with a subsequent air drying. Then the work material is immersed in solution 2 so that the alcohol will remove solvent residue (i.e., a good solvent wetting and activation will be provided). Subsequently, the sample is immersed in solution 3 for about 20 to 40 seconds, until dark gray coloration is observed. Afterwards, the specimen is immersed in solution 4 for approximately 10 to 20 seconds in order to remove carbon smut that is formed in step 3. Finally, the sample is rinsed in water, and neutralized in solution 5 to remove the remaining acid residue.

Acceptable and Unacceptable Limits:

Etching procedure causes regions rehardened by excessive heat from grinding or lapping to appear white, and the softened area due to smaller temperature will turn dark gray or black. Contrarily, areas unaffected due to heat from grinding or lapping will be uniformly light gray to light brown.

Control of Solutions:

The solutions should be changed when residue is observed in the bottom of the containers. All solutions should be discarded when proper etch colorations are not obtained. Also, all solution containers should be air-tight when they are not being used.

CHAPTER 5

MATERIALS CONSIDERATIONS

In this chapter, material analysis using scanning electron microscope is provided. The abrasives are not conductive. Therefore, for the abrasive image to be scanned with an SEM, the abrasives had to be coated with a good conductor such as gold-palladium alloy in a copper petri dish. The SEM images of the abrasives were scanned at 1000 magnification using excitation energy of 15 kilovolts.

5.1 EDS Analysis

SEM micrographs of some abrasives are illustrated in Figure 16. As can be seen in Figures 17 and 18, the number of x-rays in counts per second is plotted against each energy level in KeV, and this represents the energy dispersive spectroscopy of the abrasives.

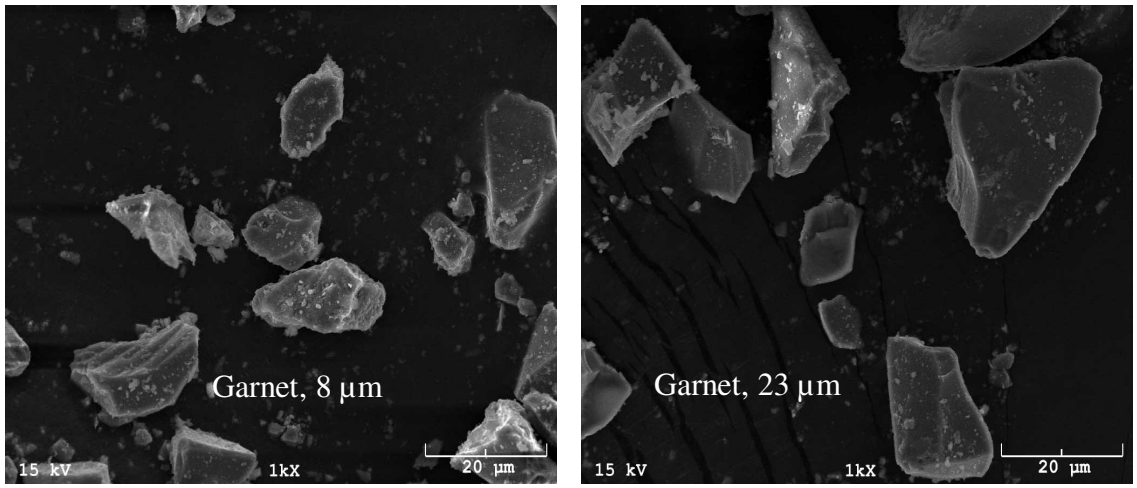

(a) Garnet - $(Mg, Mn, Fe)_3Al_2Si_3O_{12}$ and $Ca_3(Cr, Al, Fe)_2Si_3O_{12}$

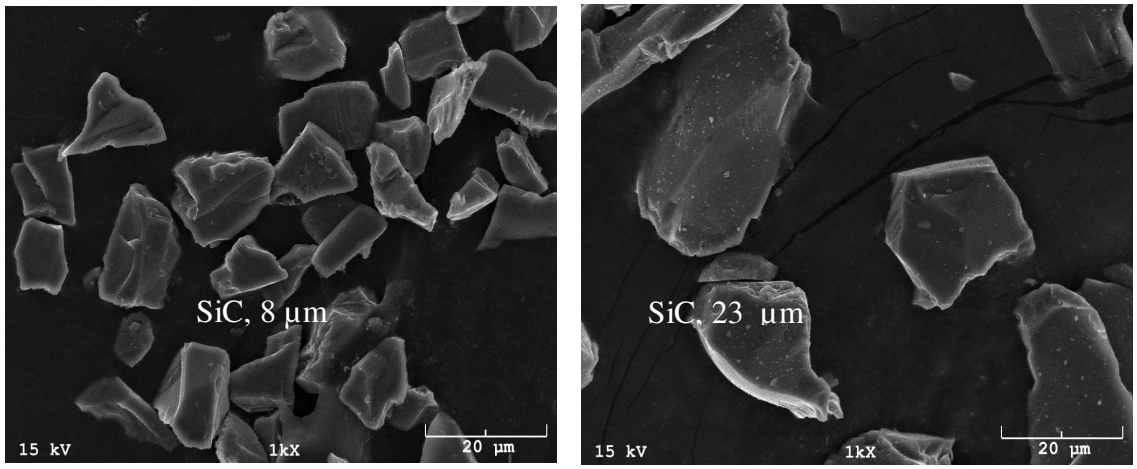

(b) Silicon Carbide (SiC)

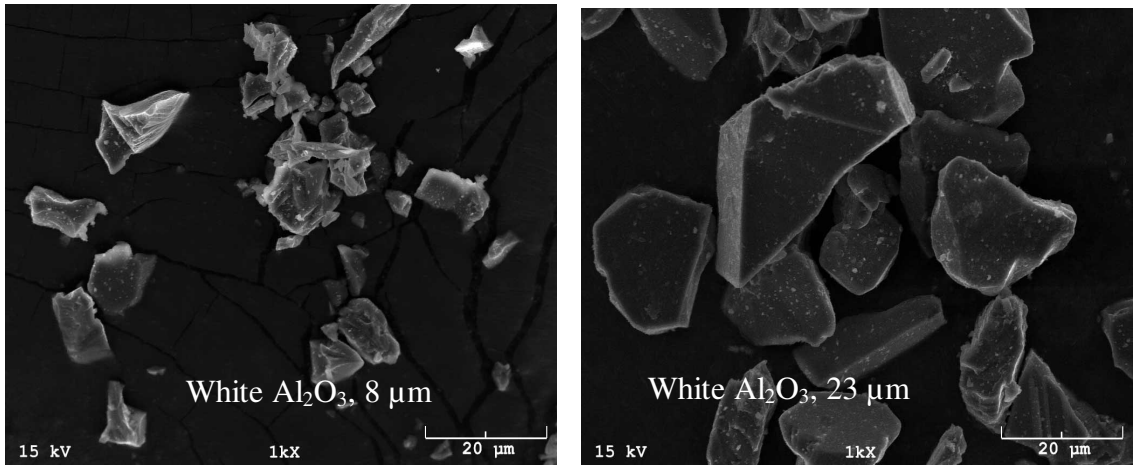

(c) White Aluminum Oxide (Al_2O_3)

Figure 16. SEM Micrographs of Abrasives Grains.

As illustrated in Figures 17 and 18, the EDS analysis of the abrasives was carried out before lapping in order to establish the actual composition of the abrasives, while EDS analysis was carried out on the work material in order to determine if the abrasives have been embedded into the workpiece or reacted with the work material. Table 7 summarizes the advantages of both EDS and WDS.

Table 7. **Advantages of EDS and WDS (Postek et al., 1980).**

Advantages Energy Dispersive Spectrometer (EDS)	**Advantages Wavelength Dispersive Spectrometer (WDS)**
1. Compact and low Cost.	1. Higher separation of elements (Resolution).
2. Rapid result (qualitative analysis).	2. Highly quantitative analysis.
3. High collection efficiency.	3. Higher sensitivity.
4. Simultaneous multi-element analysis of full x-ray spectrum.	4. Analysis of a wide range of elements (Beryllium to Uranium).
5. Display of entire spectrum in a digital format.	5. Better peak to background ratios.
	6. High count rate of individual elements.

Intensity
(count/sec)

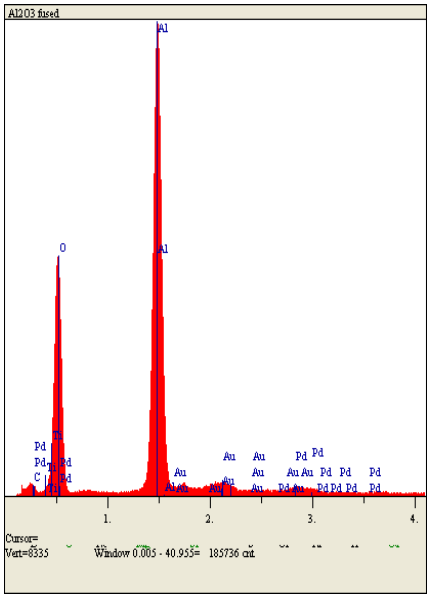

Energy (keV)

Qualitative EDS

(a) Fused Aluminum Oxide

Elt.	Line	Intensity (count/sec)	Error 2-sig	Conc. wt. %
C	K_α	7.92	0.563	2.659
O	K_α	329.62	3.631	44.566
Al	K_α	798.71	5.652	42.158
Ti	K_α	20.25	0.900	2.171
Pd	L_α	10.92	0.661	2.783
Au	L_α	0.86	0.185	5.664
				100.00

Quantitative EDS
KV: 15.0
Take-off angle: 35.0°
Elapsed live time: 100.0 seconds

Intensity
(count/sec)

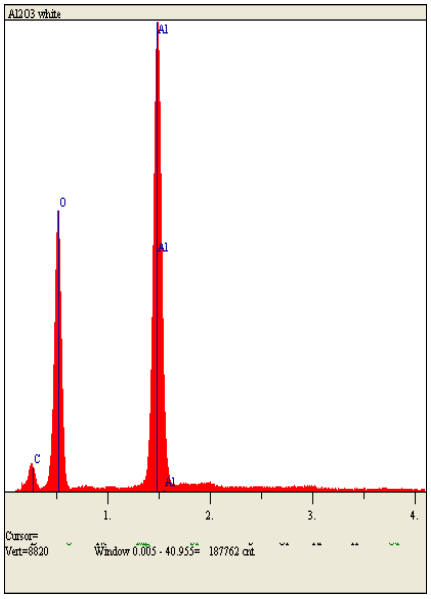

Energy (keV)

Qualitative EDS

(b) White Aluminum Oxide

Elt.	Line	Intensity (count/sec)	Error 2-sig	Conc. wt. %
C	K_α	26.13	1.022	8.607
O	K_α	414.23	4.071	50.011
Al	K_α	856.76	5.854	41.382
				100.00

Quantitative EDS
KV: 15.0
Take-off angle: 35.0°
Elapsed live time: 100.0 seconds

Figure 17. Energy Dispersive Spectrometer (EDS) of Aluminum Oxide.

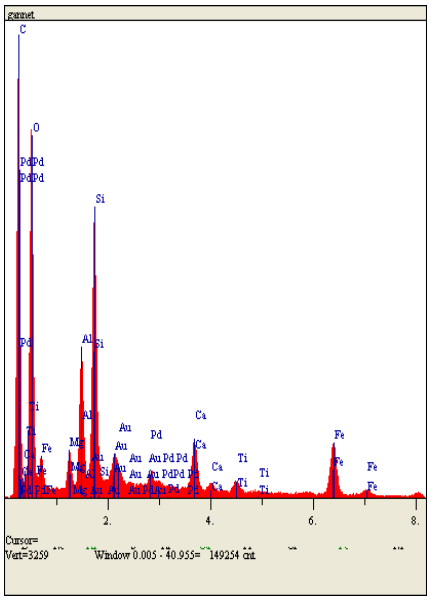

Intensity (count/sec)

Energy (keV)

Qualitative EDS

Elt.	Line	Intensity (count/sec)	Error 2-sig	Conc. wt. %
C	K_α	197.20	2.809	31.563
O	K_α	202.88	2.849	33.116
Mg	K_α	22.44	0.947	1.147
Al	K_α	88.81	1.885	4.223
Si	K_α	184.66	2.718	8.526
Ca	K_α	44.18	1.329	2.905
Ti	K_α	11.31	0.673	0.985
Fe	K_α	53.00	1.456	8.728
Pd	L_α	9.44	0.614	1.797
Au	L_α	1.27	0.226	7.009
				100.00

Quantitative EDS
KV: 15.0
Take-off angle: 35.0°
Elapsed live time: 100.0 seconds

(a) Garnet - $(Mg, Mn, Fe)_3Al_2Si_3O_{12}$ and $Ca_3(Cr, Al, Fe)_2Si_3O_{12}$

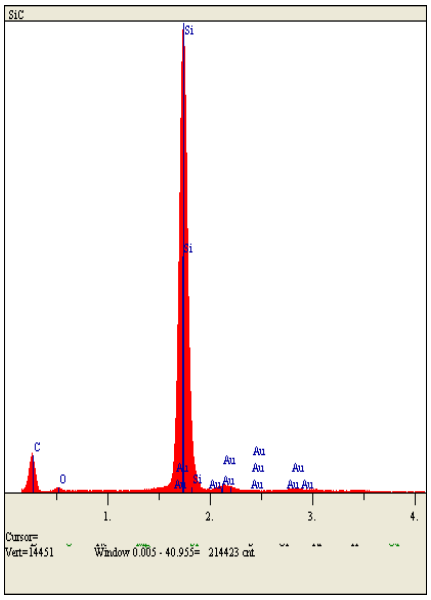

Intensity (count/sec)

Energy (keV)

Qualitative EDS

Elt.	Line	Intensity (count/sec)	Error 2-sig	Conc. wt.%
C	K_α	77.09	1.756	34.937
O	K_α	9.90	0.629	2.182
Si	K_α	1,433.36	7.572	56.026
Au	L_α	1.22	0.221	6.855
				100.00

Quantitative EDS
KV: 15.0
Take-off angle: 35.0°
Elapsed live time: 100.0 seconds

(b) Silicon Carbide

Figure 18. Energy Dispersive Spectrometer (EDS) of Garnet and Silicon Carbide.

Gold and palladium elements were detected as a result of coating the abrasives with gold-palladium alloy. Carbon peaks were mainly from carbon tape used in holding the samples. Carbon tape was used because it was a bit conductive, and carbon does not readily show in many SEM x-ray spectrums.

The chemical compositions of the aluminum 2024, 304 stainless, and 1018 steel before lapping are presented in Tables 8, 9, and 10, respectively. Furthermore, the chemical alloying elements of the Al 2024, 304 stainless, and 1018 steel after lapping are provided in Figures 19 through 21, respectively.

Table 8. Composition of Aluminum 2024 before Lapping (Metcut Research Associates Inc., 1980).

Elements	Composition (%)
Si	0.5
Fe	0.5
Cu	4.9
Mn	0.9
Mg	1.5
Cr	0.1
Zn	0.25
Ti	0.15
Al	91.2
Total	100 %

Table 9. Composition of 304 Stainless Steel before Lapping (Metcut Research Associates Inc., 1980).

Elements	Composition (%)
C	0.03
Si	1
Mn	2
P	0.04
S	0.03
Ni	11
Cr	20
Mo	0.75
Cu	0.75
Fe	64.4
Total	100 %

Table 10. Composition of 1018 Steel before Lapping (Niagara Lasalle Corp., 2005; and Cubberly et al., 1978).

Elements	Composition (%)
C	0.17
Mn	0.76
P	0.01
S	0.03
Si	0.25
Ni	0.10
Cr	0.08
Mo	0.03
Cu	0.24
Al	0.004
V	0.023
Fe	98.303
Total	100 %

Aluminum 2024 is one the best alloys of aluminum because of its high strength, low corrosion resistance, and excellent fatigue resistance. It is used to make parts and structures that require good strength-to-weight ratio. It is easily formed in the annealed condition, and can be subsequently treated by heat. Aluminum 2024 has a wide application in aircraft structural components and fittings, hardware, truck wheels, and parts for transportation industry.

Grade 304 stainless steel is the most versatile and most widely used stainless steel. It has excellent forming and welding characteristics. Grade 304L is the low carbon type of stainless steel (0.03% carbon), and does not require post-welding annealing, so it is widely used in heavy gage components. On the other hand, grade 304H (.08 to 0.1% carbon) has higher carbon content and is extensively used at elevated temperatures. Typical applications of 304 stainless steel include: food processing equipment, kitchen equipment and appliances, architectural equipment, chemical containers, heat exchangers, and mining equipment.

1018 steel is a carburizing grade of steel, which can be strengthened by cold working or surface hardened by carburizing or cyaniding. 1018 steel is soft and can easily be welded or formed.

Energy Dispersive Spectroscopy (EDS) was performed on the materials after lapping as illustrated in Figures 19 to 21. The initial concentration of silicon found in Al 2024, sample 3 before lapping was 0.635%. It was increased to 9.502% due to embedment of silicon carbide abrasives as depicted in Figures 19c. Calcium and silicon were detected in all samples lapped with garnet. Since garnet contains both calcium and silicon, these two elements were caused by the embedment of these abrasives into the lapped metals. In addition, elemental analysis indicates that aluminum and oxygen concentrations increased in materials lapped with white aluminum oxide. The initial concentration of aluminum found in 1018 steel, sample 5 before lapping was 0.065%. It was increased to 7.89 due to embedding of white aluminum oxide abrasives as shown in Figures 21e. For samples lapped with Silicon carbide, EDS results showed an increase in both carbon and silicon concentration.

As illustrated in Figure 19c, elemental analysis obtained from EDS indicated that carbon, oxygen, and silicon concentrations found in of Al 2024 lapped with SiC increased from initial values of 0%, 0.7985%, and 0.5765 to 2.755%, 25.991%, and 9.502%, respectively. As would be expected, the carbon and silicon concentrations resulted from embedment of SiC into the metal substrate. Furthermore, the increase in oxygen concentration was due to oxidation of metals when exposed to the air.

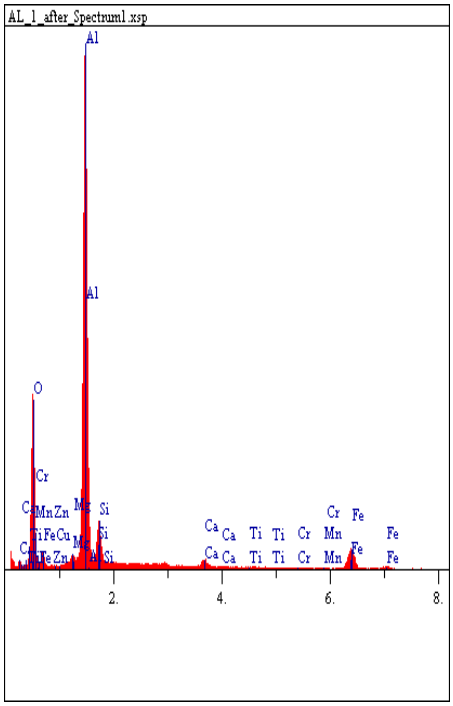

Intensity (c/sec)

Energy (keV)

Qualitative EDS

Elt.	Line	Intensity (c/s)	Error 2-sig	Conc.
C	Ka	0.00	0.000	0.000
O	**Ka**	**145.85**	**2.415**	**31.260**
Mg	Ka	9.19	0.606	0.803
Al	Ka	575.99	4.800	48.651
Si	**Ka**	**46.75**	**1.367**	**5.638**
Ca	**Ka**	**11.12**	**0.667**	**1.388**
Ti	Ka	1.02	0.202	0.167
Cr	Ka	0.60	0.155	0.126
Mn	Ka	1.37	0.234	0.356
Fe	**Ka**	**35.50**	**1.192**	**10.942**
Cu	Ka	0.60	0.154	0.396
Zn	Ka	0.30	0.110	0.274
				100.0

Quantitative EDS

Figure 19a. EDS of Al 2024, Sample 1, Lapped with Garnet.

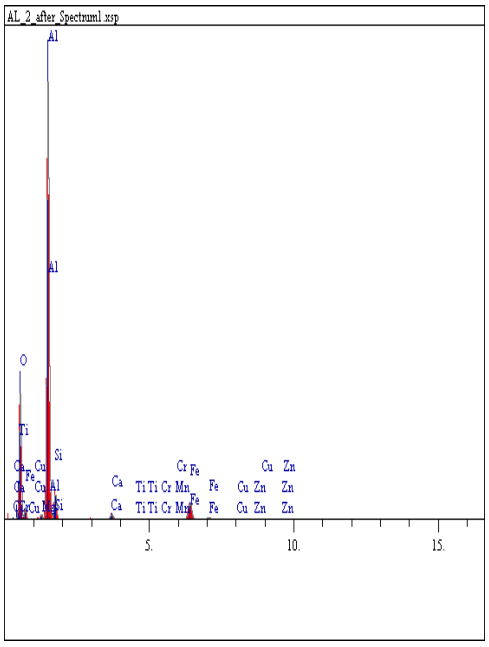

Intensity (c/sec)

Elt.	Line	Intensity (c/s)	Error 2-sig	Conc.
C	Ka	0.22	0.094	0.173
O	**Ka**	**138.42**	**2.353**	**31.428**
Mg	Ka	6.76	0.520	0.627
Al	Ka	558.84	4.728	50.038
Si	**Ka**	**34.91**	**1.182**	**4.519**
Ca	**Ka**	**9.40**	**0.613**	**1.249**
Ti	Ka	0.99	0.199	0.173
Cr	Ka	0.62	0.158	0.139
Mn	Ka	0.76	0.174	0.209
Fe	**Ka**	**32.74**	**1.144**	**10.738**
Cu	Ka	0.56	0.149	0.394
Zn	Ka	0.33	0.114	0.313
				100.0

Figure 19b of Al 2024, Sample 2, Lapped with Garnet.

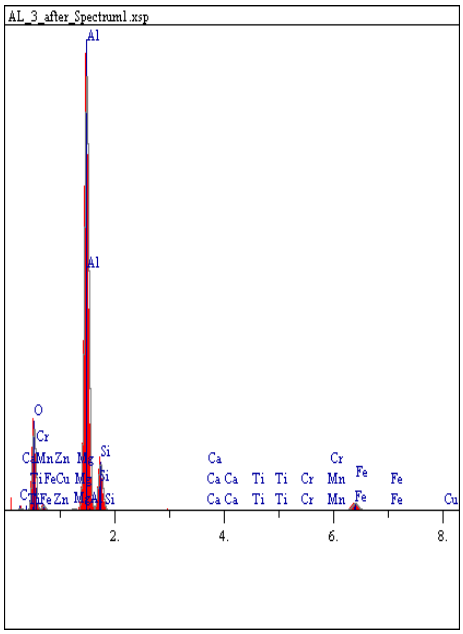

Intensity (c/sec)

Energy (keV)

Qualitative EDS

Elt.	Line	Intensity (c/s)	Error 2-sig	Conc.
C	**Ka**	**2.05**	**0.287**	**2.755**
O	**Ka**	**71.07**	**1.686**	**25.991**
Mg	Ka	1.93	0.278	0.242
Al	Ka	439.65	4.194	54.468
Si	**Ka**	**49.48**	**1.407**	**9.502**
Ca	Ka	0.49	0.140	0.098
Ti	Ka	0.43	0.132	0.113
Cr	Ka	0.46	0.135	0.153
Mn	Ka	0.49	0.139	0.200
Fe	Ka	11.62	0.682	5.662
Cu	Ka	0.24	0.098	0.250
Zn	Ka	0.40	0.126	0.565
				100.0

Quantitative EDS

Figure 19c. EDS of Al 2024, Sample 3, Lapped with SiC.

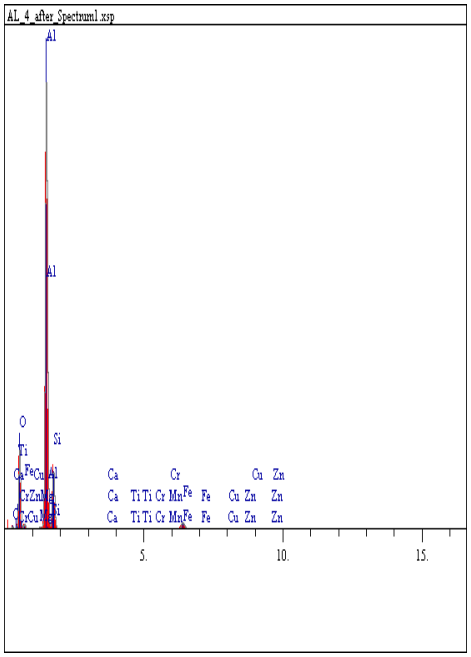

Intensity (c/sec)

Energy (keV)

Qualitative EDS

Elt.	Line	Intensity (c/s)	Error 2-sig	Conc.
C	Ka	1.65	0.257	2.622
O	**Ka**	**59.22**	**1.539**	**25.196**
Mg	Ka	2.10	0.290	0.294
Al	Ka	388.76	3.943	54.243
Si	**Ka**	**54.00**	**1.470**	**11.746**
Ca	Ka	0.48	0.138	0.109
Ti	Ka	0.44	0.132	0.131
Cr	Ka	0.36	0.120	0.140
Mn	Ka	0.16	0.079	0.073
Fe	Ka	8.75	0.592	4.875
Cu	Ka	0.17	0.083	0.204
Zn	Ka	0.22	0.095	0.367
				100.0

Quantitative EDS

Figure 19d. EDS of Al 2024, Sample 4, Lapped with SiC.

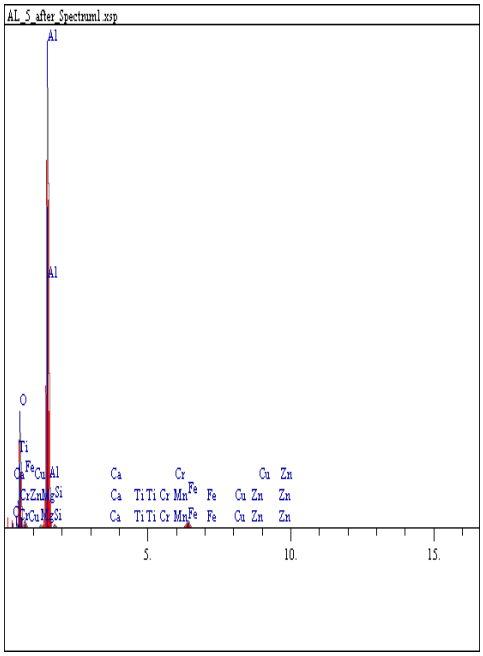

Intensity (c/sec)

Energy (keV)

Elt.	Line	Intensity (c/s)	Error 2-sig	Conc.
C	Ka	0.96	0.196	1.735
O	**Ka**	**59.94**	**1.548**	**30.002**
Mg	Ka	2.13	0.292	0.401
Al	Ka	321.06	3.584	59.760
Si	Ka	2.15	0.293	0.639
Ca	**Ka**	**0.20**	**0.089**	**0.058**
Ti	Ka	0.39	0.125	0.150
Cr	Ka	0.17	0.083	0.085
Mn	Ka	0.28	0.105	0.166
Fe	Ka	8.29	0.576	5.938
Cu	Ka	0.29	0.107	0.444
Zn	Ka	0.30	0.109	0.623
				100.0

Figure 19e. EDS Al 2024, Sample 5, Lapped with white Al_2O_3.

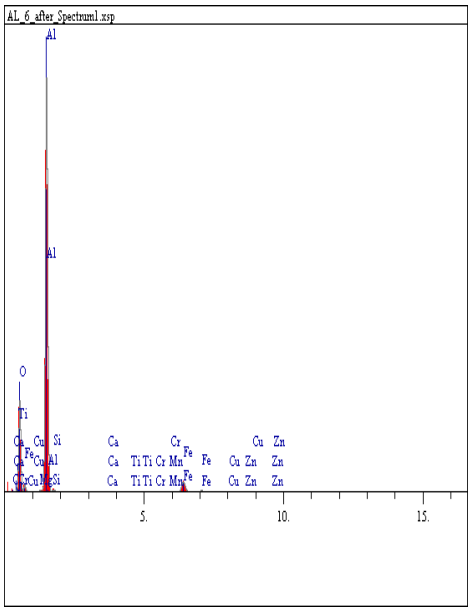

Intensity (c/sec)

Qualitative Energy (keV)

Quantitative EDS

Elt.	Line	Intensity (c/s)	Error 2-sig	Conc.
C	Ka	0.31	0.112	0.656
O	**Ka**	**51.33**	**1.433**	**29.417**
Mg	Ka	1.09	0.209	0.245
Al	Ka	270.70	3.291	59.442
Si	Ka	1.63	0.255	0.564
Ca	**Ka**	**0.45**	**0.135**	**0.154**
Ti	Ka	0.32	0.113	0.142
Cr	Ka	0.16	0.080	0.091
Mn	Ka	0.24	0.097	0.166
Fe	Ka	10.21	0.639	8.522
Cu	Ka	0.23	0.097	0.420
Zn	Ka	0.07	0.054	0.182
				100.0

Figure 19f. EDS Al 2024, Sample 6, Lapped with white Al_2O_3.

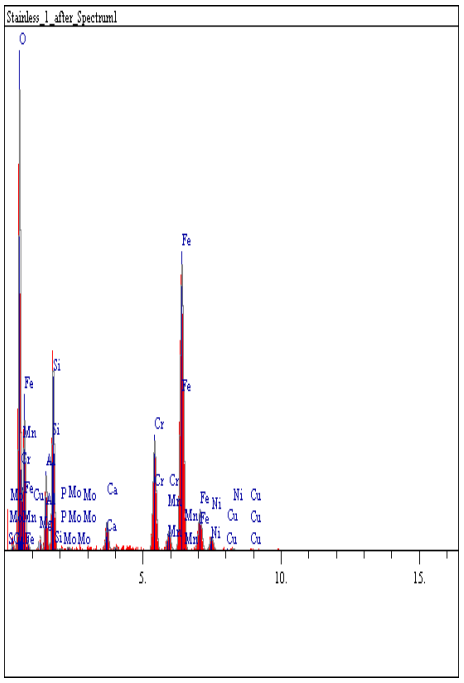

Elt.	Line	Intensity (c/s)	Error 2-sig	Conc.
C	Ka	1.33	0.231	0.795
O	**Ka**	**94.94**	**1.949**	**24.309**
Mg	Ka	3.66	0.383	0.716
Al	Ka	17.99	0.848	3.020
Si	**Ka**	**47.62**	**1.380**	**7.160**
P	Ka	0.73	0.171	0.114
S	Ka	0.00	0.000	0.000
Ca	**Ka**	**8.98**	**0.599**	**1.510**
Cr	Ka	38.53	1.241	10.081
Mn	Ka	1.98	0.282	0.704
Fe	Ka	107.72	2.076	46.801
Ni	Ka	5.67	0.476	3.948
Cu	Ka	0.44	0.133	0.419
Mo	La	0.97	0.197	0.424
				100.0

Figure 20a. EDS of 304 Stainless, Sample 1, lapped with Garnet.

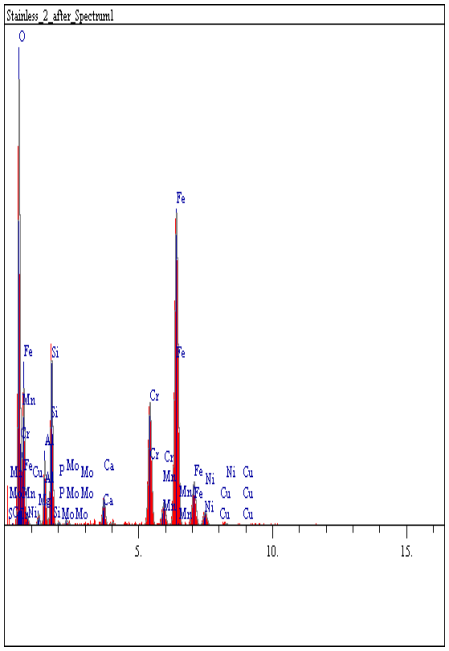

Elt.	Line	Intensity (c/s)	Error 2-sig	Conc.
C	Ka	0.00	0.000	0.000
O	Ka	95.58	1.955	22.476
Mg	Ka	2.92	0.342	0.543
Al	Ka	16.35	0.809	2.595
Si	**Ka**	**45.84**	**1.354**	**6.476**
P	Ka	0.81	0.180	0.118
S	Ka	0.00	0.000	0.000
Ca	**Ka**	**8.82**	**0.594**	**1.380**
Cr	Ka	45.22	1.345	10.969
Mn	Ka	2.91	0.341	0.960
Fe	Ka	122.97	2.218	49.778
Ni	Ka	6.00	0.490	3.898
Cu	Ka	0.23	0.095	0.200
Mo	La	1.50	0.245	0.607
				100.0

Figure 20b. EDS of 304 Stainless, Sample 2, Lapped with Garnet.

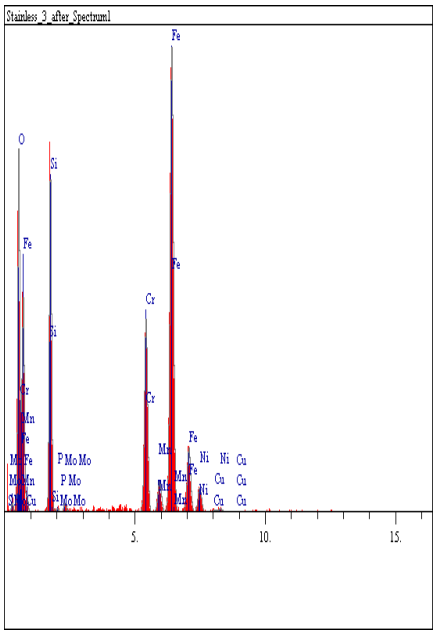

Intensity (c/sec)

Energy (keV)

Qualitative EDS

Elt.	Line	Intensity (c/s)	Error 2-sig	Conc.
C	Ka	1.92	0.277	0.955
O	**Ka**	**68.88**	**1.660**	**13.800**
Si	**Ka**	**82.58**	**1.817**	**9.823**
P	Ka	0.95	0.195	0.118
S	Ka	1.15	0.214	0.132
Cr	Ka	63.76	1.597	12.784
Mn	Ka	2.76	0.332	0.760
Fe	Ka	163.88	2.560	55.541
Ni	Ka	9.19	0.606	5.020
Cu	Ka	0.96	0.195	0.710
Mo	La	1.03	0.203	0.358
				100.0

Quantitative EDS

Figure 20c. EDS of 304 Stainless, Sample 3, Lapped with SiC.

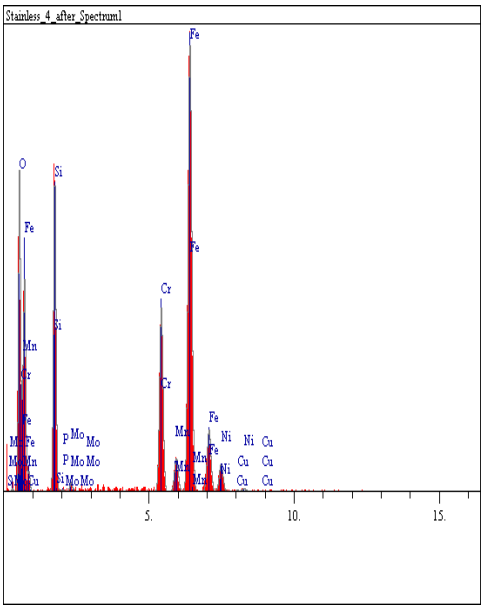

Intensity (c/sec)

Energy (keV)

Qualitative EDS

Elt.	Line	Intensity (c/s)	Error 2-sig	Conc.
C	Ka	0.57	0.150	0.316
O	**Ka**	**57.87**	**1.521**	**12.852**
Si	**Ka**	**72.16**	**1.699**	**9.659**
P	Ka	0.59	0.153	0.082
S	Ka	1.57	0.251	0.202
Cr	Ka	57.54	1.517	12.871
Mn	Ka	3.46	0.372	1.063
Fe	Ka	149.33	2.444	56.516
Ni	Ka	9.57	0.619	5.841
Cu	Ka	0.44	0.133	0.367
Mo	La	0.59	0.154	0.230
				100.0

Quantitative EDS

Figure 20d. EDS of 304 Stainless, Sample 4, Lapped with SiC.

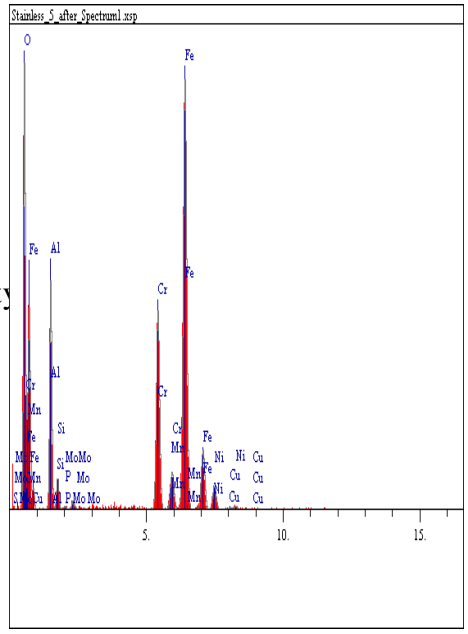

Elt.	Line	Intensity (c/s)	Error 2-sig	Conc.
C	Ka	0.23	0.096	0.100
O	**Ka**	**94.04**	**1.939**	**16.771**
Al	**Ka**	**56.70**	**1.506**	**7.369**
Si	Ka	8.45	0.581	1.004
P	Ka	0.82	0.181	0.095
S	Ka	1.20	0.219	0.129
Cr	Ka	72.15	1.699	13.790
Mn	Ka	5.01	0.448	1.309
Fe	Ka	166.85	2.583	53.683
Ni	Ka	9.38	0.612	4.853
Cu	Ka	0.72	0.170	0.508
Mo	La	1.21	0.220	0.391
				100.000

Figure 20e. EDS 304 Stainless, Sample 5, lapped with white Al_2O_3 .

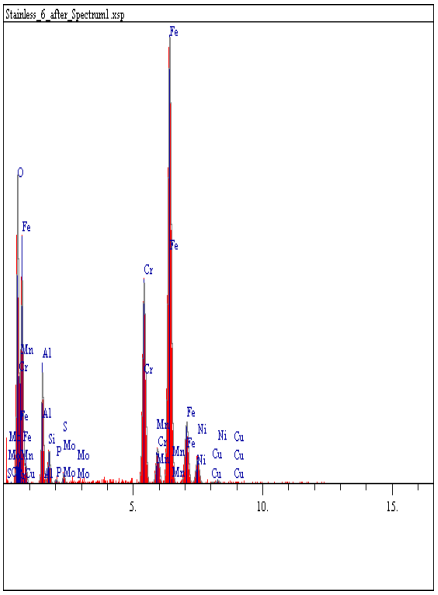

Elt.	Line	Intensity (c/s)	Error 2-sig	Conc.
C	Ka	0.00	0.000	0.000
O	**Ka**	**61.81**	**1.572**	**12.329**
Al	**Ka**	**26.54**	**1.030**	**4.000**
Si	Ka	8.68	0.589	1.159
P	Ka	1.28	0.226	0.166
S	Ka	2.41	0.310	0.290
Cr	Ka	70.28	1.677	14.755
Mn	Ka	3.48	0.373	1.013
Fe	Ka	167.06	2.585	60.092
Ni	Ka	9.90	0.629	5.751
Cu	Ka	0.56	0.150	0.444
Mo	La	0.00	0.000	0.000
				100.0

Qualitative EDS Quantitative EDS

Figure 20f. EDS 304 Stainless, Sample 6, Lapped with white Al_2O_3.

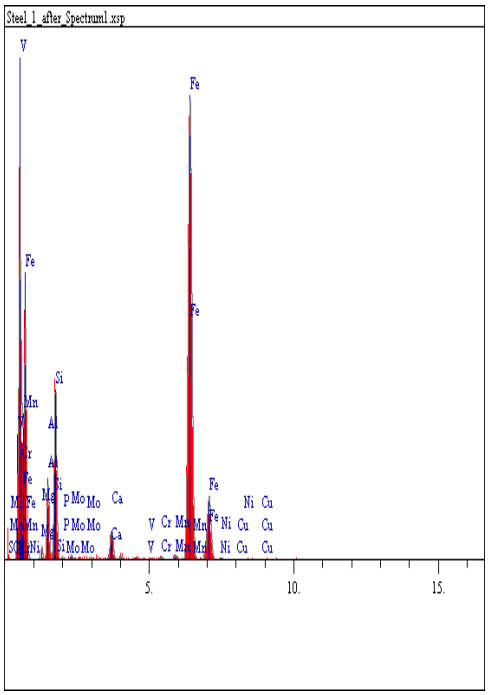

Elt.	Line	Intensity (c/s)	Error 2-sig	Conc.
C	Ka	0.00	0.000	0.000
Mg	**Ka**	**4.60**	**0.429**	**0.852**
Al	Ka	23.23	0.964	3.642
Si	**Ka**	**58.16**	**1.525**	**8.093**
P	Ka	0.91	0.190	0.128
S	Ka	0.25	0.101	0.033
Ca	**Ka**	**11.77**	**0.686**	**1.688**
V	Ka	0.42	0.129	0.075
Cr	Ka	1.49	0.244	0.274
Mn	Ka	2.10	0.290	0.614
Fe	Ka	225.72	3.005	83.277
Ni	Ka	0.74	0.172	0.449
Cu	Ka	0.40	0.127	0.329
Mo	La	1.42	0.239	0.546
				100.0

Quantitative EDS

Figure 21a. EDS of 1018 Steel, Sample 1, Lapped with Garnet.

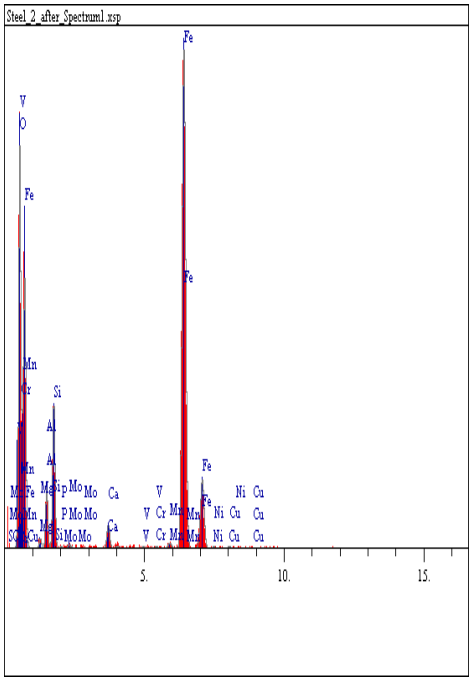

Elt.	Line	Intensity (c/s)	Error 2-sig	Conc.
C	Ka	0.00	0.000	0.000
O	Ka	73.65	1.716	15.031
Mg	**Ka**	**2.66**	**0.326**	**0.445**
Al	Ka	16.93	0.823	2.393
Si	**Ka**	**42.92**	**1.310**	**5.339**
P	Ka	0.72	0.170	0.091
S	Ka	0.05	0.046	0.006
Ca	**Ka**	**8.42**	**0.580**	**1.103**
V	Ka	0.74	0.172	0.122
Cr	Ka	0.86	0.185	0.144
Mn	Ka	2.25	0.300	0.607
Fe	Ka	214.84	2.932	73.148
Ni	Ka	0.81	0.180	0.451
Cu	Ka	0.92	0.192	0.695
Mo	La	1.24	0.222	0.426
				100.0

Figure 21b. EDS of 1018 Steel, Sample 2, Lapped with Garnet.

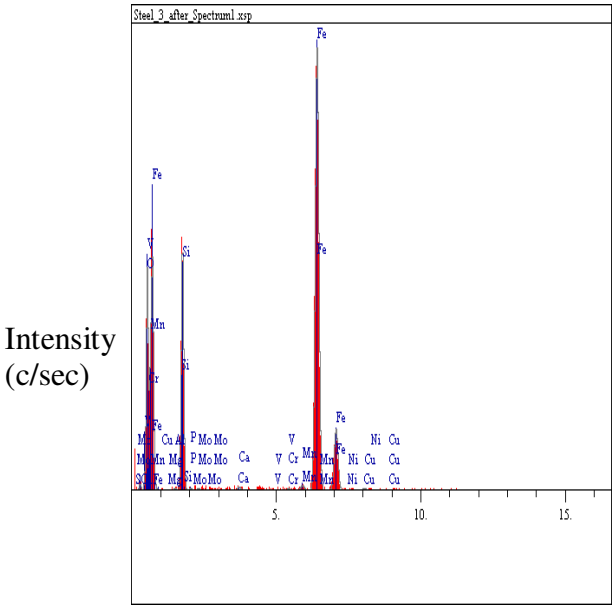

Elt.	Line	Intensity (c/s)	Error 2-sig	Conc.
C	**Ka**	**1.34**	**0.231**	**0.996**
O	Ka	34.00	1.166	10.196
Mg	Ka	0.16	0.080	0.039
Al	Ka	0.46	0.136	0.093
Si	**Ka**	**58.81**	**1.534**	**10.307**
P	Ka	0.53	0.145	0.096
S	Ka	0.00	0.000	0.000
Ca	Ka	1.12	0.211	0.210
V	Ka	0.33	0.114	0.077
Cr	Ka	0.59	0.153	0.140
Mn	Ka	1.73	0.263	0.665
Fe	Ka	155.92	2.497	75.987
Ni	Ka	0.35	0.119	0.282
Cu	Ka	0.60	0.155	0.653
Mo	La	0.52	0.144	0.259
				100.00

Figure 21c. EDS of 1018 Steel, Sample 3, Lapped with SiC.

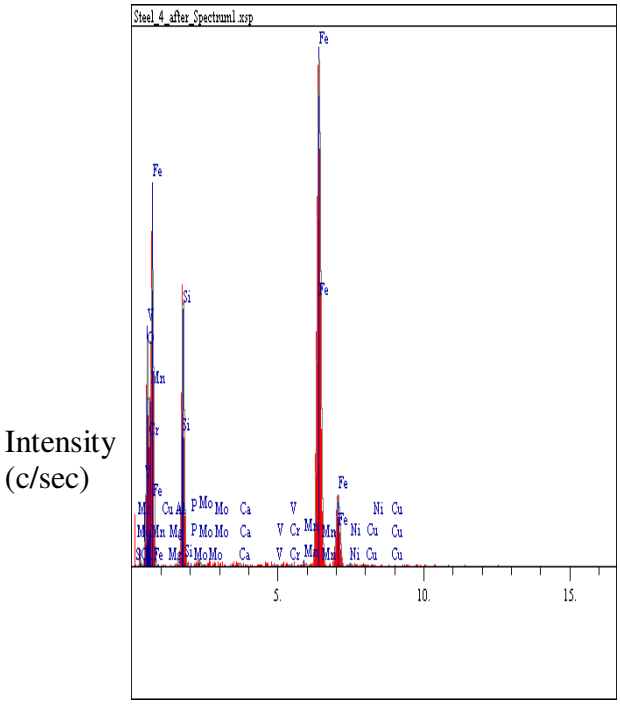

Elt.	Line	Intensity (c/s)	Error 2-sig	Conc.
C	**Ka**	**1.06**	**0.206**	**0.945**
O	Ka	22.80	0.955	8.219
Mg	Ka	0.03	0.036	0.009
Al	Ka	0.39	0.125	0.093
Si	**Ka**	**48.96**	**1.399**	**10.236**
P	Ka	0.18	0.084	0.039
S	Ka	0.31	0.111	0.061
Ca	Ka	0.71	0.168	0.157
V	Ka	0.55	0.149	0.153
Cr	Ka	0.61	0.156	0.171
Mn	Ka	1.09	0.208	0.494
Fe	Ka	134.20	2.317	77.442
Ni	Ka	0.90	0.189	0.847
Cu	Ka	0.50	0.141	0.638
Mo	La	0.83	0.182	0.493
				100.0

Figure 21d. EDS of 1018 Steel, Sample 4, Lapped with SiC.

The initial concentration of aluminum found in 1018 steel, sample 5 before lapping was 0.065%, but it was increased to 7.879 due to embedding of white Al_2O_3 abrasives as shown in Figures 25e, 28e and 28f. Also, oxygen concentration increased from zero to 17.724% after lapping. The increase in concentration came from Al_2O_3 abrasives as well as oxidation of metal when exposed to oxygen (air). As can be seen from geometric SEM and EDS analyses, some chemical components of the abrasives such as calcium and oxygen, were detected on the specimens after lapping with garnet, silicon carbide, and white aluminum abrasive particles. This was attributed to the fact that some abrasives became embedded into the samples. Due to passivation, 304 stainless steel developed a thin hard (protective) film of chromium oxide on the surface because of presence of chromium, and this prevented oxidation (rusting) or corrosion of the stainless steel. To confirm if some abrasives become embedded into the specimens, elemental analysis was carried out prior to lapping (Appendix B).

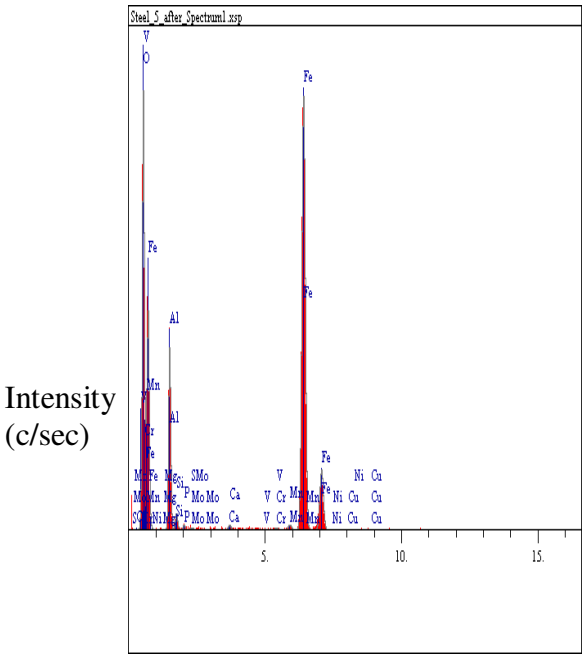

Elt.	Line	Intensity (c/s)	Error 2-sig	Conc.
C	Ka	0.00	0.000	0.000
O	**Ka**	**102.74**	**2.027**	**17.724**
Mg	Ka	0.10	0.063	0.015
Al	**Ka**	**63.08**	**1.588**	**7.879**
Si	Ka	6.16	0.496	0.704
P	Ka	1.92	0.277	0.214
S	Ka	0.00	0.000	0.000
Ca	**Ka**	**2.41**	**0.311**	**0.281**
V	Ka	0.60	0.154	0.087
Cr	Ka	1.13	0.213	0.167
Mn	Ka	2.63	0.324	0.630
Fe	Ka	234.60	3.063	71.447
Ni	Ka	0.44	0.132	0.216
Cu	Ka	0.55	0.148	0.371
Mo	La	0.86	0.186	0.265
				100.0

Figure 21e. EDS of 1018 Steel, Sample 5, lapped with white Al_2O_3.

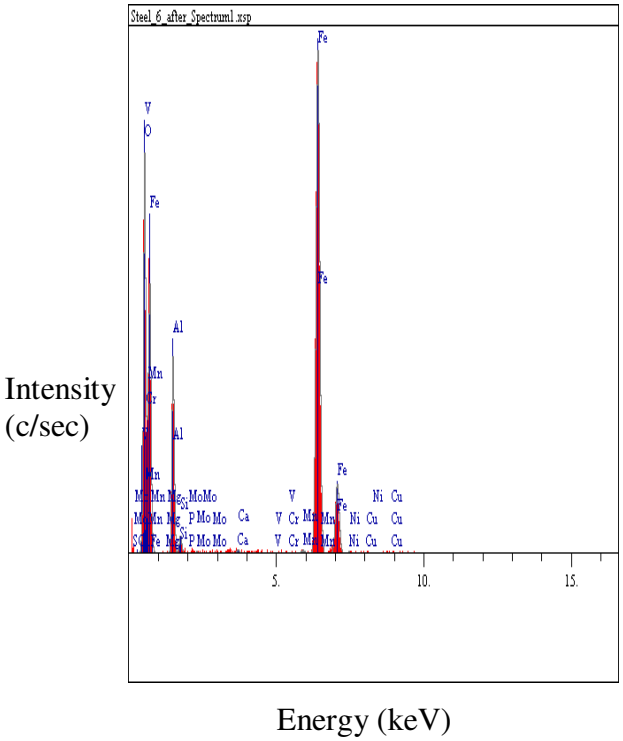

Elt.	Line	Intensity (c/s)	Error 2-sig	Conc.
C	Ka	0.00	0.000	0.000
O	**Ka**	**77.59**	**1.762**	**14.395**
Mg	Ka	0.16	0.081	0.026
Al	**Ka**	**57.72**	**1.519**	**7.808**
Si	Ka	5.45	0.467	0.673
P	Ka	0.36	0.120	0.043
S	Ka	0.00	0.000	0.000
Ca	**Ka**	**1.51**	**0.246**	**0.188**
V	Ka	0.45	0.134	0.068
Cr	Ka	0.56	0.150	0.085
Mn	Ka	1.29	0.227	0.327
Fe	Ka	232.03	3.046	75.316
Ni	Ka	0.74	0.172	0.391
Cu	Ka	0.67	0.164	0.485
Mo	La	0.59	0.154	0.194
				100.000

Figure 21f. EDS of 1018 Steel, Sample 6, Lapped with white Al_2O_3.

CHAPTER 6

IMAGE PROCESSING

Geometric SEM analysis is presented in Section 6.1 Section 6.2 presents how a 2-D image was reconstructed into a 3-D image using Scandium^{TM} software. Section 6.3 describes the MATLAB code used in separating lapped zone, scratched zone, and unfinished zone.

6.1 Geometric SEM Analysis

SEM micrographs of lapped Al 2024, 304 stainless, and 1018 steel are depicted in Figures 22, 23, and 24. Geometric analysis from the SEM indicated that some silicon carbide and white Al_2O_3 become embedded in the workpiece as illustrated in Figures 22c, 23e, 23f, 24c, 24e, and 24f. Additionally, groove was observed on steel samples lapped with white Al_2O_3 as delineated in Figure 28f. Also, microvoid was seen on steel sample lapped with SiC as shown in Figure 24d.

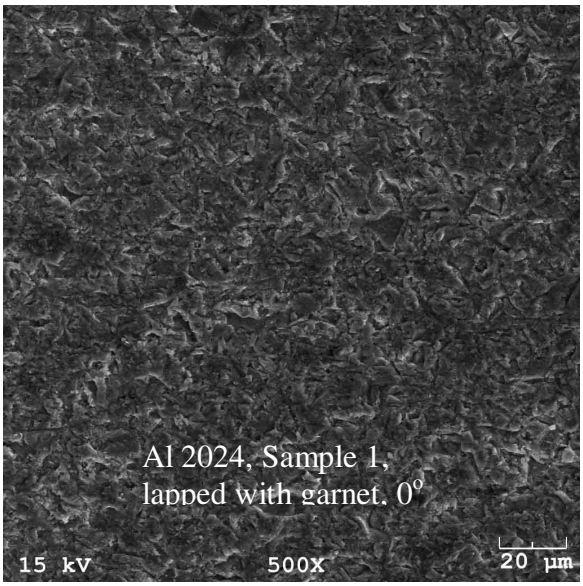

Al 2024, Sample 1, 500 Magnification

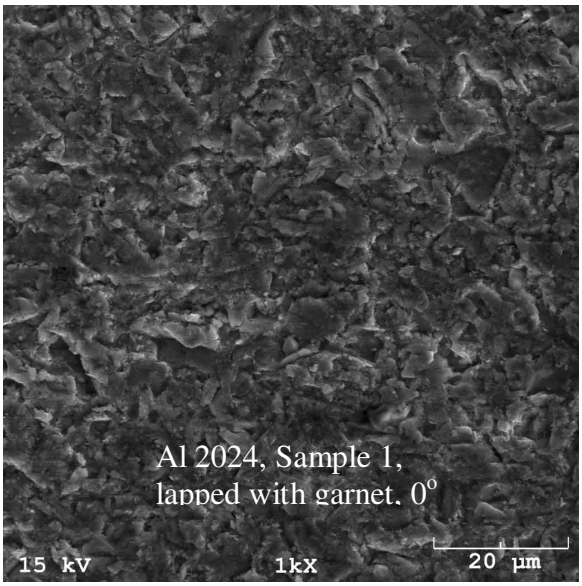

Al 2024, Sample 1, 1000 Magnification

Figure 22a. SEM Micrographs of Al 2024 - Lapped with Garnet.

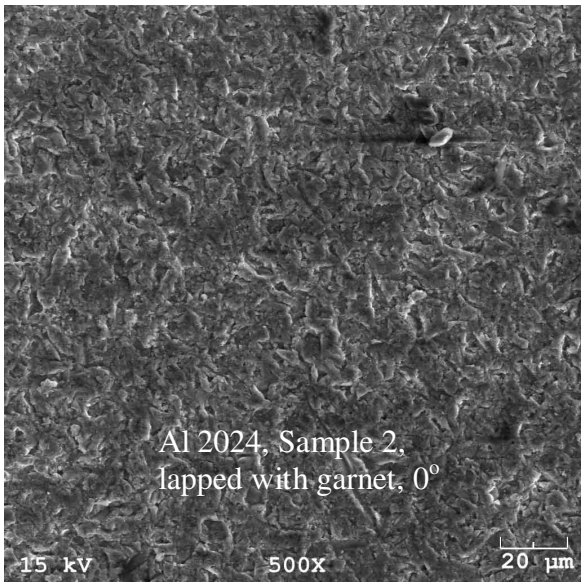

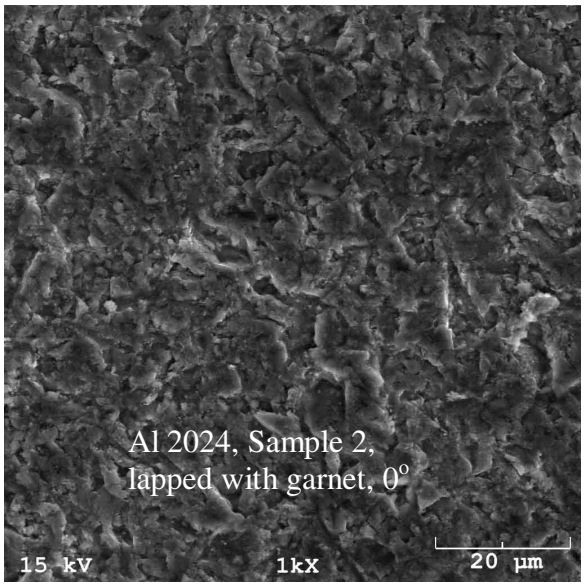

Al 2024, Sample 2, 500 Magnification Al 2024, Sample 2, 1000 Magnification

Figure 22b. SEM Micrographs of Al 2024 - Lapped with Garnet.

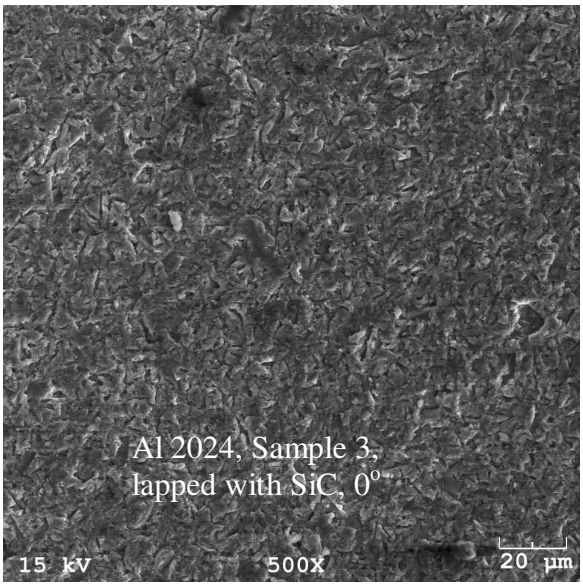

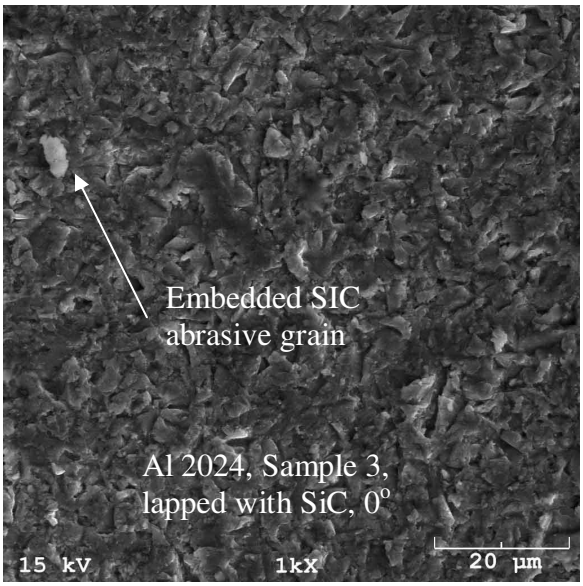

Al 2024, Sample 3, 500 Magnification Al 2024, Sample 3, 1000 Magnification

Figure 22c. SEM Micrographs of Al 2024 - Lapped with SiC.

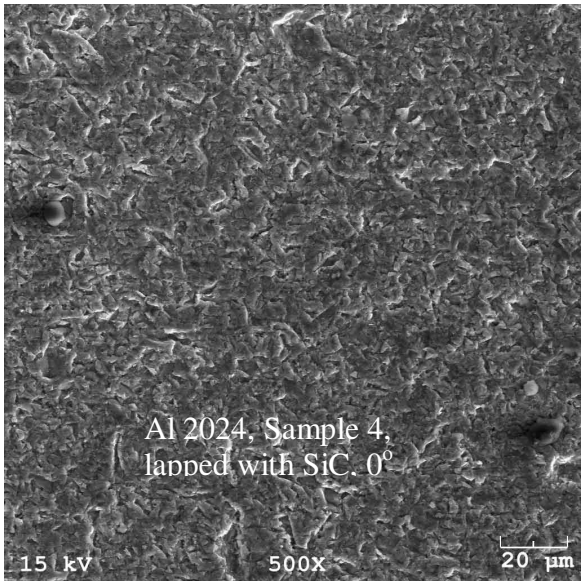

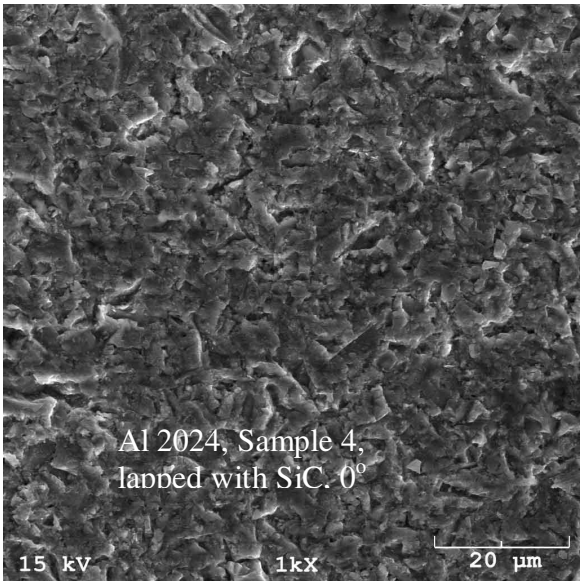

Al 2024, Sample 4, 500 Magnification Al 2024, Sample 4, 1000 Magnification

Figure 22d. SEM Micrographs of Al 2024 Lapped with SiC.

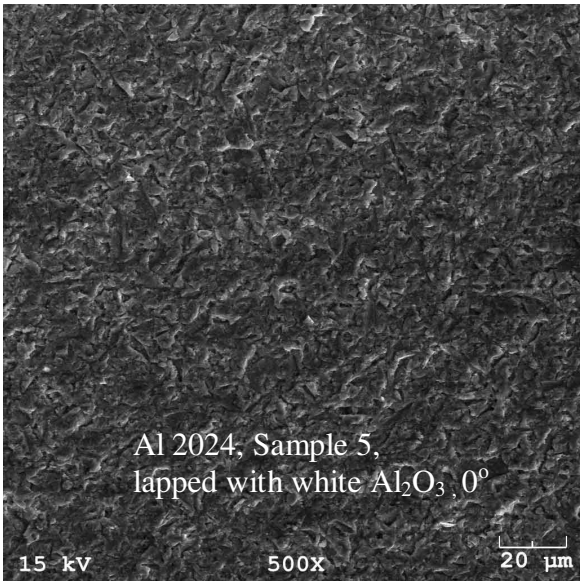

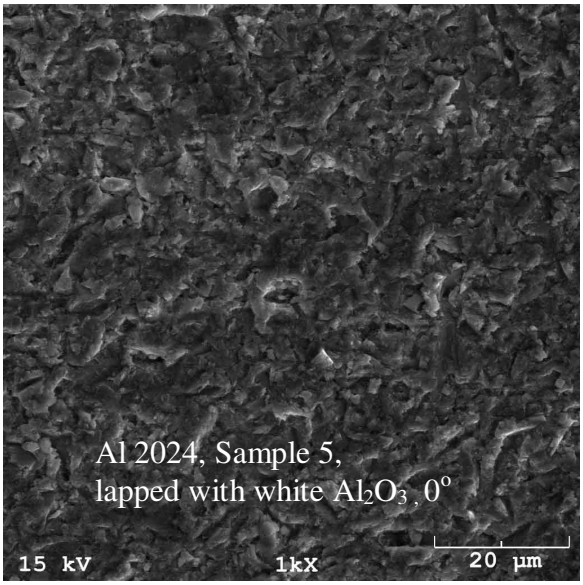

Al 2024, Sample 5, 500 Magnification Al 2024, Sample 5, 1000 Magnification

Figure 22e. SEM Micrographs of Al 2024 - Lapped with White Al_2O_3.

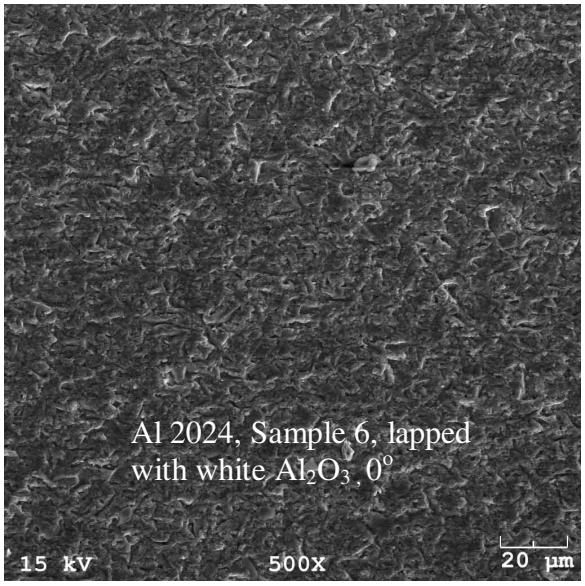

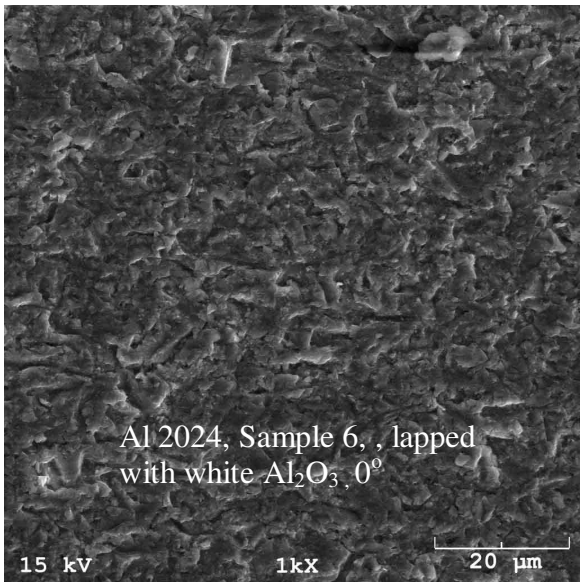

Al 2024, Sample 6, 500 Magnification Al 2024, Sample 6, 1000 Magnification

Figure 22f. SEM Micrographs of Al 2024 - Lapped with White Al_2O_3.

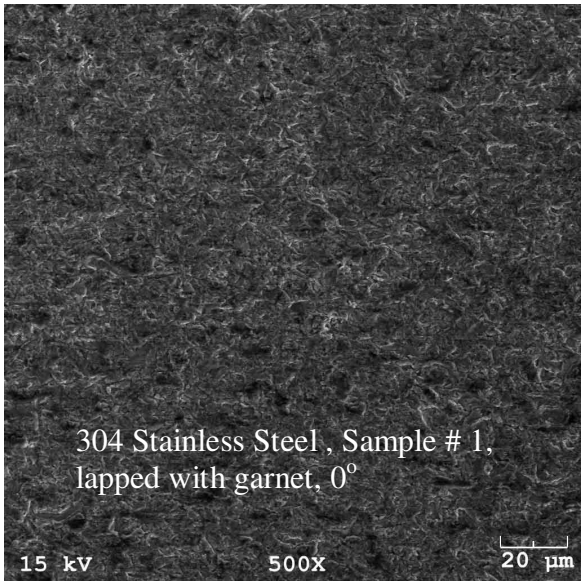

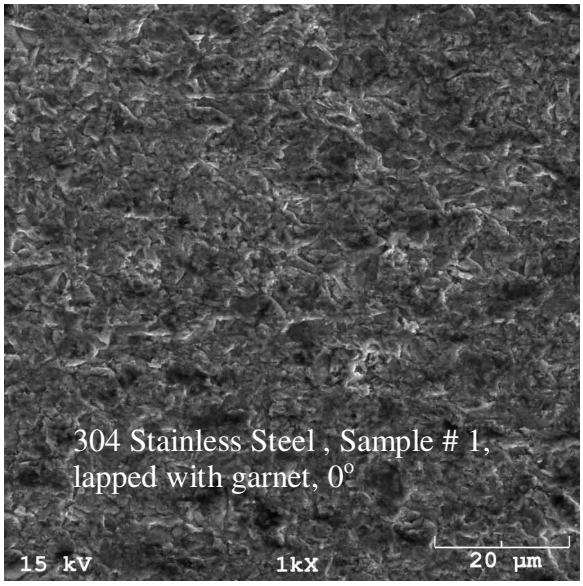

304 Stainless Steel, # 1, 500 Magnification 304 Stainless Steel, # 1, 1000 Magnification

Figure 23a. SEM Micrographs of 304 Stainless Steel - Lapped with Garnet.

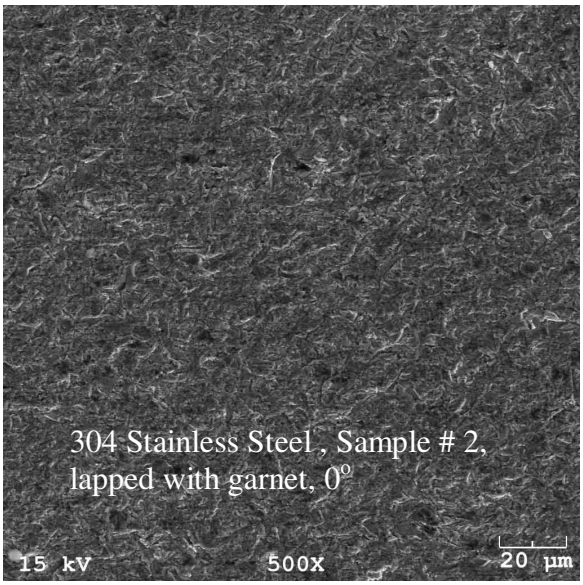

304 Stainless Steel, # 2, 500 Magnification

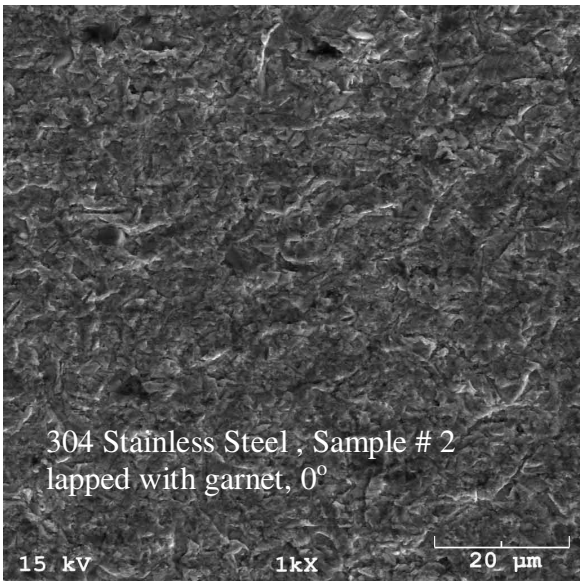

304 Stainless Steel, # 2, 1000 Magnification

Figure 23b. SEM Micrographs of 304 Stainless Steel - Lapped with Garnet.

304 Stainless Steel, # 3, 500 Magnification

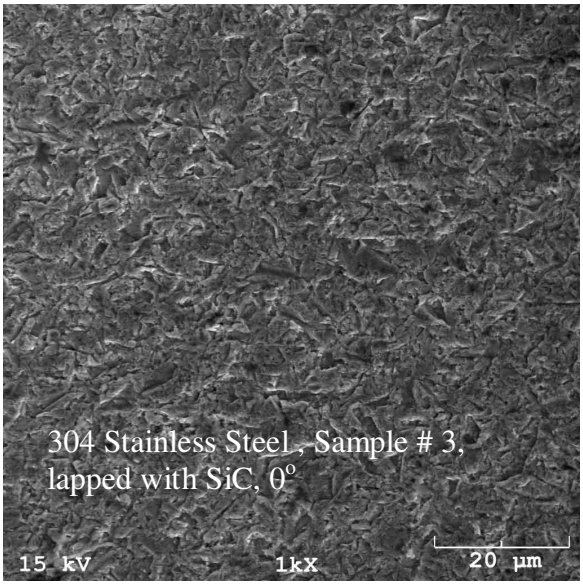

304 Stainless Steel, # 3, 1000 Magnification

Figure 23c. SEM Micrographs of 304 Stainless Steel - Lapped with SiC.

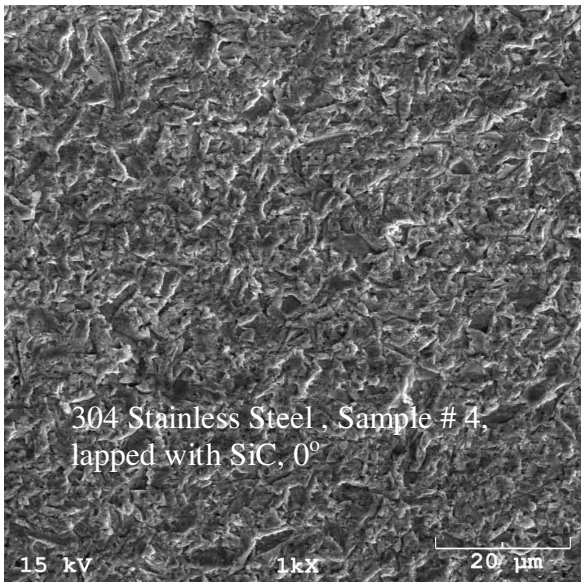

304 Stainless Steel, # 4, 500 Magnification 304 Stainless Steel, # 4 1000 Magnification

Figure 23d. SEM Micrographs of 304 Stainless Steel - Lapped with SiC.

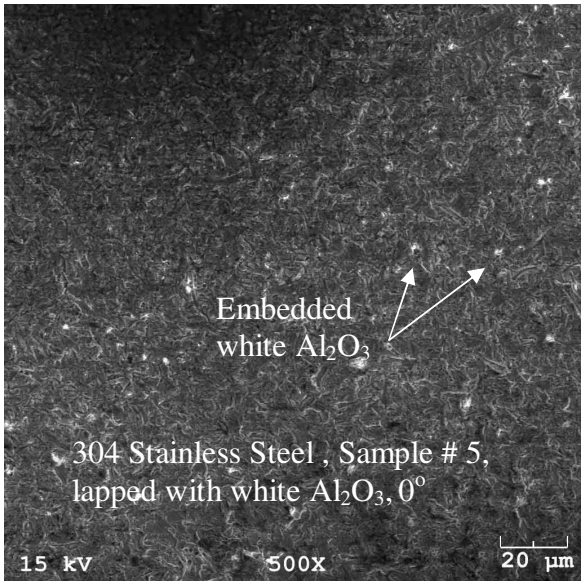

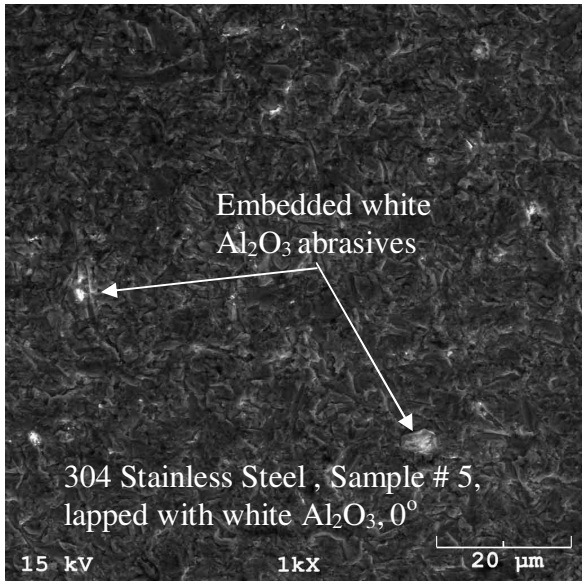

304 Stainless Steel, # 5, 500 Magnification 304 Stainless Steel, # 5, 1000 Magnification

Figure 23e. SEM Micrographs of 304 Stainless Steel - Lapped with White Al_2O_3.

Since 304 stainless steel and 1018 steel are metals (ductile materials), therefore the dominant mode of abrasive wear is plastic deformation as can be seen by the groove

and void found in Figures 28f and 29d, respectively. For ceramic materials, which are brittle, the dominant mode of abrasive wear is fracture or grain pull-out.

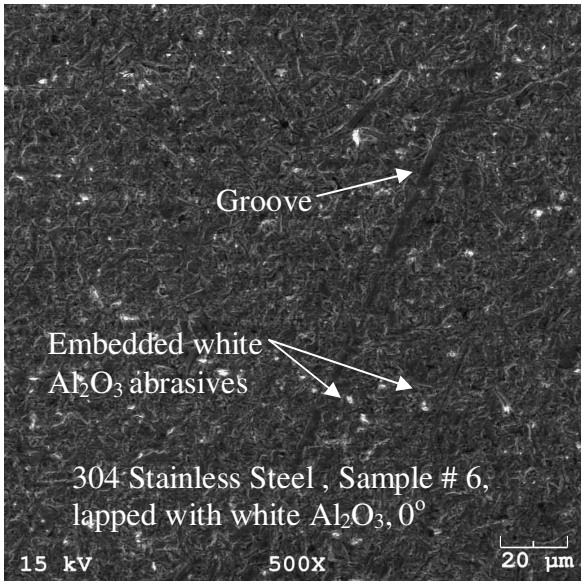

304 Stainless Steel, # 6, 500 Magnification

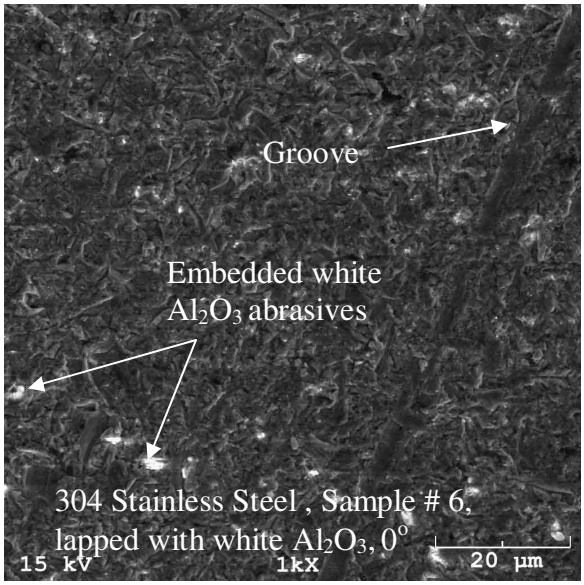

304 Stainless Steel, # 6, 1000 Magnification

Figure 23f. SEM Micrographs of 304 Stainless Steel - Lapped with White Al_2O_3.

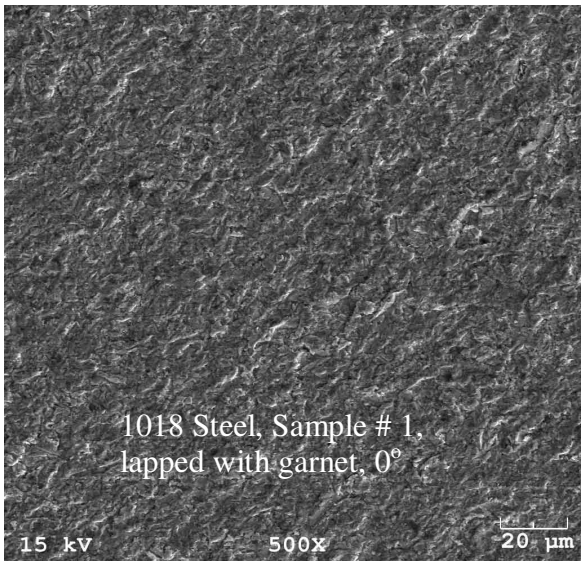

1018 Steel, Sample # 1, 500 Magnification

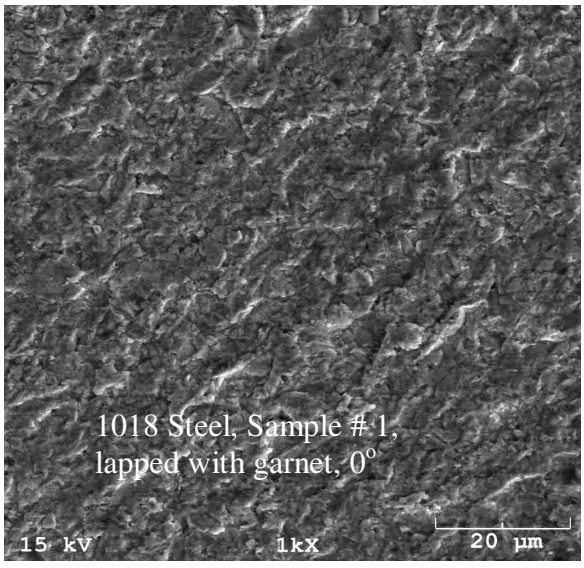

1018 Steel, Sample # 1, 1000 Magnification

Figure 24a. SEM Micrographs of 1018 Steel after Lapping with Garnet.

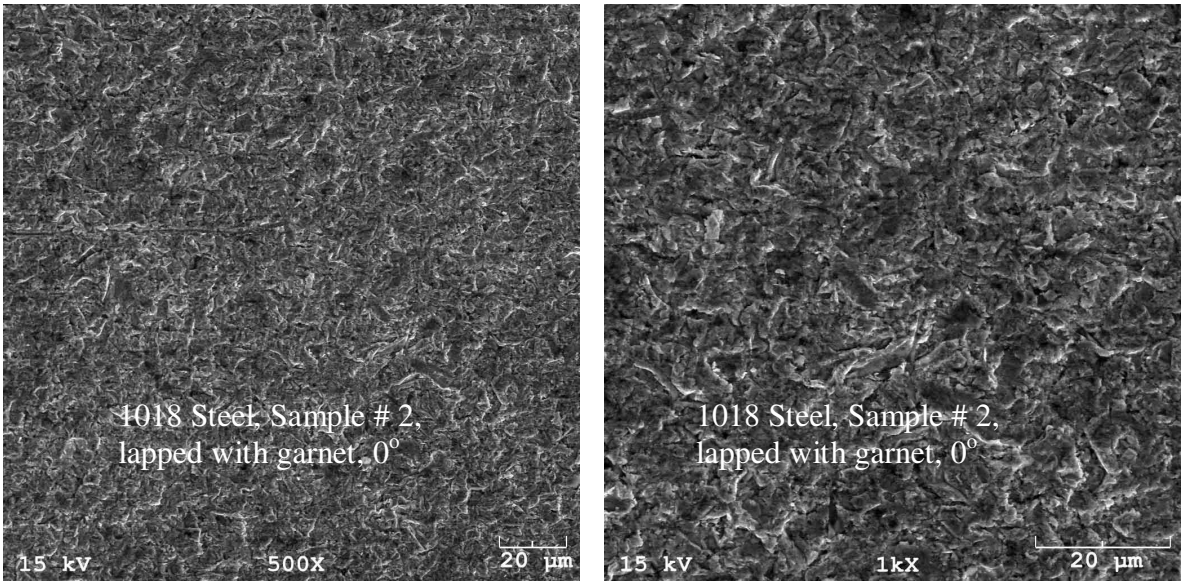

1018 Steel, Sample # 2, 500 Magnification 1018 Steel, Sample # 2, 1000 Magnification

Figure 24b. SEM Micrographs of 1018 Steel after Lapping with Garnet.

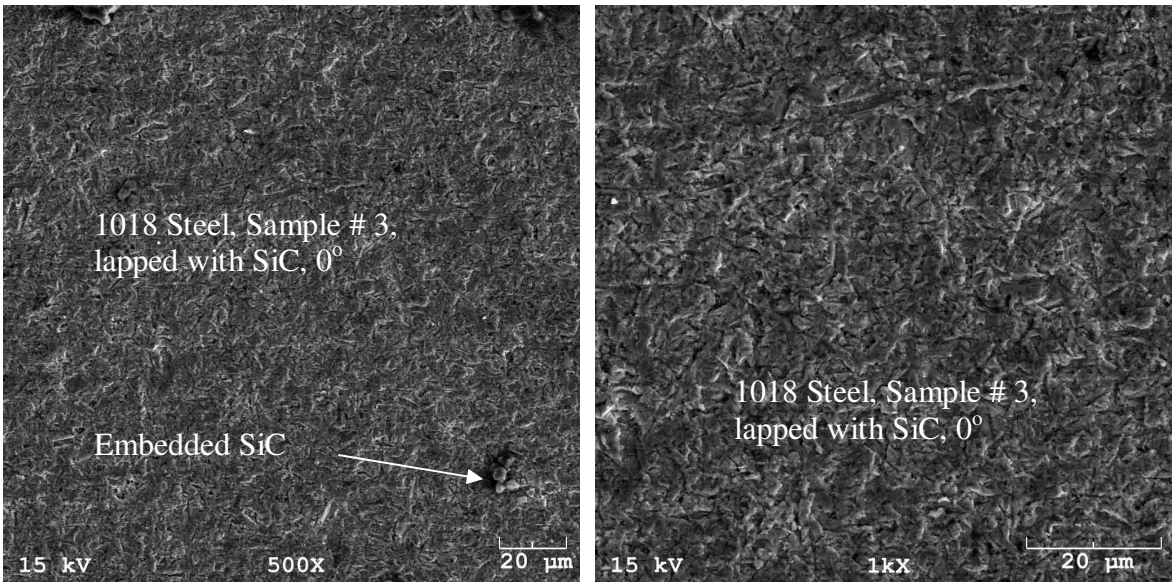

1018 Steel, Sample # 3, 500 Magnification 1018 Steel, Sample # 3, 1000 Magnification

Figure 24c. SEM Micrographs of 1018 Steel after Lapping with SiC.

Microvoid was observed in 1018 steel lapped with SiC as depicted in Figure 29d. The embedment and formation of microvoid were in agreement with earlier observations

made by Deshpande et al. (2008). In order to confirm the presence of microvoids, same location was scanned before and after lapping by making an indent on the specimens as shown in Appendix C. Although Deshpande et al. (2008) observed microvoids on some lapped samples; the same locations were not scanned before and after lapping, thereby leaving their origin unknown. Possible explanations for the formation of microvoids in the lapped samples include adhesive wear or fatigue wear mechanisms. Additionally, the microvoids observed by Deshpande et al. (2008) could also have been present on the sample prior to lapping.

These grooves and microvoids occurred as a result of two-body wear due to abrasion. More interestingly, neither microvoids nor grooves were observed in the samples lapped with garnet. This trend could have occurred because garnet is softer than SiC and white Al_2O_3 abrasives.

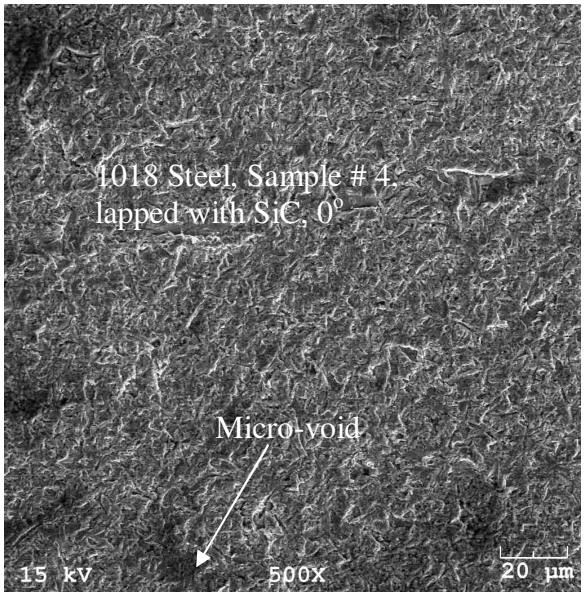

1018 Steel, Sample # 4, 500 Magnification

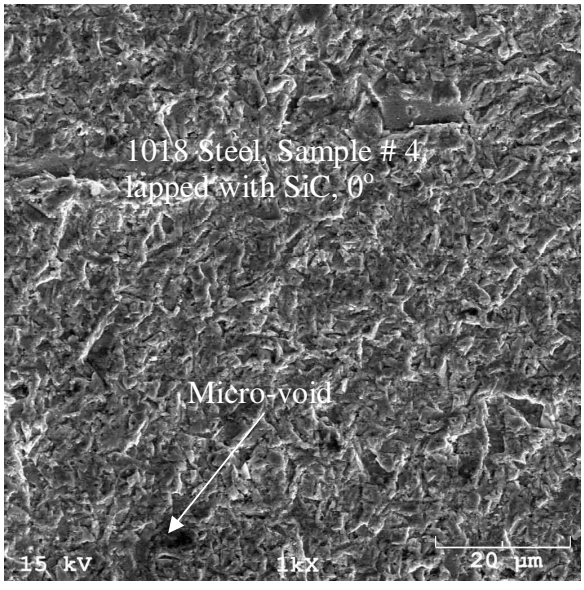

1018 Steel, Sample # 4, 1000 Magnification

Figure 24d. SEM Micrographs of 1018 Steel after Lapping with SiC.

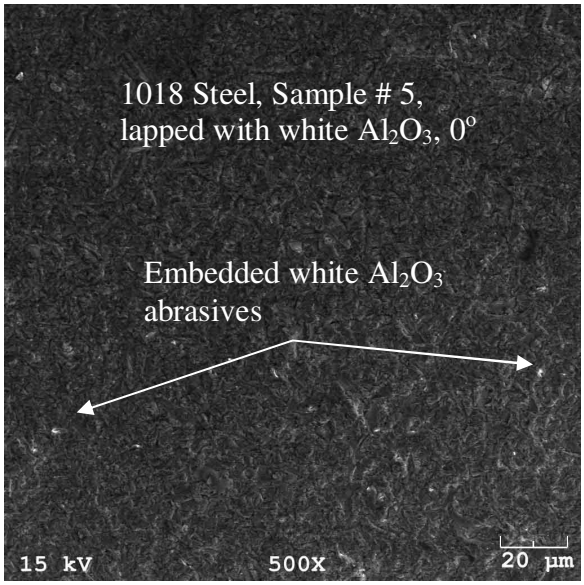

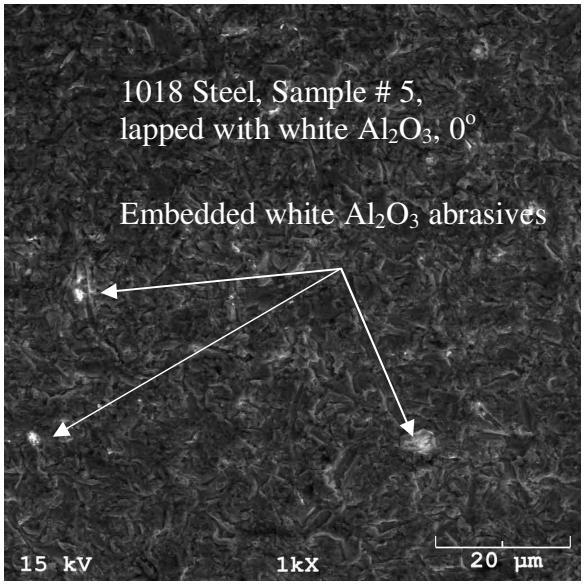

1018 Steel, Sample # 5, 500 Magnification 1018 Steel, Sample # 5, 1000 Magnification

Figure 24e. SEM Micrographs of 1018 Steel after Lapping with White Al_2O_3.

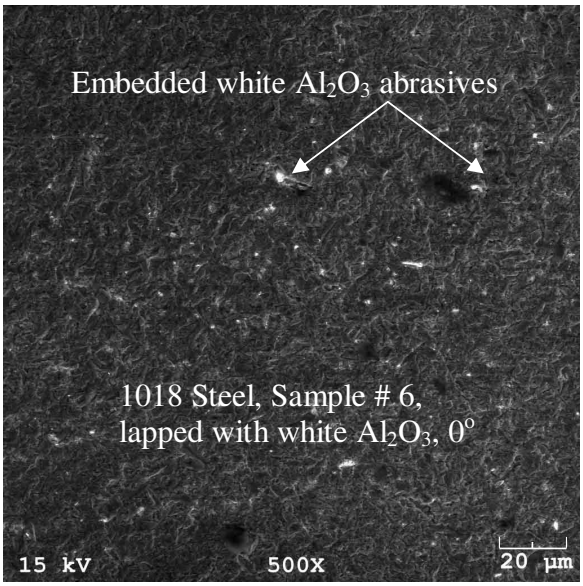

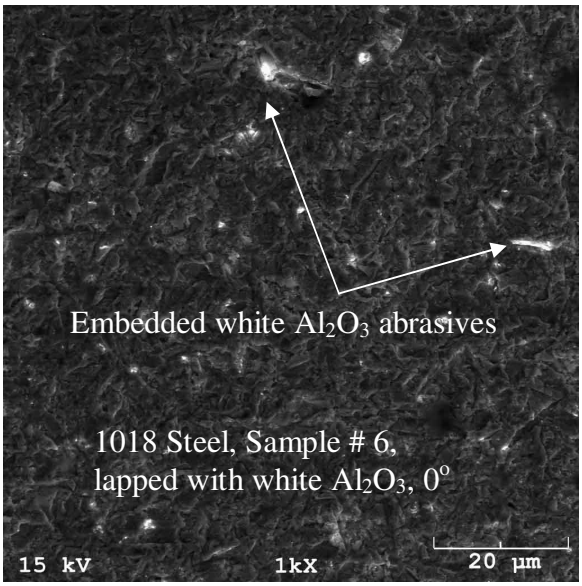

1018 Steel, Sample # 6, 500 Magnification 1018 Steel, Sample # 6, 1000 Magnification

Figure 24f. SEM Micrographs of 1018 Steel after Lapping with White Al_2O_3.

Although embedding of abrasives were observed in samples lapped with SiC and white Al_2O_3, an earlier work done in lapping of stainless steel and bronze by Deshpande (2005) did not show any embedding of Al_2O_3.

6.2 Reconstruction of 3-D Images

Scandium™ software was used to reconstruct 2-D SEM images into 3-D images. This was done by scanning each specimen at two angles (i.e., 0^o and 6^o) at a magnification of 1000x near an indent prior to lapping and after lapping as shown in Figures 25 to 30. Rockwell hardness tester was used to make an indent on the samples so that the same location was scanned before and after lapping. Three-dimensional images were constructed for Al 2024, 304 stainless steel, and 1018 steel prior and after lapping as depicted in Figures 31 through 36. Furthermore, Figures 45 through 47 in Chapter 7 illustrate anaglyph stereopair images that were reconstructed with the Scandium™ software.

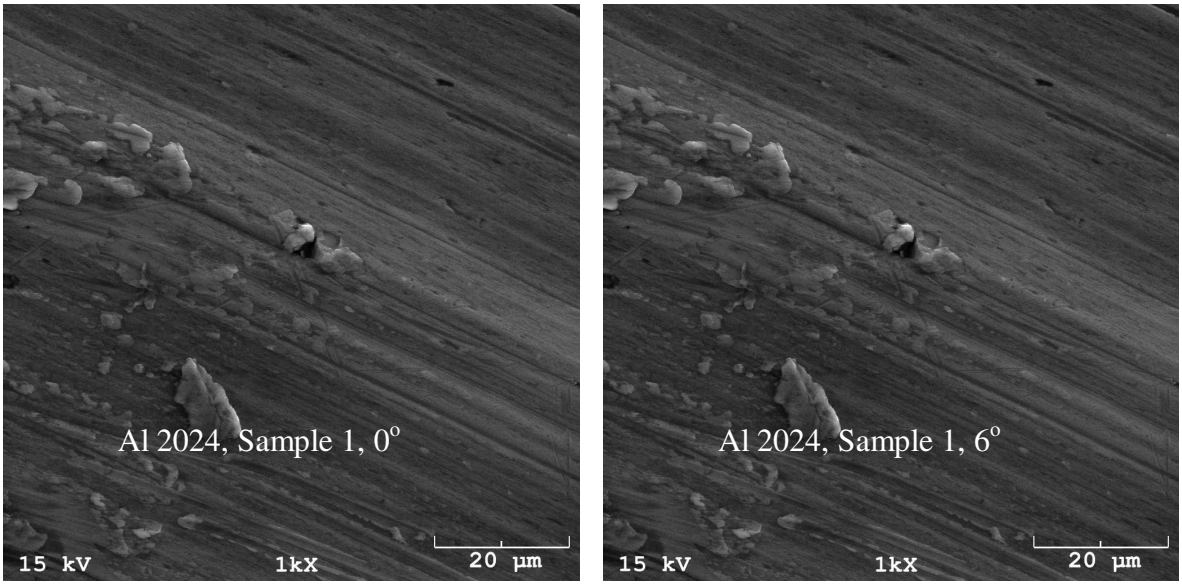

Figure 25. SEM Micrographs of Al 2024 at 0^o and 6^o prior to Lapping.

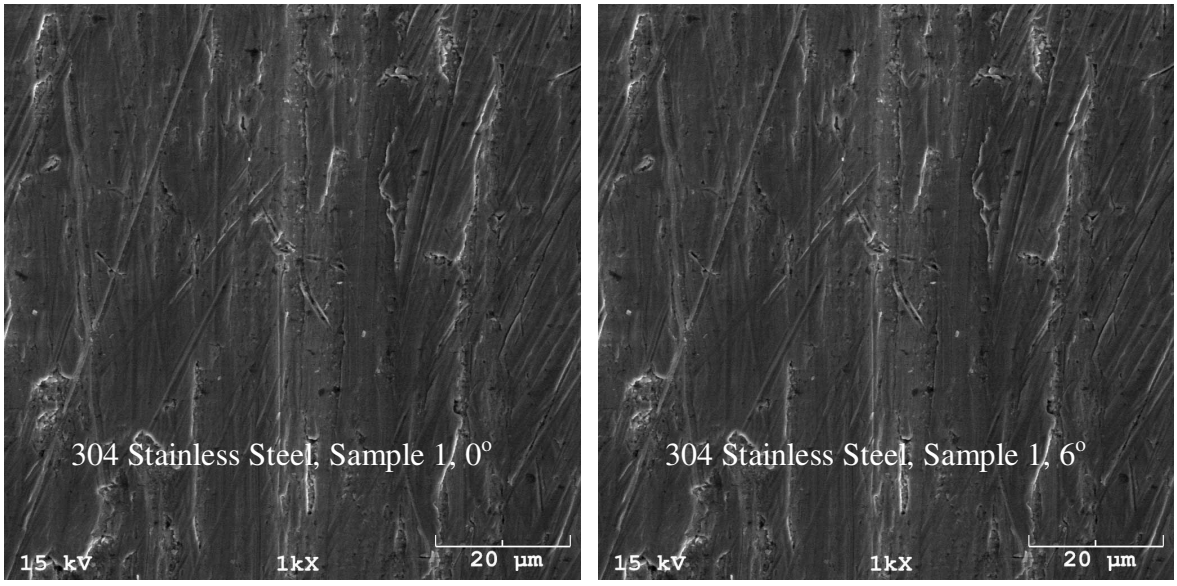

Figure 26. SEM Micrographs of 304 Stainless Steel at 0^{o} and 6^{o} prior to Lapping.

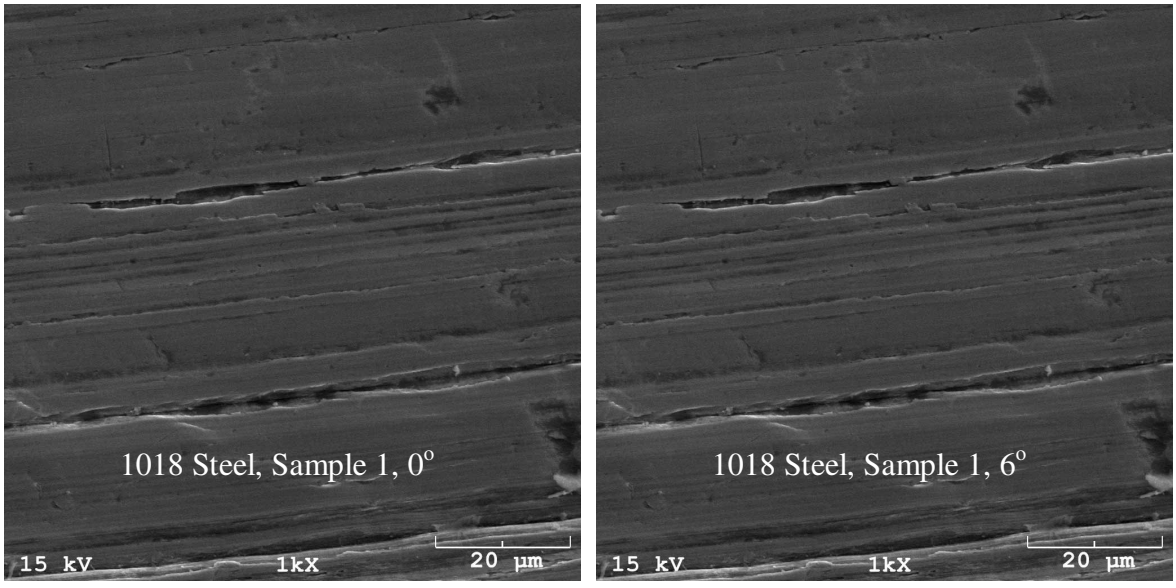

Figure 27. SEM Micrographs of 1018 Steel at 0^{o} and 6^{o} prior to Lapping.

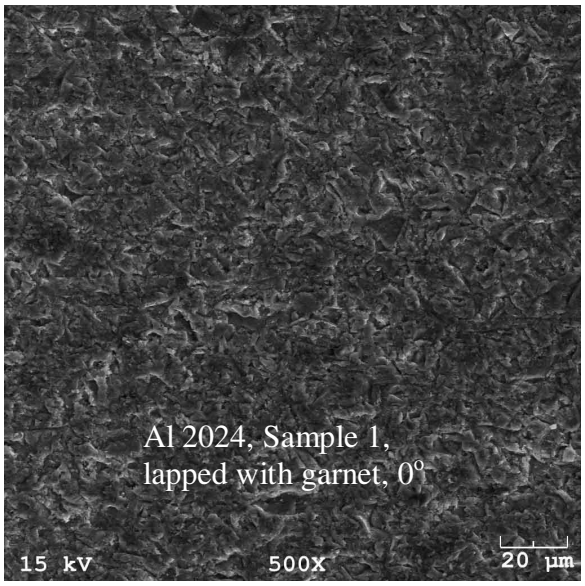

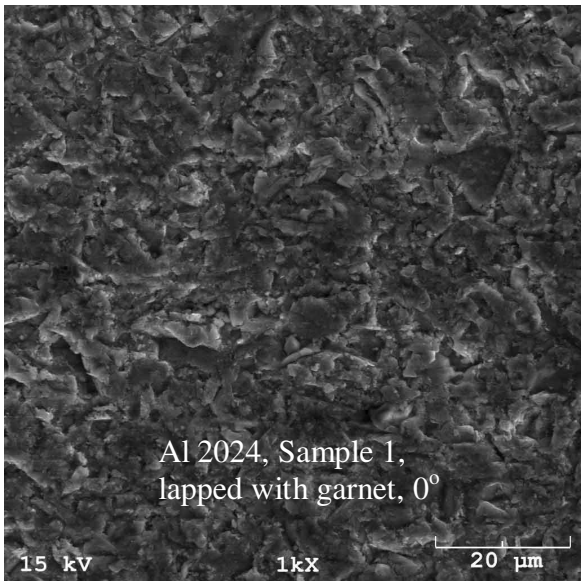

Al 2024, Sample 1, 500 Magnification Al 2024, Sample 1, 1000 Magnification

Figure 28. SEM Micrographs of Al 2024 at 0^o and 6^o - Lapped with Garnet.

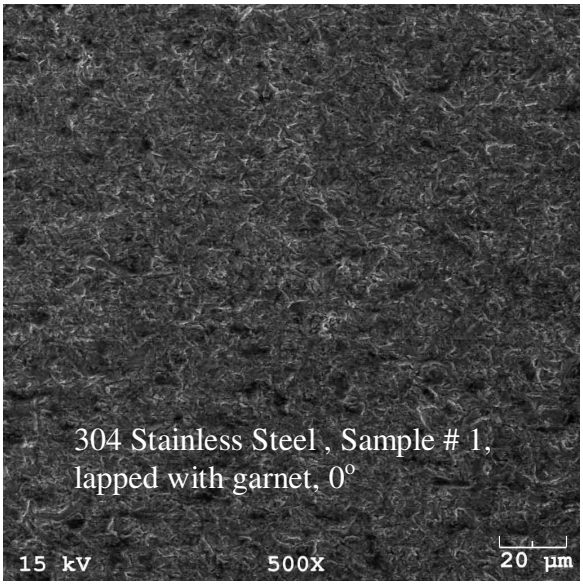

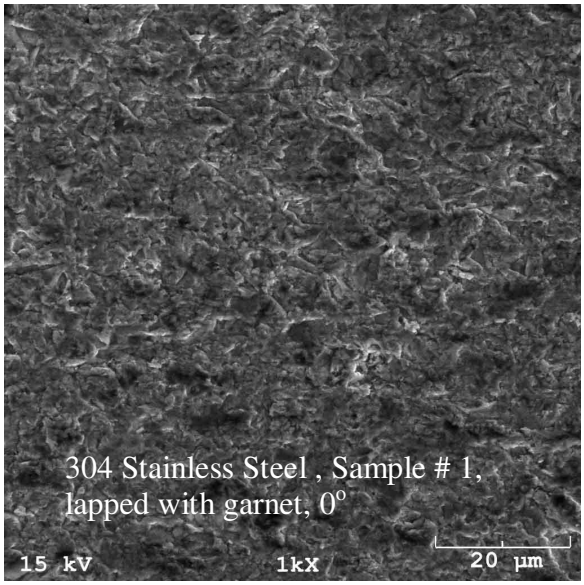

304 Stainless Steel, # 1, 500 Magnification 304 Stainless Steel, # 1, 1000 Magnification

Figure 29. SEM Micrographs of 304 Stainless Steel at 0^o and 6^o - Lapped with Garnet.

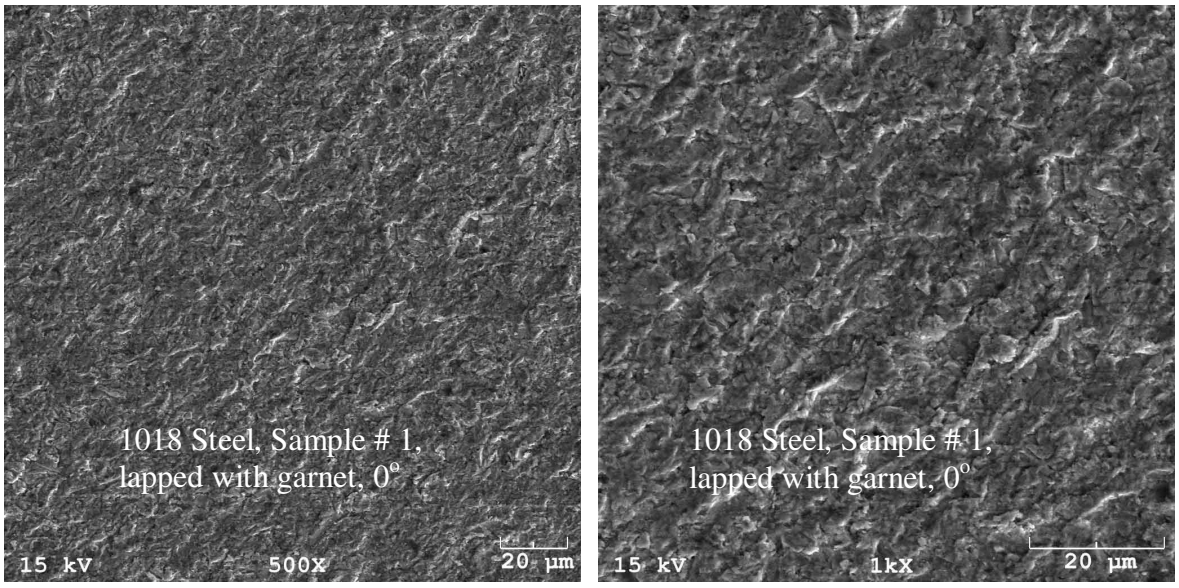

1018 Steel, Sample # 1, 500 Magnification 1018 Steel, Sample # 1, 1000 Magnification

Figure 30. SEM Micrographs of 1018 Steel at 0^o and 6^o - Lapped with Garnet.

The length, width, and height of the groove observed in 304 stainless, sample #6 shown in Figure 23f were measured using stereopairs images obtained from Scandium™ software. The length was found to be 94.4 µm, width 3.25 µm, and depth 1. 85 µm. White Al_2O_3 abrasives became embedded in 304 stainless steel and 1018 steel after lapping as illustrated with the 3-D image in Figures 35 and 36, respectively.

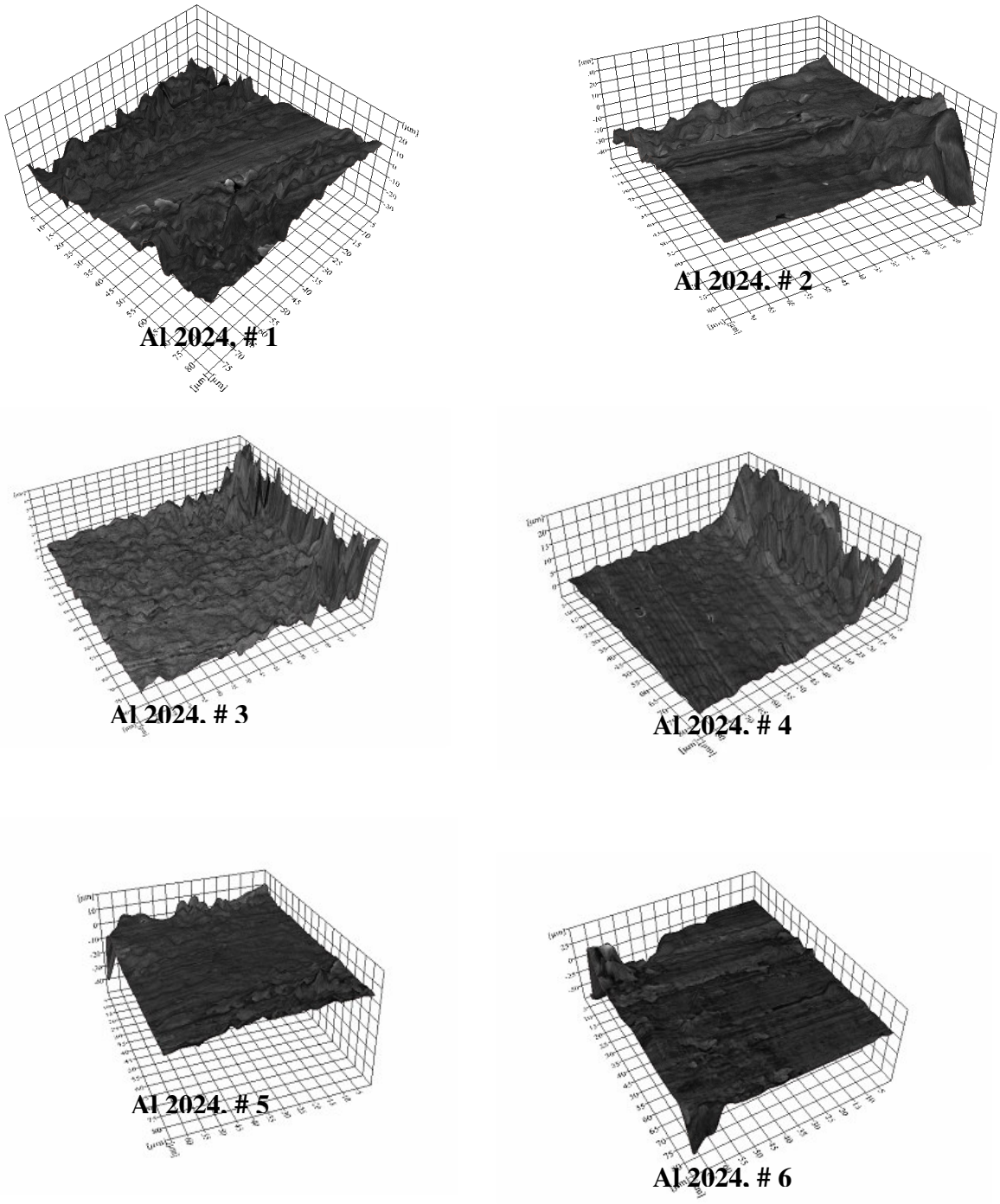

Figure 31. 3-D Images of Al 2024 before Lapping.

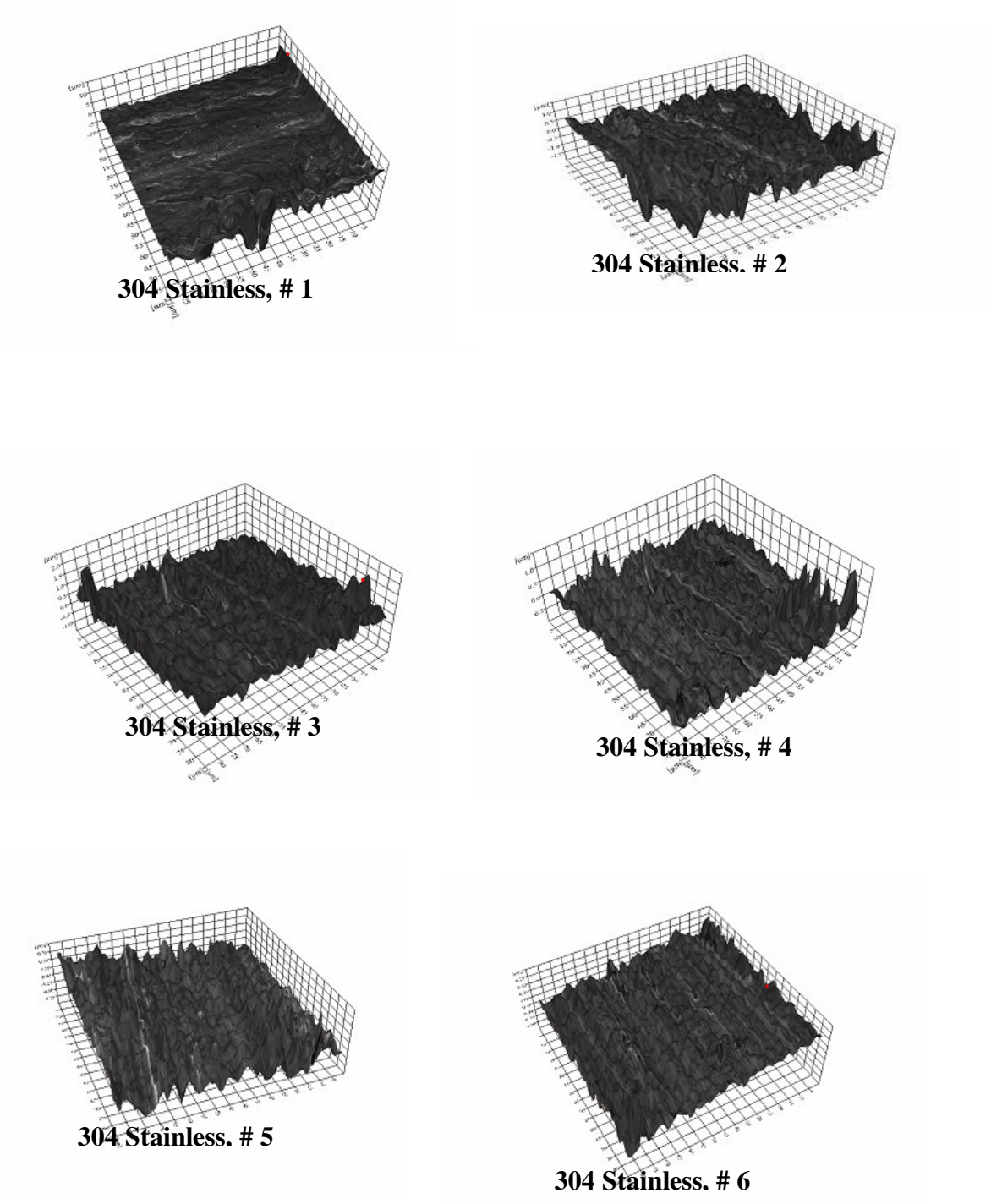

Figure 32. 3-D Images of 304 Stainless Steel before Lapping.

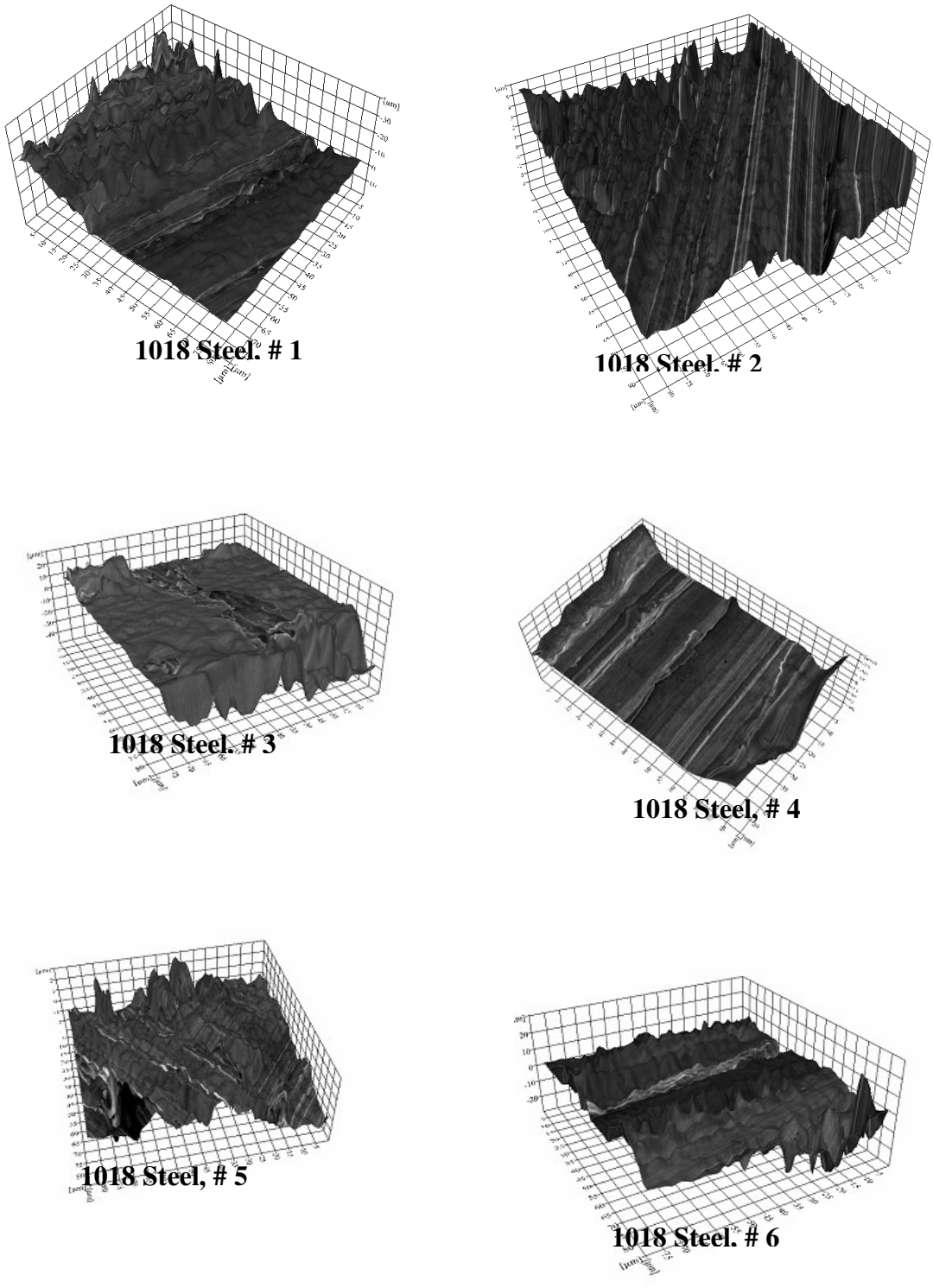

Figure 33. 3-D Images of 1018 Steel before Lapping.

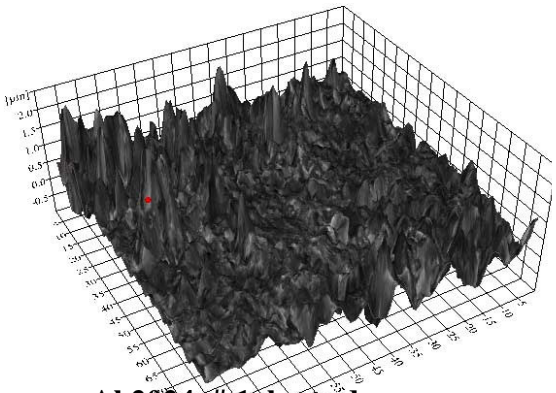

Al 2024, # 1, lapped with garnet

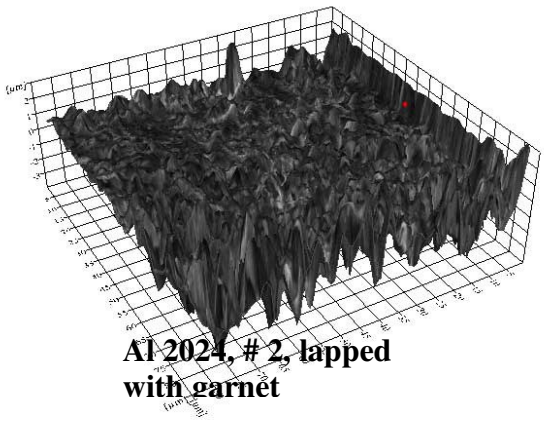

Al 2024, # 2, lapped with garnet

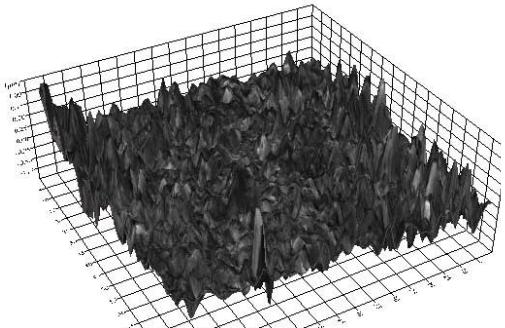

Al 2024, # 3, lapped with SiC

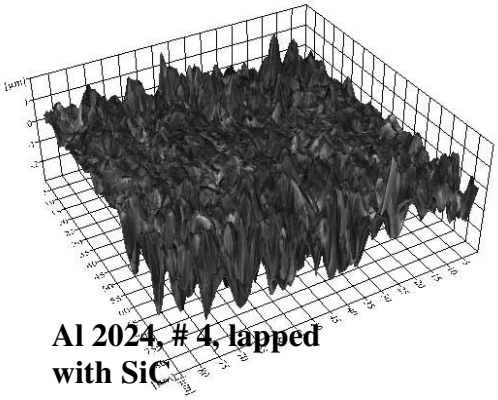

Al 2024, # 4, lapped with SiC

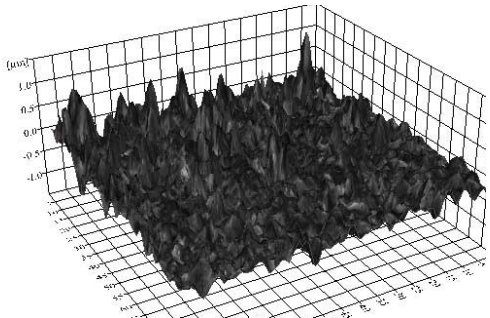

Al 2024, # 5, lapped with white Al_2O_3

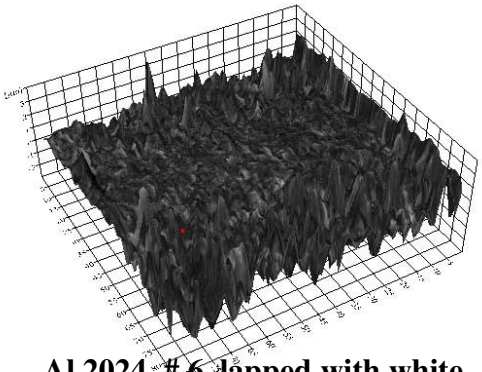

Al 2024, # 6, lapped with white Al_2O_3

Figure 34. 3-D Images of Al 2024 after Lapping.

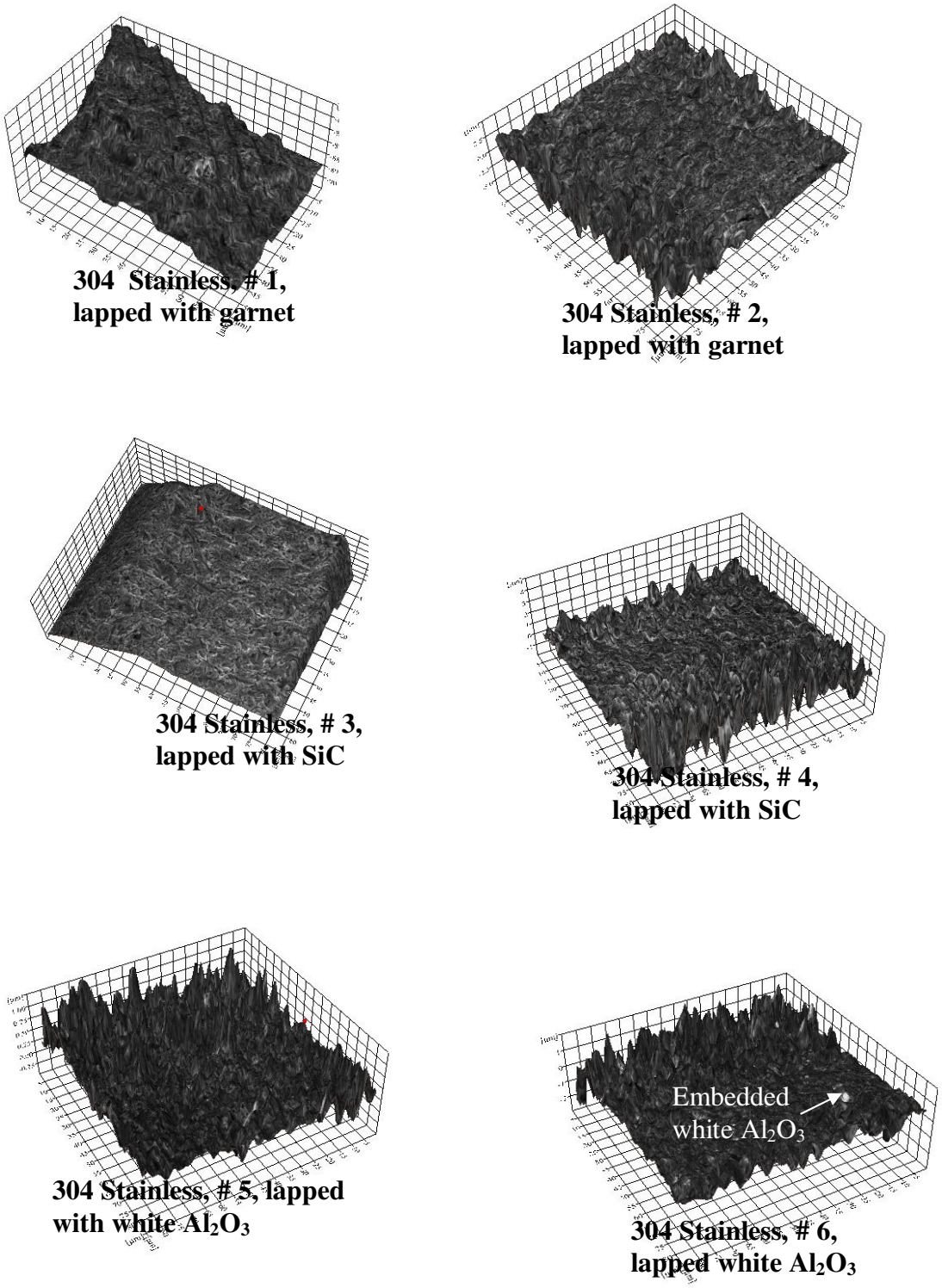

Figure 35. 3-D Images of 304 Stainless Steel after Lapping.

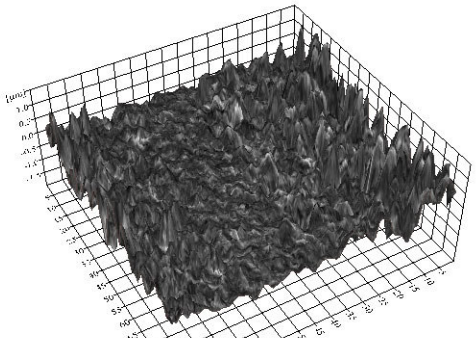

1018 Steel, # 1, lapped with garnet

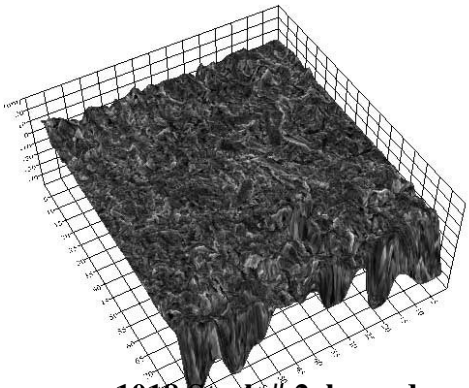

1018 Steel, # 2, lapped with garnet

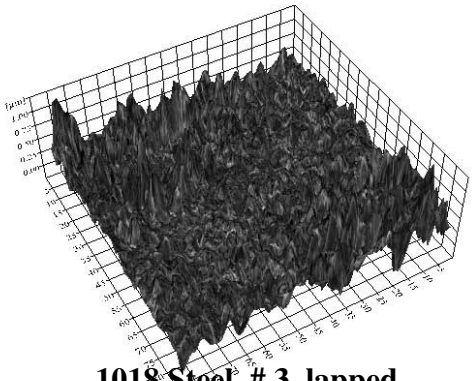

1018 Steel, # 3, lapped with SiC

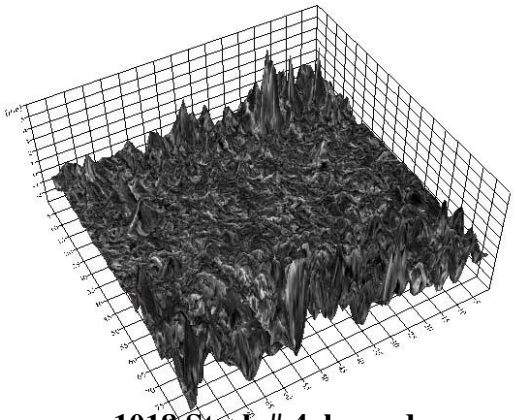

1018 Steel, # 4, lapped with SiC

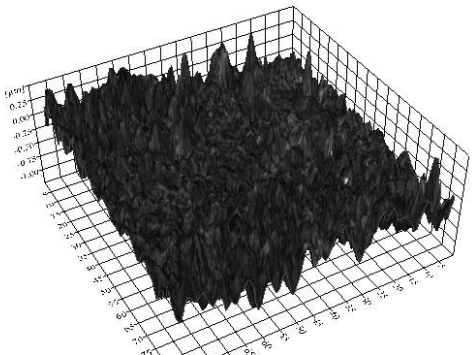

1018 Steel, # 5, lapped with white Al_2O_3

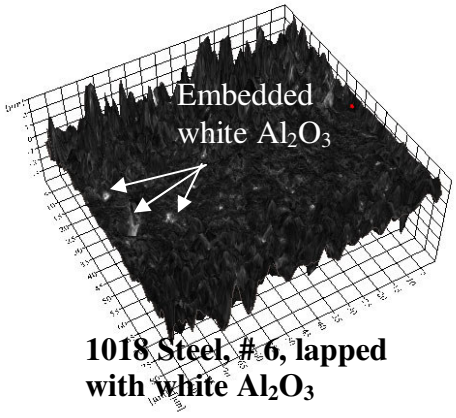

1018 Steel, # 6, lapped with white Al_2O_3

Figure 36. 3-D Images of 1018 Steel after Lapping.

6.3 MATLAB Image Processing

A program code (Appendix D) was used as a tool to obtain quality control metrics to identify lapped regions and scratched zones. There is no standard measure to determine the acceptable amount of surface defect during lapping. Therefore, this is a generic code, which can be used for lapping parameter comparison of different parts. The MATLAB image processing code was developed to determine lapped area, unfinished zone, scratched zone, and background. Although the purpose of lapping is to improve the surface finish, some of the lapped products do not meet specifications due to burn, unfinished parts (incomplete lapping), scratches, friction, and wear. This code helped to identify what portion of the wafer had met required specifications. As would be expected for a complete lapped sample, there were no unfinished or scratched zones.

The entire diameter of the wafer (50.8 mm) was scanned and saved in a bitmap format. Adobe Photoshop CS3 was used to determine the digital gray scales of the images (642 x 661 pixels). Subsequently, the MATLAB™ R2007a code which calculated the area of lapped zones, scratched zones, unfinished zones, and background. As an example, a summary of results for 304 stainless steel (specimen # 4) lapped with SiC is presented in Table 11. Scratched zones were attributed to regions of high friction, possibly due to sliding, sticking, or rolling friction. Also, the scratchy surface might have occurred in areas with low supply of abrasive slurry or due to hardness of abrasives. Figure 37 illustrates a more scratched surface, the result of using SiC, a fairly hard abrasive. Scratches and unfinished lapped parts were observed primarily in stainless steel as shown in Figure 37. Conversely, there were little or no scratches found on lapped Al 2024 and 1018 steel as illustrated in Figures 38 and 39, respectively. The two white lines

on the specimen in Figure 37 indicated the number of pixels of scratched zone, while the white area on the center of the wafer showed the unfinished zone. The small white dots on the lower end of the specimens in Figures 38 and 39 are the indentations created on the samples before lapping in order to scan the same location with the SEM after lapping.

Table 11. **Area of 304 Stainless Lapped with SiC**.

Zones	Pixels	Area (mm^2)
Scratched	2012	14.8
Lapped	252668	1863.9
Unfinished	20115	148.4
Background	149567	1103.3
Total Contact Area	254680	1878.7
Total Area	274795	2027.1
Image Area	424362	3130.4

Total Contact Area = Scratched + Lapped

Total Area = Scratched + Lapped + Unfinished

Image Area = Scratched + Lapped + Unfinished + Background

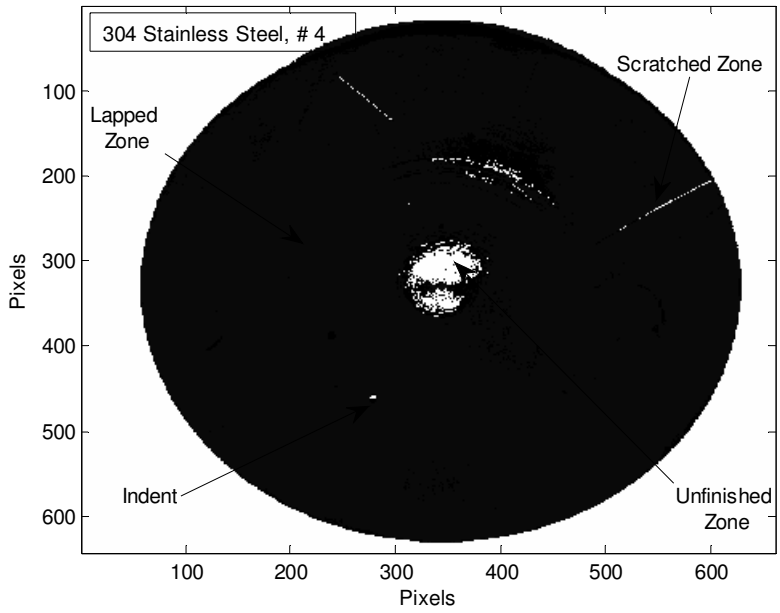

Figure 37. Graph from MATLAB Showing 304 Stainless Steel Lapped with SiC

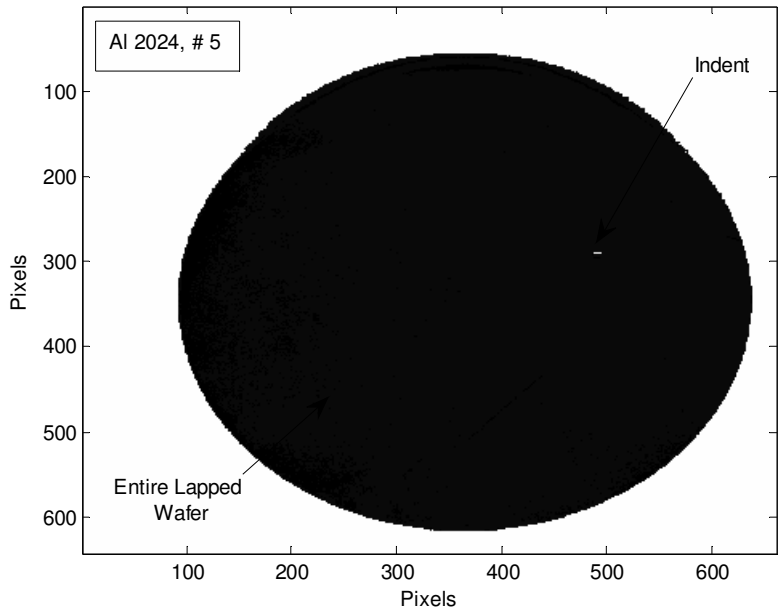

Figure 38. Graph from MATLAB Showing Al 2024 Lapped with Al_2O_3.

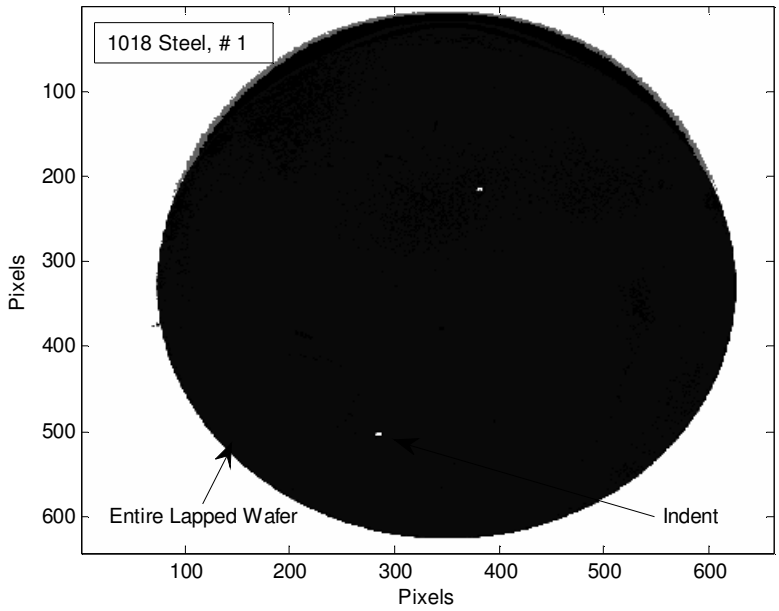

Figure 39. Graph from MATLAB Showing 1018 Steel Lapped with Garnet.

CHAPTER 7

RESULTS and ANALYSIS

Section 7.1 presents the results obtained on material removal rate and surface roughness. Section 7.2 discusses statistical analysis. Section 7.3 provides the assumptions made in the friction and lapping models. Section 7.4 describes different models that can be used to determine friction, while section 7.5 estimates the power consumption during a lapping operation. 7.6 presents finite element analysis, and section 7.7 introduces an application of redox chemistry in lapping.

7.1 Analysis of Results

The material removal rate is calculated using Equation (28). It is more accurate to measure the amount of material removed per unit time (MRR) in g/minute than inch/minute using a Coordinate Measuring Machine (CMM). This is because the CMM measures the material removal based on average values of peaks and valleys for a concave or convex part, whereas measuring the initial and final weight of the specimen with a scale gave the entire weight of the sample.

$$MRR = \frac{\Delta W}{\Delta T} = \frac{W_1 - W_2}{T_2 - T_1} \text{ or } \frac{\Delta H}{\Delta T} = \frac{H_1 - H_2}{T_2 - T_1}, \tag{28}$$

where

W_1: initial weight of sample

W_2: final weight of sample

T_1 : time at onset of lapping

T_2 : time at the end of lapping

H_1 : initial thickness of sample

H_2 : final thickness of sample.

Material removal rate (MRR) = f(abrasive grain size, lapping pressure, lapping speed, lapping time, and type of workpiece). The MRR is reported in g/minute if weight is used and in inch/minute when height is measured.

7.1.1 Initial Lapping

Larger abrasive grains (23 μm or 400 grit size) garnet, silicon carbide and white aluminum oxide were used to lap aluminum 2024, 304 stainless steel, and 1018 steel specimens in order to remove larger stocks of material before the finishing operation (i.e., final lapping process). The material removal rate for initial lapping of Al 2024, 304 stainless steel, and 1018 steel are shown in Tables 12 to 14, while the initial roughness average values are presented in Tables 15 through 17.

As shown in Table 12, material removal rates (MRR) obtained for Al 2024 (0.017 gram/min and 0.00017 inch/min) were highest for aluminum lapped with SiC (for twenty minutes test). The lowest result was obtained with aluminum lapped with garnet (0.008 g/min and 0.00006 in/min). This was due to the fact that SiC was the hardest among the three abrasives used, and hence SiC removed more material per minute. Similarly, the results obtained for 304 stainless steel in Table 13 showed that SiC removed the maximum amount of material per minute (0.009 g/min and 0.00014 in/min), followed by white Al_2O_3 (0.010 g/min and 0.00009 in/min), and lastly by garnet (0.006 g/min and 0.00005 inch).

Table 12. Material Removal Rate of Al 2024 Using 23µm Abrasive.

Sample #	23 µm	Initial wt. (g)	Final wt. (g)	MRR g/min	Initial Thk. (inch)	Final Thk. (inch)	MRR inch/min
Al-1	Garnet	18.010	17.748	0.013	0.12590	0.12440	0.00008
Al-2	Garnet	18.153	17.986	0.008	0.12780	0.12655	0.00006
Al-3	SiC	18.025	17.781	0.012	0.12600	0.12480	0.00006
Al-4	SiC	18.037	17.705	0.017	0.12469	0.12125	0.00017
Al-5	White Al_2O_3	18.299	18.051	0.012	0.12757	0.12600	0.00008
Al-6	White Al_2O_3	18.064	17.813	0.013	0.12650	0.12466	0.00009

Al: Aluminum specimen

Table 13. Material Removal Rate of 304 Stainless Steel Using 23 µm Abrasive.

Sample #	23 µm	Initial wt. (g)	Final wt. (g)	MRR g/min	Initial Thk. (inch)	Final Thk. (inch)	MRR inch/min
SS-1	Garnet	52.399	52.277	0.006	0.12469	0.12369	0.00005
SS-2	Garnet	52.335	52.194	0.007	0.12500	0.12380	0.00006
SS-3	SiC	52.411	52.247	0.008	0.12509	0.12230	0.00014
SS-4	SiC	51.934	51.758	0.009	0.12550	0.12280	0.00014
SS-5	White Al_2O_3	53.487	53.271	0.011	0.12758	0.12637	0.00006
SS-6	White Al_2O_3	51.964	51.772	0.010	0.12610	0.12435	0.00009

SS: stainless steel specimen

For the case of 1018 steel, the results obtained in Table 14 show a similar trend to those with of Al 2024 and 304 stainless steel. Table 14 indicated that the most material was removed in 1018 steel by SiC (0.014g/min and 0.00006 in/min), followed by white Al_2O_3 (0.016 g/min and 0.00004 in/min), and garnet (0.010 and 0.00004 in/min). As can be seen in Tables 12 and 14, the highest amount of material was removed from Al 2024,

followed by 304 stainless and 1018 steel. This trend was obtained because Al 2024 was the softest among the three metals used in the experiment; hence it was easier to remove material from aluminum than the other metals.

Table 14. Material Removal Rate of 1018 Steel Using 23 µm Abrasive.

Sample #	23 µm	Initial wt. (g)	Final wt. (g)	MRR g/min	Initial Thk. (inch)	Final Thk. (inch)	MRR inch/min
S-1	Garnet	52.686	52.490	0.010	0.12739	0.12660	0.00004
S-2	Garnet	52.739	52.543	0.010	0.12746	0.12670	0.00004
S-3	SiC	52.654	52.372	0.014	0.12760	0.12638	0.00006
S-4	SiC	52.656	52.421	0.012	0.12730	0.12639	0.00005
S-5	White Al_2O_3	52.596	52.271	0.016	0.12719	0.12640	0.00004
S-6	White Al_2O_3	52.721	52.471	0.012	0.12740	0.12668	0.00004

S: steel specimen

A surface profilometer was used to measure and record the surface roughness profile as depicted in Figure 14 in Chapter 4. The roughness values (R_a) obtained from initial lapping of aluminum 2024, 304 stainless, and 1018 steel are presented in Tables 15, 16, and 17, respectively. The calculation of average roughness was determined by scanning five different locations for each sample as shown in Appendix E. Mitutoyo surftest 211 profilometer and line profiles from SEM images, which were reconstructed with Scandium 3-D software were used to determine the R_a values. Scandium is a universal SEM imaging platform. Generally, the R_a values obtained from the SEM were less than those obtained with the profilometer. This was attributed to the fact that the profilometer procedure was a direct contact method and was therefore, more accurate than the SEM.

The SEM profiles were obtained by reconstructing two non-contact images at two angles (i.e., zero degrees and six degrees), hence yielded less Ra values than the profilometer. The stereopairs and line profiles obtained from SEM is about 70% accurate, however, the line from profilometer is more accurate (90%) because it is a direct contact measurement of the surface profile. The percentage roughness improvement is determined using Equation (29), and the results are summarized in Tables 15 to 17. R_a values were calculated using Equation (2) in Chapter 2.

$$Percentage\ R_a\ \text{Improvement} = \frac{(\text{Average initial } R_a - Average\ \text{final } R_a) * 100}{\text{Average initial } R_a} \tag{29}$$

Table 15. Roughness Values of Al 2024 Using 23 µm Abrasive.

Sample Number	Abrasive Grain size of 23 µm or 400 Grit	Initial Average Roughness (µm)	Final Average Roughness (µm)	% Roughness Improvement
Al-1	Garnet	0.97	0.30	69
Al-2	Garnet	0.94	0.30	68
Al-3	SiC	0.91	0.17	81
Al-4	SiC	0.95	0.17	82
Al-5	White Al_2O_3	0.99	0.12	87
Al-6	White Al_2O_3	0.97	0.11	88

As can be seen in Table 15, the highest percentage improvement (88.66%) in surface finish was found in Al 2024 lapped with white Al_2O_3, while the lowest improvement (68.09%) was found in Al 2024 lapped with garnet. Garnet being softer than SiC and white Al_2O_3 had the least improvement for surface finish. Al 2024 had the best surface finish when compared with 304 stainless and 1018 steel. This result was attributed to the softness of aluminum.

Table 16. Roughness Values of 304 Stainless Steel Using 23 µm Abrasive.

Sample Number	Abrasive Grain size of 23 µm or 400 Grit	Initial Average Roughness (µm)	Final Average Roughness (µm)	% Roughness Improvement
SS-1	Garnet	0.44	0.19	56
SS -2	Garnet	0.94	0.17	81
SS -3	SiC	0.79	0.11	86
SS -4	SiC	0.43	0.14	67
SS -5	White Al_2O_3	0.78	0.21	73
SS -6	White Al_2O_3	0.73	0.30	58

For the case of 304 stainless steel, the highest improvement of 86.08% was obtained with 304 stainless steel lapped with SiC abrasive and the lowest improvement of 56.82% was found with garnet.

It can be seen in Tables 16 that stainless steel has lower average roughness values (R_a). This implies that stainless was smoother before lapping began. Figure 45 and 46 delineate the graphs of MRR vs. hardness of abrasives, while Figure 47 illustrates the plots of average roughness vs. hardness of abrasive particles.

Table 17. Roughness Values of 1018 Steel Using 23 µm Abrasive.

Sample Number	Abrasive Grain size of 23 µm or 400 Grit	Initial Average Roughness (µm)	Final Average Roughness (µm)	% Roughness Improvement
S-1	Garnet	0.76	0.24	68
S-2	Garnet	0.86	0.29	66
S-3	SiC	1.05	0.50	52
S-4	SiC	0.67	0.27	59
S-5	White Al_2O_3	0.90	0.39	56
S-6	White Al_2O_3	0.90	0.25	72

Again, the result presented in Table 21 showed that 1018 steel lapped with white Al_2O_3 abrasive had the surface finish improvement of 72.22%, while SiC abrasive had the lowest surface finish improvement of 52.38%.

7.1.2 Final Lapping

In finish or final lapping, smaller abrasive grains (8 µm or 600 grit size) of garnet, silicon carbide, and white aluminum oxide were used in lapping of aluminum 2024, 304 stainless steel, and 1018 steel samples to improve the final surface finish of the work materials. Aluminum 2024 lapped with SiC yielded the highest MRR, 1018 steel lapped with garnet had the lowest MRR as illustrated in Tables 22 through 24. This is due to the fact that Al 2024 is softer than 304 stainless and 1018 steel. Furthermore, Figures 40 and 41 showed that SiC, being harder than garnet and white Al_2O_3, removed more material per minute. Figure 43 depicts roughness values vs. hardness of abrasives.

Table 18. Material Removal Rate of Al 2024 Using 8 µm Abrasive.

Sample #	8 µm	Initial wt. (g)	Final wt. (g)	MRR g/min	Initial Thk. (inch)	Final Thk. (inch)	MRR inch/min
Al-1	Garnet	17.748	17.642	0.005	0.12440	0.12329	0.00006
Al-2	Garnet	17.986	17.852	0.007	0.12655	0.12560	0.00005
Al-3	SiC	17.781	17.646	0.007	0.12480	0.12385	0.00005
Al-4	SiC	17.705	17.497	0.010	0.12125	0.11945	0.00009
Al-5	White Al_2O_3	18.051	17.901	0.007	0.12600	0.12500	0.00005
Al-6	White Al_2O_3	17.813	17.635	0.009	0.12466	0.12400	0.00003

Table 19. Material Removal Rate of 304 Stainless Steel Using 8 µm Abrasive.

Sample #	8 µm	Initial wt. (g)	Final wt. (g)	MRR g/min	Initial Thk. (inch)	Final Thk. (inch)	MRR inch/min
SS-1	Garnet	52.277	52.180	0.005	0.12369	0.12310	0.00003
SS-2	Garnet	52.194	52.106	0.004	0.12380	0.12280	0.00005
SS-3	SiC	52.247	52.102	0.007	0.12230	0.12000	0.00012
SS-4	SiC	51.758	51.654	0.005	0.12280	0.12079	0.00010
SS-5	White Al_2O_3	53.271	53.111	0.008	0.12637	0.12577	0.00003
SS-6	White Al_2O_3	51.772	51.554	0.011	0.12435	0.12356	0.00004

Table 20. Material Removal Rate of 1018 Steel Using 8 µm Abrasive.

Sample #	8 µm	Initial wt. (g)	Final wt. (g)	MRR g/min	Initial Thk. (inch)	Final Thk. (inch)	MRR inch/min
S-1	Garnet	52.490	52.420	0.003	0.12663	0.12617	0.00002
S-2	Garnet	52.543	52.421	0.006	0.12670	0.12610	0.00003
S-3	SiC	52.372	52.233	0.007	0.12638	0.12549	0.00004
S-4	SiC	52.421	52.241	0.009	0.12639	0.12607	0.00002
S-5	White Al_2O_3	52.271	52.105	0.008	0.12640	0.12608	0.00002
S-6	White Al_2O_3	52.471	52.309	0.008	0.12668	0.12626	0.00002

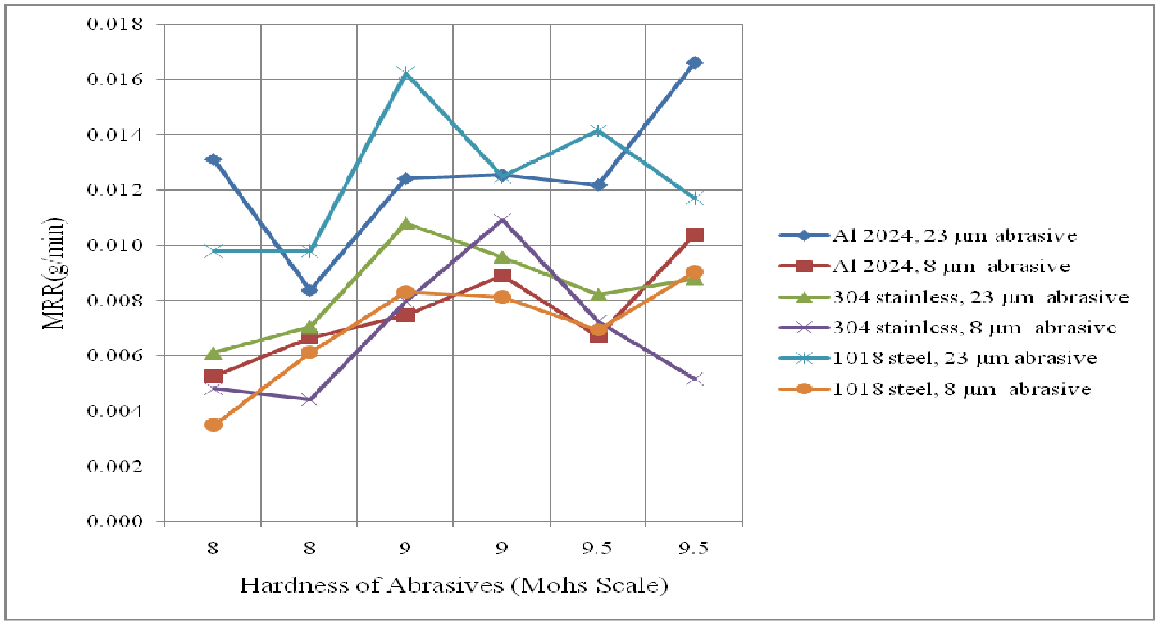

Figure 40. MRR vs. Hardness of Abrasives in Gram per Minute.

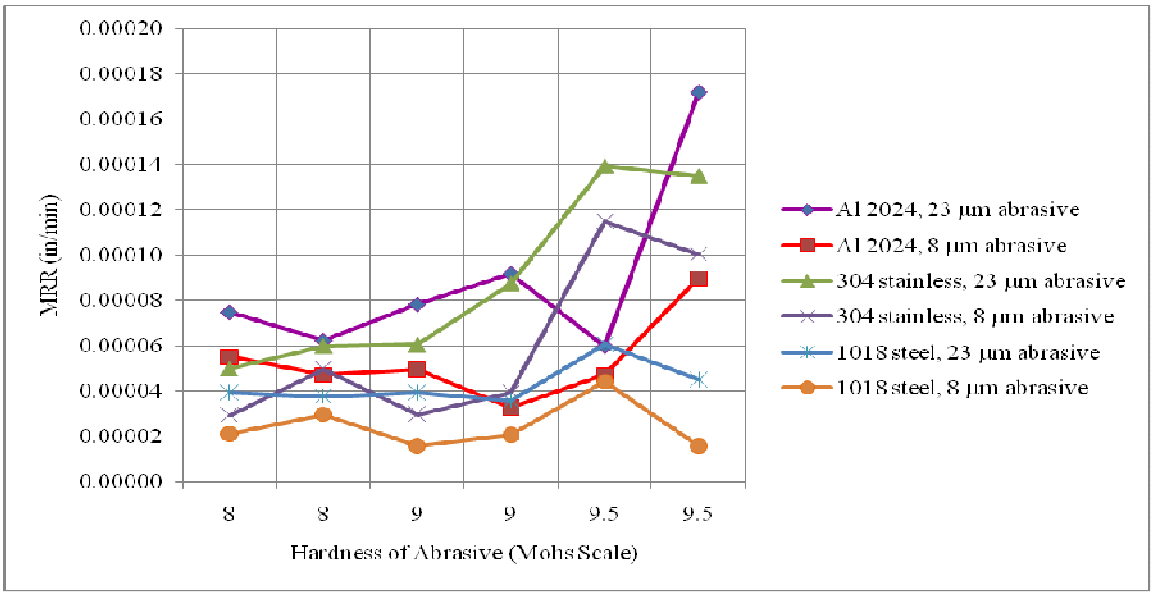

Figure 41. MRR vs. Hardness of Abrasives in inch per Minute.

Tables 21, 22, and 23 present the results of final roughness values, and percentage roughness improvement obtained from lapping of Al 2024, 304 stainless steel, and 1018 steel with 8 µm abrasive particles, respectively.

Table 21. Roughness Values of Al 2024 Using 8 µm Abrasive.

Sample #	Abrasive Grain size of 8 µm or 600 Grit Size	Initial Average Roughness (µm)	Final Average Roughness (µm)	% Roughness Improvement
Al-1	Garnet	0.30	0.18	40
Al-2	Garnet	0.30	0.16	46
Al-3	SiC	0.17	0.09	47
Al-4	SiC	0.17	0.08	52
Al-5	White Al_2O_3	0.12	0.07	41
Al-6	White Al_2O_3	0.11	0.07	36

Table 22. Roughness Values of 304 Stainless Steel Using 8 µm Abrasive.

Sample #	Abrasive Grain size of 8 µm or 600 Grit	Initial Average Roughness (µm)	Final Average Roughness (µm)	% Roughness Improvement
SS-1	Garnet	0.19	0.13	31
SS -2	Garnet	0.17	0.15	11
SS -3	SiC	0.11	0.09	18
SS -4	SiC	0.14	0.12	14
SS -5	White Al_2O_3	0.21	0.10	52
SS -6	White Al_2O_3	0.30	0.17	43

Table 23. Roughness Values of 1018 Steel Using 8 µm Abrasive.

Sample #	Abrasive Grain size of 8 µm or 600 Grit	Initial Average Roughness (µm)	Final Average Roughness (µm)	% Roughness Improvement
S-1	Garnet	0.24	0.20	16
S-2	Garnet	0.29	0.21	27
S-3	SiC	0.50	0.21	58
S-4	SiC	0.27	0.18	33
S-5	White Al_2O_3	0.39	0.16	58
S-6	White Al_2O_3	0.25	0.17	32

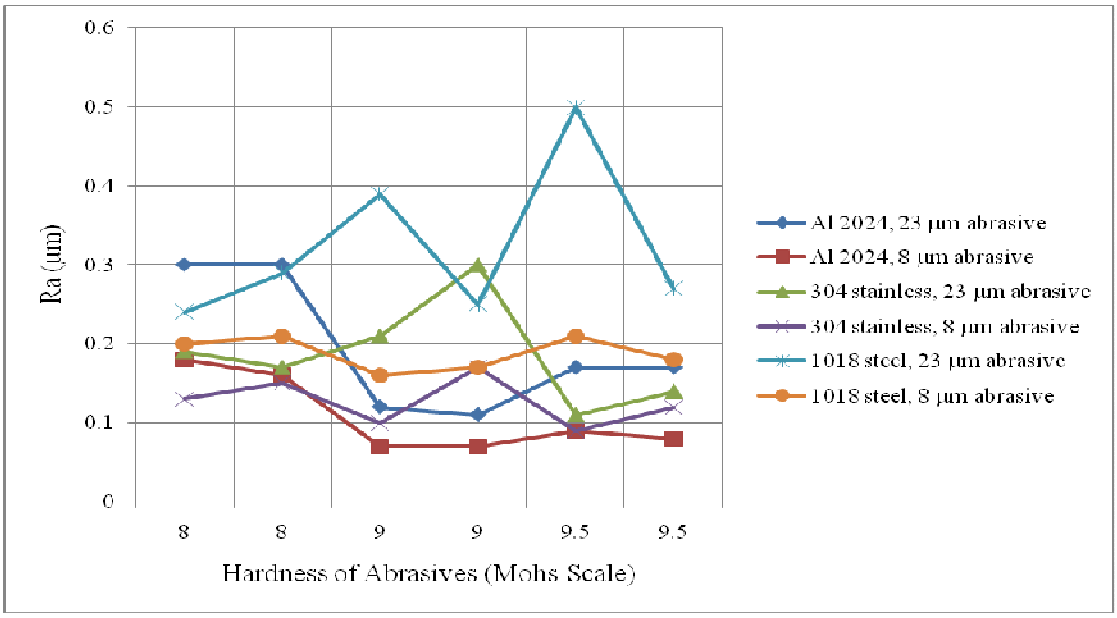

Figure 42. Surface Roughness Profile vs. Hardness of Abrasives.

7.2 Statistical Analysis

Statistical Analysis Software (SAS™ 9.1) was used as a tool to test the significance of each parameter. Table 24 presents a summary of Analysis of Variance (ANOVA) results for material removal rates. Based on the results obtained from the ANOVA for MRR (final lapping), the main effects of abrasive types, size of abrasives,

and type of work materials significantly affected the MRR with a statistical significance of $p = 0.0094$, $p < 0.0001$, and $p = 0.0005$, respectively. However, there were no significant two-way or three-way interactions for MRR.

Table 24. MRR ANOVA Summary Results.

Factors	P-value	Interpretation
Abrasives (A)	0.0094	significant
Size (S)	< 0.0001	significant
Workpiece (W)	0.0005	significant
A x S Interaction	0.0478	
A x W Interaction	0.3056	
S x W Interaction	0.8963	
A x S x W Interaction	0.9424	

A summary of ANOVA results obtained from average roughness data (final lapping) are given in Table 25. The main effects of abrasive size and type of workpiece significantly affected the roughness of the work material with $p < 0.0001$ and < 0.0001, respectively. In addition, there was a highly significant two-way interaction of abrasives and workpiece, $p = 0.0049$. Figure 43 illustrates a two-way interaction of abrasives by work materials for Ra values. The output report from SAS is presented in Appendix F.

Table 25. Ra ANOVA Summary Results.

Factors	P-value	Interpretation
Abrasives (A)	0.2123	
Size (S)	< 0.0001	significant
Workpiece (W)	< 0.0001	significant
A x S Interaction	0.7586	
A x W Interaction	0.0049	significant
S x W Interaction	0.2123	
A x S x W Interaction	0.2075	

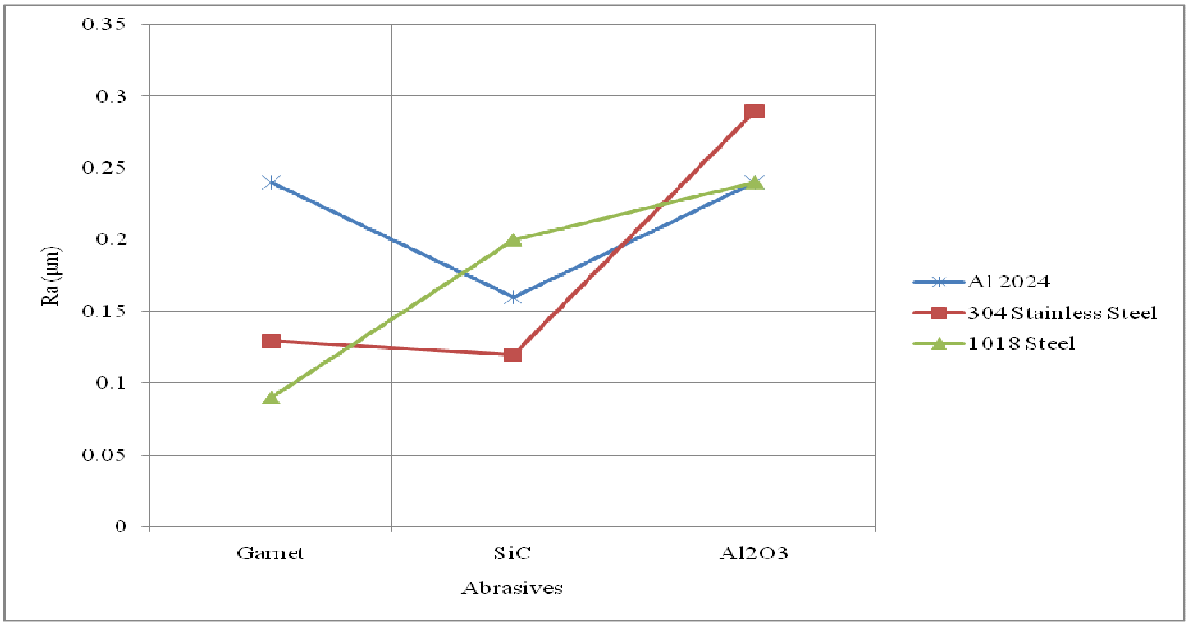

Figure 43. Two-Way Interaction between Abrasives and Workpiece.

Anaglyph stereopairs and line profiles of lapped Al 2024, 304 stainless steel, and 1018 steel reconstructed with the Scandium^{TM} software are shown in Figures 44 though 46. Line profiles from SEM images were reconstructed with Scandium^{TM} 3-D software. As can be seen in Figure 48c, SiC became embedded into aluminum sample after lapping. Furthermore, white Al_2O_3 abrasives were embedded in 1018 steel after lapping as illustrated with the 3-D image in Chapter 6. In order to obtain the 3-D images and anaglyph stereopairs described in Chapters 6 and 7, each sample was scanned at 0˚ (left hand side) and 6˚ (right hand side) at the same magnification of 1000x near an indent. Rockwell hardness tester was used to make an indent on the samples so that the same location was scanned before and after lapping.

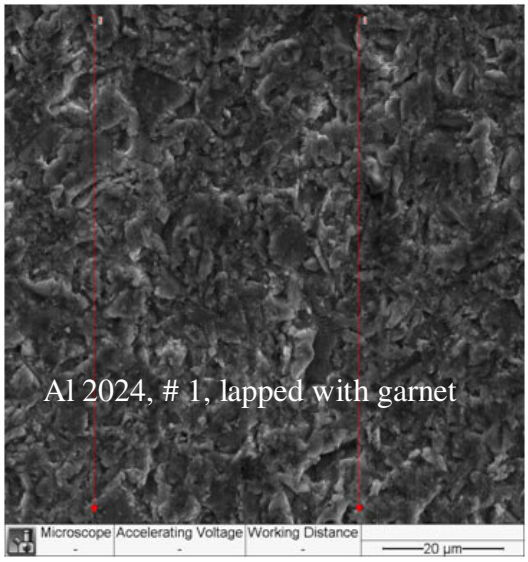

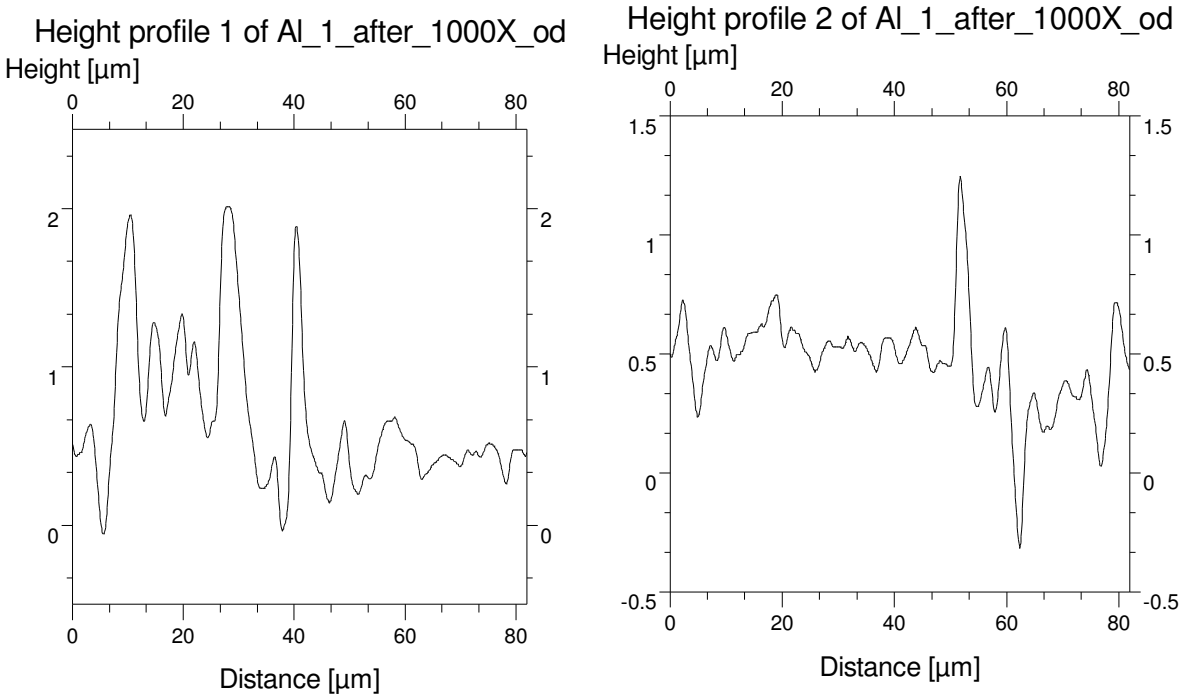

Figure 44a. Anaglyph Stereopair and Line Profile of Al 2024 Lapped with Garnet.

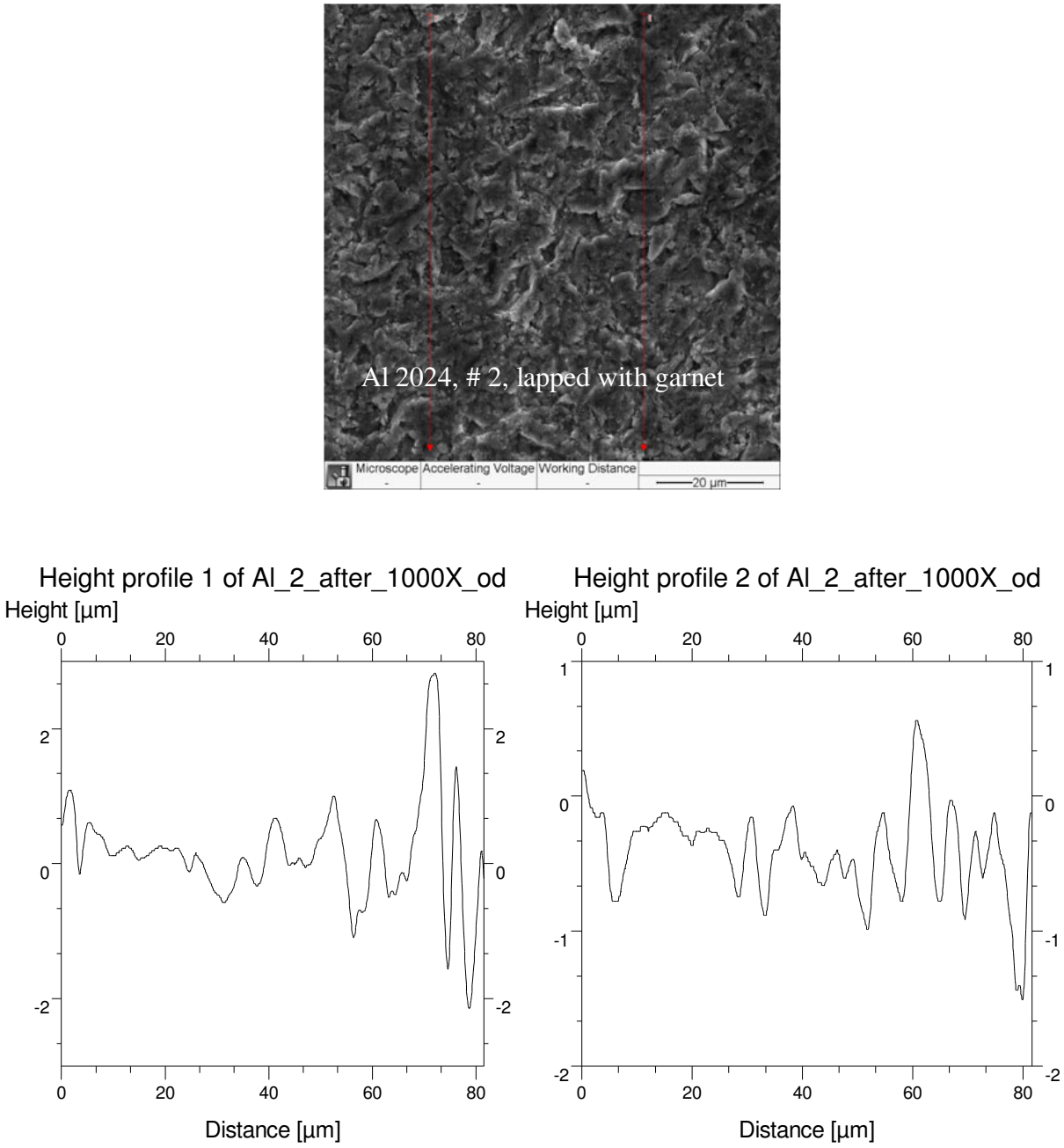

Figure 44b. Anaglyph Stereopair and Line Profile of Al 2024 Lapped with Garnet.

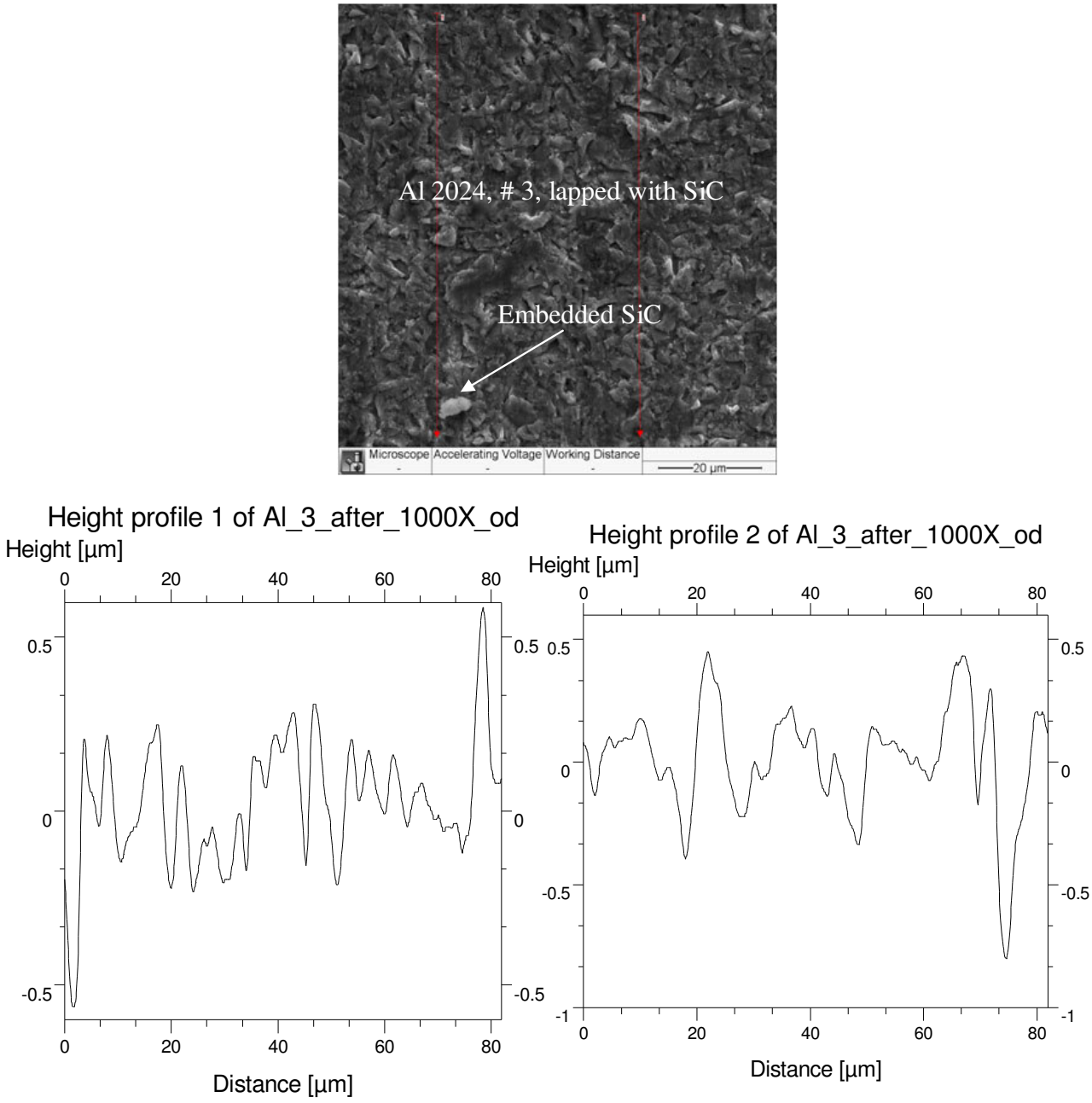

Figure 44c. Anaglyph Stereopair and Line Profile of Al 2024 Lapped with SiC.

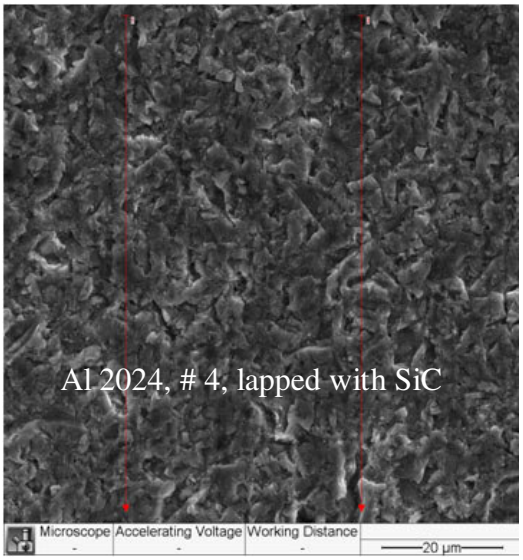

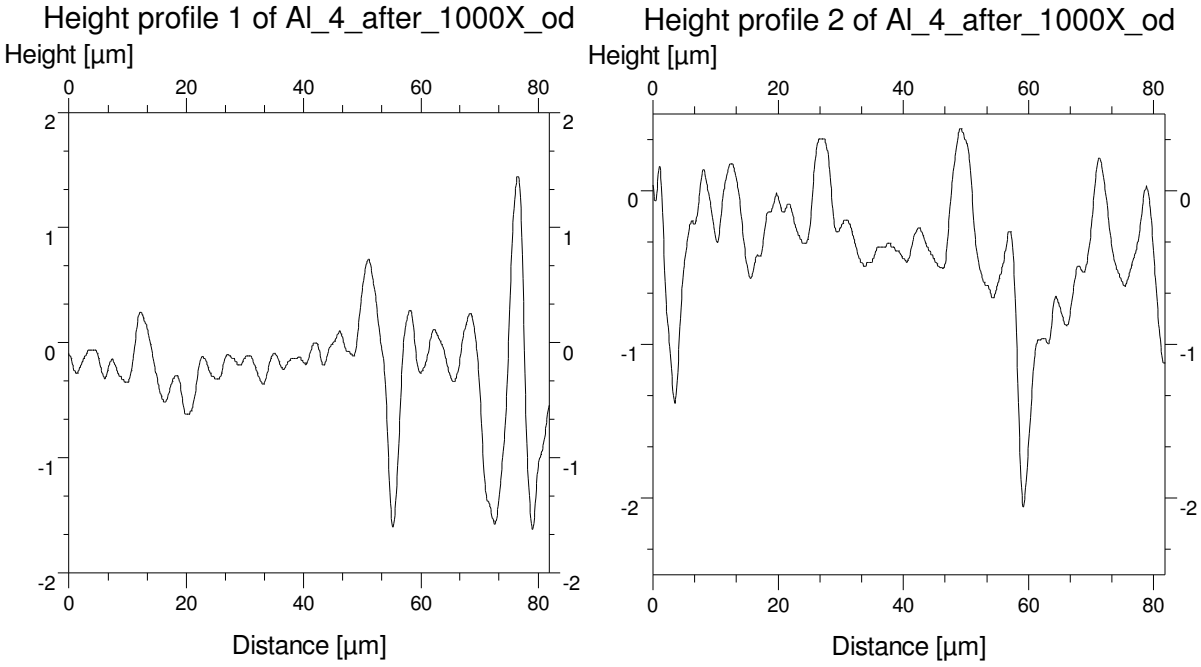

Figure 44d. Anaglyph Stereopair and Line Profile of Al 2024 Lapped with SiC.

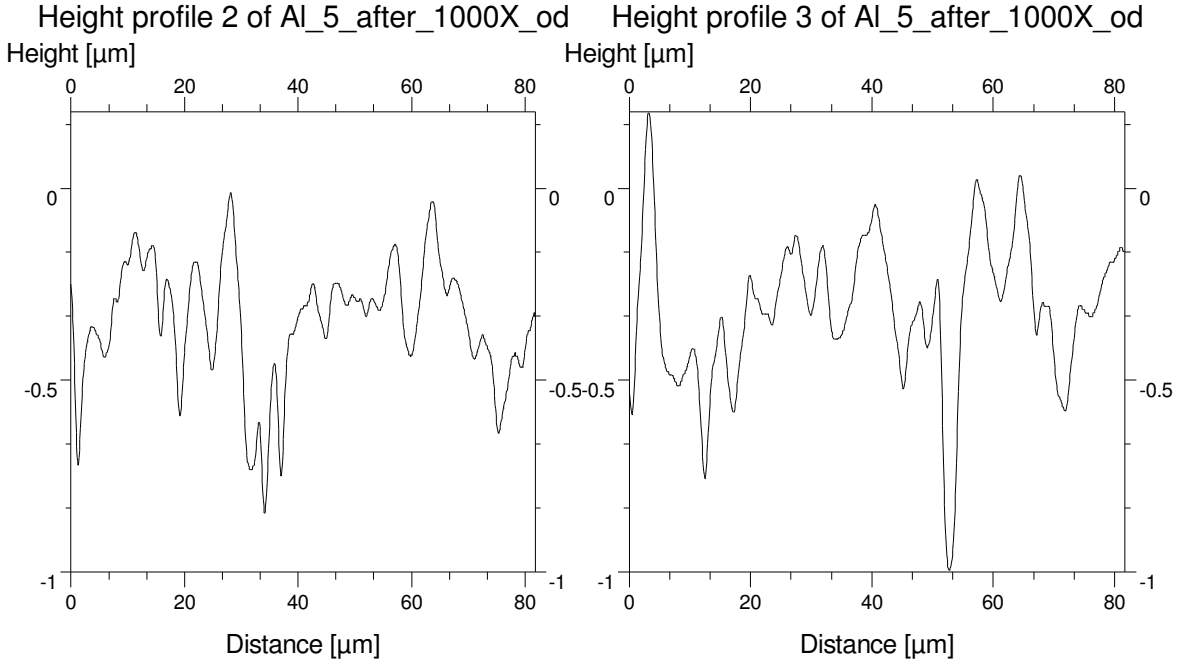

Figure 44e. Anaglyph Stereopair and Line Profile of Al 2024 Lapped with White Al_2O_3.

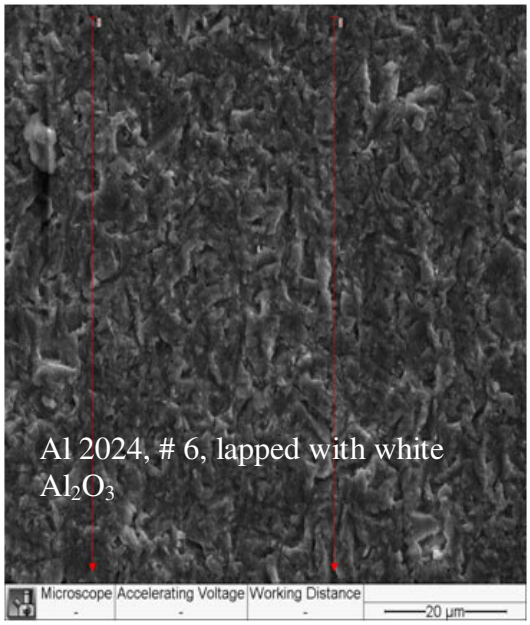

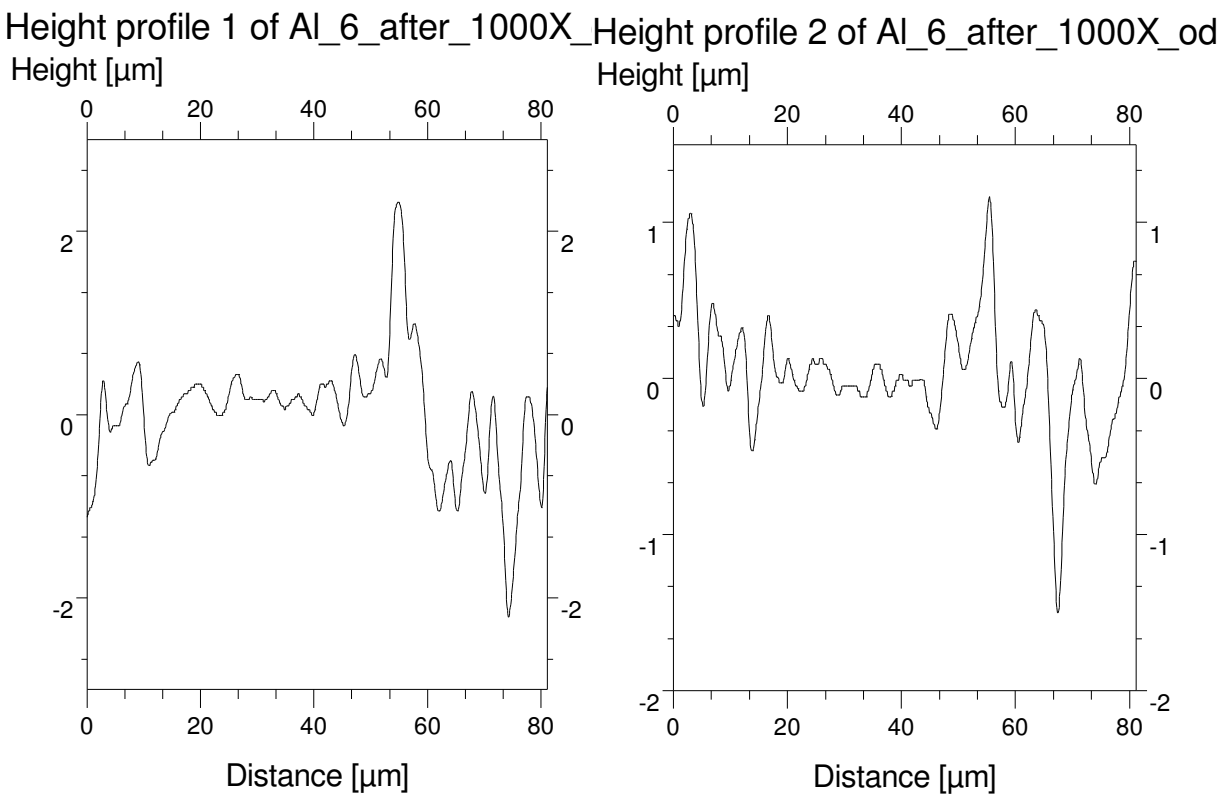

Figure 44f. Anaglyph Stereopair and Line Profile of Al 2024 Lapped with White Al_2O_3.

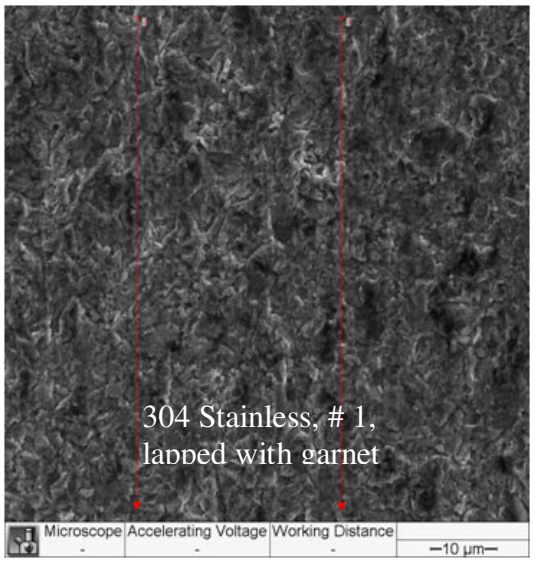

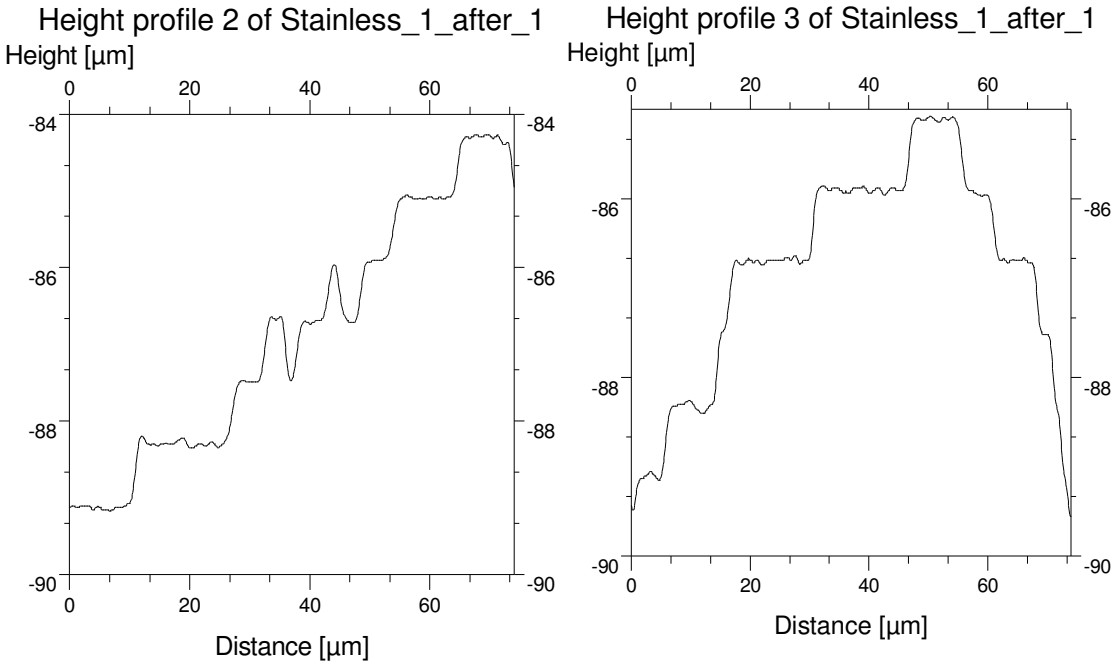

Figure 45a. Anaglyph Stereopair and Line Profile of 304 Stainless Steel Lapped with Garnet.

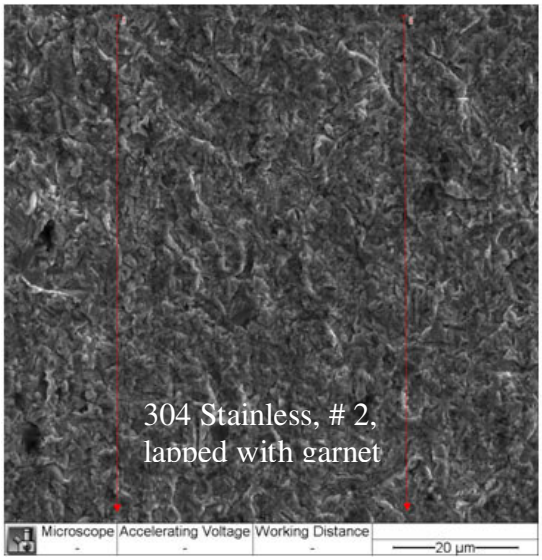

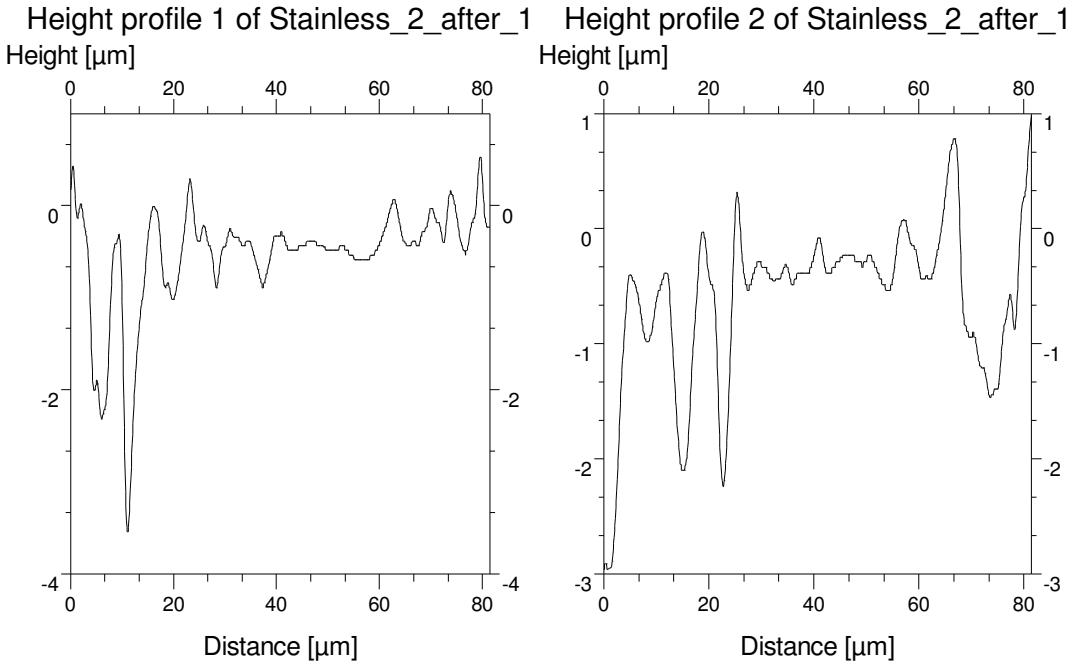

Figure 45b. Anaglyph Stereopair and Line Profile of 304 Stainless Steel Lapped with Garnet.

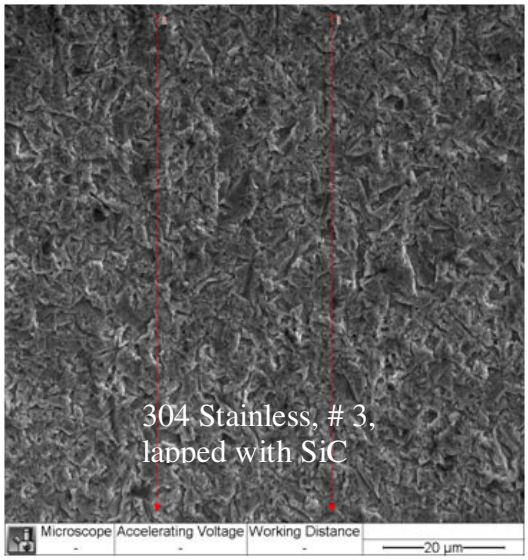

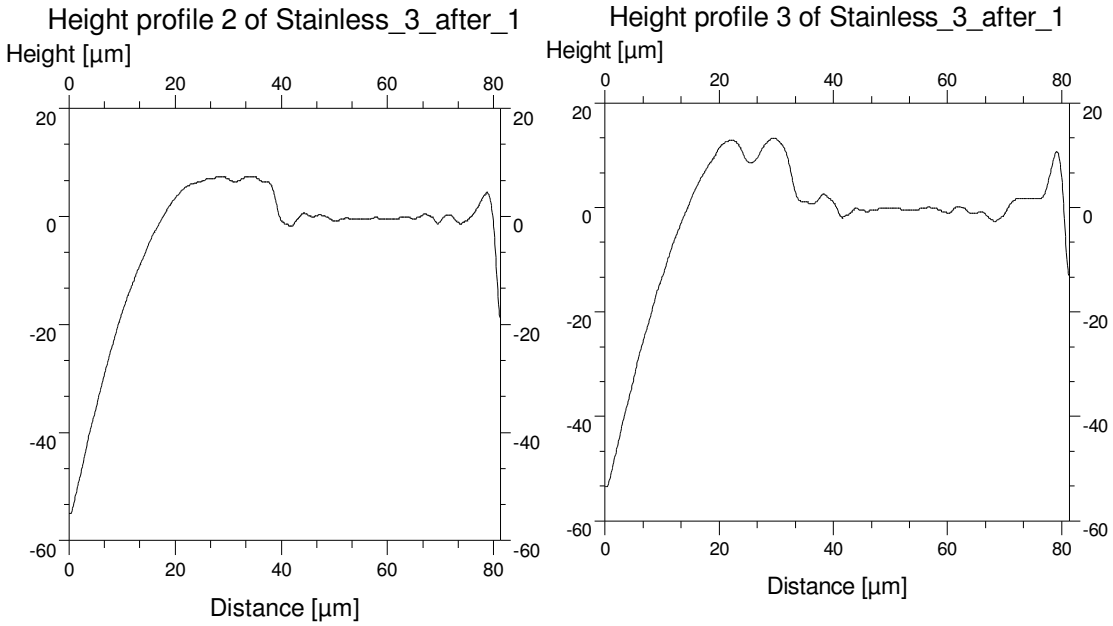

Figure 45c. Anaglyph Stereopair and Line Profile of 304 Stainless Steel Lapped with SiC.

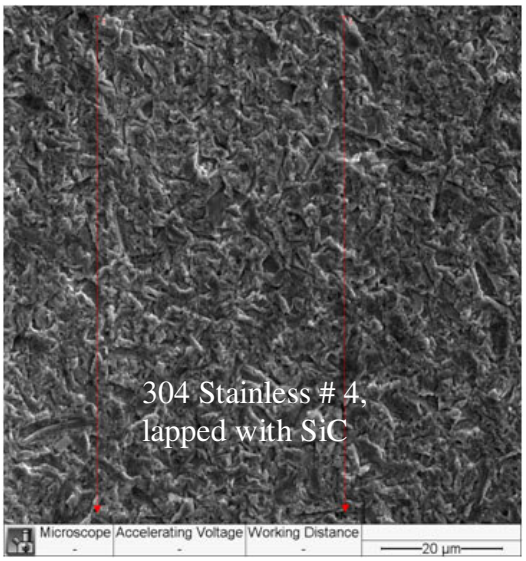

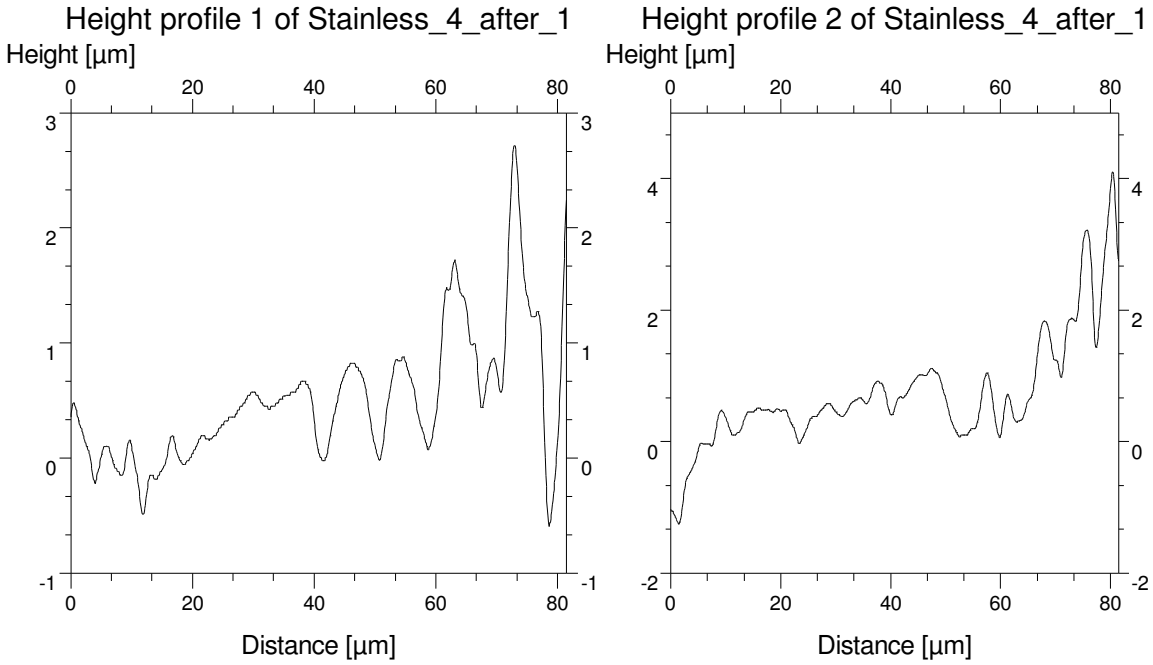

Figure 45d. Anaglyph Stereopair and Line Profile of 304 Stainless Steel Lapped with SiC.

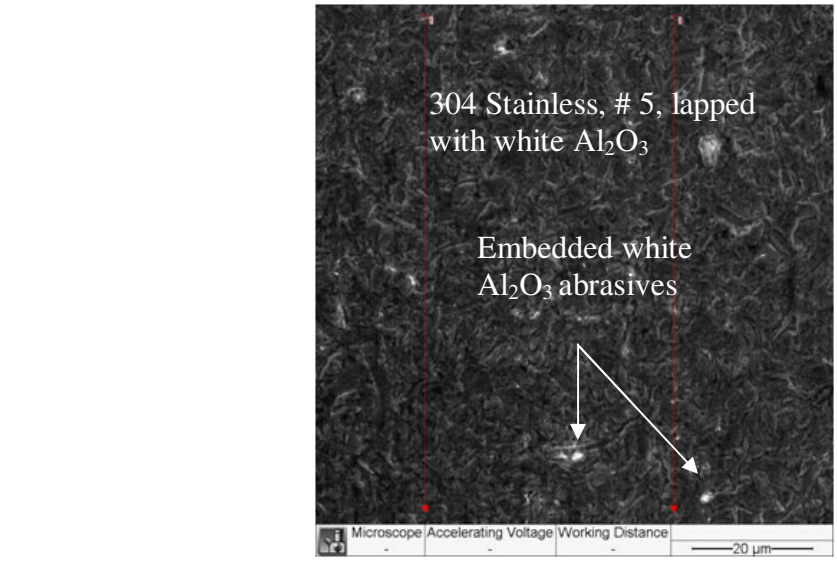

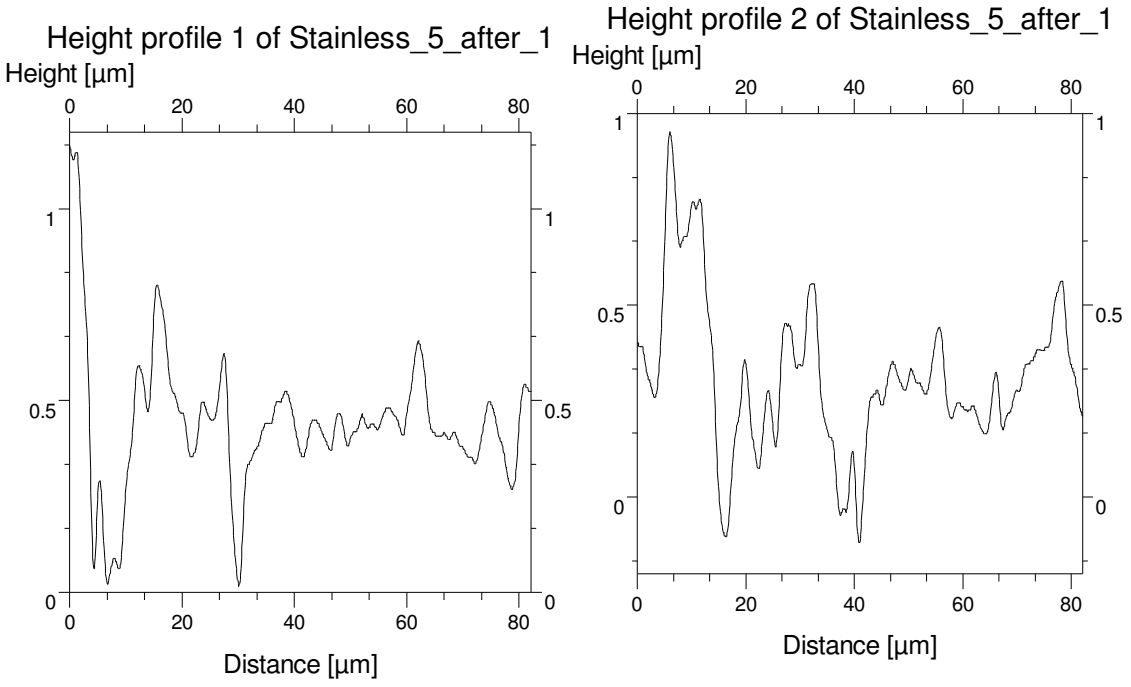

Figure 45e. Anaglyph Stereopair and Line Profile of 304 Stainless Steel Lapped with White Al_2O_3.

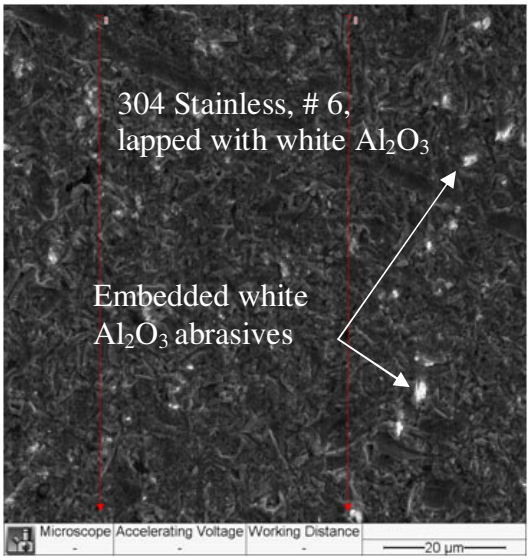

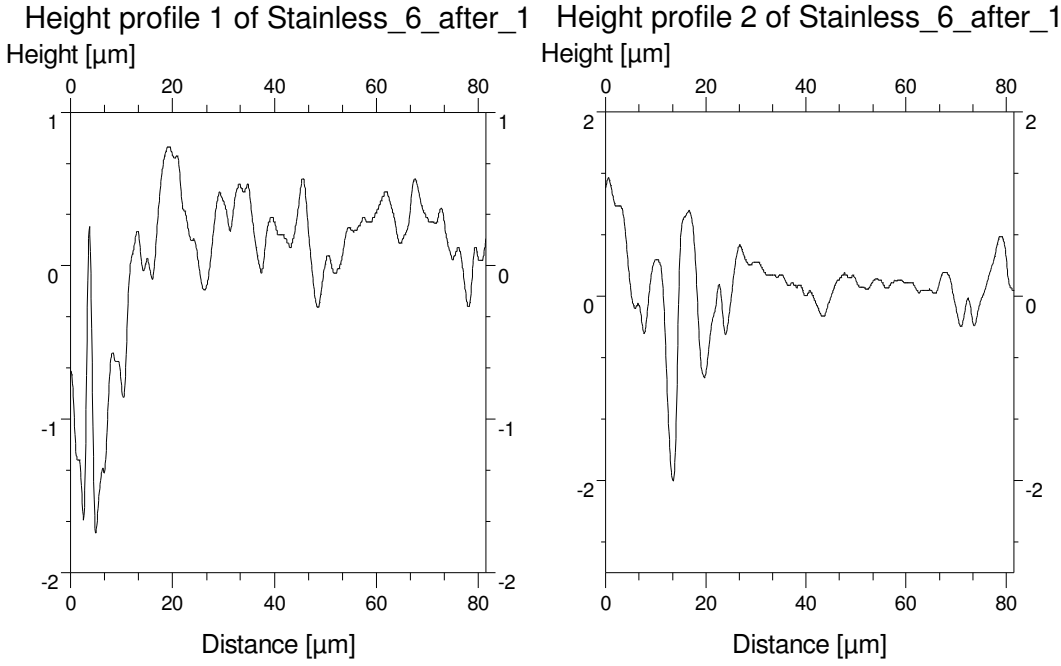

Figure 45f. Anaglyph Stereopair and Line Profile of 304 Stainless Steel Lapped with White Al_2O_3.

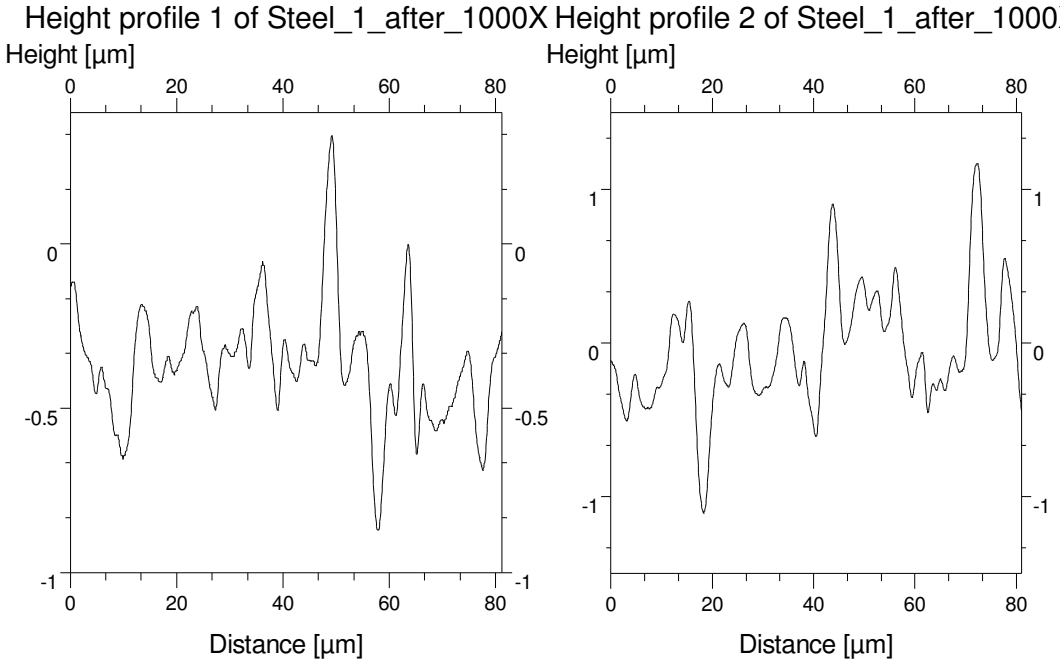

Figure 46a. Anaglyph Stereopair and Line Profile of 1018 Steel Lapped with Garnet.

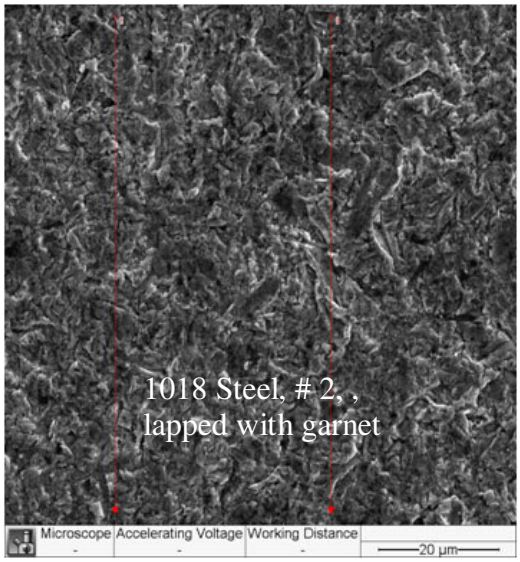

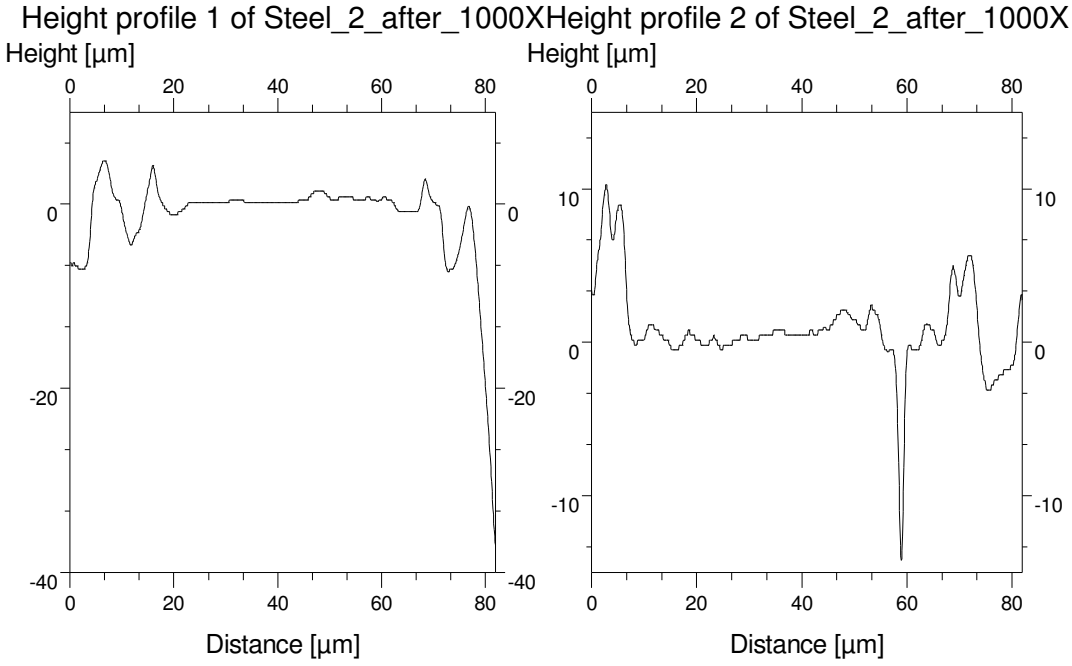

Figure 46b. Anaglyph Stereopair and Line Profile of 1018 Steel Lapped with Garnet.

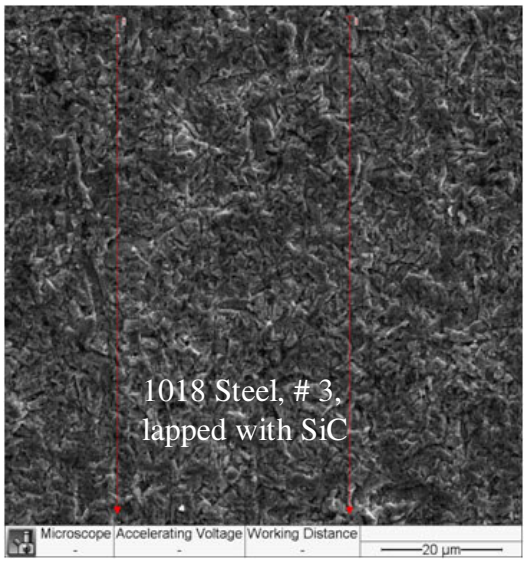

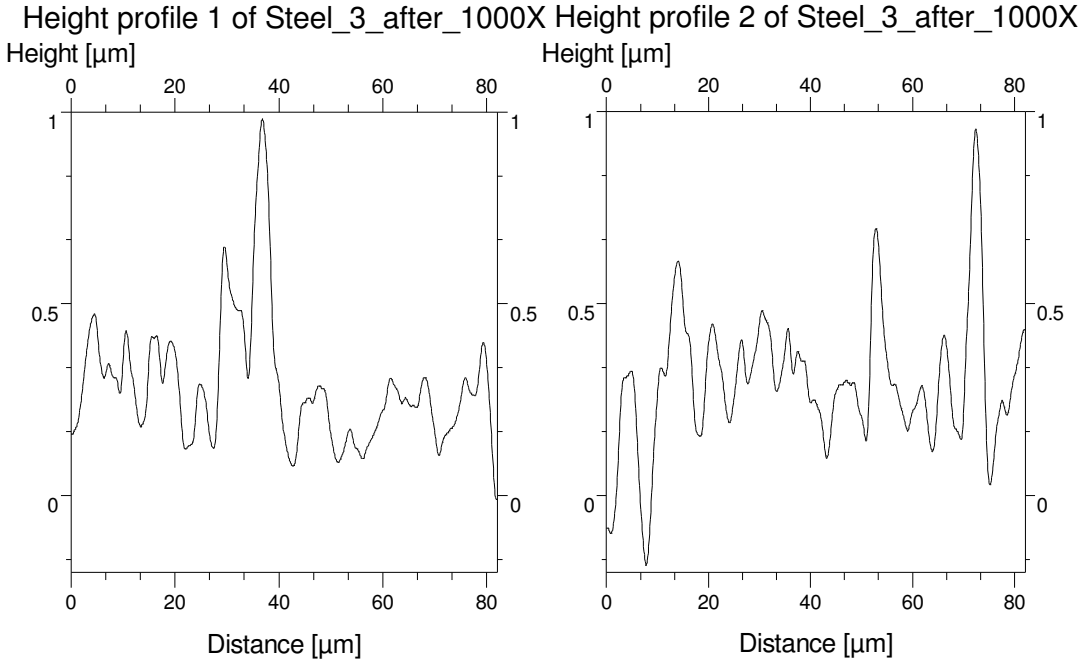

Figure 46c. Anaglyph Stereopair and Line Profile of 1018 Steel Lapped with SiC.

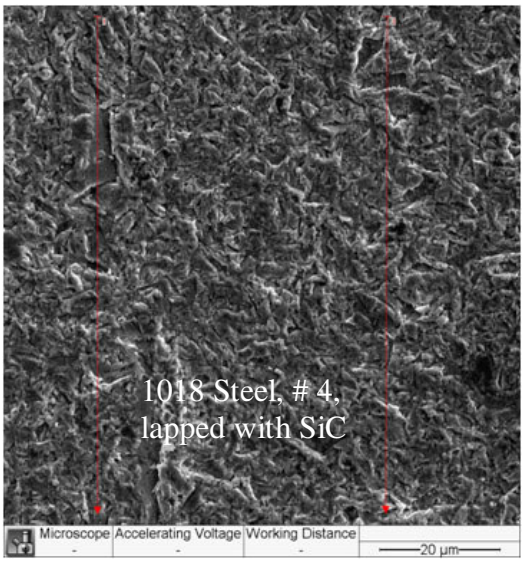

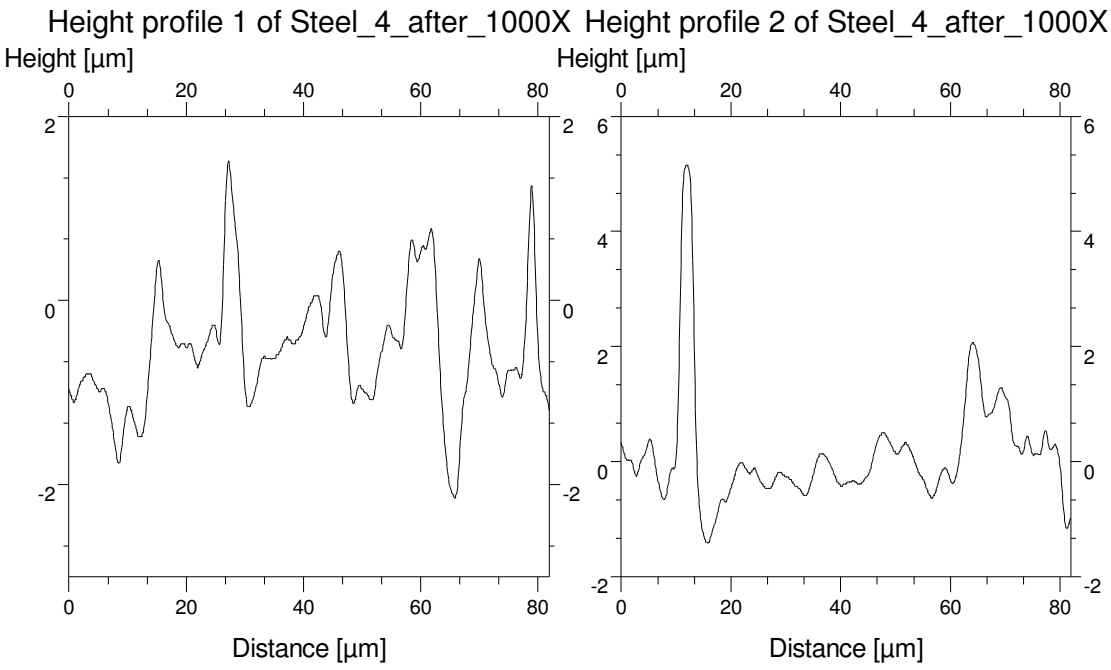

Figure 46d. Anaglyph Stereopair and Line Profile of 1018 Steel Lapped with SiC.

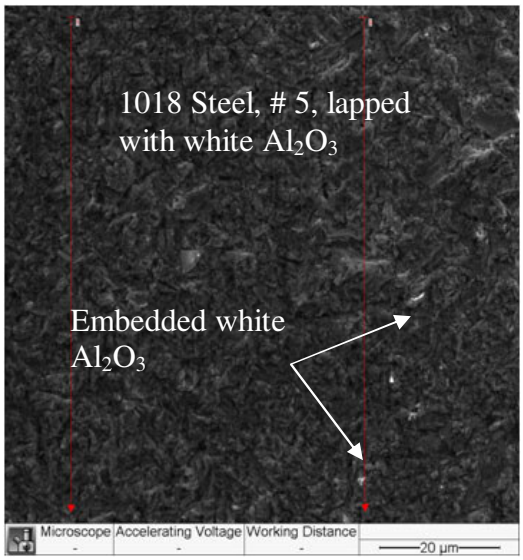

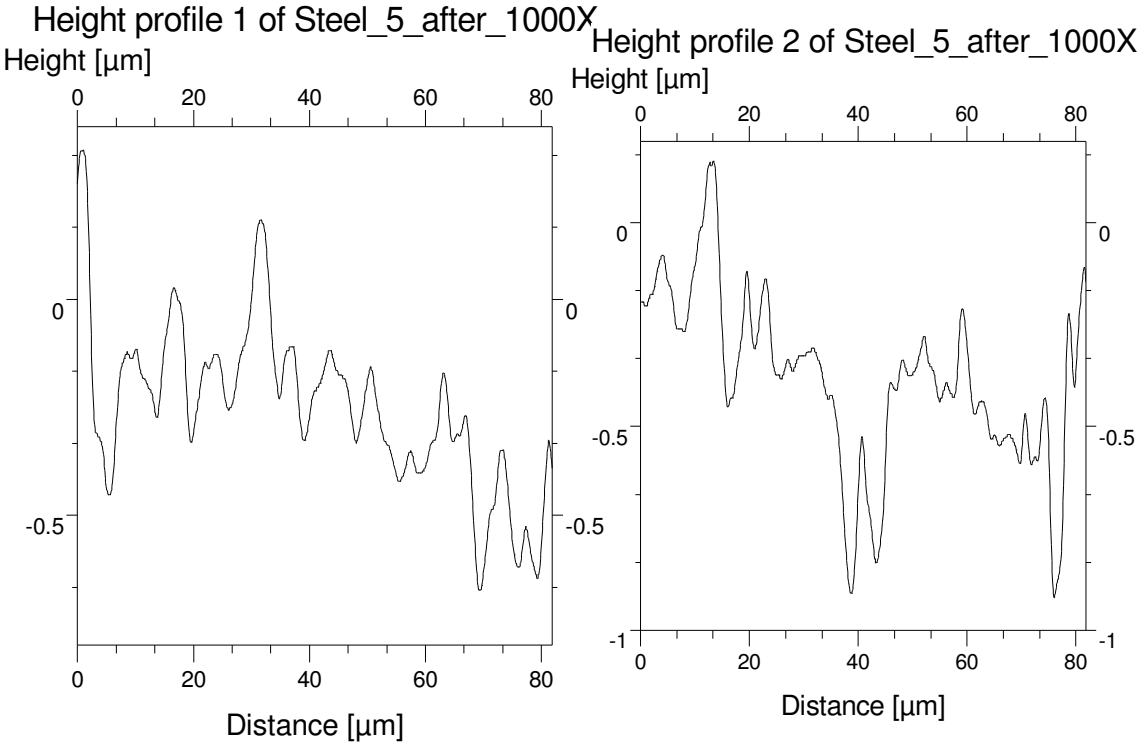

Figure 46e. Anaglyph Stereopair and Line Profile of 1018 Steel Lapped with White Al_2O_3.

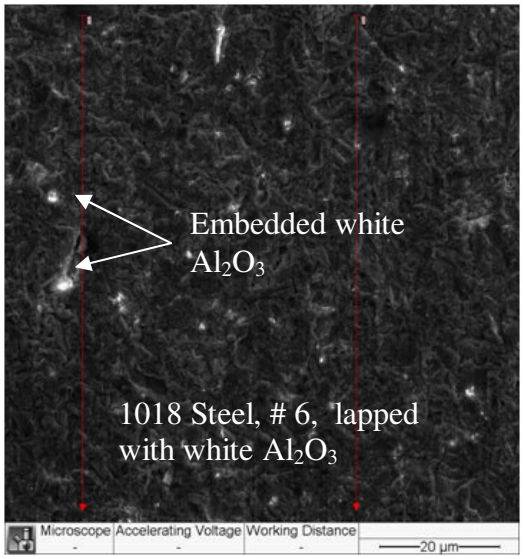

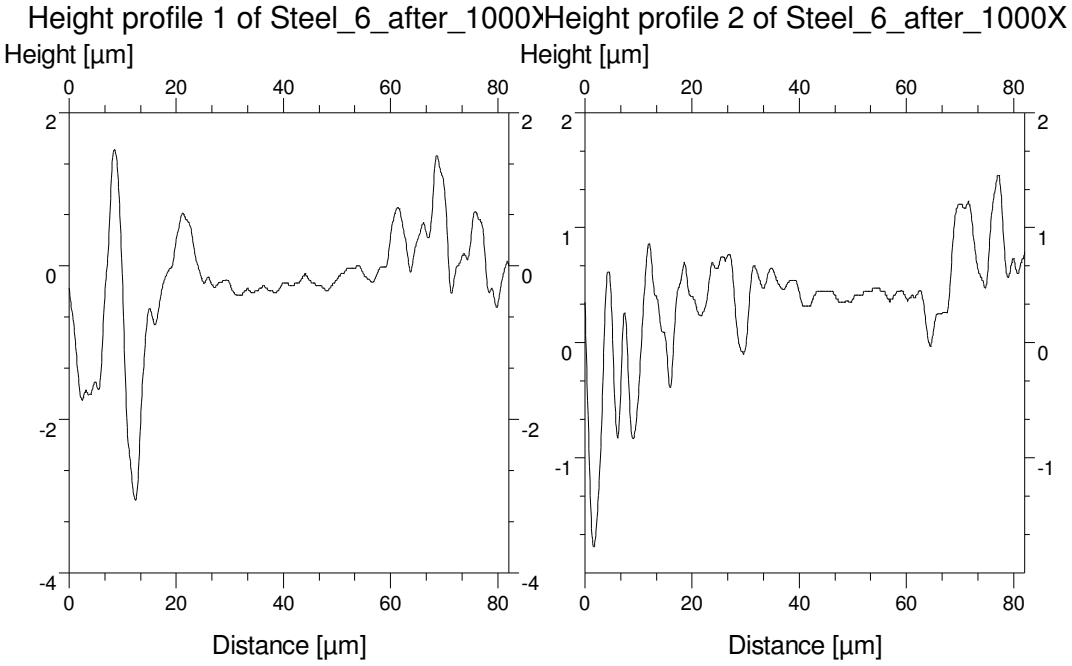

Figure 46f. Anaglyph Stereopair and Line Profile of 1018 Steel Lapped with White Al_2O_3.

The stereopair and line profiles obtained from SEM is about 70% accurate, however, the line from profilometer is more accurate (90%) because it is a direct contact measurement of the surface profile. As can be seen in Figure 44c, SiC became embedded

into aluminum sample after lapping. Furthermore, white Al_2O_3 abrasives were embedded in 304 stainless and 1018 steel after lapping as illustrated in the anaglyph stereopair images in Figures 45e, 45f, 46e, and 46f.

7.3 Assumptions

- The load applied to the work materials was assumed to be uniformly distributed on each sample lapped at every run.
- In sticking friction or two-body-friction, some abrasives become embedded into the workpiece, and the velocity is assumed to be zero in this case since there is no relative movement between the abrasives and the sample. This implies that in sticking friction, there is two-body wear at work.
- In a three-body friction, the abrasive grains, specimen, and the lapping plate are in a relative motion during the lapping operation, hence the name three-body friction.
- The abrasive grain size is assumed to be uniform, for example, a grit size of 600, allows 8 µm grains to pass through the sieve, although some grains less than 8 µm could pass through the mesh as well**.**

7.4 Tribology of Lapping

Six different methods for determining frictional force during a lapping operation are described in sections 7.4.1 through section 7.4.6. In section 7.4.1 lapping friction is derived as a function of area, viscosity of the abrasives, circumferential speed of workpiece, and distance as expressed in Equation (37). Rolling friction is determined as

function of radius of the sample (section 7.4.2), while in section 7.4.3, rolling friction is obtained, based on the sliding velocity and rolling velocity. In section 7.4.4, a force sensor can be used to measure frictional force directly during the lapping process. Finally, sections 7.4.5 and 7.4.6 described temperature and motor constant models.

7.4.1 Frictional Force as a function of Viscosity

Shear stress and shear rate can be represented in Equations (30) and (31), respectively. As can be seen in Equation (31), shear stress is directly proportional to shear strain and viscosity. Viscosity can be defined as a measure of resistance of a fluid to flow (Olson, 1973; Roberson and Crowe, 1976). In other words, viscosity is property of the fluid that restricts the force that causes the liquid to flow.

$$\tau = \frac{F}{A}, \tag{30}$$

Shear rate, γ, is stated in Equation (31).

$$\gamma = \frac{v}{d} = \frac{dv}{dy}, \tag{31}$$

Also, shear stress can be described in terms of viscosity as represented in Equation (32).

$$\tau = \mu * \gamma, \tag{32}$$

Equation (33) is obtained by combining Equations (30), (31), and (32).

$$\frac{F}{A} = \mu * \left(\frac{dv}{dy}\right) = \mu * \left[\left(\frac{dis\tan ce}{time}\right) \Big/ y\right] = \frac{\mu * v}{y}, \tag{33}$$

where

τ : shear stress (N/m^2)

F : frictional force

A : area

γ : shear rate (1/sec)

μ : viscosity of abrasives

v : velocity

y : distance.

Circumferential or cutting speed, v, is the tangential velocity of the workpiece. It is the maximum speed at the outer diameter of the work material, which is represented in Equation (34), when the diameter is measured in millimeters (Kalpakjian and Schmid, 2006). If the diameter is recorded in inches, then the circumferential speed can be calculated using Equation (35). On the other hand, rotational speed is the speed of the spindle, and can be obtained from the expression in Equation (36). Since there are three work materials, the velocity of the work materials equals 40.7 m/sec (133.5ft/min).

$$\text{v} = \left(\frac{\pi * D * N}{1000} \right) \text{ meter/min,} \tag{34}$$

D is diameter in millimeters (50.8 mm).

$$\text{v} = \left(\frac{\pi * D * N}{12} \right) \text{ ft/minute,} \tag{35}$$

D is diameter in inches (2 inches).

$$\text{Rotational speed} = 2 * \pi * N \text{ (radians per unit time)} \tag{36}$$

where

D: diameter of sample (2 inches or 50.8 mm)

N: number of revolutions per minute (85 rpm)

v: circumferential or cutting speed.

The unit of viscosity is given in centipoise, but the International System (SI) of units for viscosity is N.sec/m^2. This is derived in Equation (37), according to (Olson, 1973; Roberson and Crowe, 1976).

$$\mu = \frac{\left(\frac{F}{A}\right)}{\left(\frac{dv}{dy}\right)} = \frac{\left(\frac{N}{m^2}\right)}{\left(\frac{m}{s}\right)/m} = N.\sec/m^2 \qquad (37)$$

One centipoises equals 0.001 Newton.sec/m^2. The viscosity of fused aluminum oxide (Al_2O_3) powder, mixed with distilled water in a ratio of 1:5 by weight (180 grams of abrasives mixed with 900 grams of distilled water) at room temperature (21.9 ºC or 71.42 ºF), and spindle speed of 100 rpm was 16 centipoise (0.016 Newton.sec/m^2). Also, the viscosity of garnet $(Mg, Mn, Fe)_3Al_2Si_3O_{12}$ and $Ca_3(Cr, Al, Fe)_2Si_3O_{12}$ powder, mixed with distilled water in a ratio of 1:5 by weight at room temperature (21.9 ºC or 71.42 ºF), and spindle speed of 100 rpm was 13 centipoise (0. 013 Newton.sec/m^2). Furthermore, the viscosity of silicon carbide (SiC) powder, mixed with distilled water in a ratio of 1:5 by weight at room temperature (21.9 ºC or 71.42 ºF), and spindle speed of 100 rpm was 14 centipoise (0.014 Newton.sec/m^2). The viscometer used in measuring the viscosity was manufactured by Brookfield, model type DV-II+.

The lapping force or normal load was 24.9 N (5.6 lbf). A lapping pressure of 12.3 KPa (1.8 psi) was applied to the work material during the course of lapping and was calculated using Equation (27). The abrasives particles were dispersed or suspended in distilled water since they are not soluble in water, therefore the abrasives grains settled very quickly at the bottom of the slurry vehicle if not stirred continuously. Table 28 summarizes the results obtained by measuring of the viscosity of the abrasive particles as a function of time. Aluminum oxide had the highest viscosity of 16 centipoise, while garnet had the lowest viscosity of 13 centipoise. As delineated in Figure 47, the rate at which the abrasive particles settled at the bottom of the liquid vehicle is obtained by plotting the viscosities of the abrasives vs. time. Also, after about two minutes, the viscosity of the abrasive grains became fairly constant as presented in Table 26.

Table 26. Viscosity of Abrasives as a Function of Time.

Time	Al_2O_3		Garnet		SiC	
Minutes	Viscosity		Viscosity		Viscosity	
	Cp	N-s/m^2	Cp	N-s/m^2	Cp	N-s/m^2
0	16	0.016	13	0.013	14	0.014
0.5	12	0.012	10.9	0.0109	12.6	0.0126
1	10.9	0.0109	10.6	0.0106	12.1	0.0121
1.5	10.5	0.0105	10.5	0.0105	11.9	0.0119
2	10.5	0.0105	10.2	0.0102	11.7	0.0117

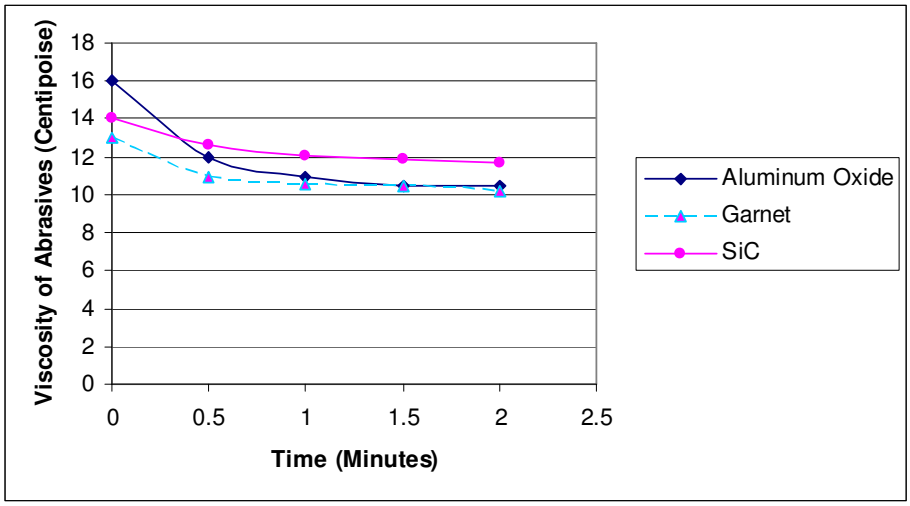

Figure 47. Viscosity of Abrasives vs. Time.

7.4.2 Rolling Friction as a Function of Radius of Specimen

Hersey (1966) cited Coulomb's law of rolling friction, which states that the resistance to rolling is proportional to the normal load, N, but independent of the speed, and inversely proportional to the radius, r, of the rolling object as expressed in Equation (38). The coefficients of friction for different materials can be obtained from handbooks, based on the assumptions that they are constant for a given material, irrespective of the radius of the specimen, r.

$$F_r = e\left(\frac{N}{r}\right), \tag{38}$$

where

F_r: rolling frictional force

e: eccentricity of the supporting force, or moment arm of rolling friction, or coefficient of rolling friction

N: normal load or force

r: radius of the sample.

7.4.3 Rolling Friction as a Function of Slip Velocity and Rolling Velocity

The force required to initiate rolling movement, F_r, is known as rolling friction, and it equal to the product of normal load, N, and tan θ as given in Equation (39) for an irregular object (Rabinowicz, 1966). It was found that the force needed to maintain rolling is less than the force required to initiate rolling. Therefore, the kinetic coefficient of rolling friction is less than the static coefficient of rolling friction. Also, Rabinowicz (1966). observed that the rolling coefficient of friction ranged from 5×10^{-3} to 5×10^{-5}. Figure 48 illustrates normal force, frictional force, and direction of circumferential speed during a lapping operation.

$$\mu_r = \frac{F_r}{N} = \tan\theta, \tag{39}$$

where

μ_r : coefficient of rolling friction

F_r : rolling frictional force

N : Normal load

$\tan\theta$: angle between the vertical, and the line joining the center of gravity of the sample, and the projection about which the rolling takes place.

Rolling is usually associated with a small fraction of slip or sliding (Rabinowicz, 1966; Bhushan, 2002). The slip velocity ranges between 1 and 10% of the overall rolling velocity. This small fraction of slip velocity produces the significant portion of resistance to rolling.

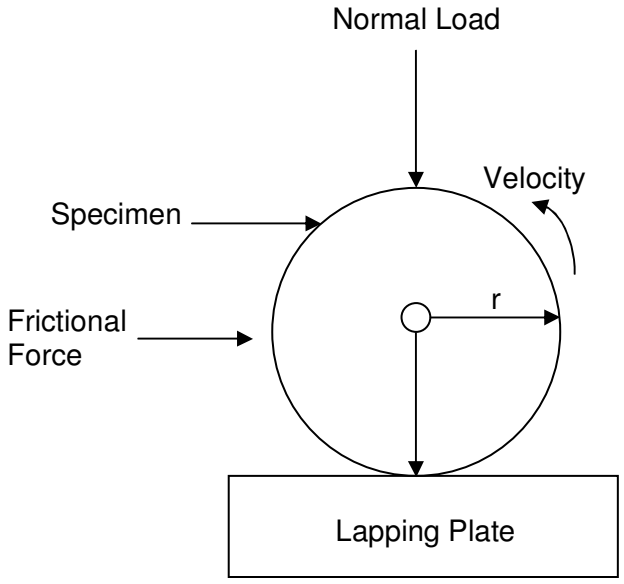

Figure 48. Lapping Forces.

According to Wolfson and Pasachoff (1990), a rolling object (cylinder) is normally associated with both kinetic energy due to sliding and rotational energy as expressed in Equations (40) and (41), respectively. The moment of inertia of a cylinder rotating about its axis, and the sliding velocity are represented in Equations (42) and (43), respectively.

$$E_K = \frac{1}{2}\left(m * u^2\right), \tag{40}$$

$$E_R = \frac{1}{2}\left(I * \omega^2\right), \tag{41}$$

$$I = \frac{1}{2}\left(mr^2\right), \tag{42}$$

$$\omega = \frac{v}{r}, \tag{43}$$

where

E_K : kinetic energy (joule)

m : mass of cylinder (52.6752 g)

u : initial sliding velocity

E_R : rotational energy (joule)

I: moment of inertia of a cylinder rotating about its axis. The moment of inertia is the sum of the product of the mass and square of the perpendicular distance to the axis of rotation of an object.

ω **:** angular velocity or rolling velocity

v: linear velocity of the sample (cylinder or disk)

r : radius of the cylinder.

Substituting Equations (42) and (43) into Equation (41), the total rolling energy becomes:

$$E_R = \frac{1}{2} * \left(\frac{1}{2} m * r^2 \right) * \left(\frac{v^2}{r^2} \right) = \frac{1}{4} * m * v^2$$

The total energy of the specimen (cylinder), E_T, is the sum of the kinetic energy and rotational energy of the workpiece as given in Equation (44).

$$E_T = E_K + E_R \tag{44}$$

$$E_T = \left(\frac{1}{4} * m * v^2 \right) + \left(\frac{1}{2} * m * v^2 \right) = \frac{6}{8} * m * v^2$$

By combining the rolling and sliding velocities, Equation (45) is obtained.

$$\frac{6}{8} * m * v^2 = \frac{1}{2} * m * u^2 \rightarrow 12 * m * v^2 = 8 * m * u^2$$

$$v^2 = \frac{8}{12} * u^2 = 0.6667 * u^2$$

Taking square roots from both sides:

$$v_{rolling} = \sqrt{(0.6667) * u^2} = 0.8165 * u_{sliding}$$

Therefore,

$$\frac{v_{rolling}}{u_{sliding}} = \frac{1}{0.8165} \tag{45}$$

This implies that the rolling velocity of the cylinder is 81.65 % that of the sliding or slip velocity. Different types of velocity observed in lapping are discussed in Appendix G.

7.4.4 Force Sensor Model

A force sensor can be used to measure frictional force directly during the lapping process as illustrated in Figure 49. Frictional force, F, is directly proportional to the normal load, N, as shown in Equation (1), described in Chapter 2 (i.e., Coulomb's law of friction).

7.4.5 Temperature Model

Frictional force was derived by from the product of specific angular velocity, lapping time, and heat capacity as expressed in Equation (46).

$$F = \frac{v * t}{r}\left[\left(M_{air} C_{air} \Delta T_{air}\right) + \left(M_{ab} C_{ab} \Delta T_{ab}\right) + \left(M_{sa} C_{sa} \Delta T_{sa}\right)\right], \tag{46}$$

where

F: frictional force (N)

v: velocity of specimen (m/min)

t: lapping time (min)

r: radius of sample

M_{air} : mass of air

C_{air} : specific heat capacity of air

ΔT_{air} : change temperature of air

M_{ab} : mass of abrasive

C_{ab} : specific heat capacity of abrasive

ΔT_{ab} : temperature change of abrasive

M_{sa} : mass of sample

C_{sa} : specific heat capacity of sample

ΔT_{sa} : temperature change of sample.

Specific heat capacity (specific heat) is the amount of heat (energy) per unit mass required to raise the temperature of a substance by one degree Celsius. The unit analysis for Equation (50) is expressed as:

$$F = \frac{v * t}{r} * \left(M * C * T\right) = \frac{(m * \min^{-1}) * (\min)}{m} * \left(Kg * \left(Jkg^{-1}K^{-1}\right) *^{o} F\right) = Newton$$

7.4.6 Motor Constant Model

The surface characteristics need to be examined at a fundamental level in order to examine friction in more detail. The embedding of abrasive particles on metal surfaces due to lapping presents some interest. According to Awtar and Craig (2004); Singer and Appelbaum (1993) motor torque is directly proportional to current as represented in

Equation (47). One horsepower (0.7457 kW) equals 36 lb-in (4. 1 Nm). This implies that 0.75 horsepower (0.56 kW) equals 27 lb-in (3.1 Nm). Therefore, the motor constant, K, at full load of 8 amperes was calculated using Equation (47).

$$T = K * i, \tag{47}$$

where

T: frictional torque

K: motor constant of lapping machine

i: current consumed during lapping.

$$K = \frac{T}{i} = \left(\frac{lb - in}{amp} \right) = 3.4 \text{ lb - in/amp or } (0.3842 \text{ Nm/amp})$$

The difference between the dry and wet run was used to evaluate the frictional torque (Appendices H and I). The initial torque, T_i, was estimated using Equation (48). Then the final torque, T_f, was calculated. Frictional force was determined by dividing the frictional torque with the radius of the specimen as shown in Equation (48). Coefficient of friction was calculated using Equation (49). A normal load of 24.9 N (5.6 lbf) was applied during the lapping operation.

$$F = \frac{\Delta T}{r}, \tag{48}$$

$$\mu = \frac{F}{\mathrm{N}}, \tag{49}$$

where

F : frictional force

r: radius of sample

Δ T : difference between wet and dry torque (frictional torque)

μ : coefficient of friction

N : Normal load.

Figures 49 to 51 delineate the plots of frictional force vs. time for wet run (i.e., the actual duration of the lapping operation). The slopes of the frictional force vs. time were positive, suggesting that more current was consumed as lapping progressed. Therefore, as the lapped surface became smoother with time, the higher area of contact resulted in an increased friction.

This was in agreement with the findings of Rabinowicz (1966); Garzino-Demo and Lama (1994). Rabinowicz (1966) stated that friction force is higher for smoother surfaces than for rougher surfaces since the actual area of contact for smoother surfaces is greater than that of rougher surfaces. Garzino-Demo and Lama (1994) evaluated the effects of friction and wear for coated and uncoated stainless steel; and for coated and uncoated aluminum. They concluded that smoother surface increased adhesion between two surfaces. This implied that an adhesive force had to be applied to the weight, hence causing abrasive wear, which eventually led to an increase in frictional force.

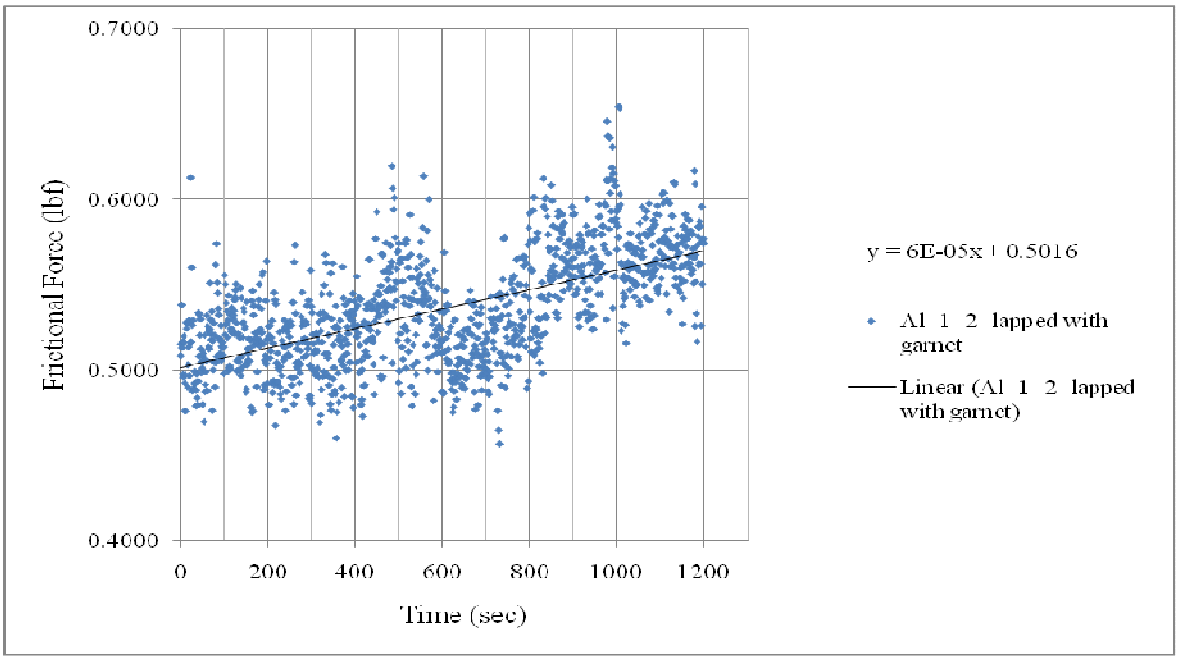

Figure 49a. Frictional Force vs. Time for Al 2024 Lapped with Garnet.

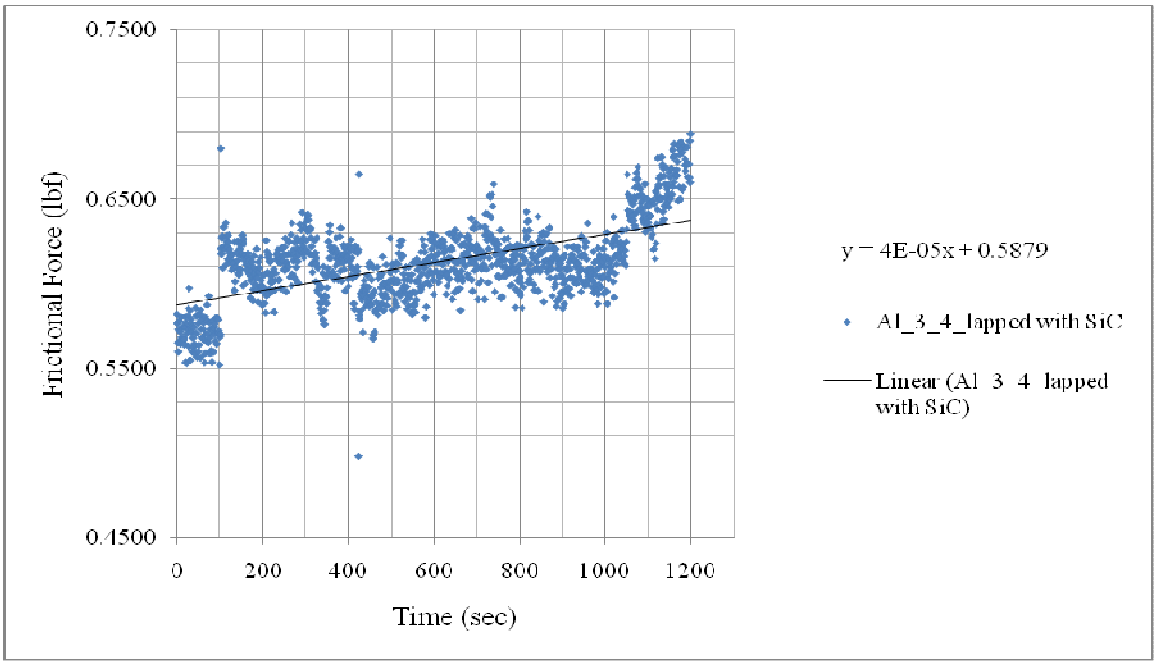

Figure 49b. Frictional Force vs. Time for Al 2024 Lapped with SiC.

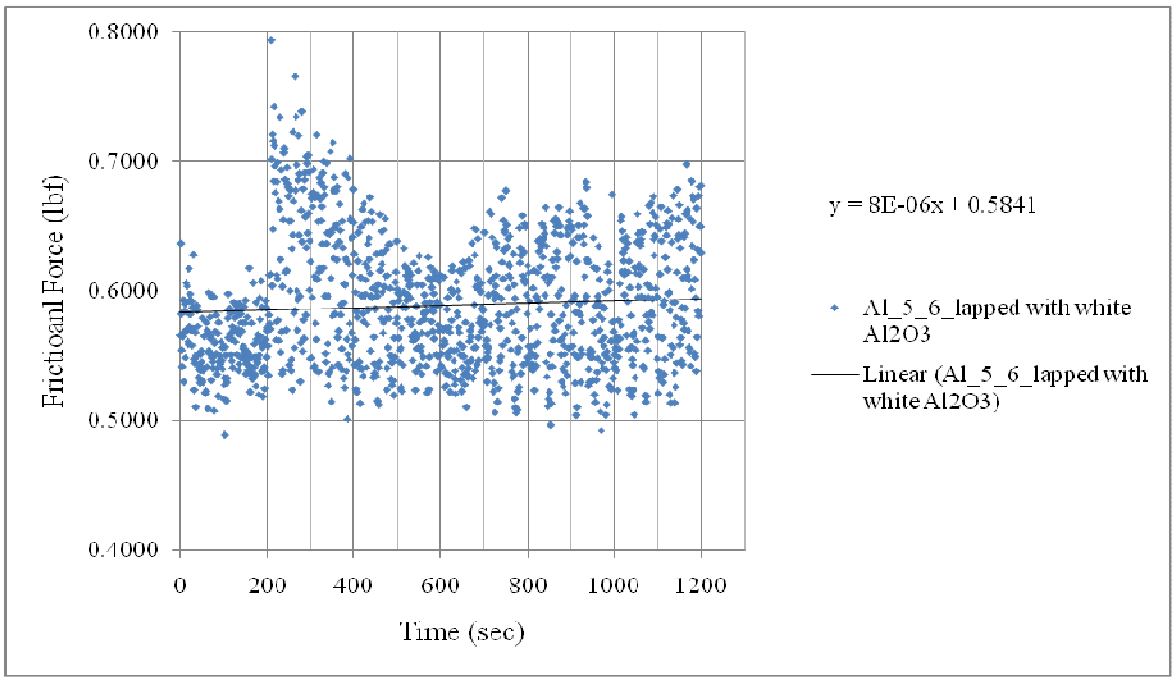

Figure 49c. Frictional Force vs. Time for Al 2024 Lapped with White Al_2O_3.

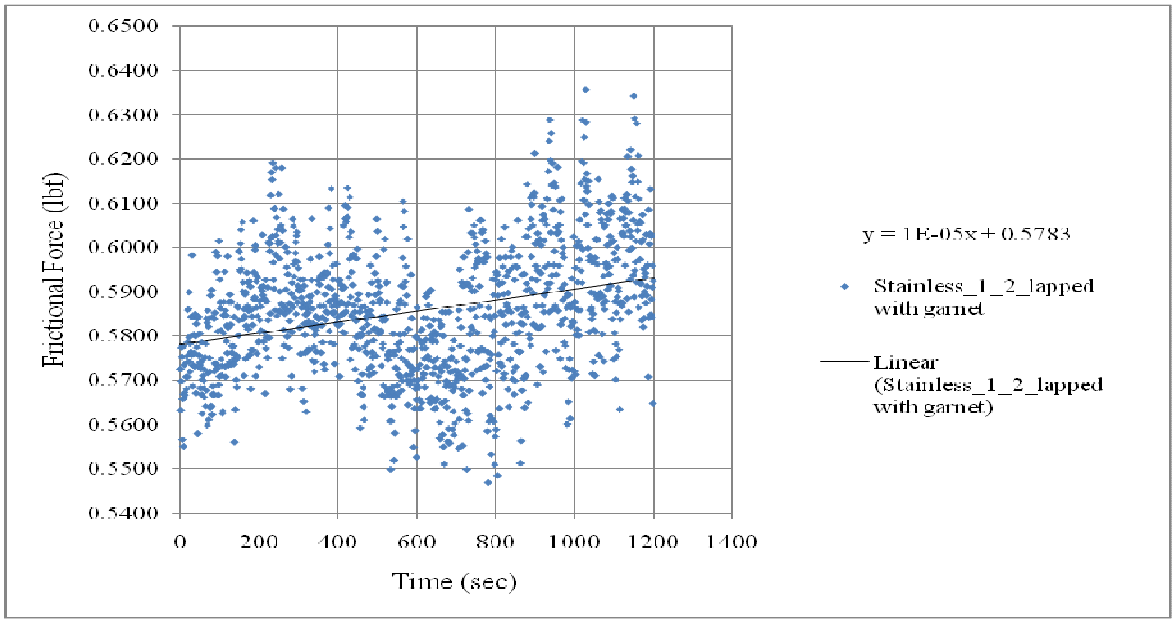

Figure 50a. Frictional Force vs. Time for 304 Stainless Steel Lapped with Garnet.

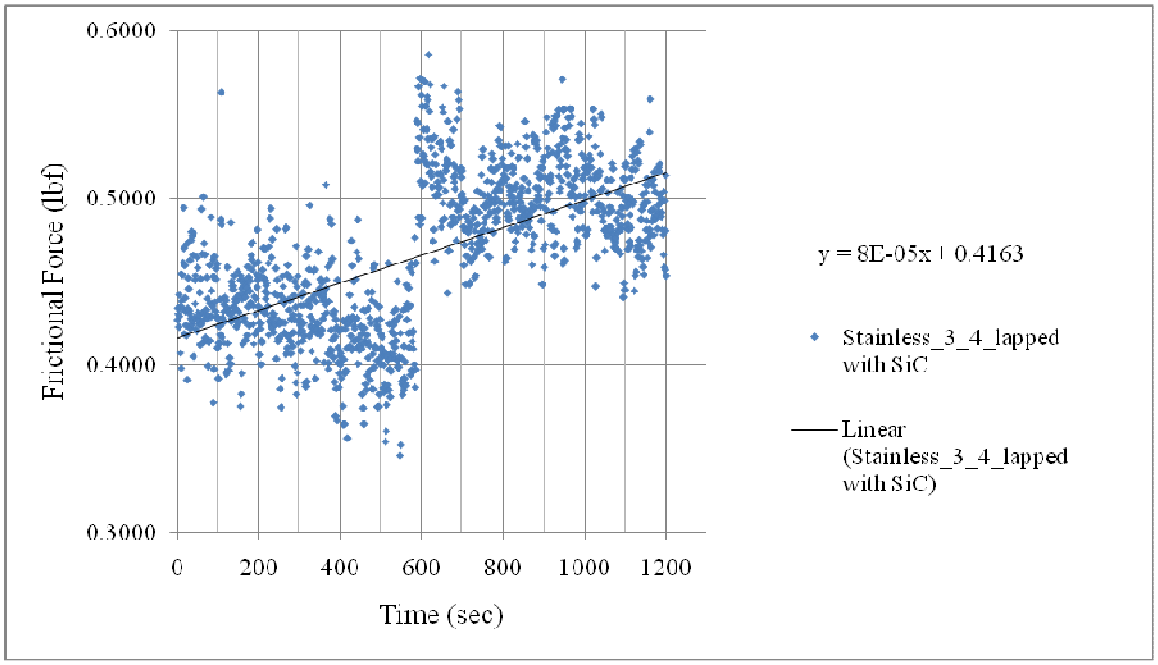

Figure 50b. Frictional Force vs. Time for 304 Stainless Steel Lapped SiC.

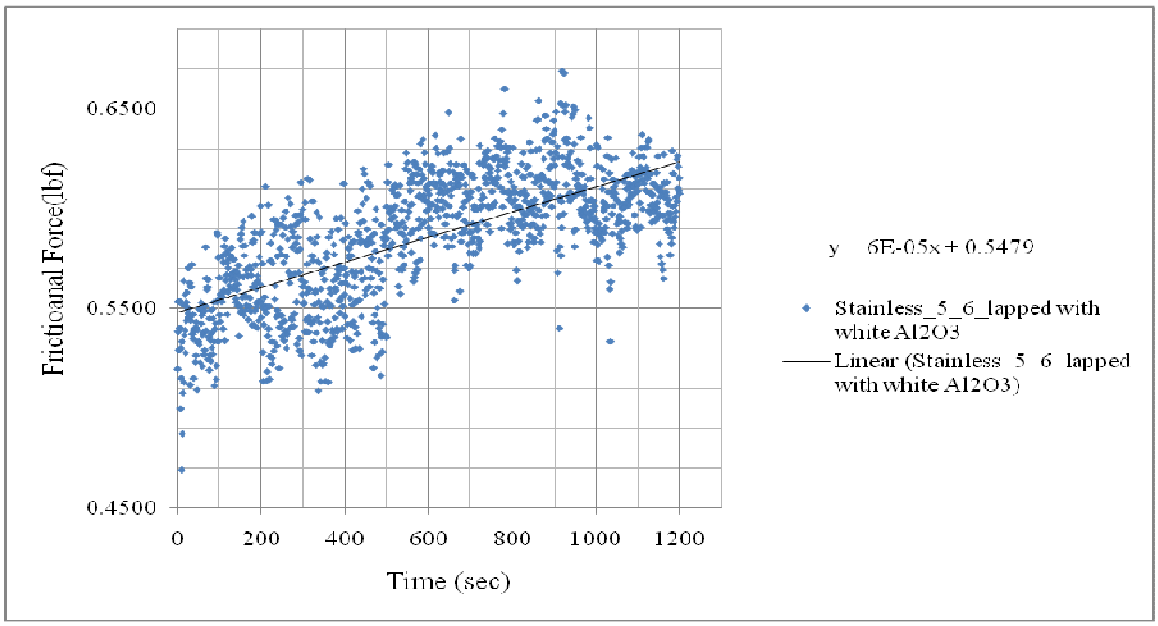

Figure 50c. Frictional Force vs. Time for 304 Stainless Steel Lapped with White Al_2O_3.

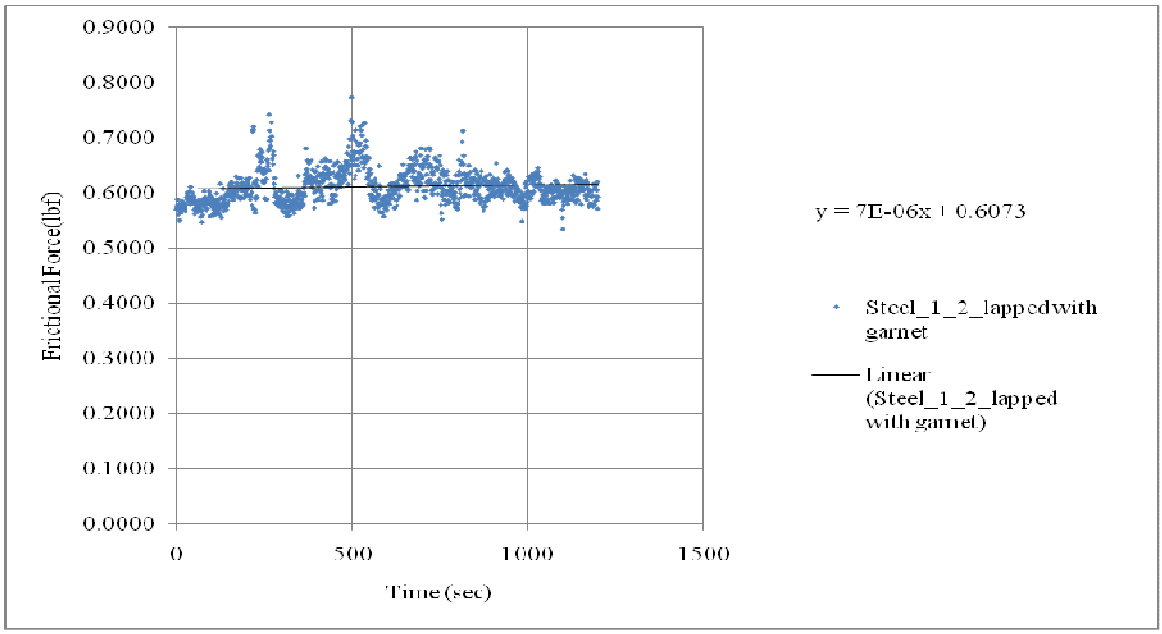

Figure 51a. Frictional Force vs. Time for 1018 Steel Lapped with Garnet.

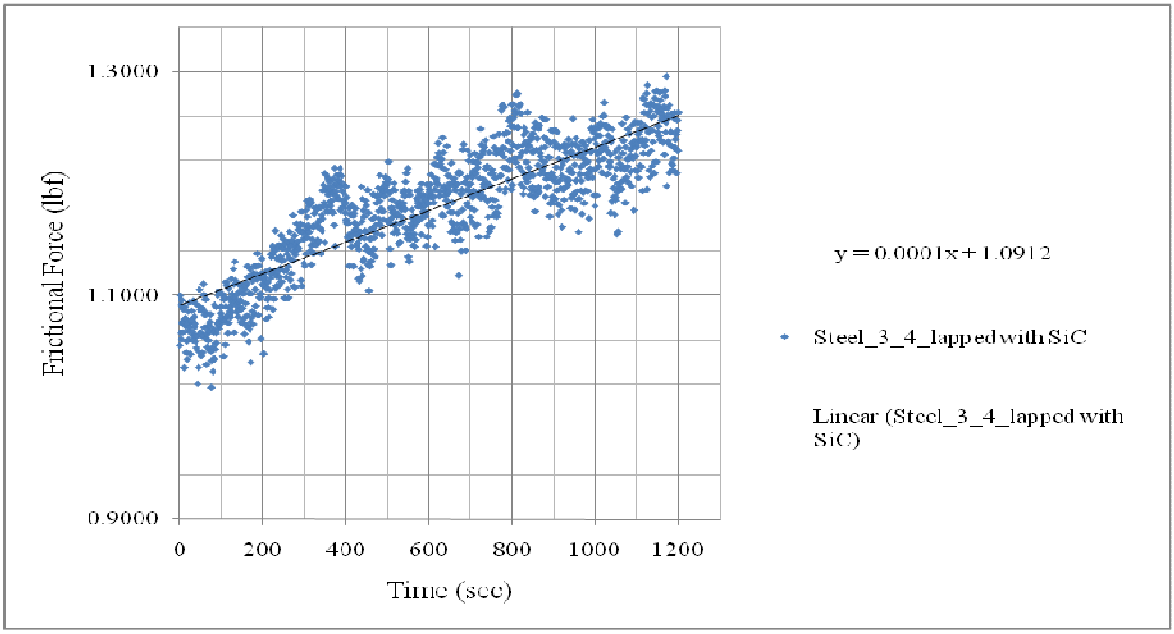

Figure 51b. Frictional Force vs. Time for 1018 Steel Lapped with SiC.

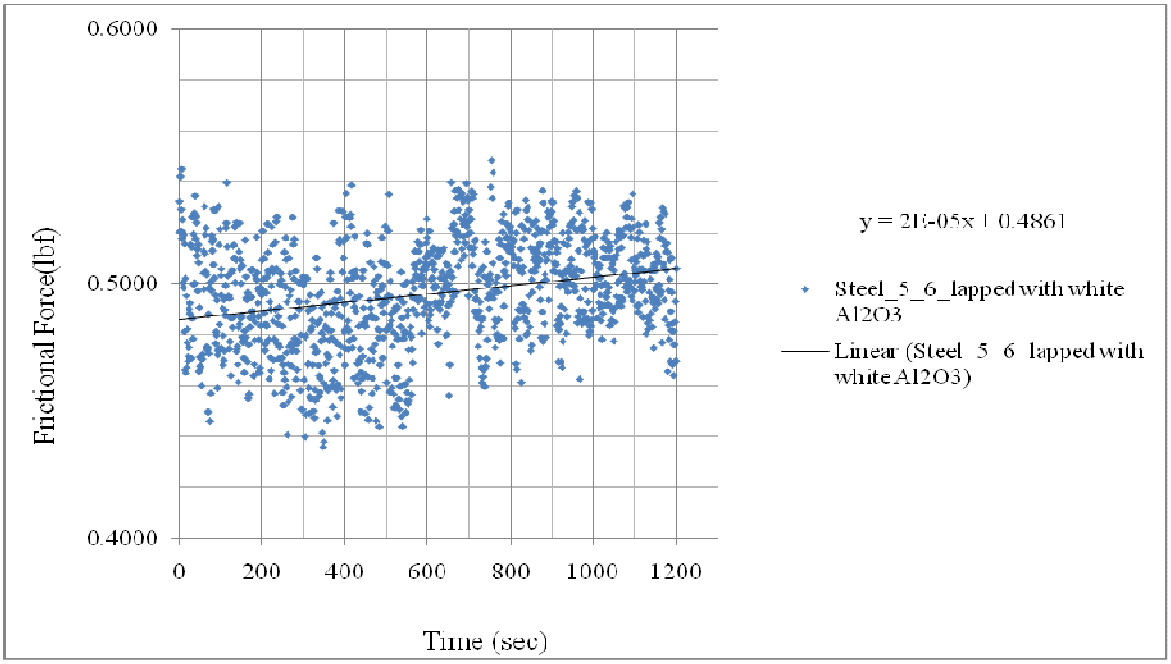

Figure 51c. Frictional Force vs. Time for 1018 Steel Lapped with White Al_2O_3.

The mean coefficient of friction obtained ranged from 0.0832 to 0.1094 as shown in Table 27, and this was in agreement with the reporting of (Kalpakjian, and Schmid, 2006) for cold working operation. According to their book, the coefficient of friction varies from 0.03 for a cold working to 0.7 for a hot working in metalworking processes. Also, the coefficient of friction varies from 0.5 to 2 for machining operations (Kalpakjian, and Schmid, 2006). Figure 52 depicts the plot of coefficient of friction vs. time for 1018 steel lapped with SiC.

Table 27. Mean Frictional Force and Mean Coefficient of Friction.

Material	Mean Frictional Force, lbf	Mean Coefficient of Friction, μ
Al 2024 lapped with garnet	0.5359	0.0957
Al 2024 lapped with SiC	**0.6126**	**0.1094**
Al 2024 lapped with white Al_2O_3	**0.5892**	**0.1052**
304 Stainless steel lapped with garnet	0.5865	0.1047
304 Stainless steel lapped with SiC	**0.4659**	**0.0832**
304 Stainless steel lapped with white Al_2O_3	0.5858	0.1046
1018 Steel lapped with garnet	0.5865	0.1047
1018 Steel lapped with SiC	0.5881	0.1050
1018 Steel lapped with white Al_2O_3	**0.4961**	**0.0886**

As would be expected, Al 2024 had a better surface finish, hence a higher area of contact. Therefore, the highest mean frictional force and mean coefficient of friction were obtained using aluminum lapped with SiC and white Al_2O_3 abrasives. In contrast, the lowest mean frictional force was obtained using 304 stainless steel lapped with SiC because the stainless steel had more scratches and there was less area of contact.

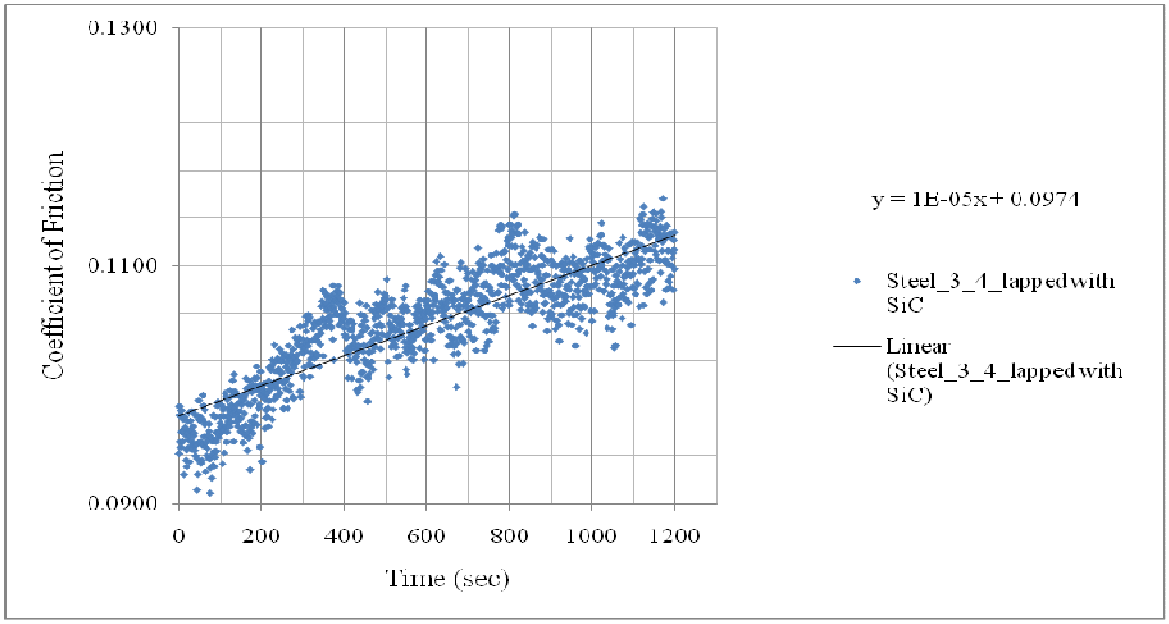

Figure 52. Coefficient of Friction of 1018 Steel Lapped with SiC vs. Time.

7.4.7 Three-body Wear Model in Flat Lapping of Metals

Bingley and Schnee (2005) assumed a square packing distribution for abrasive particles in order to determine a three-body abrasive wear in metals. As shown in Figure 16, the shapes of the abrasives are not square; therefore the assumption of Bingley and Schnee (2005) is relaxed and a cube is assumed in this research. A proper geometric shape for the abrasives is a cube. The maximum number of particle contacts with the sample, N_p, is given in Equation (50). Also, the cross-sectional area of indentations produced is considered to be independent of the number of particles. Rather it is directly proportional to the applied load, W, and inversely proportional to the hardness of the sample, H, as represented in Equation (51), (Schnee, 2005)

$$N_p = \frac{A_s}{d^2}, \tag{50}$$

$$A = \frac{W}{H}, \tag{51}$$

where

N_p: maximum number of particle contacts

A_s: cross-sectional area of sample

d: diameter of particles

A: cross-sectional area of indentations produced

W: normal load

H: hardness of work material.

Assuming the shape of the abrasive particles to be a cube, the total volume of indentation made is expressed in Equation (52), with the number of indentations made per particle given in Equation (53). Equation (54) represents the total volume of particle

indentations made in a sliding, s, and is obtained by combining Equations (52) through (54).

$$V = a^3 = Ah = \frac{Wh}{H}, \tag{52}$$

$$I_p = \frac{sc}{\pi d}, \tag{53}$$

$$V = \frac{Whsc}{\pi dH} = \frac{Ahsc}{\pi d} = \frac{a^3 sc}{\pi d}, \tag{54}$$

where

V: volume of indentations made at a given time (in^3/min)

h: height of a cube (i.e., for abrasive particles)

I_p: number of indentations per particle

s: sliding distance

c: number of sharp-corner contacts (i.e., indentations produced per rotation of particle).

7.5 Power Consumed in Lapping

The power consumed during lapping can be determined using Equations (55), (56), and (57). The lapping force used was 24.9 N (5.6 lbf).

$$\text{Power} = \frac{w}{t} \quad \text{(kw or hp)}$$

Work = f*d

Distance = v*t

Therefore, work = f*v*t

$$\text{Thus, Power} = \frac{f * v * t}{t} = f * v, \tag{55}$$

where

w: work

t: time

f: force

d: distance

D: diameter of sample (1 inch)

N: number of revolutions per minute

v: circumferential or cutting speed.

According to Metcut Research Associates Inc., (1980), power in English unit and metric unit are given in Equations (56) and (57), respectively.

$$\text{Power} = \frac{f * v}{33{,}000} \text{ (horsepower)}, \tag{56}$$

where

f : force (lbf)

v : velocity in ft/min.

$$\text{Power} = \frac{f * v}{60{,}000} \text{ (kilowatts)}, \tag{57}$$

where

f : force (Newton)

Normally, power consumed in friction has to be minimized in order to achieve an optimal and efficient lapping rate. If more power is used up in friction, then the lapping

operation will be become more difficult, and less efficient. According to Kalpakjian and Schmid (2006), torque, that is, turning, twisting or the moment of a force or system of forces tending to cause rotation is given in Equation (58). Torque is the force that produces rotation or torsion (twisting). In machinery, it is the ability of the rotating element to overcome turning resistance. It consists of product of force, and the perpendicular distance from the line of action of the force to the axis of rotation, hence the unit Newton meter. A metric unit of torque equals 0.01 Newton meter.

$$Torque = \frac{Power}{Rotational\ speed} = \frac{f * v}{2 * \pi * N} \tag{58}$$

where f is force, v is velocity, and N is number of revolutions per minute.

7.6 Finite Element Analysis

In order to determine the stress distribution when a normal load of 24.9 N (5.6 lbf) was applied on the specimen, Finite Element Analysis (FEA) was performed using Pro/Mechanica. As illustrated in Figures 53 through 55, the result obtained from FEA showed a maximum stress of 2.025 x 10^{-2} N/mm^2 at the edge of the samples. This high stress at the edges indicates a stress concentration. On the other hand, a minimum stress of 1.772 x 10^{-4} N/mm^2 was found on the inner ring of the cylinder. Some samples were lapped better at the edges than on the inner ring. This confirms the FEA results, which showed higher stress concentration at outer ring than the inner ring of the specimen. Appendix j shows FEA results for stress, strain, and displacement.

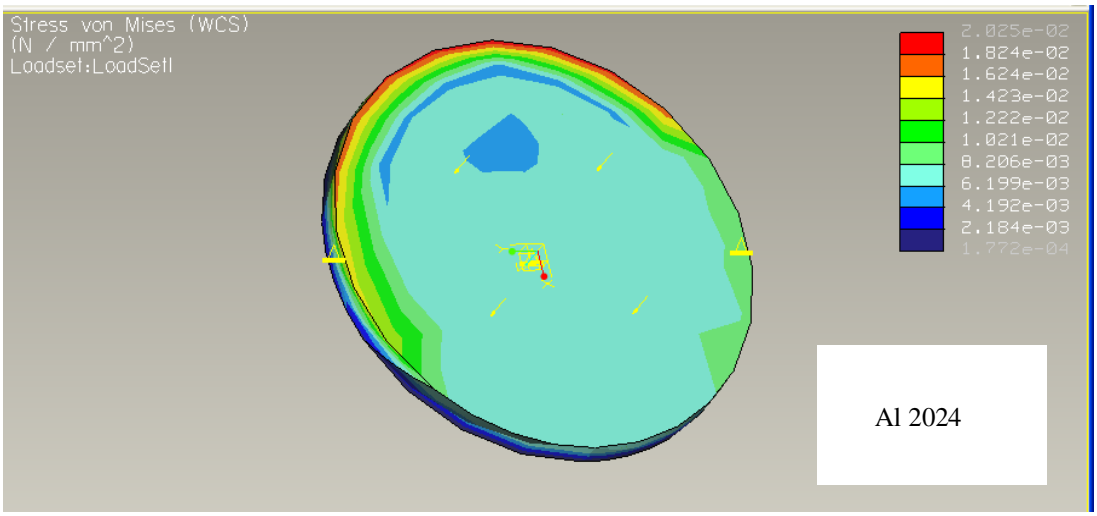

Figure 53. Von Mises Stress Map of Al 2024.

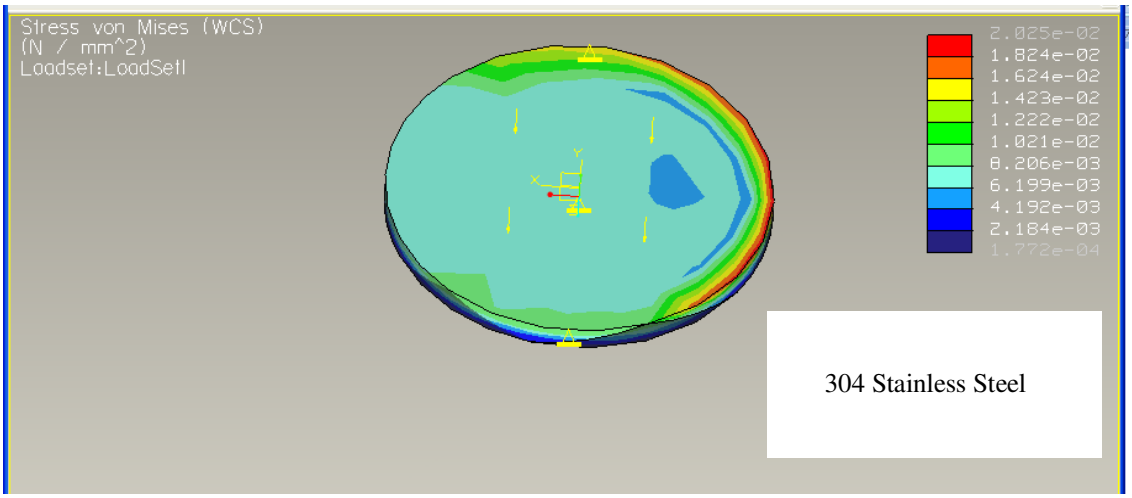

Figure 54. Von Mises Stress Map of 304 Stainless.

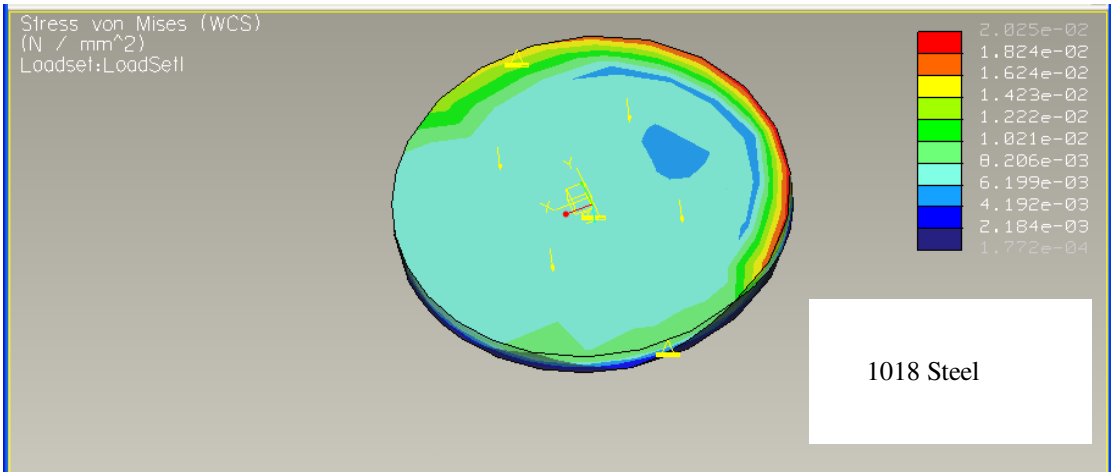

Figure 55. Von Mises Stress Map of 1018 Steel.

7.7 Redox Chemistry in Lapping

Oxidation occurs under any of the following conditions: when a molecule loses electrons, loses hydrogen, or gains oxygen. On the contrary, **reduction** happens when a molecules gains electrons, gains hydrogen, or loses oxygen. Redox reactions (oxidation-reduction reactions) are similar to acid-base reactions. Therefore, every redox reaction must have an oxidant and a reductant. Redox reactions are concerned with the transfer of electrons between species. In a redox reaction, oxidation and reduction reactions take place simultaneously. A pH paper was used to determine if the abrasive slurry was acidic or basic. Garnet and SiC abrasives have a pH of 6 (weak acids), while the pH of white Al_2O_3 abrasive is 8 (weak base).

Half-reactions of the abrasive elements and the alloying elements are presented in Table 28 (Harris, 2007; Lide, 2002; Greenwood, 1997). These reactions are reversible. The purpose of investigating the redox chemistry in lapping is to determine if there are

any possible reactions between the abrasives and the metal alloys. If the abrasives react with the work materials, this can affect the material removal rate and the type of surface finish obtained after lapping. Moreover, a chemical reaction between the abrasives and the workpiece could produce toxic chemicals as can be seen in the redox chemistry of metal alloys containing sulfur (304 stainless steel) presented in Table 28. If the difference between the standard redox potential of the abrasives and the metal alloying element were to be positive, hydrogen sulfide, which is toxic, could have been produced during the lapping process.

Table 28. Redox Chemistry of White Al_2O_3 Abrasives and Metal Alloys.

Redox Reactions of White Al_2O_3 Abrasives with Al 2024, 304 Stainless, and 1018 Steel	**Standard Potential, E^o (volts)**	**Net Potential, E (volts)**
$Al^{3+} + 3e^- \rightarrow Al(s)$	**-1.677***	**-**
$FeOH^+ + H^+ + 2e^- \rightarrow Fe(s) + H_2O$	-0.16	-1.704
$Cu^+ + e^- \rightarrow Cu(s)$	0.518	-1.968
$Cu^{2+} + 2e^- \rightarrow Cu(s)$	0.339	-1.966
$Cu(OH)_2(s) + 2e^- \rightarrow Cu(s) + 2OH^-$	-0.222	-0.518
$C(s) + 4H^+ + 4e^- \rightarrow CH_4$	-1.583	0.1315
$Mn^{2+} + 2e^- \rightarrow Mn(s)$	-1.182	-0.445
$Mn(OH)_2(s) + 2e^- \rightarrow Mn(s) + 2OH^-$	-1.565	-0.417
$Mg(OH)^+ + H^+ + 2e^- \rightarrow Mg(s) + H_2O$	-2.022	**0.356***
$Mg(OH)_2(s) + 2e^- \rightarrow Mg(s) + 2OH^-$	-2.690	**1.950***
$Mg^{2+} + 2e^- \rightarrow Mg(s)$	-2.360	**0.603***
$Cr^{3+} + 3e^- \rightarrow Cr(s)$	-0.74	-0.946
$Cr^{2+} + 2e^- \rightarrow Cr(s)$	-0.89	-0.737
$TiO_2(s) + 4H^+ + 4e^- \rightarrow Ti(s) + 2H_2O$	-1.076	-1.113
$Ti^{2+} + 2e^- \rightarrow Ti(s)$	-1.60	-0.027
$H_3PO_4 + 5H^+ + 5e^- \rightarrow 1/4P_4(s, \text{white}) + 4H_2O$	-0.402	-1.805
$H_3PO_2 + H^+ + e^- \rightarrow 1/4P_4(s) + 2H_2O$	-0.51	-1.413
$Ni^{2+} + 2e^- \rightarrow Ni(s)$	-0.236	-1.391
$Ni(OH)_2(s) + 2e^- \rightarrow Ni(s) + 2OH^-$	-0.714	-1.268
$V^{2+} + 2e^- \rightarrow V(s)$	-1.125	-0.501
$Zn^{2+} + 2e^- \rightarrow Zn(s)$	-0.762	-0.865
$ZnOH^+ + H^+ + 2e^- \rightarrow Zn(s) + H_2O$	-0.497	-1.367
$Zn(OH)_3^- + 2e^- \rightarrow Zn(s) + 3OH^-$	-1.183	-0.977
$Zn(OH)_4^{2-} + 2e^- \rightarrow Zn(s) + 4OH^-$	-1.199	-1.138
$ZnO(s) + H_2O + 2e^- \rightarrow Z(s) + 2OH^-$	-1.405	-2.432
$MoO_2(s) + 2H_2O + 4e^- \rightarrow Mo(s) + 4OH^-$	-2.610	-0.980
$SiO_2(s, \text{quartz}) + 4\text{H}^+ + 4e^- \rightarrow Si(s) + 2H_2O$	-0.990	-1.144
$S(s) + 2H^+ + 2e^- \rightarrow +H_2S(aq)$	0.144	-1.475
$SO_4^{2-} + 4H_2O + 6e^- \rightarrow S(s) + 8OH^-$	-0.751	-1.468
$SO_2 + 4H^+ + 4e^- \rightarrow S(s) + 2H_2O$	0.450	-2.639

The abbreviations "aq" and "s" denote aqueous or solid, respectively. The symbol "e-" represents a free electron with a negative charge, which can reduce some other species such as in the half-reaction. E^o is the standard reduction potential in volts at 25˚ C (298˚ K) and atmospheric pressure. The notation, (*) represents reactions with a net positive cell reaction potential, E.

A reaction will occur if the net potential between the standard reduction potential of the elements of the abrasive in aqueous solution and that of the solid metals is positive. A spontaneous reaction occurs at standard conditions (i.e., 25 degrees Celsius and atmospheric pressure). On the other hand, if the difference between the potential is negative, the reaction tends to stay as reactants and does not form the products. The half-reactions in Equations (59) and (60) show that aluminum ion and magnesium ion (with positive charges) are being reduced through the addition of three electrons and two electrons, respectively to form solid aluminum and magnesium solid, respectively. The possible reactions with white Al_2O_3 abrasives are reactions with magnesium and its hydroxides as represented in Equations (64) and (65).

$$Al^{3+} + 3e^- \rightarrow Al(s), \mathrm{E}^0 = -1.677 \text{ volts} \tag{59}$$

$$\mathrm{Mg}^{2+} + 2e^- \rightarrow Mg(s), \mathrm{E}^0 = -2.360 \text{ volts} \tag{60}$$

Therefore, (-1.677) - (-2.360) = +0.683 volts.

The two half-reactions in Equations (59) and (60) are combined to form a redox reaction in Equation (61), a balanced reaction showing six electrons each on left/right half-cell reactions. Equation (61) indicates that solid magnesium (with no charge) is being oxidized (losing two electrons) to form a magnesium ion with a +2 charge, while aluminum ion with a positive charge is reduced to aluminum solid. Al^{3+} from the white

Al_2O_3 abrasives is the oxidizing agent because it causes Mg(s) to lose electrons, while Mg(s) is the reducing agent because it causes Al^{3+} to gain electrons. These reactions are possible when Al 2024 is lapped with white Al_2O_3 since Al 2024 contains magnesium.

$$2Al^{3+} + 3Mg(s) \rightarrow 2Al(s) + 3Mg^{2+} \quad (61)$$

The Nernst equation was used to find out if any of the metal solids reacted as the anode with the aluminum abrasive ion as the cathode. This means that the metal solid would be giving up its electrons to the aluminum abrasive ion. First, the concentration of Al^{3+} in distilled water was determined as stated below:

$$Al_2O_3 + 3H_2O \rightarrow 2Al^{3+} + 6OH^-$$

pH of Al_2O_3 = 8

$$Al^{3+} \text{ Concentration} = [10^{-6}] * \frac{[2 \text{ moles of } Al^{3+}]}{[6 \text{ moles of OH}]} = 3.3333\, x 10^{-7} \text{ moles}$$

If the difference between the two half-cell potentials ($E_{cathode}$ and $E_{anode)}$ is positive, then the reaction is spontaneous in the forward direction. For example, the half-reactions of white aluminum oxide abrasive and copper are given as:

$$E_{cell} = E_{cathode} - E_{anode}$$

(**Nernst equation)**

$$Al^{3+} + 3e^- \rightarrow Al(s)$$

$$Cu^+ + e^- \rightarrow Cu(s)$$

A complete Nernst equation of the reaction is represented in Equation (62), (Harris, 2007). If there is hydrogen ion concentration $[H^+]$, then Equation (62) changes to Equation (63).

$$E_{cell} = \left(E^0 - \left(\frac{0.05916}{n} \right) * \log(half\ reaction) \right) - \left(E_M^0 - \frac{0.05916}{n} * \log(half\ reaction) \right) \tag{62}$$

$$E_{cell} = \left(E_{Al}^0 - \left(\frac{0.05916}{n} \right) * \log\left(\frac{1}{[Al^{3+}]} \right) \right) - \left(E_M^0 - \frac{0.05916}{n} * \log(half\ reaction) \right)$$

$$\left(1.677 - \left(\frac{0.05916}{3} \right) * \log\left(\frac{1}{[Al^{3+}]} \right) \right) - \left(E_M^0 - \left(\frac{0.05916}{n} \right) * \log(half\ reaction) \right)$$

$$\left(-1.677 - \left(\frac{0.05916}{3} \right) * \log\left(\frac{1}{[3.3333\,x10^{-7}]} \right) \right) - \left(0.518 - \left(\frac{0.05916}{1} \right) * \log \frac{1}{[Cu^+]} \right)$$

$$\left(-1.677 - \left(\frac{0.05916}{3} \right) * \log\left(\frac{1}{[3.3333\,x10^{-7}]} \right) \right) - \left(0.518 - \left(\frac{0.05916}{1} \right) * \log \frac{1}{[10^{-6}]} \right)$$

For white aluminum oxide abrasive and phosphorus, the half-reactions are given as:

$$Al^{3+} + 3e^- \rightarrow Al(s)$$

$$H_3PO_4 + 5H^+ + 5e^- \rightarrow 1/4P_4(s, \text{white}) + 4H_2O$$

$$\left(-1.677 - \left(\frac{0.05916}{3} \right) * \log\left(\frac{1}{[3.3333\,x10^{-7}]} \right) \right)$$

$$- \left(0.402 - \left(\frac{0.05916}{5} \right) * \log\left(\frac{1}{[H_3PO_4\ ] * [H^+]^C} \right) \right) \tag{63}$$

$$\left(-1.677 - \left(\frac{0.05916}{3} \right) * \log\left(\frac{1}{[3.3333\,x10^{-7}]} \right) \right)$$

$$- \left(0.402 - \left(\frac{0.05916}{5} \right) * \log\left(\frac{1}{[1x10^{-6}] * [1x10^{-8}]^5} \right) \right)$$

where

Cathode: electrode where reduction occurs

Anode: electrode where oxidation occurs

E^o: standard reduction potential (in volts at 298° K)

E_{cell} or E: net cell reaction potential

s: solid

n: number of electrons transferred in a half-reaction

Half-reaction: product/reactant

M: metal

C: coefficient of $[H^+]$

$[H_3PO_4]$: 1 x 10^{-6} moles

$[H^+]$: 1 x 10^{-8} (pH of abrasive)

Note: Spontaneous reaction occurs at room temperature (25 degrees Celsius) and atmospheric pressure. Solids and water are not considered as products in the Nernst equation.

The only possible reactions are those occurring between magnesium and its hydroxides and white aluminum oxide abrasive since they have positive net potential as presented in Table 28. The three reactions with positive net potentials in Table 28 indicate that each could have occurred during the lapping process. If net E > 0, then net cell reaction is spontaneous in the forward direction and vice versa. The balanced cell reactions of magnesium hydroxides and Al_2O_3 abrasives are stated below.

Half-cell reactions

$Al^{3+} + 3e^- \rightarrow Al(s), \mathrm{E}^0 = -1.677$ volts

$\mathrm{Mg}^{2+} + 2e^- \rightarrow Mg(s), \mathrm{E}^0 = -2.360$ volts

$$Mg(OH)^{+} + H^{+} + 2e^{-} \rightarrow Mg(s) + H_2O, \mathrm{E}^0 = -2.022 \text{ volts}$$

$$Mg(OH)_2(s) + 2e^{-} \rightarrow Mg(s) + 2OH^{-}, \mathrm{E}^0 = -2.690 \text{ volts}$$

Balanced net cell reactions

$$2\mathrm{Al}^{3+} + 3Mg(s) \rightarrow 2Al(s) + 3Mg^{2+}, \text{Net E} = +0.603$$

$$2Al^{3+} + 3Mg(s) + 3H_2O \rightarrow 2Al(s) + 3Mg(OH)^{+} + 3H^{+}, \ Net \text{ E} = +0.356 \qquad (64)$$

$$2Al^{3+} + 3Mg(s) + 6OH^{-} \rightarrow 2Al(s) + 3Mg(OH)2(s), Net \text{ E} = +1.950 \qquad (65)$$

The reaction of SiC with water and air is represented in Equation (66). Silicon does not undergo a redox reaction. Its oxidation state is +4 in the SiC and remains +4 in the SiO_2. The redox species in this reaction are the carbon and the oxygen. The carbon is oxidized from -4 in the SiC to +4 oxidation state in the H_2CO_3, and the oxygen from O_2 is reduced from 0 to -2 oxidation state. The only pertinent reaction in the product is the SiO_2 as stated in Equation (66).

$$SiC + H_2O + 2O_2 \rightarrow SiO_2 + H_2CO_3 \qquad (66)$$

$$SiO_2(s, \text{quartz}) + 4\mathrm{H}^{+} + 4e^{-} \rightarrow Si(s) + 2H_2O, \mathrm{E}^0 = -0.990 \text{ volts} \qquad (67)$$

To calculate the net reduction potential of the half-reaction in Equation (68), the Nernst equation (62) was used. The cathode is the SiO_2 reaction and the various anodes are the metal ion reactions as seen in Table 29**.** The pH of SiC abrasive is 6, which is the H^{+} concentration. The Nernst equation for SiO_2 is stated in Equation (68).

$$E_{cell} = \left(-0.990 - \left(\frac{0.05916}{n}\right) * \log\left(\frac{1}{[H^{+}]^4}\right)\right) - \left(E_M^0 - \frac{0.05916}{n} * \log(half\ reaction)\right) \qquad (68)$$

$$E_{cell} = \left(-0.990 - \left(\frac{0.05916}{4}\right) * \log\left(\frac{1}{[1x10^{-6}]^4}\right)\right) - \left(E_M^0 - \frac{0.05916}{n} * \log(half\ reaction)\right)$$

Table 29. Redox Chemistry of SiC Abrasives and Metal Alloys.

Redox Reactions of SiC Abrasives with Al 2024, 304 Stainless, and 1018 Steel	**Standard Potential, E^o (volts)**	**Net Potential, E (volts)**
$Al^{3+} + 3e^- \rightarrow Al(s)$	-1.677	**0.450***
$FeOH^+ + H^+ + 2e^- \rightarrow Fe(s) + H_2O$	-0.16	-1.244
$Cu^+ + e^- \rightarrow Cu(s)$	0.518	-1.508
$Cu^{2+} + 2e^- \rightarrow Cu(s)$	0.339	-1.506
$Cu(OH)_2(s) + 2e^- \rightarrow Cu(s) + 2OH^-$	-0.222	-0.058
$C(s) + 4H^+ + 4e^- \rightarrow CH_4$	-1.583	-1.123
$Mn^{2+} + 2e^- \rightarrow Mn(s)$	-1.182	**0.015***
$Mn(OH)_2(s) + 2e^- \rightarrow Mn(s) + 2OH^-$	-1.565	**0.043***
$Mg(OH)^+ + H^+ + 2e^- \rightarrow Mg(s) + H_2O$	-2.022	**0.816***
$Mg(OH)_2(s) + 2e^- \rightarrow Mg(s) + 2OH^-$	-2.690	**2.410***
$Mg^{2+} + 2e^- \rightarrow Mg(s)$	-2.360	**1.063***
$Cr^{3+} + 3e^- \rightarrow Cr(s)$	-0.74	-0.487
$Cr^{2+} + 2e^- \rightarrow Cr(s)$	-0.89	-0.277
$TiO_2(s) + 4H^+ + 4e^- \rightarrow Ti(s) + 2H_2O$	-1.076	-0.654
$Ti^{2+} + 2e^- \rightarrow Ti(s)$	-1.60	**0.433***
$H_3PO_4 + 5H^+ + 5e^- \rightarrow 1/4P_4(s, \text{white}) + 4H_2O$	-0.402	-1.345
$H_3PO_2 + H^+ + e^- \rightarrow 1/4P_4(s) + 2H_2O$	-0.51	-0.953
$Ni^{2+} + 2e^- \rightarrow Ni(s)$	-0.236	-0.931
$Ni(OH)_2(s) + 2e^- \rightarrow Ni(s) + 2OH^-$	-0.714	-0.808
$V^{2+} + 2e^- \rightarrow V(s)$	-1.125	-0.041
$Zn^{2+} + 2e^- \rightarrow Zn(s)$	-0.762	-0.405
$ZnOH^+ + H^+ + 2e^- \rightarrow Zn(s) + H_2O$	-0.497	-0.907
$Zn(OH)_3^- + 2e^- \rightarrow Zn(s) + 3OH^-$	-1.183	-0.517
$Zn(OH)_4^{2-} + 2e^- \rightarrow Zn(s) + 4OH^-$	-1.199	-0.678
$ZnO(s) + H_2O + 2e^- \rightarrow Z(s) + 2OH^-$	-1.405	-1.972
$MoO_2(s) + 2H_2O + 4e^- \rightarrow Mo(s) + 4OH^-$	-2.610	-2.150
$SiO_2(s, \text{quartz}) + 4\text{H}^+ + 4e^- \rightarrow Si(s) + 2H_2O$	-0.990	-
$S(s) + 2H^+ + 2e^- \rightarrow +H_2S(aq)$	0.144	-1.016
$SO_4^{2-} + 4H_2O + 6e^- \rightarrow S(s) + 8OH^-$	-0.751	-1.008
$SO_2 + 4H^+ + 4e^- \rightarrow S(s) + 2H_2O$	0.450	-2.180

The significance of the reaction between aluminum ion abrasive and magnesium is that some Mg^{2+} ions are released into the solution (abrasive slurry) from the solid Mg in the steel. Also, some solid aluminum will be plated out. This aluminum solid could adhere to the steel metal substrate, or it might stay suspended as a particle in the slurry. In either case, the impact is likely to be very small since the concentration of aluminum ion is low, and the magnesium solid is only a part of the composition of the steel.

Silicon dioxide oxidized the Al(s), Mg(s), Mn(s), and Ti(s) in Al 2024 to form the Si(s) as shown in Equations (69) to (73). In addition, SiO_2 oxidized the Mn(s) in 304 stainless steel and 1018 steel. SiO_2 reacted with Mg(s) in Al 2024 to form $Mg(OH)_2$(s). Also, because the reduction potential for the reaction that produces $Mg(OH)_2$(s) is so much larger than all the rest, this is the predominant reaction (i.e., it is the only reaction that occurs to any significant extent).

$$3SiO_2(s, \text{quartz}) + 12\text{H}^+ + 4Al(s) \rightarrow 4Al^{3+} + 3Si(s) + 6H_2O, Net\ \text{E} = +0.450 \quad (69)$$

$$SiO_2(s, \text{quartz}) + 4\text{H}^+ + 2Mn(s) \rightarrow 2Mn^{2+} + Si(s) + 2H_2O, Net\ \text{E} = +0.015 \quad (70)$$

$$SiO_2(s, \text{quartz}) + 4\text{H}^+ + 2Mg(s) \rightarrow 2Mg^{2+} + Si(s) + 2H_2O, Net\ \text{E} = +1.063 \quad (71)$$

$$SiO_2(s, \text{quartz}) + 4\text{H}^+ + 2Ti(s) \rightarrow 2Ti^{2+} + Si(s) + 2H_2O, Net\ \text{E} = +0.433 \quad (72)$$

$$SiO_2(s, \text{quartz}) + 2\text{H}^+ + 2Mg(s) \rightarrow 2Mg(OH)^+ + Si(s), Net\ \text{E} = +0.816 \quad (73)$$

Alternatively, a reaction can be spontaneous (clearly favored) if the Gibbs free energy is negative, that is, ΔH is a negative (heat is given off) and ΔS is a positive (more disorder of the system) as represented in Equation (74). Furthermore, there is a relationship between the potential of a reaction and the change in free energy as stated in Equation (76), (Harris, 2007).

$$\Delta G = \Delta H - \Delta(TS), \quad (74)$$

$$\Delta G = -nFE, \tag{75}$$

where

ΔG : change in Gibbs free energy (joules),

ΔH : *enthapy* (joule),

T: temperature (Kelvin),

S: joule per Kelvin,

n: number of electrons (mol electrons),

F: Faraday's constant (96485 Coulombs / mol electrons),

E: net potential of the reaction.

For example, from Equation (71), the change in free energy can be calculated using Equation (75).

$$\Delta G = -(4 \text{ mol electron}) * (9.649 x 10^4 \text{ Coulombs/mol})(1.063 \text{ volts})$$

$$\Delta G = -410275.48 \text{ Coulombs volts}$$

Since volts is in joules/Coulomb, ΔG equals -410.2755 KJ, which implies a favored reaction.

CHAPTER 8

CONCLUSIONS and RECOMMENDATIONS

8.1 Forces in Sliding Friction

Monitoring frictional force during a lapping operation is vital because current increases as friction increases and this implies that power consumption increases as well. Frictional force during the flat lapping of aluminum 2024, 304 stainless steel, and 1018 steel was determined by converting the current consumed in lapping to frictional torque. The slopes of the frictional force vs. time were found to be positive. This suggests more current was consumed as lapping progressed. Therefore, as the lapped surface became smoother with time, both the area of contact and friction increased. Rather than installing a rotary torque sensor on the lapping machine, this method serves as a relatively cheap and easy procedure for calculating frictional force. This method is introduced in this research as a cheaper alternative to existing torque and force determination methods.

The resulting mean coefficient of friction ranged from 0.0832 to 0.1094. This was in agreement with the report in literature for cold working operations. The normal force was very low and consequently coulombic friction can be used to quantify frictional force. The cold working range for coefficient of friction is expected since there is no apparent deformation and flow of material at the frictional interface. As would be expected, Al 2024 had a better surface finish, hence a higher area of contact. Therefore, the highest mean frictional force and mean coefficient of friction were obtained using Al 2024 lapped with SiC and white Al_2O_3 abrasives. In contrast, the lowest mean frictional

force was obtained using 304 stainless steel lapped with SiC because the stainless had more scratches and there was less area of contact.

Overall, the frictional force obtained was minimal. Frictional force is a function of sliding velocity, properties of work material, contact area, and surface finish of the workpiece. The more power consumed in friction, the higher the cost of lapping. However, an abrasive slurry acts as a lubricant which reduces the frictional force.

8.2 Three-body Friction Defects

The friction in lapping has been proposed in literature as a three-body friction because the abrasive grains, specimen, and lapping plate move in relation to one another. The friction between the abrasive particles, lapping plate, and sample caused scratches or voids on some samples. In addition, the friction between the lapping plate, sample, and abrasive particles caused abrasive wear and fatigue on the lapping plate after a period of time. Three-body abrasive wear occurs in loose abrasive techniques such as buffing, lapping, and ultrasonic machining. Two-body wear occurs when loose abrasives become embedded in the lapping plate as well as in fixed abrasive machining processes such as grinding, honing, polishing, rotary ultrasonic machining, and wire brushing. Wear rate is inversely proportional to hardness of lapping plate material, workpiece, and abrasive grain particles.

Based upon results obtained using ANOVA, the main effects of size and type of abrasives, along with the type of work materials used had a statistically significant effect on the MRR and surface finish of the work materials. Furthermore, there was a

significant two-way interaction of abrasives by work materials. However, the three-way interaction did not produce any significant effect.

8.3 Effects of Lapping Parameters

Finite element analysis (FEA) showed a maximum stress of 2.025×10^{-2} N/mm^2 at the edge of the samples. On the other hand, a minimum stress of 1.772×10^{-4} N/mm^2 was found on the inner ring of the cylinder. Experimentally, some samples were lapped better at the edges than on the inner ring, confirming the FEA trends.

8.4 Qualitative Observation of the Interface

Material removal rate (MRR) during a lapping operation is a function of abrasive grain size, the type of workpiece, lapping pressure, speed, time, and lapping plate. MRR is directly proportional to lapping pressure, speed, and time. However, MRR is inversely proportional to the hardness of the work material. During tests, silicon carbide and white aluminum oxide abrasives were able to remove more material per minute than a softer garnet abrasive. Therefore, it is necessary to evaluate the influence of all the listed independent variables during a lapping operation. Cheap abrasives that could achieve high MRR should be used in a lapping operation, and MRR should not adversely affect the dimensional accuracy which is required.

Geometric and Energy Dispersive Spectroscopy (EDS) analysis obtained through an SEM confirmed that some abrasives became embedded in the lapped samples. After lapping with garnet, silicon carbide, and white aluminum oxide abrasives, chemical components such as calcium and oxygen were detected on the specimens. The geometric

and EDS analyses showed that more white aluminum oxide abrasives became embedded into the metal substrates than garnet and silicon carbide abrasive particles.

Metal samples lapped with SiC and white Al_2O_3 abrasives resulted in embedding, while in 304 stainless lapped with white Al_2O_3 abrasives resulted in grooves. Furthermore, microvoids were observed in 1018 steel lapped with SiC. These grooves and microvoids occurred as a result of two-body wear due to abrasion or adhesion. More interestingly, there were neither microvoids nor grooves observed in the samples lapped with garnet. This trend could have occurred because garnet is softer than SiC and white Al_2O_3 abrasives. Since 304 stainless steel and 1018 steel are metals (ductile materials), the dominant mode of abrasive wear is plastic deformation. There was originally only a small amount of oxygen in the composition of Al 2024, but when the metal was oxidized, aluminum oxide formed. This is similar to stainless steel which may develop a thin hard protective film of chromium oxide on its surface which prevents oxidation or corrosion. If the protective film of chromium oxide is scratched, a new adherent film of chromium oxide film begins to form again.

Overall, white Al_2O_3 yielded the best surface finish and garnet yielded the worst surface finish. Al 2024 had a better surface finish than 304 stainless and 1018 steel. This could be because Al 2024 is softer than both 304 stainless steel and 1018 steel. Therefore, it was easier to improve the surface finish of Al 2024. The highest amount of material was removed from Al 2024, followed by 304 stainless and 1018 steel. This trend follows logically because Al 2024 was the softest of the three metals used in the experiment. Additionally, it was found that silicon carbide and white aluminum oxide abrasives removed more material per minute than the softer garnet.

8.5 Substantiating Theories

Based on the net cell reaction potentials using the Nernst equation, the possible reactions which occur during the lapping process are reactions between magnesium and its hydroxides and white aluminum oxide abrasives. These reactions are possible when Al 2024 is lapped with white Al_2O_3 since Al 2024 contains magnesium. Also, SiO_2 from SiC abrasives oxidized Al, Mn, Mg, and Ti in Al 2024 as well as Mn in 304 stainless steel, and Al and Mn in 1018 steel. These trends need to be investigated further.

In summary, the factors influencing the quality of a lapped product include the following:

- Lapping speed
- Lapping time
- Determination of optimum lapping pressure which would not damage the work material
- Flatness of the lapping plate
- Flow rate of the abrasive slurry
- Lapping vehicle fluids (oil-based or water-based fluids)
- Preparation of the workpiece
- Selection of adequate abrasive through hardness verifications
- Selection of an adequate lapping machine
- Size of the abrasive grain
- Temperature of the lapping plate

8.6 Contributions

A qualitative and quantitative evaluation of the lapping process was done to determine surface characterizations, roughness and material removal rate. These could all be considered within a single model for future studies.

- A statistical evaluation of lapping parameters was conducted to determine the influence of these parameters on material removal rate and surface roughness.
- Quanlitative evaluation using Scanning Electron Microscope (SEM) and Energy Dispersive Spectrometer (EDS) was conducted to gain a better understanding of the effects of lapping.
- A method of calculating frictional force during a flat lapping operation was developed by relating frictional torque to the current consumed.
- A theoretical temperature model for predicting friction during lapping was also developed, but not experimentally verified.
- Bingley and Schnee's Three-body Wear Model was modified using a cube as the shape of the abrasive particles.
- A method for image analysis for calculating the area of lapped zone, unfinished area, and scratched zone was developed for quantitative evaluation of the lapped surfaces.
- Redox chemistry in lapping was investigated and it was found that there are possible reactions between magnesium and its hydroxides and white aluminum oxide abrasives. These reactions are possible when Al 2024 is lapped with white Al_2O_3 since Al 2024 contains magnesium.

8.7 Recommendations for Further Work

In order to improve the lapping research and data analysis, the following steps are recommended:

- An amp meter display or rotary torque transducer should be incorporated in the design of the lapping machine so that the frictional torque resulting from lapping can be estimated better.
- More samples and runs must be studied for a comparative statistical analysis.
- It is essential to optimize lapping pressure to avoid the breaking of work material.
- Subsurface damage must be suitably controlled to fully understand the friction of lapping.
- Stepwise use of different abrasive grain sizes must be investigated in order to obtain good surface finish.
- A better procedure for determining material removal rate must be derived.
- A mechanism adequate for stirring the abrasives is required. The abrasive grains settle easily at the bottom of the slurry carrier. Therefore, additives that could prevent settling of the abrasives should be developed.
- In order to avoid production of toxic chemicals and environmental effects, better study of the physiochemical reaction is required.

REFERENCES

Aerospace Specification Metals, Inc. http://asm.matweb.com/search/SpecificMaterial.asp?bassnum=MA2024T4, accessed July 12, 2006.

Aircraft Spruce & Specialty CO. http://www.aircraftspruce.com, accessed July 7, 2006.

Akagaki, T., Hokkirigawa, K., Okabe, T., and Saito, K. (1999). Friction and wear of woodceramics under oil and water lubricated sliding contacts. *Journal of Porous Materials*, *Vol. 6*, 197-204.

Allan, G.A., and Sutherland, K.H. (1962). A preliminary study of the lapping process. *The Production Engineer*; *the Journal of the Institution of Production Engineers*, *Vol. 41*, *No. 4*, 195-202.

Archard, J. F. (1953). Contact and rubbing of flat surface. *Journal of Applied Physics*, *Vol. 24*, *No. 8,* 981-988.

Ashkerov, Y.V. (1992). Role of frictional forces in grinding and polishing processes in machines that operate by the lapping method. *Soviet Journal of Optical Technology*, *Vol. 59*, *No. 4*, 250-254.

Awtar, S., and Craig, K.C. (2004). Electromagnetic coupling in a dc motor and tachometer assembly. *Journal of Dynamic Systems, Measurement, and Control*: *Transactions of the ASME, Vol. 126*, 684-691.

Baleri, M, Sassani, F., and Ko, P.L. (2003). Stick-slip vibration between two large concentric circular discs in rotational contact with multiple points loads. *Journal of Mechanical Design*, *Transactions of the ASME*, *Vol. 125*, 786-792.

Belyaev, G.S. (1984). Microcutting process during lapping of sealing surfaces. *Chemical and Petroleum Engineering*, *Vol. 20*, *No. 7.* 356-357.

Bhushan, B. (2002). *Introduction to tribology* (*1st ed.*), (pp. 15, 347-377). New York: John Wiley & Sons, Inc.

Bingley, M.S., and Schnee, S. (2005). A study of the mechanisms of abrasive wear for ductile metals under wet and dry three-body conditions. *Wear*, *Vol. 258*, pp. 50-61.

Blau, P.J. (1981). An investigation of the unlubricated friction and wear break-in behavior of a dual-phase steel. *Wear*, *Vol. 72*, *No. 1*, 67-80.

Blau**,** P.J, Henry, S.D, Davidson, G.M, Zorc, T.B., and Levicki, D.R. (1992). Friction,

lubrication, and wear technology. *ASM Handbook*, *Vol. 18*, 9-11.

Buijs, M., and Houten, K.K. (1993a). A model for lapping of glass. *Journal of Material Science*, *Vol. 28*, 3014-3020.

Buijs, M., and Houten, K.K. (1993b). Three-body abrasion of brittle materials as studied by lapping. *Wear*, *Vol. 166*, 237-245.

Chandrasekar, S., and Kotini, K. (1990). Influence of abrasive properties on residual stresses in lapped ferrite and alumina. *Journal of American Ceramic Society*, *Vol. 73*, *No. 7*, 1907-1911.

Chang, Y.P., Hashimura, M., and Dornfeld, D.A. (2000). An investigation of material removal mechanisms in lapping with grain size transition. *Journal of Manufacturing Science and Engineering*, *Vol. 122*, 413-419.

Chen, C., Sakai, S., and Inasaki, I. (1991). Lapping of advanced ceramics. *Materials & Manufacturing Processes*, *Vol. 6*, *No. 2*, 211-226.

Cotell**,** C.M., Sprague, J.A., and Smidt, F.A., Jr. (1994). Surface engineering. *ASM Handbook*, *Vol. 5*, 948-971.

Cubberly, W.H., Bardes, B.P., Baker, H., Benjamin, D., and Unterweiser, P.M. (1978). Properties and selection: Irons and steels. *Metals Handbook*, *Vol. 1*, 125, 145.

Cubberly, W.H., Baker, H., Benjamin, D., and Unterweiser, P.M. (1979). Properties and selection: Nonferrous alloys and pure metals. *Metals Handbook*, *Vol. 2*, 75.

Cubberly, W.H, Unterweiser, P.M., Benjamin, D., Kirkpatrick, C.W., Knoll, C., and Nieman, K. (1980). Properties and selection: Stainless steels, tool materials and special purpose metals. *Vol. 3*, *No.* 9, 5, 19.

Dai, Y., Yuan, J.L., Zhou, Z.Z., Zheng, J.J., and Zhao, P. (2006). Modeling and simulation of lapping processes based on grain size sensitivity model. *Key Engineering Materials*, *Vols. 304-305*, 389-392.

Davis, C.E. (1974). Study of the influences on flat lapping with diamond micron abrasives em dash 2. *Industrial Diamond Review*, 94-99.

Davis, J.R. (1994). Surface engineering of carbon and alloy steels. *ASM Handbook*, *Vol. 5*, 701-710.

Deshpande, L.S (2005). Influence of Abrasive Material Properties on the Surface Generated in Flat Lapping. *Unpublished master's thesis, University of Oklahoma*, Norman, OK (pp. 48-65).

Deshpande L. S., Raman S., Sunanta O., and Agbaraji, C. (2008). Observations in the

flat lapping of stainless steel and bronze. *Wear*, *Vol. 265*, *No.1-2*, pp. 105-116.

Dong, W.D., Putilin, E.S., Rudin, Y.V. (2003). Modeling the velocity and trajectory of the relative motion of a zone of a workpiece during surface lapping. *Journal of Optical Technology*, *Vol. 70*, *No. 8*, 573-575.

EATON Corporation (1977). Instructions on maintaining wheel flatness. *Bulletin B-210*, (pp. 1-15). Shawnee, Oklahoma: EATON Corporation.

Eugene, F. (1947). Investigation of the lapping process. *Industrial Diamond Review*, *Vol. 7*, 35-40, 67-71.

Fuller, D.D. (1984). *Theory and practice of lubrication for engineers* (*2nd ed.),* (pp. 1-13, 549-581). New York: John Wiley & Sons.

Garzino-Demo, G.A., and Lama, F.L. (1994). Friction and wear of uncoated or SiO_2-coated 329 stainless and of uncoated or AlN-coated aluminum surfaces. *Surface and Coatings Technology*, *Vol. 68/69*, 507-511.

Goldstein, J.I., Newbury, D.E., Echlin, P., Joy, D.C. Lyman, C.E., Lifshin, E., Sawyer, L., and Michael, J.R. (2003). *Scanning electron microscope and x-ray microanalysis* (*3rd ed.*), (271-276, 297, 302, 323). New York: Springer Science + Business Media, Inc.

Gordon England Independent Metallurgist and Thermal Spray Coating Consultant. http://www.gordonengland.co.uk/hardness, accessed November 4, 2005.

Greenwood, N.N. and Earnshaw, A. (1997). *Chemistry of the elements* (*2nd ed.*), (pp. 242-43, 334, 348). Oxford: Reed Educational and Professional Publishing, Ltd.

Groshart, E. (1989). The new world of finishing - Friction and lubrication, *Metal Finishing*, *Vol. 87*, *No. 2*, 65-66.

Guha, S.K., and Chatterjee, S. (1980). Effects of lapping and polishing on the strength of alumina ceramics. *Transactions of the Indian Ceramic Society*, *Vol. 39*, *No. 4*, 127-130.

Harris, D.C. (2007). *Quantitative chemical analysis* (*7th ed.*), (pp. 98, 273-75, 279-81, AP 20-27). New York: W.H. Freeman and Company.

Hersey, M.D. (1966). *Theory and research in lubrication* (*1st ed.*), (pp. 1-17). New York: John Wiley & Sons, Inc.

Hryniewicz, P., Szeri, A.Z., and Jahanmir, S. (2001a). Application of lubrication theory to fluid in grinding: Part I-Flow between smooth surfaces. *Journal of Tribology*: *Transactions of The ASME*, *Vol. 123*, 94-100.

Hryniewicz, P., Szeri, A.Z., and Jahanmir, S. (2001b). Application of lubrication theory to fluid in grinding: Part II-Influence of wheel and workpiece roughness. *Journal of Tribology*: *Transactions of The ASME*, *Vol. 123*, 101-107.

http://www.ambiostech.com/profiler.html , accessed May 23, 2007.

Ichida, Y., and Kishi, K. (1985). Consideration of material removal mechanism of MC type carbide in precision lapping of high-carbon high-vanadium steel. *Proceedings of the Japan Congress on Materials Research* (pp. 107-111). Kyoto, Japan: Society of Material Science.

Jiandong, Y., Changgen, R., and Changxing, W. (1998). Theoretical analyses movement between press head and press disc in lapping. *Proceeding of SPIE - The International Society for Optical Engineering* (pp. 225-228).

Kalpakjian, S., and Schmid, S.R. (2001). *Manufacturing engineering and technology* (*4th ed.*), (pp. 69-71, 144-145, 558, 704-735, 871-891). New Jersey: Pearson Prentice Hall, Inc.

Kalpakjian, S., and Schmid, S.R. (2006). *Manufacturing engineering and technology* (*5th ed.*), (pp. 54-83, 123, 135, 159, 347, 685, 728, 790-794, 818-829, 1043-1044). New Jersey: Pearson Prentice Hall, Inc.

Kang, J., and Hadfield, M. (2005). Examination of the material removal mechanisms during the lapping process of advanced ceramic rolling elements. *Wear*, *Vol. 258*, 2-12.

Knight, W.A., and Case, A.A. (1915). An investigation of the cutting properties of abrasives when used with different laps and different lubricants. *Transactions of the American Society of Mechanical Engineers*, *Vol. 37*, *No. 1488*, 297-338.

Kurtus, R. http://www.school-for-champions.com/science/friction.htm, accessed June 15, 2006.

Larsen-Basse, J. (1992). Introduction to friction. *ASM Handbook*, Vol. 18, 35-37.

Le, X., and Peterson, M.L. (1999). Material removal rate in flat lapping. *Journal of Manufacturing Processes*, *Vol. 1*, *No. 1*, 71-78.

Letner, H.R., and Synder, H.J. (1953). Grinding and lapping stresses in manganese oil hardening tool steel. *Transactions of the ASME*, 874-882.

Lide, D.R. (2002). *Handbook of chemistry and physics*, (*82nd ed.*), (pp. 8-117). Florida: CRC Press.

Lynah, P., and Hoffman, P.R. (1989). Lapping. *ASM Handbook*, *Vol. 16*, 492-

505.

Montgomery, D.C. (2001). *Design and analysis of experiments* (*5th ed.*), (pp. 14-15, 392). New York: John Wiley & Sons, Inc.

Moore, D.F. (1972). *The friction and lubrication of elastomers* (*1st ed.*), (pp. 1-17). New York: Pergamon Press, Inc.

Metcut Research Associates Inc. (1980). *Machining data handbook* (*3rd ed.*), (pp. 26-39, 26-68, 26-61). Cincinnati, Ohio: C.J. Krebel Co.

Niagara Lasalle Corp. (2005). Material Description. Midlothian: TX.

O'Brien, W.J., http://www.lib.umich.edu/dentlib/Dental_tables/Knoophard.html, accessed October 28, 2005.

Olson**,** R.M. (1973). *Essentials of engineering fluid mechanics* (*3rd ed.*), (pp. 28-40). New York: Intext Educational Publishers.

Overney, R. http://depts.washington.edu/nanolab/ChemE554, accessed July 3, 2006.

Player, S. (1930). Maintaining precision in production lapping. *The Iron Age*, *Vol. 125*, *No. 13*, 943.

Postek, M.T., Howard, K.S., Johnson, A.H., and McMichael, K.L. (1980). *Scanning electron microscope - A student's handbook* (*1st ed.*), (pp. 47-59, 69-91). Vermont: Ladd Research Industries, Inc.

Preston, F.W. (1927). The theory and design of plate glass polishing machines. *Journal of the Society of Glass Technology*, *Vol. 11*, 214-256.

Rabinowicz, E. (1966). *Friction and wear of material* (*2nd ed.*), (pp. 52-79, 85, 95-123). New York: John Wiley and Sons, Inc.

Roberson, J.A., and Crowe, C.T. (1976). *Engineering Fluid mechanics* (*2nd ed.*), (pp. 17-21). Boston: Houghton Mifflin Company.

Schey, J.A. (1983). *Tribology in metalworking* (*1st ed.*), (pp. 94-101). Ohio: American Society for Metals.

Schey, J.A. (1987). *Introduction to manufacturing processes* (*2nd ed.*), (pp. 514-523). New York: McGraw-Hill, Inc.

Schmitz, T.L., Action, J.E., Ziegert, J.C., and Sawyer, G.W. (2005). The difficulty of measuring low friction: Uncertainty analysis for friction coefficient

measurements. *Journal of Tribology*, *Transactions of the ASME*, *Vol. 127*, *No. 3*, 673-677.

Singer, S., and Appelbaum, J. (1993). Starting characteristics of direct current motors powered by solar cells. *IEEE Transactions on Energy Conversion*, *Vol. 8*, *No. 1*, 47-53.

Spitler, D., Lantrip, J., Nee, J.G., and Smith, D.A. (2003). *Fundamentals of tool design* (*5th ed.*), (pp. 14-32, 376). Dearborn, Michigan: Society of Manufacturing Engineers.

Strasbaugh (1999). Operation and maintenance manual, (pp. IN-2, MS-4). California: Technical Publication Group.

Subramanian, K. (1994). Finishing methods using multipoint or random cutting edges. *ASM Handbook*, *Vol. 5*, 102-109.

Suh, N.P. (1986). *Tribophysics* (*1st ed.*), (pp. 1-25, 63-102, 196). Englewood Cliffs, New Jersey: Prentice-Hall, Inc.

Synlube. http://www.synlube.com/tribolog.htm, accessed September 26, 2006.

Szeri, A.Z. (1998). *Fluid film lubrication*: *Theory and design* (*1st ed.*), (pp. 9-31). Cambridge, United Kingdom: Cambridge University Press.

Trent, E.M., and Wright, P.K. (2000). *Metal Cutting* (*4th ed.*), (pp. 39-40). Woburn, Massachusetts: Butterworth-Heinemann.

Tweedy, I.M. (1928). Machine-lapping steel and cast iron. *American Mechanist*, 265.

Tylczak, J. H. (1992). Abrasive wear. *ASM Handbook*, *Vol. 18*, 184-190.

United States Products CO., (2006). Grinding and lapping compounds. Pittsburgh: PA: United States Products CO.

Vogelpohl, G. (1951). One third of world's energy may be conserved by suitable lubrication. *Scientific Lubrication*, *Vol. 3*, *No. 9*, 9.

Vidrine, D.W, http://www.vidrine.com/iropmat3.htm, accessed November 23, 2005.

Wolfson, R., and Pasachoff, J.M. (1990). P*hysics*: *Extended with modern physics* (*1st ed.*), (pp.284-289). Glenview, Illinois: Foresman and Company.

APPENDIX A

DEFINITIONS AND PROPERTIES OF MATERIALS

Table A-1 presents the mechanical properties of the work material (Cubberly et al., 1979). Hardness is the resistance to permanent indentation (scratch) or the ability of a material to withstand abrasion or resist penetration. Young's modulus, E, is the measure of stiffness of a material, that is, the ratio of engineering stress to engineering strain in the elastic region ($E = \frac{\sigma}{e}$). Kalpakjian and Schmid (2006) defined engineering stress and strain as follows: Engineering stress, σ, is the ratio of the applied load, P, to the original cross-section area, A_o, that is, $\frac{P}{A_o}$. On the other hand, true stress, S, is the ratio of the applied load, P, to the actual or instantaneous cross-sectional area, A, that is, $S = \frac{P}{A}$. Engineering strain, e, is a molecular displacement or deformation divided by original dimension $\left(e = \frac{l - l_o}{l_o} \right)$. Note, l_o is the initial length, and l is the final elongation. **True strain**, $\varepsilon = \ln\left(\frac{l}{l_o} \right)$

Stiffness is defined as the ability of a material to retain its dimension and shape under an application of an external load. **Density** is a property of a material that is expressed in terms of mass per unit volume. **Toughness** is the amount of energy per unit volume that a material dissipates prior to fracture. **Strength** is the ability of a material to withstand load without fracture or the ability of a material to resist deformation. **Tensile stress or ultimate tensile stress (UTS)** of a material is the maximum engineering stress

that is obtained from a plot of engineering stress vs. engineering strain. **Yield point** of a material is the level at which the stress and strain are no longer proportional as opposed to elastic region where there is a uniform elongation.

Table A-1. Mechanical Properties of Workpiece (Cubberly et al., 1979 and 1980).

Mechanical Properties	Work Material		
	Al 2024 T4	304 Stainless Steel	1018 Cold Rolled Steel
Hardness (Rockwell , B Scale)	58	91	92
Young Modulus (GPa)	73.1	193	190
Density (Kg/m^3)	2780	8000	7700
Ultimate Tensile Strength (MPa)	579	515	634
Yield Strength (MPa)	421	240	386

- **Types of Steel**

According to Kalpakjian, and Schmid (2006), carbon steels are classified based on the percentage of carbon present in the steel. Carbon steels contain less than 1% carbon, unlike cast iron that has about 2.11% to 4.5% carbon, and about 3% silicon. Table A-2 summarizes the mechanical properties of some carbon and alloy steels, while Table A-3 presents a summary of mechanical properties of some annealed stainless steel. Three classes of carbon steels are:

(i) Low-carbon steel or mild steel: It contains less than 0.3% carbon. It is used in production of bolts, nuts, sheet, plate, and tubes as well as for machine components that do not require high strength.

(ii) Medium-carbon steel: It contains 0.3 to 0.6% carbon. Generally, it is used in applications that require higher strength such as machinery, automotive parts, and railroad equipments.

(iii) High-carbon steel: It has greater than 0.6% carbon. Generally, it used for components that require high strength, high hardness, and wear resistance, for example, cutting tools, cable, music wire, spring, and cutlery.

Table A-2. Mechanical Properties of Some Carbon and Alloy Steels (Kalpakjian and Schmid, 2006).

AISI	Condition	Ultimate Tensile Strength (Mpa)	Yield Strength (Mpa)	Hardness HB
1020	Hot-rolled	448	346	143
	Normalized	441	330	131
	Annealed	393	294	111
1080	Hot-rolled	1010	586	293
	Normalized	965	524	293
	Annealed	615	375	174
3140	Normalized	891	599	262
	Annealed	689	422	197
4340	Normalized	1279	861	363
	Annealed	744	472	217
8620	Normalized	632	385	183
	Annealed	536	357	149

- **Annealing**

It is the restoring of a cold-worked or heated treated alloy to its original properties. The steel is heated at elevated temperature, and then cooled slowly. Annealing reduces hardness and strength, but improves ductility, machinability, and dimensional stability.

- **Normalizing**

In order to avoid excess softness from the annealing of steels, the cooling cycle is performed in still air, and this process is known as normalizing. It involves heating the material to a temperature, ranging from 100 to 200 ^{o}F before cooling in still air, so that fine grain structures that have been altered will be restored (Spitler, Lantrip, Nee, and Smith, 2003).

- **Tempering**

This is a heating and quenching process, whereby hardened steels and alloys are heated to some temperature below the lower critical temperature in order to reduce internal stresses caused by hardening (Spitler, Lantrip, Nee, and Smith, 2003). During tempering, hardness is reduced, while toughness is improved.

- **Rolling**

This is a process of reducing the thickness of the work material by applying compressive forces though a series of rolls.

Table A-3. Mechanical Properties of Some Annealed Stainless Steel (Kalpakjian and Schmid, 2006).

AISI (UNS)	Ultimate Tensile Strength (Mpa)	Yield Strength (Mpa)
303 (S30300)	550-620	240-260
304 (S30400)	5-620	240-290
316 (S31600)	50-590	210-290
410 (S41000)	480-520	240-310
416 (S41600)	480-520	275

Notations:

AISI: The American Iron and Steel Institute

SAE: The Society of Automotive Engineers

UNS: The Unified Numbering System. It consists of a letter that indicates the general class of alloy, and then is followed by five digits which indicate the chemical composition of the material. Normally, the Unified Numbering System starts with the following letters:

G: AISI and SAE Carbon and alloy steels.

J: Cast steels

K: Miscellaneous steels and ferrous alloys

S: Stainless Steels and super-alloys. A **Super-alloy** or **high-performance alloy** is a nickel, cobalt or nickel-iron based alloy, which is capable of withstanding very high temperatures, normally used for high temperature applications such as jet engine components, rockets, nuclear power plants, chemical processing equipment, coins, etc.

T: Tool steels

- **Effects of Different Elements on Steel**

According to Kalpakjian and Schmid (2001), different types of elements are added to steels, to improve certain properties such as hardenability, hardness, machinability, strength, toughness, wear resistance, weldability, and workability. The elements that are added to steel include:

- Boron: It improves hardenability (i.e., the capability of an alloy to be hardened by heat treatment).

- Calcium: This deoxidizes steel and improves toughness, which is the energy that a material dissipates before fracture.
- Carbon: The presence of carbon in steels improves hardenability, hardness (resistance to permanent indentation), and strength. However, it decreases ductility, weldability, and toughness.
- Cerium: This deoxidizes steel, controls the shape of inclusion, and improves toughness.
- Chromium: Addition of chromium to steel improves hardenability, high-temperature strength, toughness, corrosion resistance, and wear.
- Cobalt: It improves hardness and strength at elevated temperatures.
- Copper: This improves resistance to atmospheric corrosion, and strength (ability of a material to withstand load without fracture). However, it severely affects hot-working and surface quality.
- Lead: It improves machinability. However, it causes liquid-metal embrittlement (i.e., cracking of metals under very low stresses).
- Magnesium: This deoxidizes steel, controls the shape of inclusion, and improves toughness.
- Manganese: The presence of manganese in steels improves abrasion resistance, hardenability, machinability, and strength. Also, it deoxidizes molten steel, and minimizes hot shortness (i.e., local melting of the component in the grain boundary, usually below the melting point of the metal). However, it reduces weldability.

- Molybdenum: This improves creep resistance, elevated-temperature strength, hardness, hardenability, toughness, and resistance to wear. In addition, it reduces temper embrittlement (movement of impurities to the grain boundary). **Creep** is permanent elongation of a material under a static load.
- Nickel: Addition of nickel to steels improves corrosion resistance, hardenability, strength, and toughness.
- Niobium or Columbium: It improves fineness of grain size, strength, and toughness. Also, it decreases transition temperature (i.e., a sharp change in ductility of metals across a narrow range of temperature).
- Phosphorus: The presence of phosphorus in steel imparts properties such as corrosion resistance, hardenability, machinability, and strength. On the contrary, it adversely decreases ductility and toughness.
- Selenium: This improves machinablity, which implies a good surface finish, prolonged tool life, low force and power requirements, low critical speed, and good chip control.
- Silicon: It improves corrosion resistance, electrical conductivity, hardness and strength. Conversely, it reduces machinability, and cold formability.
- Sulfur: If sulfur is combined with manganese, it improves machinability. On the other hand, it reduces ductility, impact strength, surface quality, and weldablity (ability of a metal to be welded into a specific structure).
- Tantalum: It improves fineness of grain size, strength, and toughness. Also, it decreases transition temperature.
- Tellurium: This improves machinability, formability, and toughness.

- Titanium: It deoxidizes steel and improves hardenability.
- Tungsten: It improves hardness and strength at elevated temperatures.
- Vanadium: Addition of vanadium to steel, improves abrasion resistance, hardness at elevated temperature, strength, and toughness. However, it prevents grain growth during heat treatment.
- Zirconium: This deoxidizes steel, controls the shape of inclusion, and improves toughness.

- **Types of Aluminum**

Properties of some aluminum alloys at room temperature are summarized in Table A-4.

Table A-4. Properties of Some Aluminum Alloys at Room Temperature (Kalpakjian and Schmid, 2006).

Alloy (UNS)	Temper	Ultimate Tensile Strength (MPa)	Yield Strength (MPa)
1100 (A91100)	O	90	35
1100	H14	125	120
2024 (A92024)	O	190	75
2024	T4	470	325
3003 (A93003)	O	110	40
3003	H14	150	145
5052 (A95052)	O	190	90
5052	H34	260	215
6061 (A96061)	O	125	55
6061	T6	310	275
7075 (A97075)	O	230	105
7075	T6	570	500

Temper Notations:

F: Fabricated by cold or hot working or casting.

O: Annealed from cold worked or casting.

H: Strain hardening by cold working.

H1: Strain hardened only.

H2: Strain hardened, and then partially annealed.

H2: Strain hardened, then stabilized.

T: Heat treated. The letter, T, is followed by one or more digits. The digits indicate the method that is used to obtain the stable tempers as stated below:

T3: Solution is heat treated, followed by cold working.

T351: Solution is heat treated, stress relieved, and then cold worked.

T4: Solution is heat treated, and naturally aged.

T451: Solution is heat treated, and stress relieved.

T5: Artificially aged only.

T6: Solution is heat treated, and artificially aged.

T651: Solution is heat treated, stress relieved, and then artificially aged (precipitation heat treatment).

T652: Solution is heat treated, stress relieved by compression, and then artificially aged.

T7: Solution is heat treated, then stabilized.

T8: Solution is heat treated, cold worked, and then artificially aged.

T851: Solution is heat treated, cold worked, stress-relieved, then artificially aged.

T9: Solution is heat treated, artificially aged, and then cold worked.

T10: Artificially aged, and then cold worked.

W: Solution treated only (i.e., unstable temper)

During **Solution treatment,** the alloy is heated to solid-solution, and then cooled rapidly, for example, by quenching in water. **Aging** is a precipitation process, which is a function of time and temperature. **Artificial aging** is when aging is carried out above room temperature. **Natural aging** occurs when alloys harden and become stronger at room temperature. If natural aging is slowed down by refrigeration of quenched alloy, this process is called **cryogenic treatment.**

Aluminum and other nonferrous metals and alloys are identified internationally by the Unified Numbering System similar to that of steel. It consists of a letter, indicating the general class of the alloy, followed by five digits that indicate the chemical composition. In the UNS, 2024 wrought aluminum is designated as A92024. For example, the following metals are represented as:

A: represents aluminum

C: Copper

N: Nickel alloys

P: Precious metals

Z: zinc.

- **Treatments of Metals**

Some of the treatments listed below are performed on materials in order to improve their chemical, mechanical, and physical properties.

- **Cold working**:

Cold working is plastic deformation that is generally carried out at room temperature with some exceptions like lead. Deformation of lead at room temperature is hot working since recrystallization temperature of lead is at room temperature. In cold working, the homologous temperature, this is, the ratio of working temperature, T, to that of melting temperature, T_m, is less than 0.3. The temperatures are measured on the absolute scale. For example, absolute zero equals -273.5 ^oC or zero on the Kelvin scale.

Plastic or permanent deformation: The material does not return to is original shape after the external force is removed, although some portion of the elastic deformation could be recovered. Plastic deformation involves breaking of atomic bonds of the material due to movement of dislocations. In the case of **elastic deformation**, the material or the object returns to its original shape if the external force is removed. In other words, a temporary change in shape at a low stress, which can be recovered after the load is removed, is called elastic deformation.

- **Warm working**:

Warm working is carried out at intermediate temperatures between cold and hot working. T/T_m ranges from 0.3 to 0.5.

- **Hot working**

Hot working is plastic deformation carried out above recrystallization. temperature. $T/T_m > 0.6$.

- **Recrystallization**

At certain temperature ranges, new equiaxed and strain-free grains are formed to replace the old grains, and this is known as recrystallization. It occurs approximately between 0.3 and 0.5 T_m on the absolute scale.

- **Strain hardening or work hardening**

An increase in shear stress causes an increase in strength and hardness of the metal. Therefore, the greater the deformation, the greater the amount of entanglements, and this eventually leads to an increase in the metal's strength, especially when work hardening is done at room temperature.

- **Elemental Analysis**

Material analysis was performed on the work material using a Scanning Electron Microscope (SEM), to check if the alloying elements have been affected by lapping operation. The composition obtained was compared with the original composition before lapping. This was done in order to determine if lapping operation has altered the original composition of the work material.

- **SEM Signals**

SEM was used to observe the topography of the lapped specimen in order to determine if the abrasive grains cause some voids or surface damage on the lapped sample. According to Postek et al. (1980), seven possible signals are generated by primary electron beam with specimen interaction and they are illustrated in Figure A-1. The seven possible signals include: backscattered electrons, secondary electrons, x-rays, specimen current, transmitted electrons, Auger electrons, and cathodoluminescence.

During scanning, primary electrons lose some energy due to their interaction with atoms of the specimen. SEM images obtained from secondary electrons and some back scattered electrons were used for image analysis of the specimen, that is, for obtaining topographical information of the samples. If there are no voids, the secondary images and backscattered images will appear light in color. If there are voids, the areas that appear dark in the SEM micrographs indicate the presences of voids in the lapped specimen. Also, the x-rays were used for determination of chemical composition of the specimen.

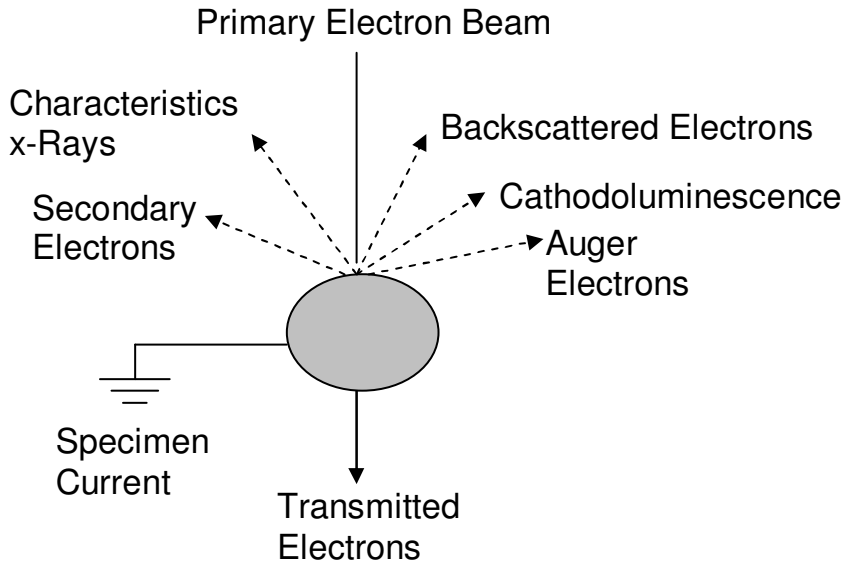

Figure A-1. Seven Signals Generated by Primary Electron Beam in SEM Analysis (Postek et al., 1980).

- **Backscattered Electrons**

It occurs when a primary electron beam comes in close contact with a nucleus of the sample or outer shell electron. Then the primary electron rebounds with a negligible amount of energy loss, and it normally possesses energy > 50 eV. This is referred to as an elastic interaction. The scattered electrons in this operation are regarded as backscattered electrons. As the atomic number of the sample increases, the backscattering electron increases, and this linear relationship is the basis for a contrast mode in SEM. The backscattered electrons are collected with backscattering detectors and they give information about atomic number contrast as well as the information about the topography of the material. For example, if the specimen is composed of gold and carbon, the gold portion will appear lighter in color, while the carbon area will appear darker in color in the SEM micrograph.

- **Secondary Electrons**:

Another type of scattering effect is known as an inelastic collision. This occurs when the primary electron beam collides with an electron from the sample, and loses an enormous amount of energy. It usually possesses energy < 50 eV because of the atom of the workpiece. During the inelastic collision, the energy communicated to the sample will cause it to ionize. In the case of inelastic collision, the kinetic energy between the two particles is transformed to another form of energy, but the total amount of energy remains the same. As a result of ionization processes, electrons are emitted and these are termed as secondary electrons. The secondary electrons are good for studying the topography of the specimen.

- **Auger Electrons**:

This phenomenon occurs when an electron from an atom of the sample falls from an outside shell to an inner shell, and the excess energy may be expended in a form of emission by another electron or by emission of electromagnetic radiation. An emission of a low energy electron occurs near the surface in this stabilization process. This is known as an Auger electron, named after the first person that observed this type of emission (Postek et al., 1980).

- **Cathodoluminescence**

Another from of energy stabilization that occurs during electron beam-sample interaction is cathodoluminesacence. It is the emission of photons of infrared, visible or ultraviolet wavelengths in order to dissipate excess energy that occurs within the material.

- **Transmitted Electrons**

In this type of electron beam-specimen interaction, the electrons that have enough energy will pass through the specimen. For example, if the sample is prepared with thickness < one micron, the electrons that have enough energy to move through the work material will be accumulated.

- **X-rays**

If the nucleus of the atom of the specimen scatters electrons, the excess energy is released as x-rays of different wavelengths. This radiation is known as white Bremstralung radiation or x-ray continuum. This gives information about the composition of the material. The peaks obtained from x-rays are correlated with the periodic table to determine the actual composition of the material.

- **Specimen Current**

The last signal generated by primary electron beam-specimen interaction is called the specimen current. This occurs as a result of negative, charged electrons, including the electrons that are incident to the sample and emitted by the sample. The difference in current between the backscattered electrons and the incident electrons is referred to as the absorbed current. In any case, the specimen current will give a lower value due to loss of electrons from secondary electrons and Auger electrons.

If oxygen is detected after lapping, it is due to oxidation. Oxygen increases the strength of steels slightly, but it adversely decreases toughness. The presence of manganese and sulfur indicates that the steel is a free-cutting steel. Manganese and sulfur act as a lubricant, thereby making the steel easy to cut, and the chip will be easy to control as well.

- **Sample Preparation**

Coating is very important in x-ray analysis. For example, the gold or gold-palladium alloy, hinder the escape of many characteristic x-rays of the specimen. X-rays are excited from both the specimen and the coating material. Thus, this absorption of the characteristic x-rays from the sample by the coating material reduces the count rate. Also, the characteristic x-rays generated by the coating material can overlap with the peaks of the specimen, thereby making the results indistinct. Therefore, heavy coating of metals should be avoided. Electrical conductivity should be provided to nonmetallic or nonconductive materials using carbon coating. Carbon coating is recommended because the low density of carbon allows most x-rays generated to pass through the coating, and any false carbon x-rays produced are blocked by the beryllium window of the detector.

- **X-Ray Spectrum**

From basic knowledge of physics, the electrons of any given atom occupy clearly defined energy levels called shells (Postek et al., 1980). Conventionally, the shell closest to the nucleus is known as the K shell, and contains up to two electrons as shown in Figure A-2. The shell following the K shell is called the L shell, and contains up to 8 electrons. In that order, M shell comes next, with up to 18 electrons, and N shell with up to 32 electrons, etc. The atomic number determines the number of shells present in an atom. In other words, the number of electrons present in an atom is equal to the number of protons present in its nucleus.

For a most stable configuration, it is required that that lower energy level be filled first. For instance, iron has an atomic number of 26. This implies that k shell has 2 electrons, L has 8 electrons, and the remaining 16 electrons occupy the M shell. Electrons usually occupy the lowest energy level. Therefore, if an electron is removed from a low energy inner shell, an electron from a higher energy outer shell will immediately replace the vacancy. Hence, the second electron loses energy in this form of transfer, and this is referred to as an "electron jump." In this process, energy is released in the form of an x-ray, whose energy is equal to the difference in energy between the two shells. This means that a spectrum of x-ray exists for each element.

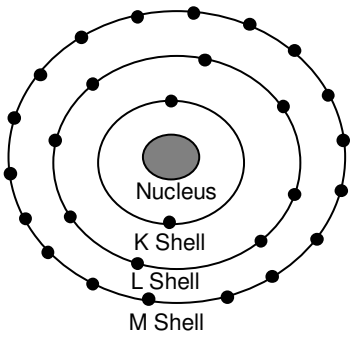

Figure A-2. Diagram of an Atom Showing Electron Shells (Postek et al., 1980).

As can be seen in Figure A-3, an alphanumeric system of nomenclature is used to identify the resultant x-rays. Each x-ray is first named after the shell, which is initially vacated to create the x-ray. For example, an x-ray created by filling of a vacancy in a K shell is known a K x-ray. Also, the filling of a vacancy in L shell is termed as an L x-ray.

Furthermore, the x-ray is distinguished by the size of the "electron jump." For instance, if a vacancy is filled by an electron from an adjacent cell, this creates an x-ray referred to as an α x-ray. In that manner, a difference between two shells creates a β x-ray, and a difference between three shells creates an x-ray called a γ x-ray. Therefore, an electron jump from an L shell to a K shell creates K_α x-ray, and if an electron jumps from an N shell to an L shell, this results in an L_β x-ray, and so on. According to Goldstein et al. (2003), the difference in energy between the K shell and the L shell equals the energy of the K_α x-ray that is produced. Most of the elements produce k x-rays, ranging from 1 to 10 KeV. If K_α x-rays are generated, K_β x-rays are produced as well.

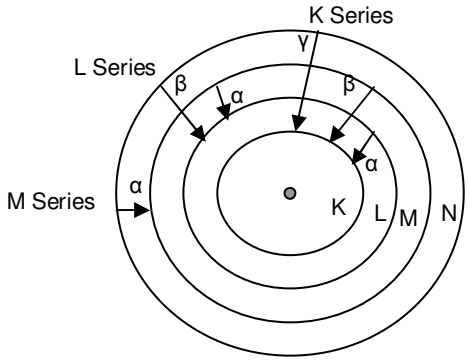

Figure A-3. Spectrum of X-ray Generated from a Single Element (Postek et al., 1980).

- **Analysis of X-Ray spectrum**

The interaction of electron beam with a specimen in SEM produces x-ray signal. The x-rays produced in the SEM have wavelengths and energies that characterize the elements present in the sample. Two techniques used for evaluation of x-ray spectrum include: Wavelength Dispersive Spectrometer (WDS) and Energy Dispersive Spectrometer (EDS).

- **Wavelength Dispersive Spectrum (WDS)**

As the name implies, WDS identifies and counts the x-rays based on the wavelengths, which are characteristic of elements present in the specimen. According to Postek et al. 1980, Equations (A-1) and (A-3) can be used to relate energy and wavelength, respectively. If Equation (A-2) is substituted into Equation (A-1), then the wavelength can be represented with Equation (A-3). As can be seen, Equations (A-1) and (A-3) are the basis for x-ray analysis of specimens since the x-rays have wavelengths and energies that are characteristic of the elements present in the sample to be analyzed.

The electron jump between shells in an atom, which shows the energy of each x-ray can be expressed with Equation (A-1).

$$E = hv, \tag{A-1}$$

$$v = \frac{c}{\lambda}, \tag{A-2}$$

$$\lambda = \frac{hc}{E}, \tag{A-3}$$

where

E : Energy of an x-ray

h : Plank's constant = 6.6262 x 10^{-34} joule x sec

v : x-ray's wave frequency

c : speed of light = 3.0 x 10^{8} m/sec

λ : wavelength of x-ray.

- **Energy Dispersive Spectrum (EDS)**

In order to characterize the material composition of a specimen, the x-rays produced in a scanning electron microscope have energies that correspond to the elements present in the sample. Chemical analysis in the SEM and electron microprobe are usually done by measuring the energy, and the intensity distribution of x-ray signal produced by a focused beam (Goldstein et al., 2003). A typical EDS system is a dispersion with a semiconductor as illustrated in Figure A-4. Postek et al. (1980) defined the **take-off angle** as the angle between the surface of the sample and center of the

detector. If the take-off angle is too low, the x-rays generated travel a greater distance through the sample before reaching the detector, thus leading to greater absorption of the x-rays at a lower count rate. A take-off angle, less than 30 degrees leads to excessive absorption by the specimen, that is, lower energy x-rays will be absorbed to a greater extent. Contrarily, if the take-off angle is too high, the paths of some of the rays can be blocked by the collimator.

Also, the authors defined **solid angle** as the fraction of the x-rays that reach the face of the detector, assuming the source of x-rays comes from one particular point of the sample. Furthermore, **count rate** is defined as the number of x-rays that reach the detector per unit time. A low count rate results in long periods of analysis, which may damage the specimen, due to long interaction of the primary electron beam. Additionally, the number of background noise increases due to low count rate, hence the signal-to-noise ratio decreases.

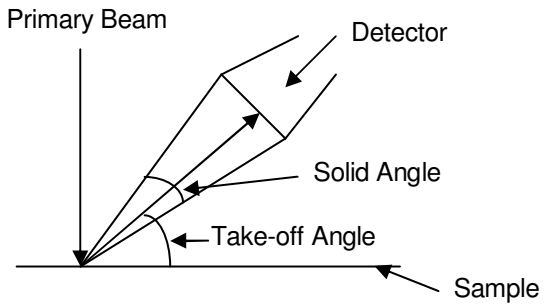

Figure A-4. Solid Angle and Take-off Angle of an EDS System (Postek et al., 1980).

The detector used by the SEM is an oxford detector, which consists of semiconductor crystals made of Si(Li). When an x-ray strikes a semiconductor crystal, each electron in the crystal absorbs a given amount of energy. If the energy of the x-ray

increases, the number of electrons excited also increases. Subsequently, the energy absorbed by the electrons is converted to electrical energy, which is emitted and amplified as depicted in Figure A-5. The first part of the preamplifier is the Field Effect Transistor (FET), and this provides the mechanism by which the electrical signal produced by the Si(Li) crystal is separated from the bias voltage. Furthermore, from the field effect transistor, the voltage pulse is amplified by another preamplifier, and then modified by a linear amplifier as illustrated in Figure A-5.

The field effect transistor performs efficiently at low temperatures because reduced temperatures decrease extraneous signals such as thermal noise, thereby increasing the signal-to-noise ratio. Also, low temperature operation of filed effect transistor improves the resolution of the signals. In order to obtain a low temperature, the field effect transistor is cooled in a Dewar (vacuum flask) of liquid nitrogen at $-196^{o}C$. The liquid nitrogen also cools the Si(Li) crystals. Since the detector crystal and the field effect transistor are operated in a vacuum, small amounts of liquid could leak into the system, thereby contaminating the crystal and short out the field effect transistor.

Another function of the liquid nitrogen is to freeze any moisture in the system without causing any damage to the vacuum. This process helps in maintaining a vacuum, and it is known as "cryogenic pumping**."** The vacuum should be maintained even when the specimen chamber is vented because extreme cold to the detector can condense water from the air. To remedy this situation, the semiconductor crystal is isolated from the specimen chamber by a very thin layer of beryllium (7.5 μm thick), and this is referred to as a "beryllium window." The x-ray must pass through the beryllium window before reaching the crystal detector from the specimen. The low energy x-ray can be easily

absorbed by the beryllium window. According to Goldstein et al. (2003), to measure an accurate x-ray signal, noise minimization is very essential. Therefore, the detector crystals have to be kept close to the liquid nitrogen in order to reduce effects from thermal noise.

If the EDS system warms up, the ice melts, the preamplifier with high voltage bias shorts out, and the semiconductor detector could be damaged. To remedy this problem, modern EDS systems have liquid nitrogen monitors that shut off the system if the liquid nitrogen supply becomes low. A multichannel analyzer sorts the number of electrical energy signals and counts the number of x-rays at each energy level that strikes the semiconductor crystals.

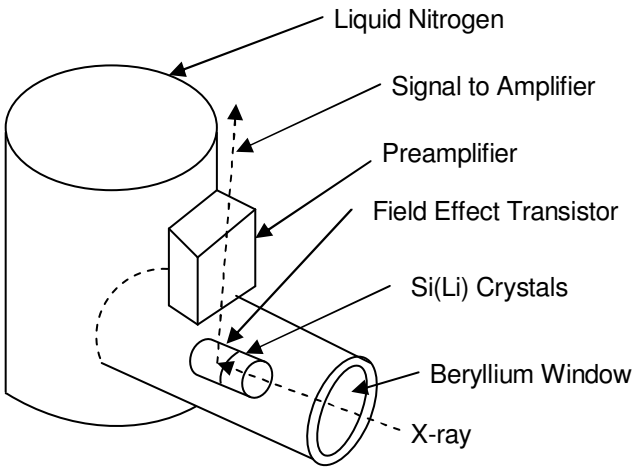

Figure A-5. Components of an EDS (Postek et al., 1980).

The abrasives are not conductive. Therefore, for the abrasive image to be scanned with an SEM, the abrasives had to be coated with a good conductor such as gold-

palladium alloy in a copper petri dish. The SEM images of the abrasives were scanned at 1000 magnification using excitation energy of 15 kilovolts.

APPENDIX B

EDS AND ANAGLYPH STEREOPAIRS OF SPECIMENS BEFORE LAPPING

EDS OF ALUMINUM 2024 BEFORE LAPPING

Intensity (c/sec)

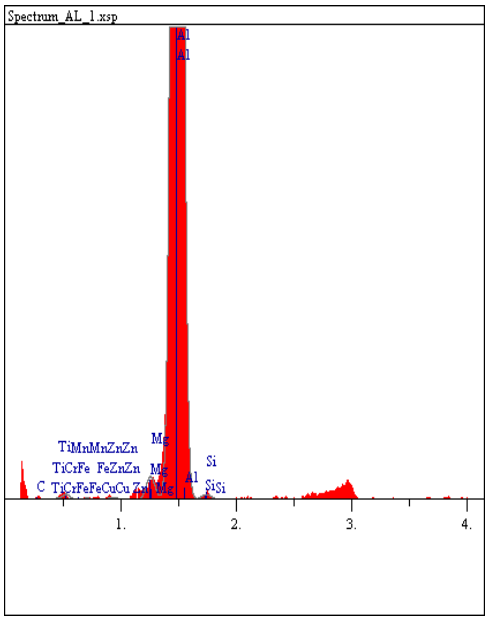

Energy (keV)
Qualitative EDS
Al 2024, Sample 1

Elt.	Line	Intensity (c/s)	Error 2-sig	Conc. wt. %
C	Ka	0.00	0.000	0.000
O	Ka	2.80	0.335	0.807
Mg	Ka	13.87	0.745	0.830
Al	Ka	1,329.63	7.293	95.937
Si	Ka	3.30	0.363	0.530
Ti	Ka	0.95	0.195	0.172
Cr	Ka	1.05	0.205	0.244
Mn	Ka	0.41	0.129	0.116
Fe	Ka	1.96	0.280	0.647
Cu	Ka	0.59	0.154	0.416
Zn	Ka	0.31	0.112	0.302
				100.0

Quantitative EDS
KV: 15.0
Take-off angle: 35.0°
Elapsed live time: 100.0 seconds

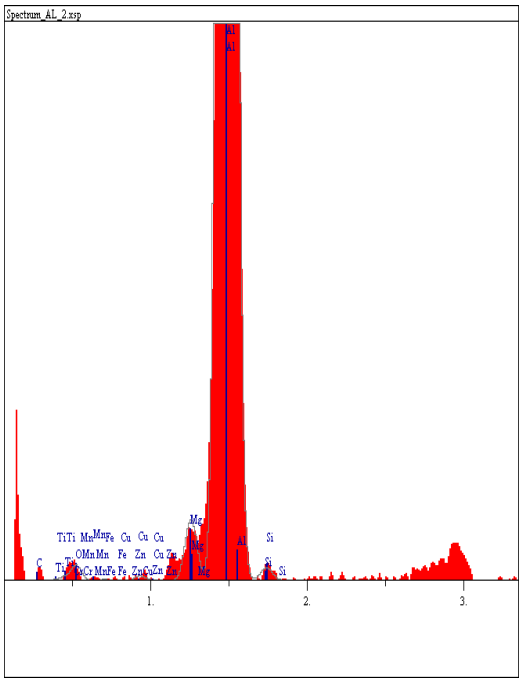

Elt.	Line	Intensity (c/s)	Error 2-sig	Conc. wt. %
C	Ka	0.00	0.000	0.000
O	Ka	2.31	0.304	0.871
Mg	Ka	10.46	0.647	0.814
Al	Ka	1,022.87	6.396	96.168
Si	Ka	2.34	0.306	0.491
Ti	Ka	0.53	0.146	0.125
Cr	Ka	0.65	0.161	0.196
Mn	Ka	0.52	0.144	0.189
Fe	Ka	0.94	0.194	0.406
Cu	Ka	0.47	0.137	0.430
Zn	Ka	0.25	0.099	0.310
				100.0

Quantitative EDS

Qualitative EDS

Al 2024, Sample 2

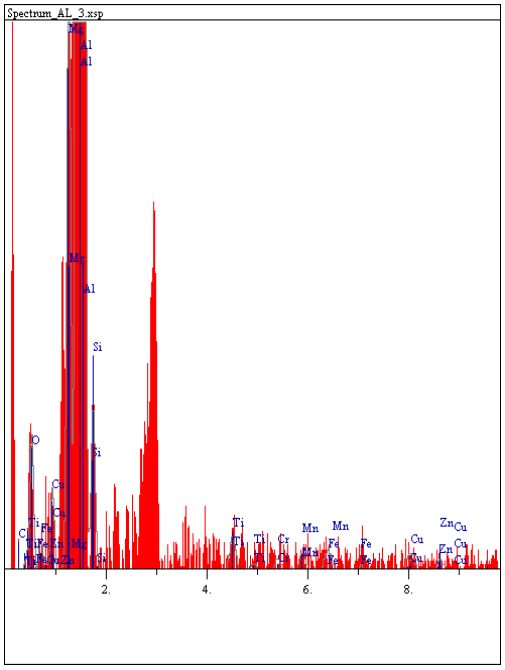

Elt.	Line	Intensity (c/s)	Error 2-sig	Conc. wt. %
C	**Ka**	**0.00**	**0.000**	**0.000**
O	Ka	2.10	0.290	0.780
Mg	Ka	11.28	0.672	0.863
Al	Ka	1,039.86	6.449	96.165
Si	**Ka**	**3.07**	**0.351**	**0.635**
Ti	Ka	0.86	0.185	0.198
Cr	Ka	0.31	0.111	0.092
Mn	Ka	0.46	0.135	0.163
Fe	Ka	0.61	0.156	0.256
Cu	Ka	0.56	0.149	0.504
Zn	Ka	0.28	0.106	0.344
				100.0

Quantitative EDS

Qualitative EDS

Al 2024, Sample 3

ANAGLYPH STEREOPAIR AND LINE PROFILE OF AL 2024 BEFORE LAPPING

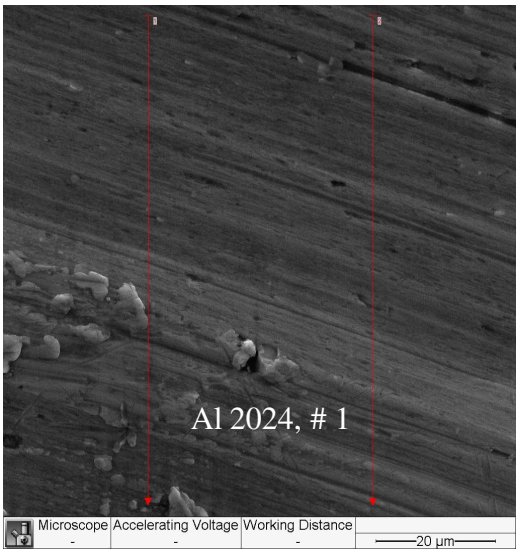

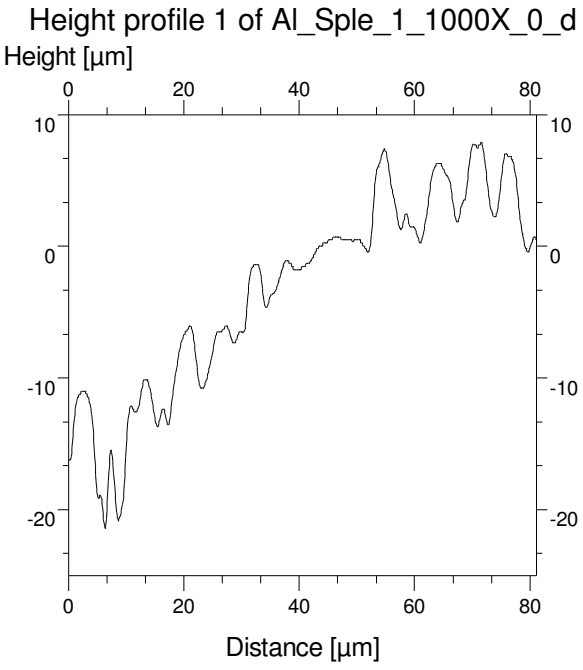

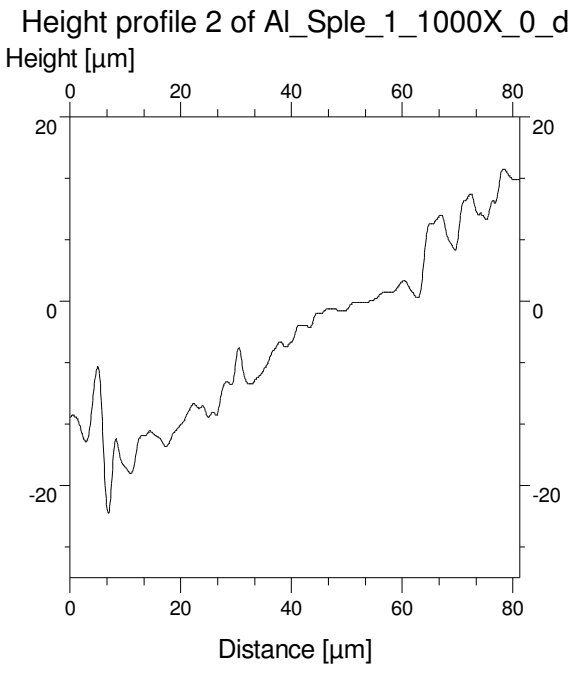

Al 2024, Sample 1

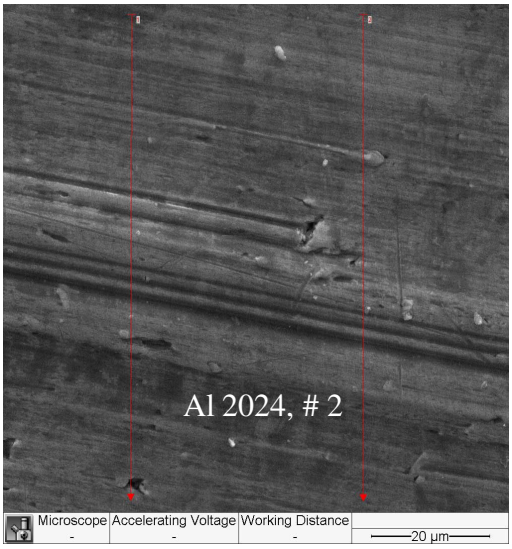

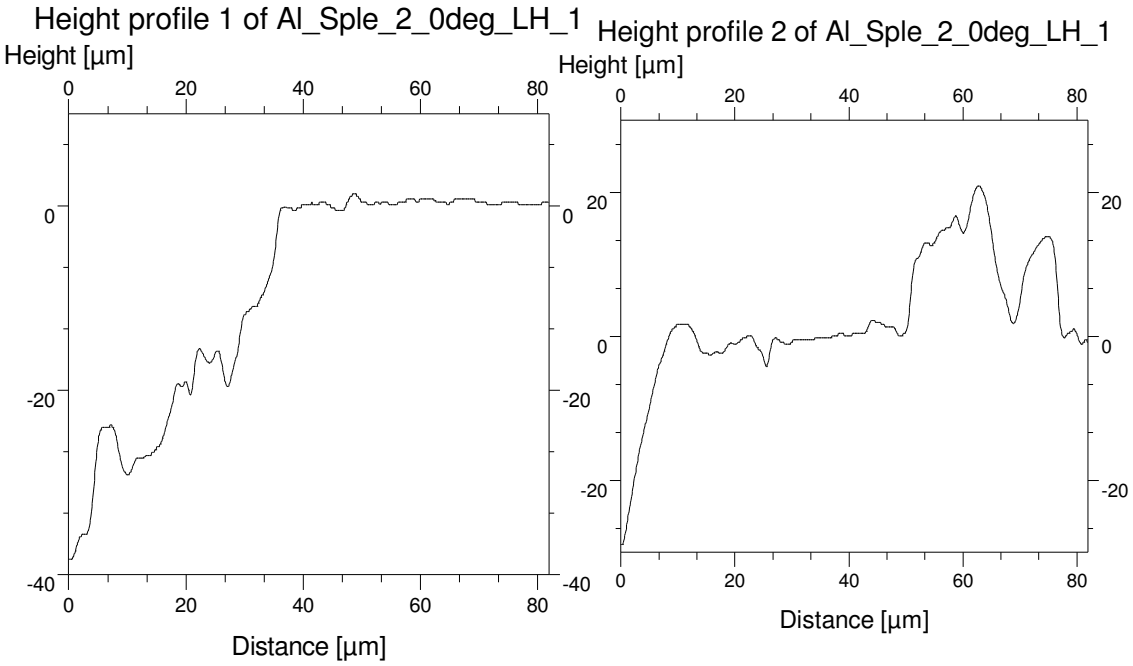

Al 2024, Sample 2

SEM MICROGRAPHS OF ALUMINUM 2024 BEFORE LAPPING

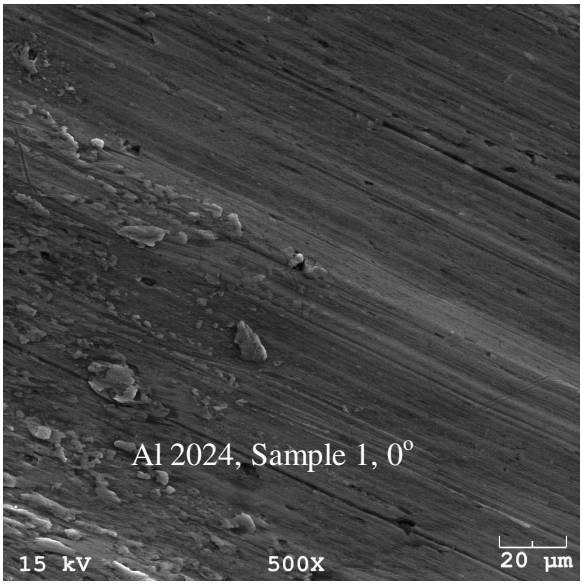

Al 2024, Sample 1, 500 Magnification

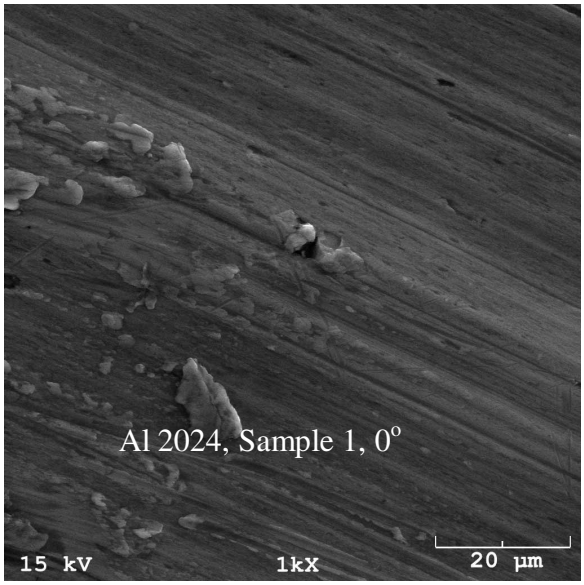

Al 2024, Sample 1, 1000 Magnification

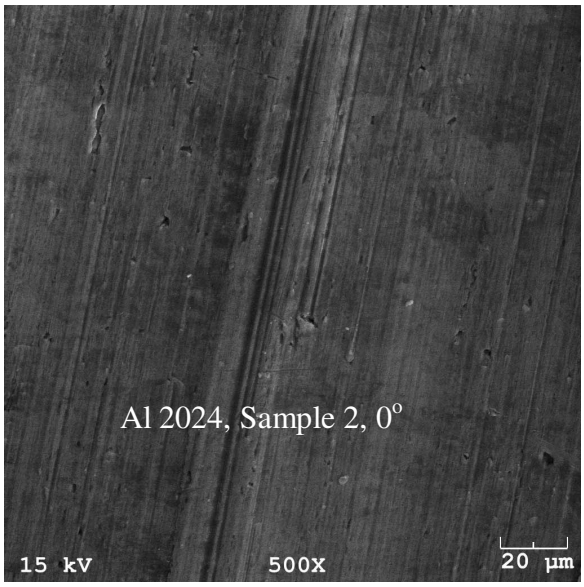

Al 2024, Sample 2, 500 Magnification

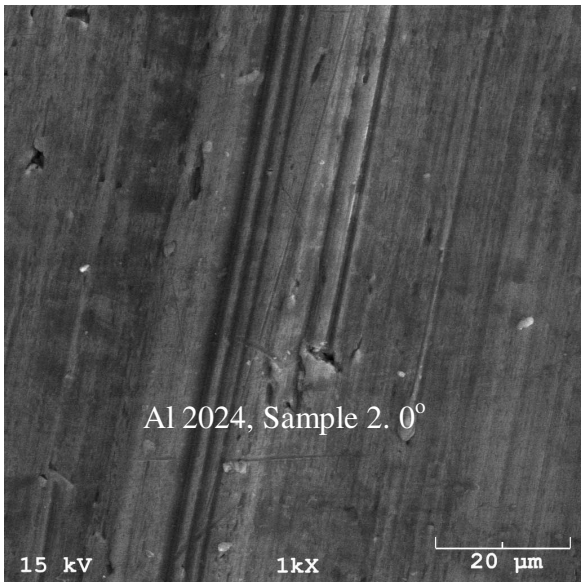

Al 2024, Sample 2, 1000 Magnification

EDS OF 304 STAINLESS STEEL BEFORE LAPPING

Intensity (c/sec)

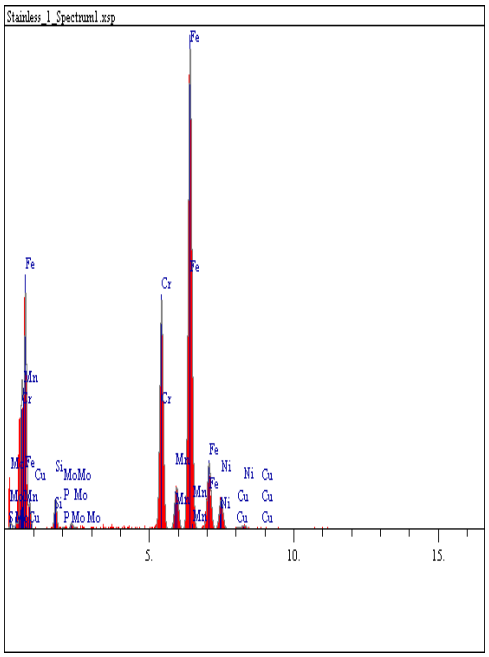

Elt.	Line	Intensity (c/s)	Error 2-sig	Conc.
C	Ka	0.00	0.000	0.000
Si	Ka	12.39	0.704	1.123
P	Ka	0.72	0.170	0.064
S	Ka	0.00	0.000	0.000
Cr	Ka	131.73	2.295	18.173
Mn	Ka	8.60	0.586	1.650
Fe	Ka	294.85	3.434	70.182
Ni	Ka	19.51	0.883	7.536
Cu	Ka	1.22	0.221	0.637
Mo	La	2.67	0.327	0.636
				100.0

Quantitative EDS

Energy (keV)
Qualitative EDS
304 Stainless Steel, Sample 1

Conditions:

KV: 15.0
Take-off angle: 35.0°
Elapsed live time: 100.0 seconds

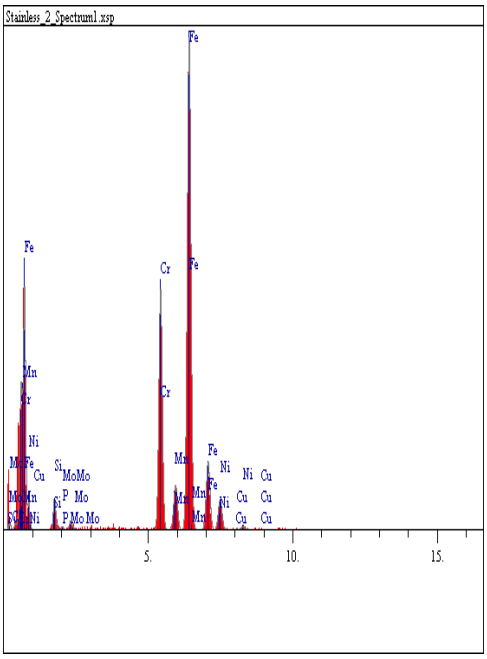

Intensity (c/sec)

Energy (keV)

Elt.	Line	Intensity (c/s)	Error 2-sig	Conc.
C	Ka	0.00	0.000	0.000
Si	Ka	14.20	0.754	1.181
P	Ka	1.34	0.232	0.109
S	Ka	0.00	0.000	0.000
Cr	Ka	146.08	2.417	18.596
Mn	Ka	9.55	0.618	1.688
Fe	Ka	319.42	3.574	69.993
Ni	Ka	20.34	0.902	7.227
Cu	Ka	0.94	0.194	0.452
Mo	La	3.45	0.371	0.754
				100.0

Quantitative EDS

Qualitative EDS

304 Stainless Steel, Sample 2

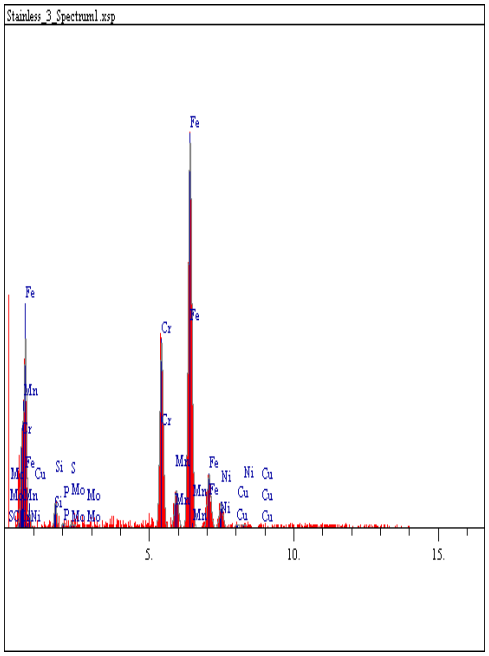

Intensity (c/sec)

Energy (keV)

Elt.	Line	Intensity (c/s)	Error 2-sig	Conc.
C	Ka	0.00	0.000	0.000
Si	Ka	0.89	0.189	1.210
P	Ka	0.18	0.085	0.238
S	Ka	0.00	0.000	0.000
Cr	Ka	8.66	0.589	18.033
Mn	Ka	0.75	0.173	2.161
Fe	Ka	19.24	0.877	68.687
Ni	Ka	1.27	0.226	7.379
Cu	Ka	0.20	0.090	1.599
Mo	La	0.19	0.088	0.693
				100.0

Quantitative EDS

Qualitative EDS

304 Stainless, Sample 3

ANAGLYPH STEREOPAIR AND LINE PROFILE OF PRELAPPED 304 STAINLESS STEEL

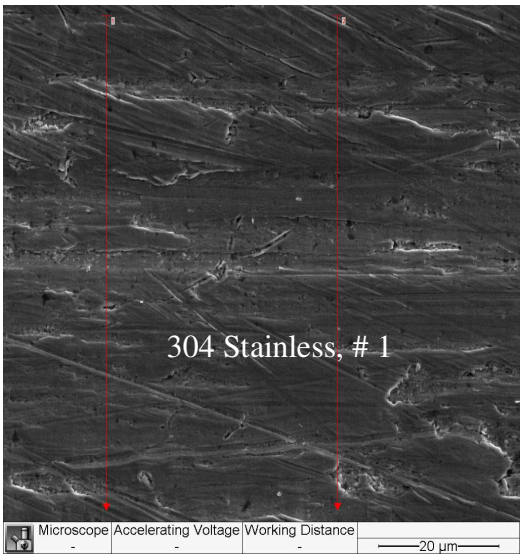

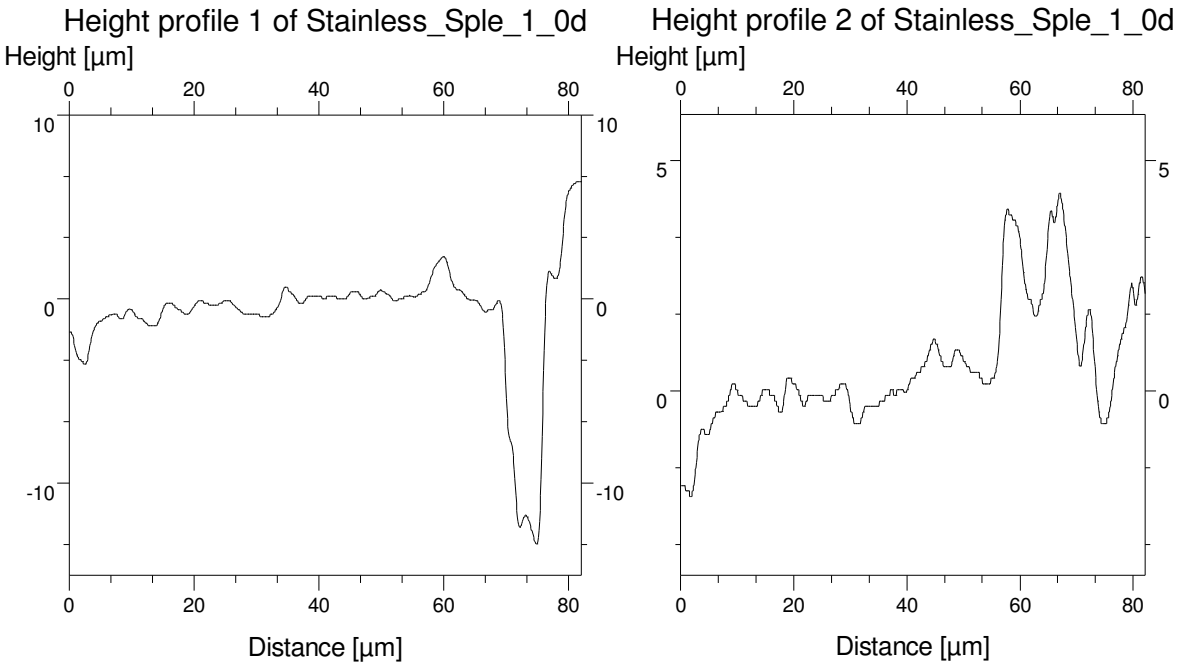

304 Stainless Steel, Sample 1

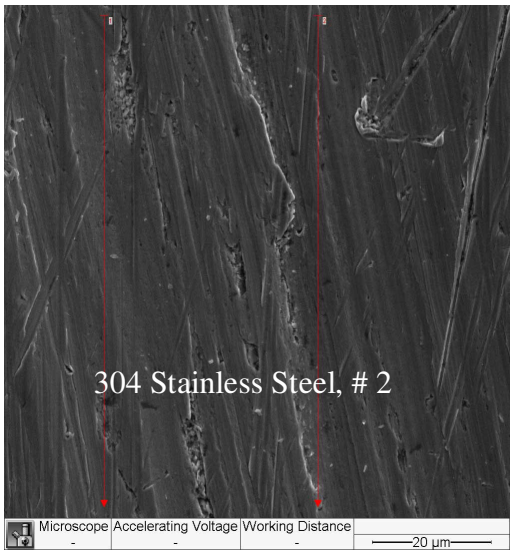

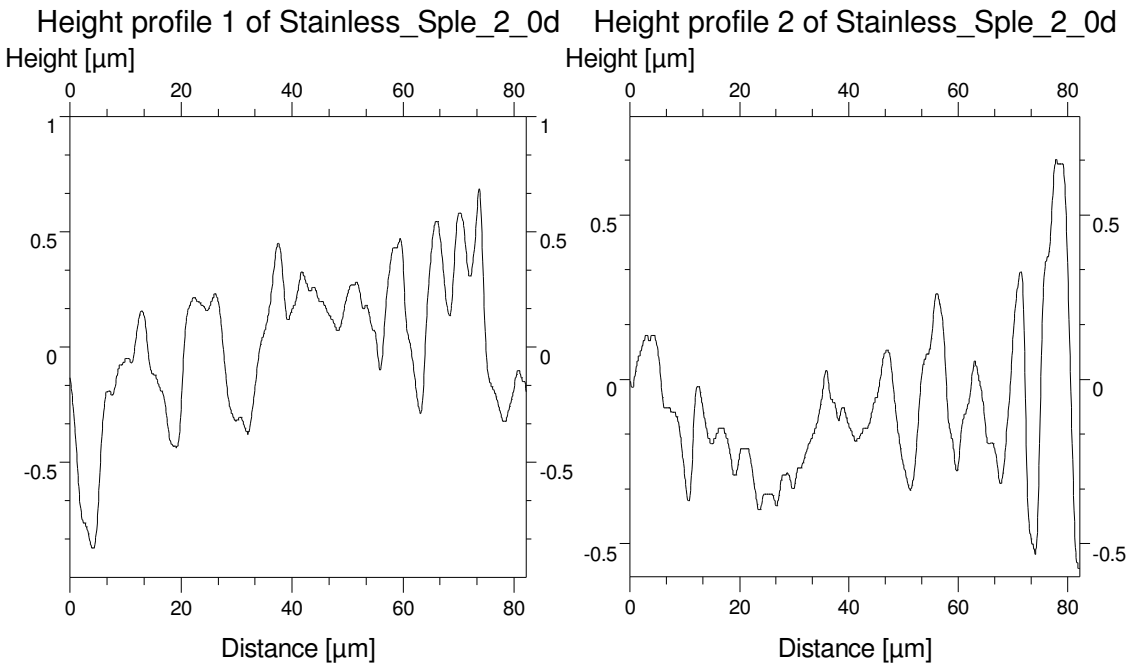

304 Stainless Steel, Sample 2

SEM MICROGRAPHS OF 304 STAINLESS STEEL BEFORE LAPPING

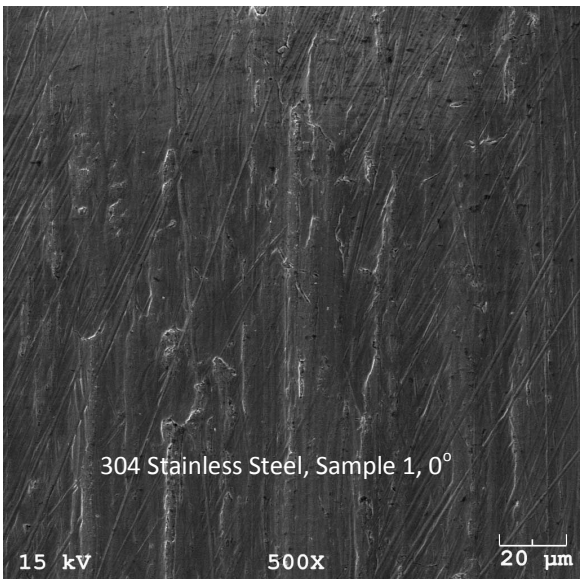

304 Stainless Steel, # 1, 500 Magnification

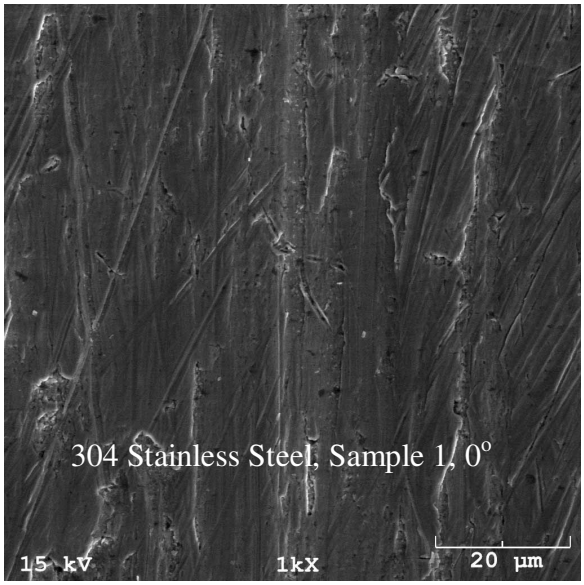

304 Stainless Steel, #1, 1000 Magnification

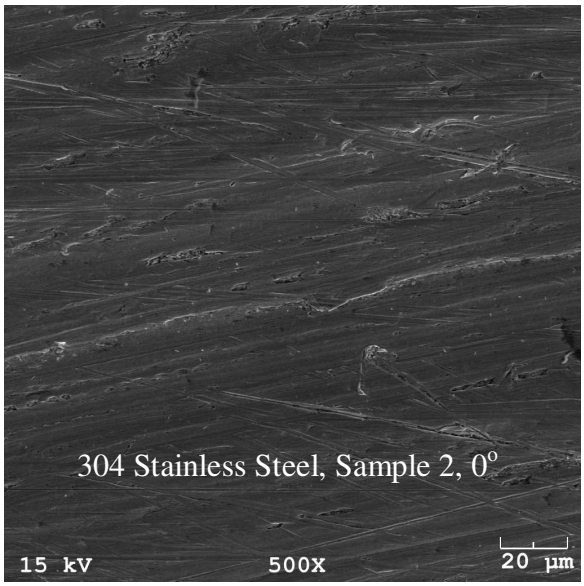

304 Stainless Steel, # 2, 500 Magnification

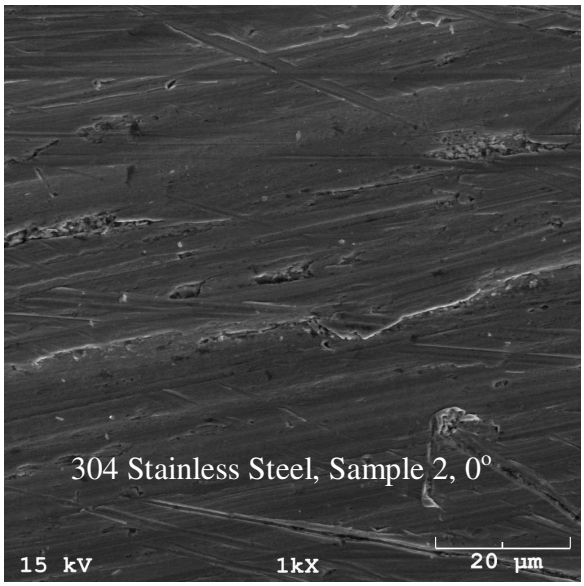

304 Stainless Steel, # 2, 1000 Magnification

INITIAL EDS OF 1018 STEEL BEFORE LAPPING

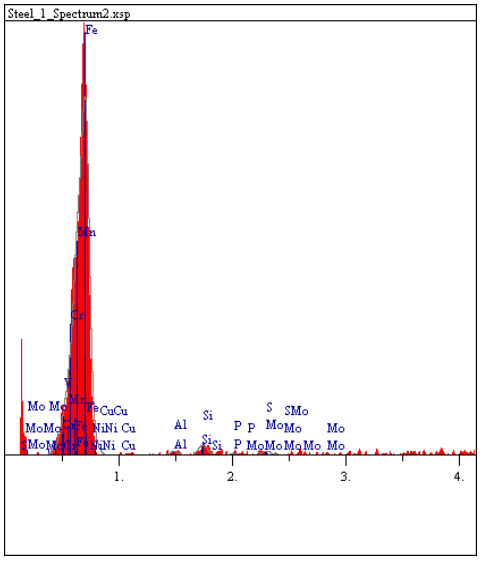

Intensity (c/sec)

Energy (keV)

Qualitative EDS

1018 Steel, Sample 1

Elt.	Line	Intensity (c/s)	Error 2-sig	Conc. wt. %
C	Ka	0.00	0.000	0.000
Al	Ka	1.53	0.350	0.225
Si	Ka	4.14	0.575	0.515
P	Ka	0.74	0.243	0.089
S	Ka	0.00	0.000	0.000
V	Ka	0.97	0.278	0.127
Cr	Ka	1.36	0.330	0.171
Mn	Ka	3.04	0.493	0.725
Fe	Ka	301.96	4.915	96.270
Ni	Ka	1.03	0.287	0.543
Cu	Ka	1.20	0.309	0.854
Mo	La	1.52	0.348	0.480
				100.0

Quantitative EDS

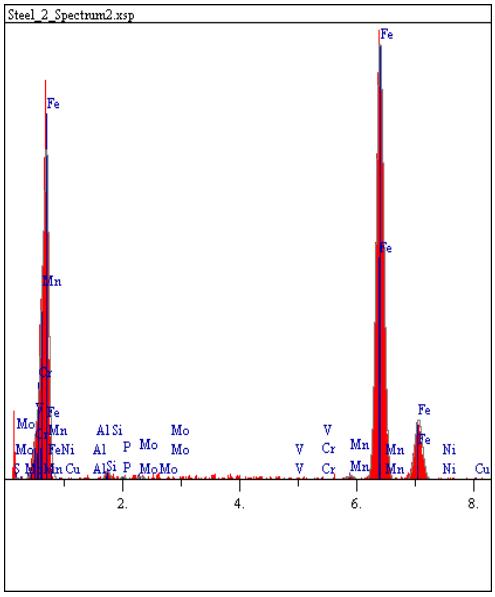

Intensity (c/sec)

Energy (keV)

Qualitative EDS

1018 Steel, Sample 2

Elt.	Line	Intensity (c/s)	Error 2-sig	Conc. wt. %
C	Ka	0.00	0.000	0.000
Al	Ka	0.24	0.138	0.032
Si	Ka	4.29	0.586	0.495
P	Ka	1.55	0.352	0.172
S	Ka	1.24	0.315	0.127
V	Ka	0.87	0.264	0.104
Cr	Ka	0.90	0.268	0.101
Mn	Ka	3.10	0.498	0.680
Fe	Ka	327.72	5.120	96.984
Ni	Ka	0.80	0.253	0.391
Cu	Ka	1.10	0.297	0.732
Mo	La	0.62	0.223	0.181
				100.0

Quantitative EDS

ANAGLYPH STEREOPAIR AND LINE PROFILE OF 1018 STEEL

BEFORE ALPPING

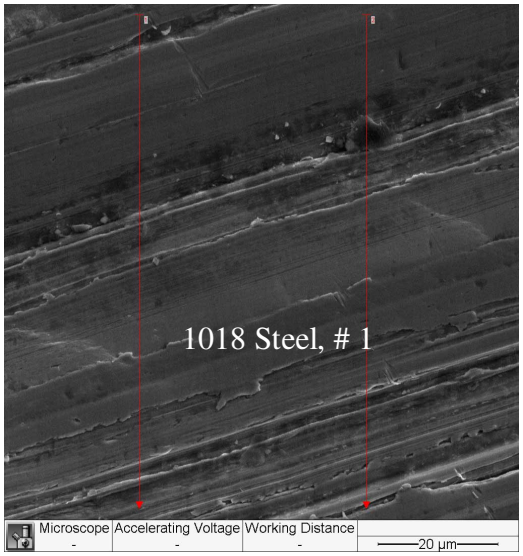

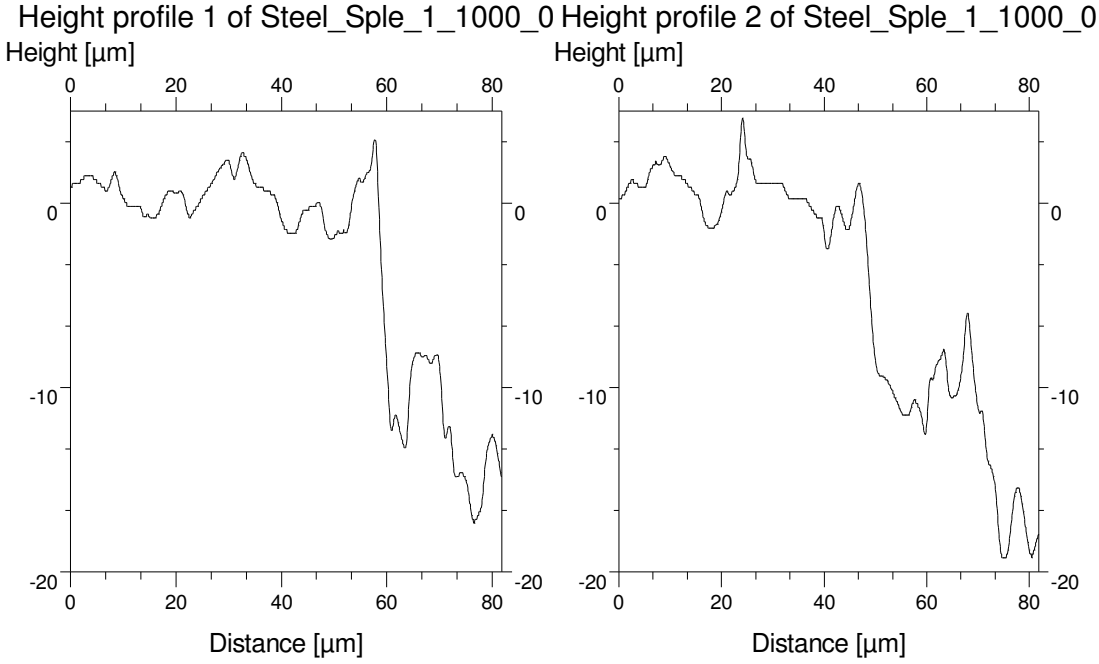

1018 Steel, Sample 1

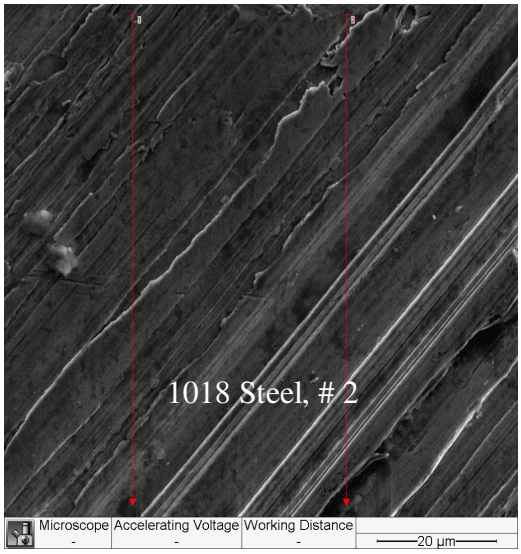

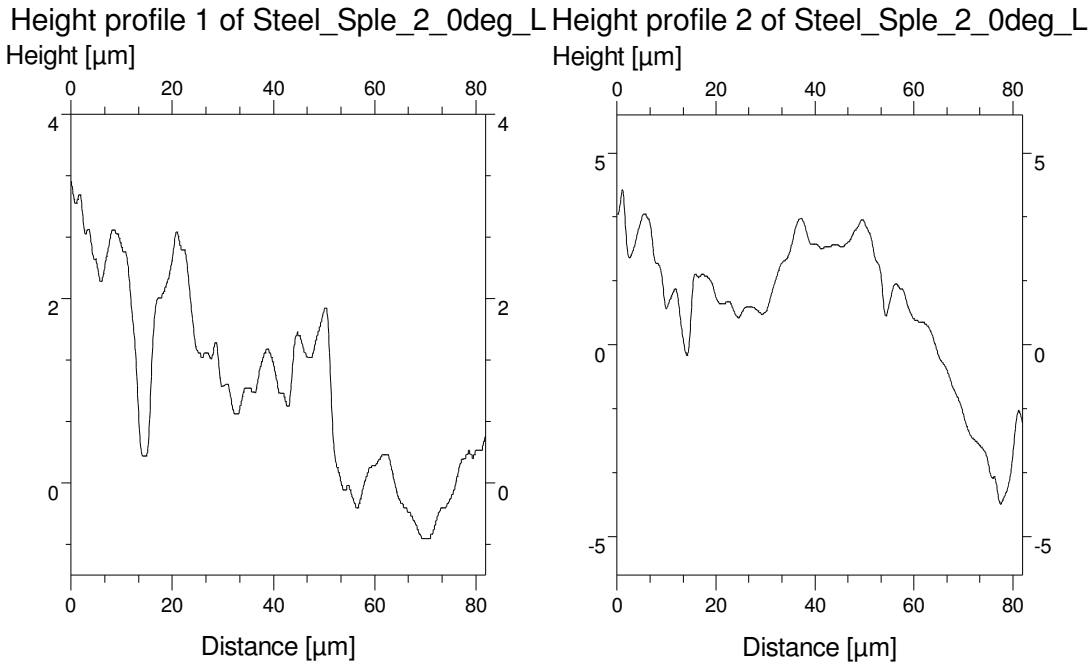

1018 Steel, Sample 2

SEM MICROGRAPHS OF 1018 STEEL BEFORE LAPPING

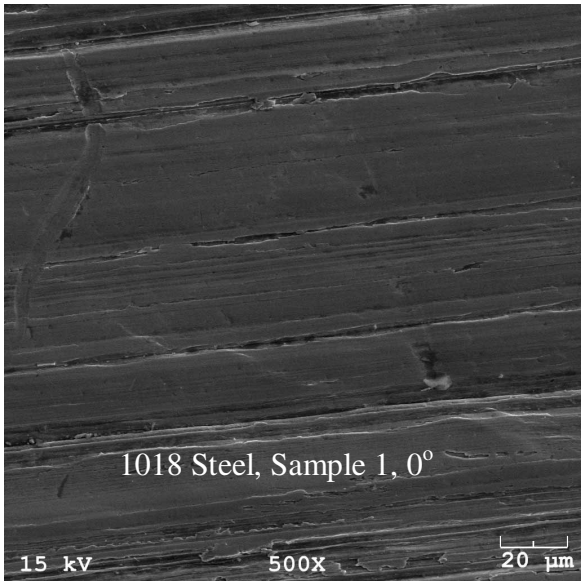

1018 Steel, Sample 1, 500 Magnification

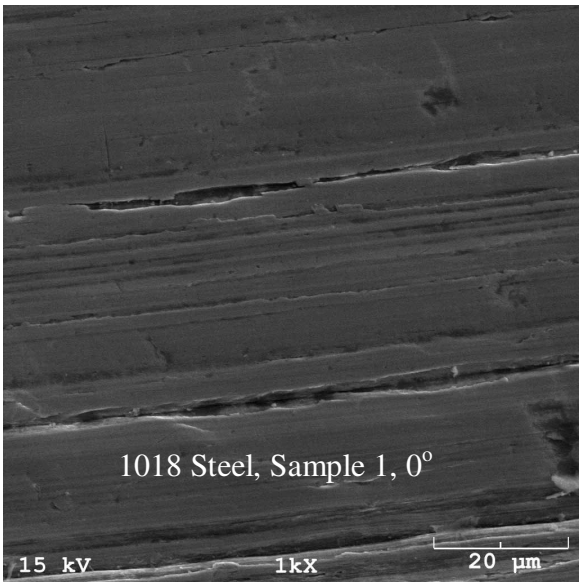

1018 Steel, Sample 1, 1000 Magnification

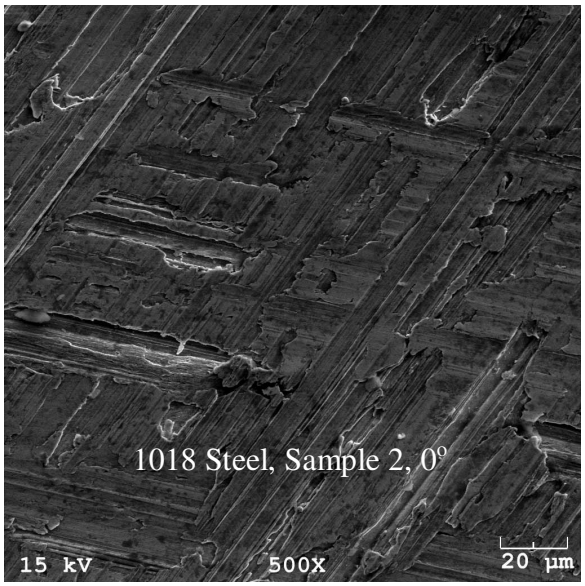

1018 Steel, Sample 2, 500 Magnification

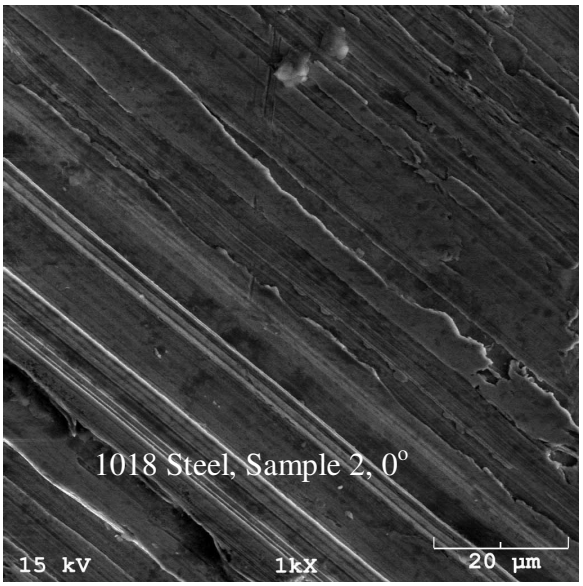

1018 Steel, Sample 2, 1000 Magnification

APPENDIX C

INDENTATION MADE ON SAMPLES BEORE LAPPING

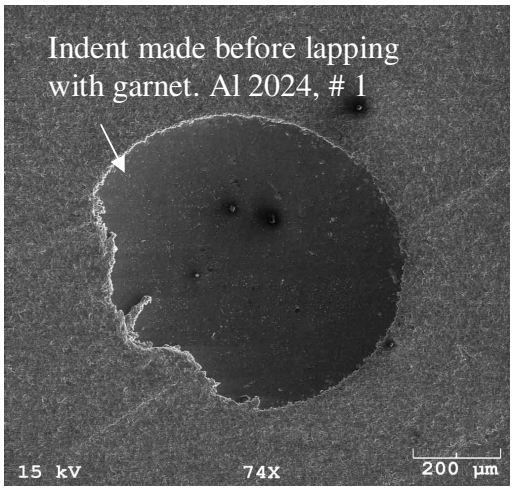

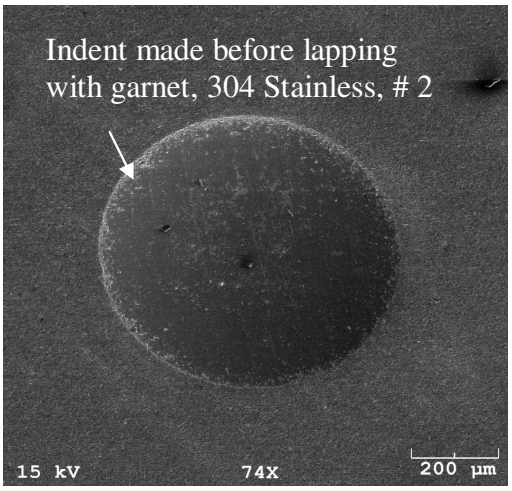

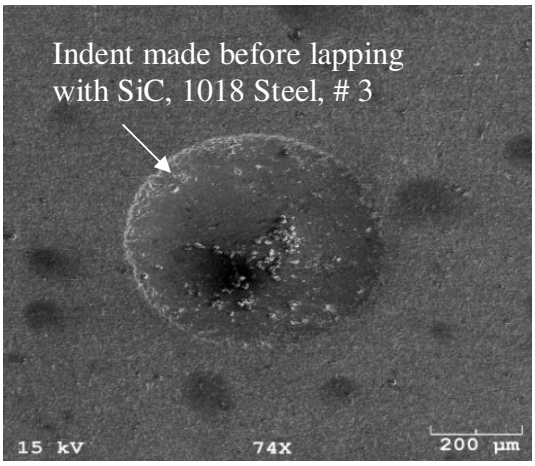

APPENDIX D

MATLAB CODE FOR IMAGE PROCESSING

```
clear
clc
[X,map]=imread('Stainless_4.bmp');
im = rgb2gray(X);

% ######## COUNTING AREAS ###################################
Scratched=0;
Lapped=0;
Unfinished=0;
background=0;

for i=1:642
   for j=1:661
      if im(i,j)>=128 && im(i,j)<=135;
         Scratched = Scratched + 1;
      elseif im(i,j)>=95 && im(i,j)<=116;
          Lapped = Lapped + 1;
      elseif im(i,j)>=20 && im(i,j)<=158;
          Unfinished=Unfinished+1;
      else
          background=background+1;
      end
   end
end


% ######## CREATING IMAGES ################################


for i=1:642
   for j=1:661

      if (im(i,j) >= 135||(im(i,j)<20)); %Not on the wafer (background)
         u(i,j) = 255; %Stainless_4.bmp
         v(i,j) = 255; %Scratched Area
         w(i,j) = 255; %Lapped Area
         x(i,j) = 255; %Unfinished Area
         y(i,j) = 255; %Total Contact Area
         z(i,j) = 255; %Entire Wafer
      end
      if (im(i,j)>=128 && im(i,j)<=135);%Scratched
```

```
            u(i,j) = 25; %Stainless_4.bmp
            v(i,j) = 25; %Scratched Area
            w(i,j) = 255; %Lapped Area
            x(i,j) = 255; %Unfinished Area
            y(i,j) = 100; %Total Contact Area
            z(i,j) = 100;  %Entire Wafer

        end
        if (im(i,j)>=95 && im(i,j)<=116); %Lapped
            u(i,j) = 50;
            v(i,j) =255;
            w(i,j) = 50;
            x(i,j) = 255;
            y(i,j) = 10;
            z(i,j) = 10;
        end
        if (im(i,j)>=125 && im(i,j)<=158); %Unfinshed
            u(i,j) = 200;
            v(i,j) = 255;
            w(i,j) = 255;
            x(i,j) = 255;
            y(i,j) = 255;
            z(i,j) = 10;
        end
    end
end
% read image may not be gray scale..hence assign
%Write Everything Image
map = colormap(gray(256));
figure(1)
colormap(gray(256))
image(u)
colormap(gray(256))
imwrite(u,map,'Run2Stainless_4.bmp');

figure(2)
colormap(gray(256))
image(v)
imwrite(v,map,'Scratched.bmp');

figure(3)
colormap(gray(256))
image(w)
imwrite(w,map,'Lapped.bmp');

figure(4)
```

```
colormap(gray(256))
image(x)
imwrite(x,map,'Unfinished.bmp');

figure(5)
colormap(gray(256))
image(y)
imwrite(y,map,'TotalContact.bmp');

figure(6)
colormap(gray(256))
image(z)
imwrite(z,map,'Entirewafer.bmp');
 imtool('Stainless_4.bmp')

 Scratched
 Lapped
 Unfinished
 background
 TotalContactArea=Scratched+Lapped
 TotalArea=Scratched+Lapped+Unfinished
 ImageArea=Scratched+Lapped+Unfinished+background
```

APPENDIX E

AVERAGE ROUGHNESS

Initial	**Roughness**			
Al 2024 #1 + Garnet	**Ra (µm)**		**Al 2024 #4 + SiC**	**Ra (µm)**
a	0.92		a	0.85
b	0.92		b	0.95
c	1.00		c	1.00
d	1.00		d	0.97
e	1.00		e	0.97
Mean	**0.97**		**Mean**	**0.95**
Al 2024 #2 + Garnet			**Al 2024 #5 + white Al_2O_3**	
a	0.90		a	1.00
b	0.90		b	1.00
c	0.97		c	0.97
d	0.97		d	0.97
e	0.95		e	1.03
Mean	**0.94**		**Mean**	**0.99**
Al 2024 #3 + SiC			**Al 2024 #6 + white Al_2O_3**	
a	0.92		a	0.97
b	0.92		b	1.00
c	0.95		c	1.00
d	0.90		d	0.95
e	0.87		e	0.95
Mean	**0.91**		**Mean**	**0.97**

Al lapped with 23 µm abrasives				
Al 2024 #1 + Garnet	**Ra (µm)**		**Al 2024 #4 + SiC**	**Ra (µm)**
a	0.54		a	0.67
b	0.05		b	0.05
c	0.05		c	0.05
d	0.46		d	0.05
e	0.41		e	0.05
Mean	**0.30**		**Mean**	**0.17**
Al 2024 #2 + Garnet			**Al 2024 #5 + white Al_2O_3**	
a	0.44		a	0.15
b	0.05		b	0.03
c	0.41		c	0.05
d	0.15		d	0.31
e	0.46		e	0.05
Mean	**0.30**		**Mean**	**0.12**
Al 2024 #3 + SiC			**Al 2024 #6 + white Al_2O_3**	
a	0.67		a	0.05
b	0.05		b	0.05
c	0.05		c	0.05
d	0.05		d	0.18
e	0.05		e	0.21
Mean	**0.17**		**Mean**	0.11

Al lapped with 8 µm abrasives				
Al 2024 #1 + Garnet	**Ra (µm)**		**Al 2024 #4 + SiC**	**Ra (µm)**
a	0.33		a	0.15
b	0.05		b	0.05
c	0.05		c	0.05
d	0.10		d	0.05
e	0.36		e	0.05
Mean	**0.18**		**Mean**	**0.07**
Al 2024 #2 + Garnet			**Al 2024 #5 + white Al_2O_3**	
a	0.33		a	0.05
b	0.33		b	0.05
c	0.05		c	0.05
d	0.05		d	0.23
e	0.05		e	0.03
Mean	**0.16**		**Mean**	**0.08**
Al 2024 #3 + SiC			**Al 2024 #6 + white Al_2O_3**	
a	0.05		a	0.10
b	0.05		b	0.05
c	0.05		c	0.05
d	0.05		d	0.08
e	0.23		e	0.05
Mean	**0.09**		**Mean**	**0.07**

Initial	**Roughness**			
304 SS #1 + Garnet	**Ra (µm)**		**304 SS #4+ SiC**	**Ra (µm)**
a	0.44		a	0.41
b	0.44		b	0.44
c	0.38		c	0.46
d	0.49		d	0.46
e	0.46		e	0.38
Mean	**0.44**		**Mean**	**0.43**
304 SS #2 + Garnet			**304 SS #5 + white Al_2O_3**	
a	0.90		a	0.90
b	1.00		b	0.67
c	0.97		c	0.62
d	0.87		d	0.95
e	0.97		e	0.79
Mean	**0.94**		**Mean**	**0.78**
304 SS #3 + SiC			**304 SS #6 + white Al_2O_3**	
a	0.95		a	0.72
b	0.87		b	0.74
c	0.67		c	0.72
d	0.79		d	0.74
e	0.67		e	0.72
Mean	**0.79**		**Mean**	**0.73**

304 SS lapped with 23 µm abrasives				
304 SS #1 + Garnet	**Ra (µm)**		**304 SS #4 + SiC**	**Ra (µm)**
a	0.23		a	0.23
b	0.23		b	0.05
c	0.23		c	0.31
d	0.23		d	0.05
e	0.03		e	0.08
Mean	**0.19**		**Mean**	**0.14**
304 SS #2 + Garnet			**304 SS #5 + white Al_2O_3**	
a	0.13		a	0.33
b	0.23		b	0.28
c	0.08		c	0.08
d	0.18		d	0.05
e	0.26		e	0.28
Mean	**0.17**		**Mean**	**0.21**
304 SS #3 + SiC			**304 SS #6 + white Al_2O_3**	
a	0.31		a	0.31
b	0.08		b	0.31
c	0.05		c	0.31
d	0.05		d	0.33
e	0.05		e	0.23
Mean	**0.11**		**Mean**	**0.30**

304 SS lapped with 8 µm abrasives				
304 SS #1 + garnet	**Ra (µm)**		**304 SS #4 + SiC**	**Ra (µm)**
a	0.05		a	0.13
b	0.15		b	0.13
c	0.15		c	0.13
d	0.15		d	0.08
e	0.15		e	0.15
Mean	**0.13**		**Mean**	**0.12**
304 SS #2 + garnet			**304 SS #5 + white Al_2O_3**	
a	0.15		a	0.21
b	0.15		b	0.13
c	0.15		c	0.05
d	0.15		d	0.05
e	0.15		e	0.05
Mean	**0.15**		**Mean**	**0.10**
304 SS #3 + SiC			**304 SS #6+ white Al_2O_3**	
a	0.10		a	0.15
b	0.10		b	0.18
c	0.10		c	0.23
d	0.08		d	0.08
e	0.05		e	0.21
Mean	**0.09**		**Mean**	**0.17**

Initial	**Roughness**			
1018 Steel #1 + Garnet	**Ra (µm)**		**1018 Steel #4 + SiC**	**Ra (µm)**
a	0.56		a	0.72
b	0.85		b	0.54
c	0.69		c	0.82
d	0.85		d	0.79
e	0.87		e	0.49
Mean	**0.76**		**Mean**	**0.67**
1018 Steel #2 + Garnet			**1018 Steel #5 + white Al_2O_3**	
a	0.92		a	0.95
b	1.15		b	0.92
c	0.62		c	1.10
d	0.82		d	0.69
e	0.77		e	0.85
Mean	**0.86**		**Mean**	**0.90**
1018 Steel #3 + SiC			**1018 Steel #6 + white Al_2O_3**	
a	1.15		a	0.72
b	1.08		b	0.82
c	0.77		c	0.82
d	1.05		d	1.05
e	1.18		e	1.10
Mean	**1.05**		**Mean**	**0.90**

1018 steel lapped with 23 µm abrasives				
Steel #1 + Garnet	**Ra (µm)**		**Steel #4 + SiC**	**Ra (µm)**
a	0.33		a	0.38
b	0.03		b	0.05
c	0.23		c	0.05
d	0.26		d	0.46
e	0.33		e	0.41
Mean	**0.24**		**Mean**	**0.27**
Steel #2 + Garnet			**Steel #5 + white Al_2O_3**	
a	0.28		a	0.36
b	0.23		b	0.41
c	0.33		c	0.44
d	0.31		d	0.38
e	0.31		e	0.38
Mean	**0.29**		**Mean**	**0.39**
Steel #3 + SiC			**Steel #6 + white Al_2O_3**	
a	0.59		a	0.36
b	0.49		b	0.15
c	0.51		c	0.05
d	0.44		d	0.36
e	0.49		e	0.31
Mean	**0.50**		**Mean**	**0.25**

1018 steel lapped with 8 µm abrasives				
Steel #1 + Garnet	**Ra (µm)**		**Steel #4 + SiC**	**Ra (µm)**
a	0.21		a	0.18
b	0.21		b	0.18
c	0.18		c	0.18
d	0.18		d	0.18
e	0.23		e	0.21
Mean	**0.20**		**Mean**	**0.18**
Steel #2 + Garnet			**Steel #5 + white Al_2O_3**	
a	0.21		a	0.15
b	0.21		b	0.15
c	0.21		c	0.15
d	0.21		d	0.15
e	0.23		e	0.18
Mean	**0.21**			**0.16**
Steel #3 + SiC			**Steel #6 + white Al_2O_3**	
a	0.23		a	0.15
b	0.23		b	0.15
c	0.23		c	0.15
d	0.18		d	0.18
e	0.18		e	0.23
Mean	**0.21**		**Mean**	**0.17**

APPENDIX F

SAS OUTPUT

Dissertation 23:43 Wednesday, September 10, 2008 1

Obs	abrasives	size	workpiece	MRR
1	1	23	1	0.013
2	1	23	1	0.008
3	1	8	1	0.005
4	1	8	1	0.007
5	1	23	2	0.012
6	1	23	2	0.013
7	1	8	2	0.007
8	1	8	2	0.009
9	1	23	3	0.012
10	1	23	3	0.017
11	1	8	3	0.007
12	1	8	3	0.010
13	2	23	1	0.006
14	2	23	1	0.007
15	2	8	1	0.005
16	2	8	1	0.004
17	2	23	2	0.011
18	2	23	2	0.010
19	2	8	2	0.008
20	2	8	2	0.011
21	2	23	3	0.008
22	2	23	3	0.009
23	2	8	3	0.007
24	2	8	3	0.005
25	3	23	1	0.010
26	3	23	1	0.010
27	3	8	1	0.003
28	3	8	1	0.006
29	3	23	2	0.016
30	3	23	2	0.012
31	3	8	2	0.008
32	3	8	2	0.008
33	3	23	3	0.014
34	3	23	3	0.012
35	3	8	3	0.007
36	3	8	3	0.009

Dissertation 23:43 Wednesday, September 10, 2008 2

The GLM Procedure

Class Level Information

Class	Levels	Values
abrasives	3	1 2 3

size	2	8 23
workpiece	3	1 2 3

Number of Observations Read 36
Number of Observations Used 36

The GLM Procedure

Dependent Variable: MRR

Source	DF	Sum of Squares	Mean Square	F Value	Pr > F
Model	17	0.00031489	0.00001852	5.65	0.0003
Error	18	0.00005900	0.00000328		
Corrected Total	35	0.00037389			

R-Square	Coeff Var	Root MSE	MRR Mean
0.842199	19.99285	0.001810	0.009056

Source	DF	Type I SS	Mean Square	F Value	Pr > F
abrasives	2	0.00004006	0.00002003	6.11	0.0094
size	1	0.00015211	0.00015211	46.41	<.0001
workpiece	2	0.00007872	0.00003936	12.01	0.0005
abrasives*size	2	0.00002372	0.00001186	3.62	0.0478
abrasives*workpiece	4	0.00001711	0.00000428	1.31	0.3056
size*workpiece	2	0.00000072	0.00000036	0.11	0.8963
abrasiv*size*workpie	4	0.00000244	0.00000061	0.19	0.9424

Source	DF	Type III SS	Mean Square	F Value	Pr > F
abrasives	2	0.00004006	0.00002003	6.11	0.0094
size	1	0.00015211	0.00015211	46.41	<.0001
workpiece	2	0.00007872	0.00003936	12.01	0.0005
abrasives*size	2	0.00002372	0.00001186	3.62	0.0478
abrasives*workpiece	4	0.00001711	0.00000428	1.31	0.3056
size*workpiece	2	0.00000072	0.00000036	0.11	0.8963
abrasiv*size*workpie	4	0.00000244	0.00000061	0.19	0.9424

The GLM Procedure

Tukey's Studentized Range (HSD) Test for MRR

NOTE: This test controls the Type I experimentwise error rate, but it generally has a higher
Type II error rate than REGWQ.

Alpha	0.05
Error Degrees of Freedom	18
Error Mean Square	3.278E-6
Critical Value of Studentized Range	3.60930
Minimum Significant Difference	0.0019

Means with the same letter are not significantly different.

Tukey Grouping	Mean	N	abrasives
A	0.0100000	12	1
A			
A	0.0095833	12	3
B	0.0075833	12	2

The GLM Procedure

Tukey's Studentized Range (HSD) Test for MRR

NOTE: This test controls the Type I experimentwise error rate, but it generally has a higher
Type II error rate than REGWQ.

Alpha	0.05
Error Degrees of Freedom	18
Error Mean Square	3.278E-6
Critical Value of Studentized Range	2.97115
Minimum Significant Difference	0.0013

Means with the same letter are not significantly different.

Tukey Grouping	Mean	N	size
A	0.0111111	18	23
B	0.0070000	18	8

The GLM Procedure

Tukey's Studentized Range (HSD) Test for MRR

NOTE: This test controls the Type I experimentwise error rate, but it generally has a higher
Type II error rate than REGWQ.

Alpha	0.05
Error Degrees of Freedom	18
Error Mean Square	3.278E-6
Critical Value of Studentized Range	3.60930
Minimum Significant Difference	0.0019

Means with the same letter are not significantly different.

Tukey Grouping	Mean	N	workpiece
A	0.0104167	12	2
A			
A	0.0097500	12	3
B	0.0070000	12	1

The GLM Procedure

Level of abrasives	Level of size	N	MRR Mean	MRR Std Dev
1	8	6	0.00750000	0.00176068
1	23	6	0.01250000	0.00288097
2	8	6	0.00666667	0.00258199
2	23	6	0.00850000	0.00187083
3	8	6	0.00683333	0.00213698
3	23	6	0.01233333	0.00233809

The GLM Procedure

Level of abrasives	Level of workpiece	N	MRR Mean	MRR Std Dev
1	1	4	0.00825000	0.00340343
1	2	4	0.01025000	0.00275379
1	3	4	0.01150000	0.00420317
2	1	4	0.00550000	0.00129099
2	2	4	0.01000000	0.00141421
2	3	4	0.00725000	0.00170783
3	1	4	0.00725000	0.00340343
3	2	4	0.01100000	0.00382971
3	3	4	0.01050000	0.00310913

The GLM Procedure

Level of size	Level of workpiece	N	MRR Mean	MRR Std Dev
8	1	6	0.00500000	0.00141421
8	2	6	0.00850000	0.00137840
8	3	6	0.00750000	0.00176068
23	1	6	0.00900000	0.00252982
23	2	6	0.01233333	0.00206559
23	3	6	0.01200000	0.00328634

The GLM Procedure

Level of abrasives	Level of size	Level of workpiece	N	MRR Mean	MRR Std Dev
1	8	1	2	0.00600000	0.00141421
1	8	2	2	0.00800000	0.00141421
1	8	3	2	0.00850000	0.00212132
1	23	1	2	0.01050000	0.00353553
1	23	2	2	0.01250000	0.00070711
1	23	3	2	0.01450000	0.00353553
2	8	1	2	0.00450000	0.00070711
2	8	2	2	0.00950000	0.00212132
2	8	3	2	0.00600000	0.00141421
2	23	1	2	0.00650000	0.00070711
2	23	2	2	0.01050000	0.00070711
2	23	3	2	0.00850000	0.00070711
3	8	1	2	0.00450000	0.00212132
3	8	2	2	0.00800000	0.00000000
3	8	3	2	0.00800000	0.00141421
3	23	1	2	0.01000000	0.00000000
3	23	2	2	0.01400000	0.00282843
3	23	3	2	0.01300000	0.00141421

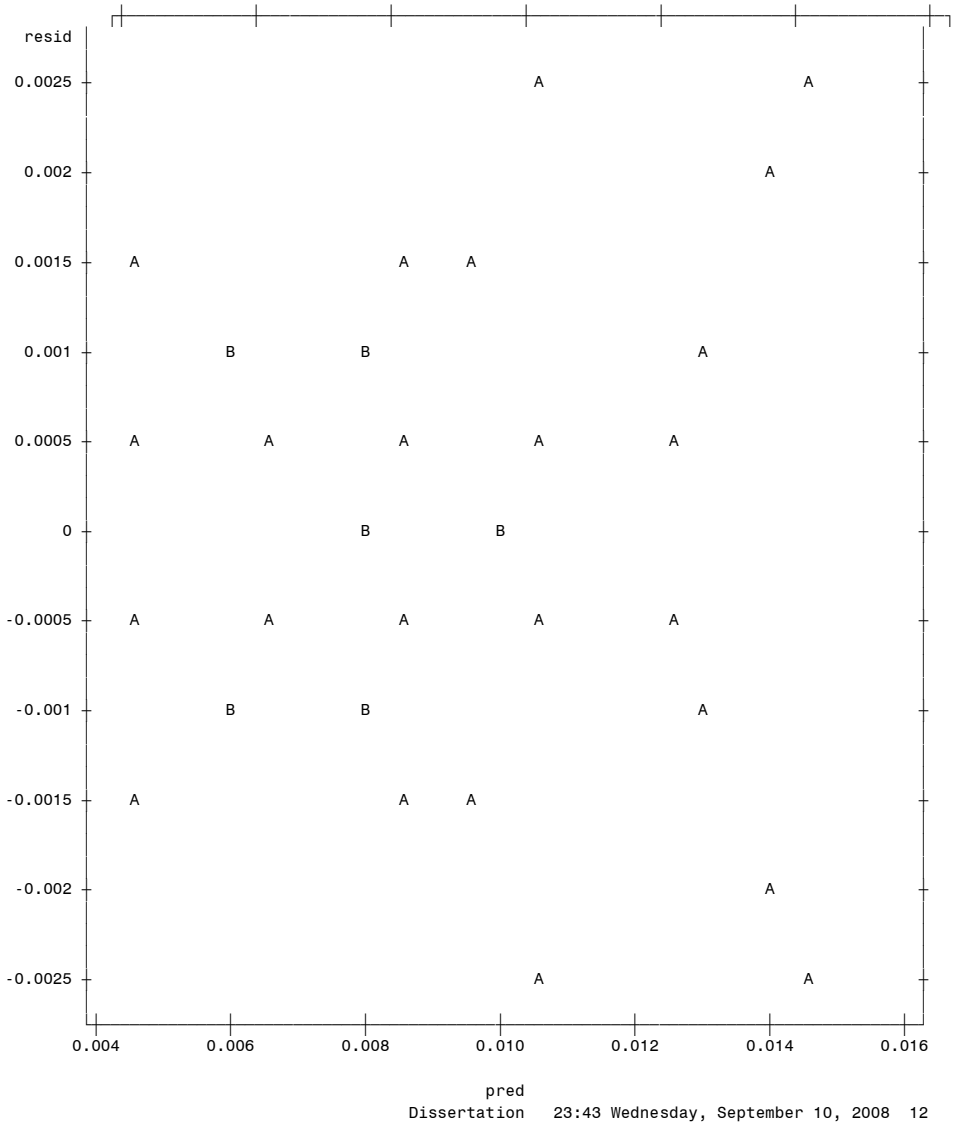
Plot of resid*pred. Legend: A = 1 obs, B = 2 obs, etc.
resid
0.0025
0.002
0.0015
0.001
0.0005
0
-0.0005
-0.001
-0.0015
-0.002
-0.0025
0.004
0.006
0.008
0.010
0.012
0.014
0.016
pred
Dissertation 23:43 Wednesday, September 10, 2008 12

Plot of resid*abrasives. Legend: A = 1 obs, B = 2 obs, etc.

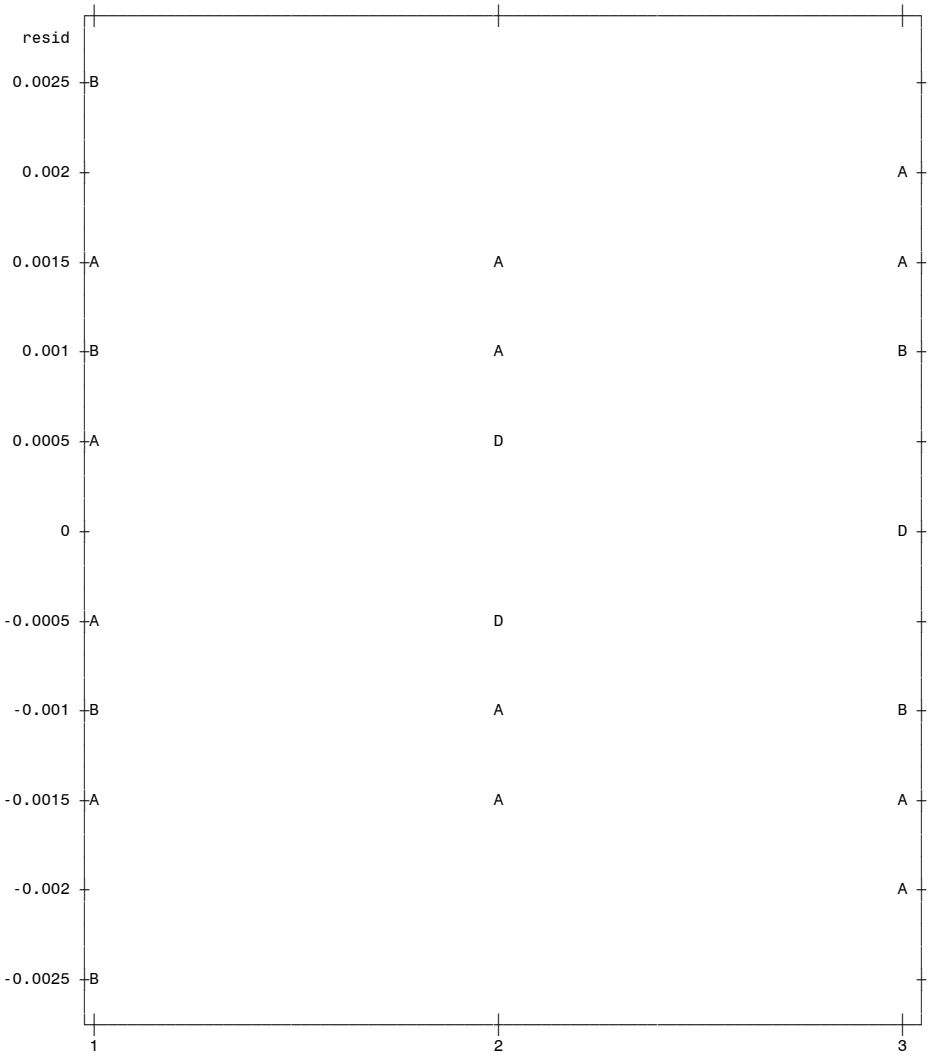

Plot of resid*size. Legend: A = 1 obs, B = 2 obs, etc.

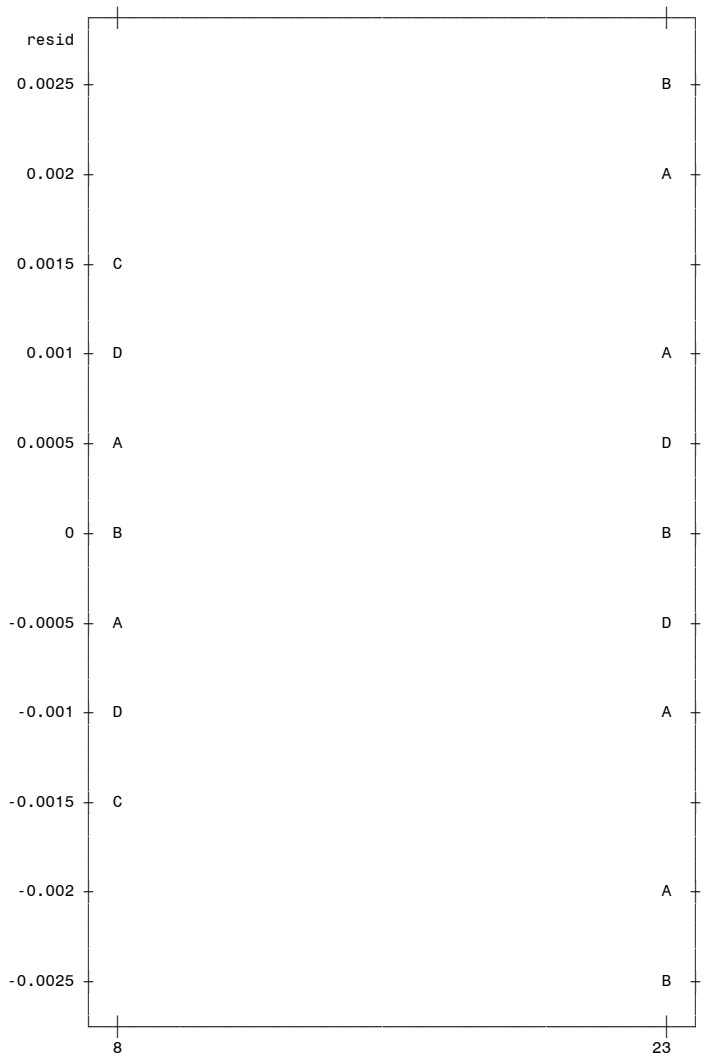

Plot of resid*workpiece. Legend: A = 1 obs, B = 2 obs, etc.

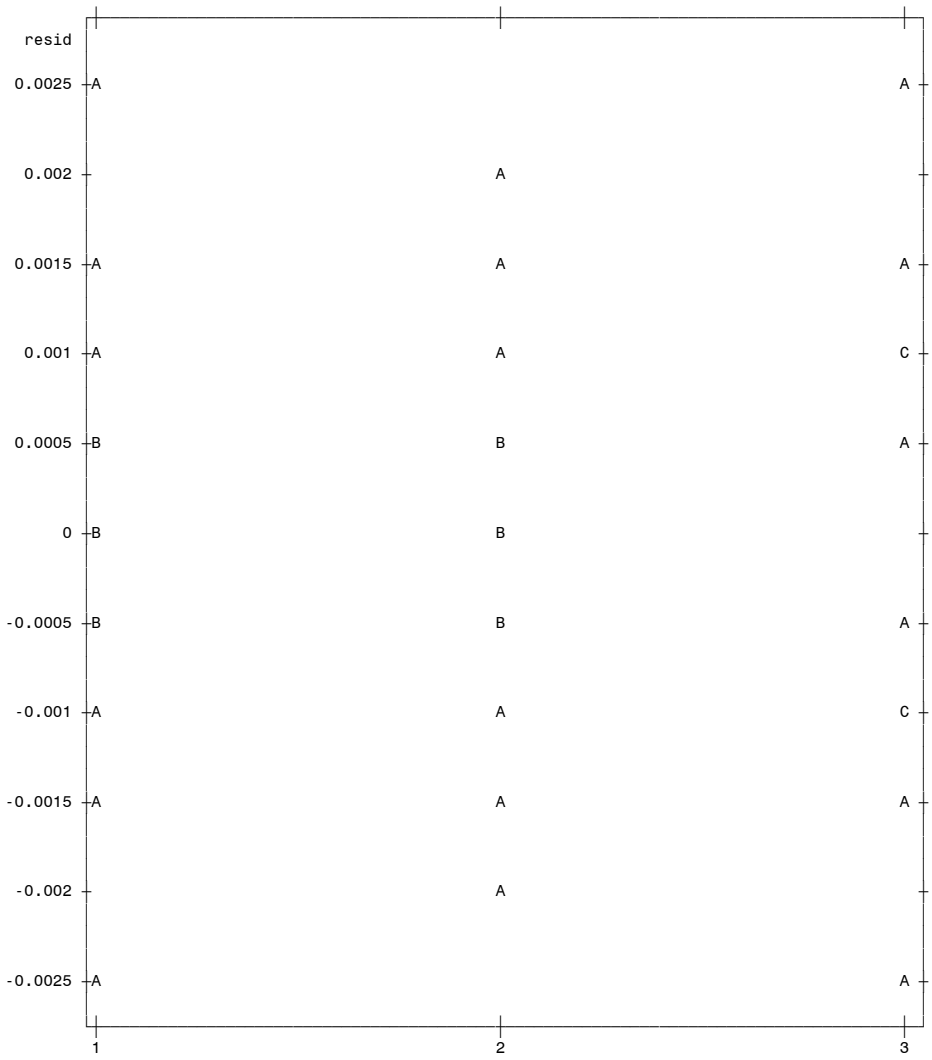

workpiece

The UNIVARIATE Procedure
Variable: resid

Moments

N	36	Sum Weights	36
Mean	0	Sum Observations	0
Std Deviation	0.00129835	Variance	1.68571E-6
Skewness	0	Kurtosis	-0.5389686
Uncorrected SS	0.000059	Corrected SS	0.000059
Coeff Variation	.	Std Error Mean	0.00021639

Basic Statistical Measures

Location Variability

Mean	0.00000	Std Deviation	0.00130
Median	0.00000	Variance	1.68571E-6
Mode	-0.00100	Range	0.00500
		Interquartile Range	0.00200

NOTE: The mode displayed is the smallest of 6 modes with a count of 2.

Tests for Location: MuO=O

Test	-Statistic-		-----p Value------	
Student's t	t	0	Pr > |t|	1.0000
Sign	M	1	Pr >= |M|	0.8642
Signed Rank	S	1	Pr >= |S|	0.9867

Tests for Normality

Test	--Statistic---		-----p Value------	
Shapiro-Wilk	W	0.975414	Pr < W	0.5903
Kolmogorov-Smirnov	D	0.094364	Pr > D	>0.1500
Cramer-von Mises	W-Sq	0.049642	Pr > W-Sq	>0.2500
Anderson-Darling	A-Sq	0.29595	Pr > A-Sq	>0.2500

Quantiles (Definition 5)

Quantile	Estimate
100% Max	0.0025
99%	0.0025
95%	0.0025
90%	0.0015
75% Q3	0.0010

The UNIVARIATE Procedure
Variable: resid

Quantiles (Definition 5)

Quantile	Estimate
50% Median	0.0000
25% Q1	-0.0010
10%	-0.0015
5%	-0.0025
1%	-0.0025
0% Min	-0.0025

Extreme Observations

```
          -----Lowest-----        -----Highest----

            Value      Obs          Value      Obs

          -0.0025        9         0.0015       12
          -0.0025        2         0.0015       20
          -0.0020       30         0.0020       29
          -0.0015       27         0.0025       10
          -0.0015       11         0.0025        1


        Stem Leaf                     #             Boxplot
           2 55                       2                |
           2 0                        1                |
           1 555                      3                |
           1 00000                    5               +-----+
           0 55555                    5               |     |
           0 0000                     4               *--+--*
          -0                                          |     |
          -0 55555                    5               |     |
          -1 00000                    5               +-----+
          -1 555                      3                |
          -2 0                        1                |
          -2 55                       2                |
             ----+----+----+----+
         Multiply Stem.Leaf by 10**-3
```


The UNIVARIATE Procedure
Variable: resid

Normal Probability Plot

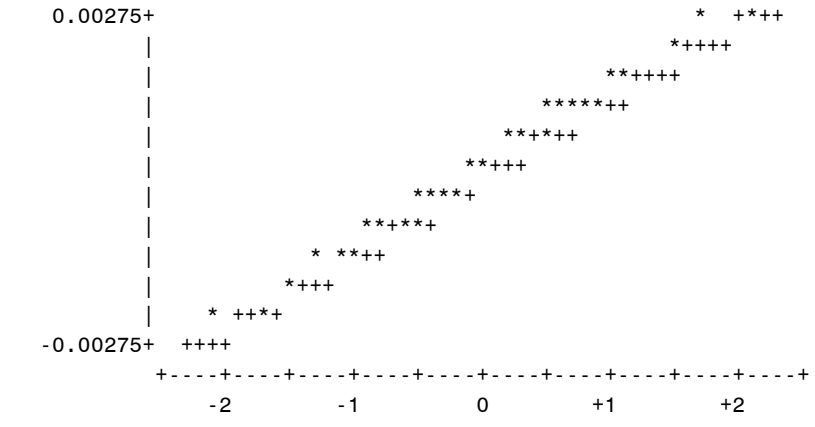

Surface Roughness Output

Dissertation 15:48 Wednesday, December 5, 2007 1

Obs	abrasives	size	workpiece	roughness
1	1	23	1	0.30
2	1	23	1	0.30
3	1	8	1	0.18
4	1	8	1	0.16
5	1	23	2	0.19
6	1	23	2	0.17
7	1	8	2	0.13
8	1	8	2	0.15
9	1	23	3	0.24
10	1	23	3	0.29
11	1	8	3	0.20
12	1	8	3	0.21
13	2	23	1	0.17
14	2	23	1	0.17
15	2	8	1	0.09
16	2	8	1	0.08
17	2	23	2	0.11
18	2	23	2	0.14
19	2	8	2	0.09
20	2	8	2	0.12
21	2	23	3	0.50
22	2	23	3	0.27
23	2	8	3	0.21
24	2	8	3	0.18
25	3	23	1	0.12
26	3	23	1	0.11
27	3	8	1	0.07
28	3	8	1	0.07
29	3	23	2	0.21
30	3	23	2	0.30
31	3	8	2	0.10
32	3	8	2	0.17
33	3	23	3	0.39
34	3	23	3	0.25
35	3	8	3	0.16
36	3	8	3	0.17

Dissertation 15:48 Wednesday, December 5, 2007 2

The GLM Procedure

Class Level Information

Class	Levels	Values
abrasives	3	1 2 3
size	2	8 23
workpiece	3	1 2 3

Number of Observations Read 36
Number of Observations Used 36

The GLM Procedure

Dependent Variable: roughness

Source	DF	Sum of Squares	Mean Square	F Value	Pr > F
Model	17	0.25321389	0.01489493	5.81	0.0003
Error	18	0.04615000	0.00256389		
Corrected Total	35	0.29936389			

R-Square	Coeff Var	Root MSE	roughness Mean
0.845840	26.92548	0.050635	0.188056

Source	DF	Type I SS	Mean Square	F Value	Pr > F
abrasives	2	0.00867222	0.00433611	1.69	0.2123
size	1	0.07933611	0.07933611	30.94	<.0001
workpiece	2	0.08283889	0.04141944	16.15	<.0001
abrasives*size	2	0.00143889	0.00071944	0.28	0.7586
abrasives*workpiece	4	0.05542778	0.01385694	5.40	0.0049
size*workpiece	2	0.00867222	0.00433611	1.69	0.2123
abrasiv*size*workpie	4	0.01682778	0.00420694	1.64	0.2075

Source	DF	Type III SS	Mean Square	F Value	Pr > F
abrasives	2	0.00867222	0.00433611	1.69	0.2123
size	1	0.07933611	0.07933611	30.94	<.0001
workpiece	2	0.08283889	0.04141944	16.15	<.0001
abrasives*size	2	0.00143889	0.00071944	0.28	0.7586
abrasives*workpiece	4	0.05542778	0.01385694	5.40	0.0049
size*workpiece	2	0.00867222	0.00433611	1.69	0.2123
abrasiv*size*workpie	4	0.01682778	0.00420694	1.64	0.2075

The GLM Procedure

Tukey's Studentized Range (HSD) Test for roughness

NOTE: This test controls the Type I experimentwise error rate, but it generally has a higher Type
II error rate than REGWQ.

Alpha	0.05
Error Degrees of Freedom	18
Error Mean Square	0.002564
Critical Value of Studentized Range	3.60930
Minimum Significant Difference	0.0528

Means with the same letter are not significantly different.

Tukey Grouping	Mean	N	abrasives
A	0.21000	12	1
A			
A	0.17750	12	2
A			
A	0.17667	12	3

The GLM Procedure

Tukey's Studentized Range (HSD) Test for roughness

NOTE: This test controls the Type I experimentwise error rate, but it generally has a higher Type
II error rate than REGWQ.

Alpha	0.05
Error Degrees of Freedom	18
Error Mean Square	0.002564
Critical Value of Studentized Range	2.97115
Minimum Significant Difference	0.0355

Means with the same letter are not significantly different.

Tukey Grouping	Mean	N	size
A	0.23500	18	23
B	0.14111	18	8

The GLM Procedure

Tukey's Studentized Range (HSD) Test for roughness

NOTE: This test controls the Type I experimentwise error rate, but it generally has a higher Type II error rate than REGWQ.

Alpha	0.05
Error Degrees of Freedom	18
Error Mean Square	0.002564
Critical Value of Studentized Range	3.60930
Minimum Significant Difference	0.0528

Means with the same letter are not significantly different.

Tukey Grouping	Mean	N	workpiece
A	0.25583	12	3
B	0.15667	12	2
B			
B	0.15167	12	1

The GLM Procedure

Level of abrasives	Level of size	N	roughness Mean	roughness Std Dev
1	8	6	0.17166667	0.03060501
1	23	6	0.24833333	0.05776389
2	8	6	0.12833333	0.05419102
2	23	6	0.22666667	0.14431447
3	8	6	0.12333333	0.04885352
3	23	6	0.23000000	0.10751744

The GLM Procedure

Level of abrasives	Level of workpiece	N	roughness Mean	roughness Std Dev
1	1	4	0.23500000	0.07549834
1	2	4	0.16000000	0.02581989
1	3	4	0.23500000	0.04041452
2	1	4	0.12750000	0.04924429
2	2	4	0.11500000	0.02081666
2	3	4	0.29000000	0.14491377
3	1	4	0.09250000	0.02629956

3	2	4	0.19500000	0.08346656
3	3	4	0.24250000	0.10626225

The GLM Procedure

Level of size	Level of workpiece	N	roughness Mean	roughness Std Dev
8	1	6	0.10833333	0.04875107
8	2	6	0.12666667	0.03011091
8	3	6	0.18833333	0.02136976
23	1	6	0.19500000	0.08502941
23	2	6	0.18666667	0.06592926
23	3	6	0.32333333	0.10191500

The GLM Procedure

Level of abrasives	Level of size	Level of workpiece	N	roughness Mean	roughness Std Dev
1	8	1	2	0.17000000	0.01414214
1	8	2	2	0.14000000	0.01414214
1	8	3	2	0.20500000	0.00707107
1	23	1	2	0.30000000	0.00000000
1	23	2	2	0.18000000	0.01414214
1	23	3	2	0.26500000	0.03535534
2	8	1	2	0.08500000	0.00707107
2	8	2	2	0.10500000	0.02121320
2	8	3	2	0.19500000	0.02121320
2	23	1	2	0.17000000	0.00000000
2	23	2	2	0.12500000	0.02121320
2	23	3	2	0.38500000	0.16263456
3	8	1	2	0.07000000	0.00000000
3	8	2	2	0.13500000	0.04949747
3	8	3	2	0.16500000	0.00707107
3	23	1	2	0.11500000	0.00707107
3	23	2	2	0.25500000	0.06363961
3	23	3	2	0.32000000	0.09899495

Plot of resid*pred. Legend: A = 1 obs, B = 2 obs, etc.

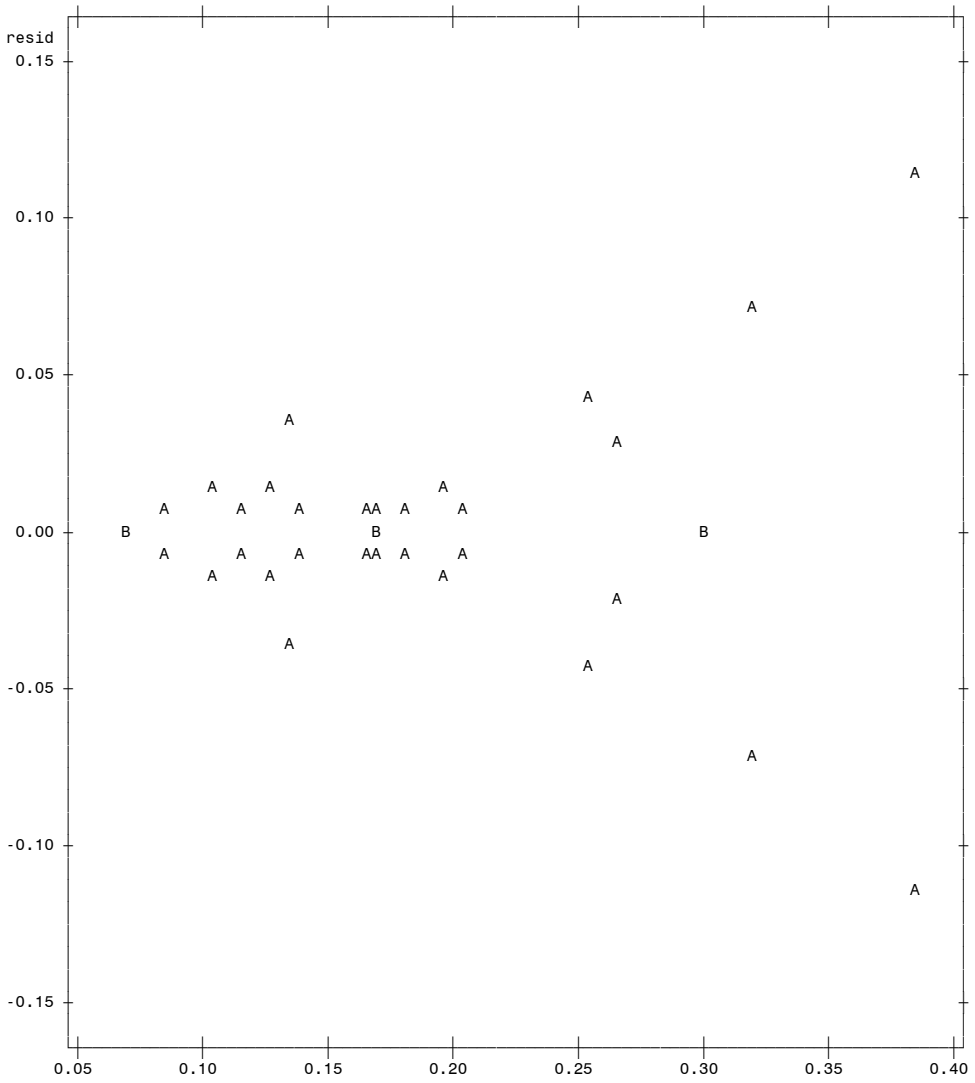

Dissertation 15:48 Wednesday, December 5, 2007 12

Plot of resid*abrasives. Legend: A = 1 obs, B = 2 obs, etc.

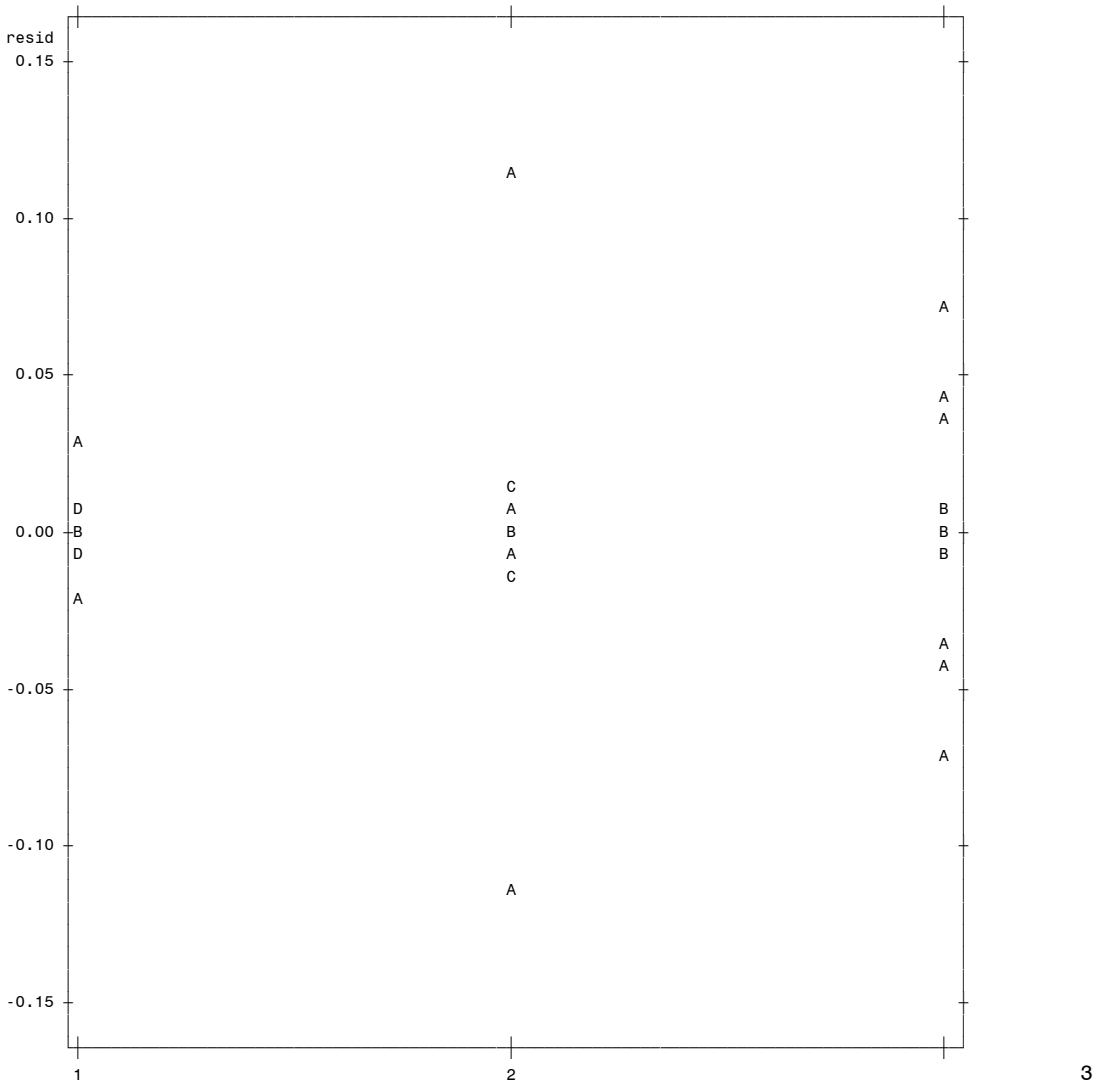

Dissertation 15:48 Wednesday, December 5, 2007 13

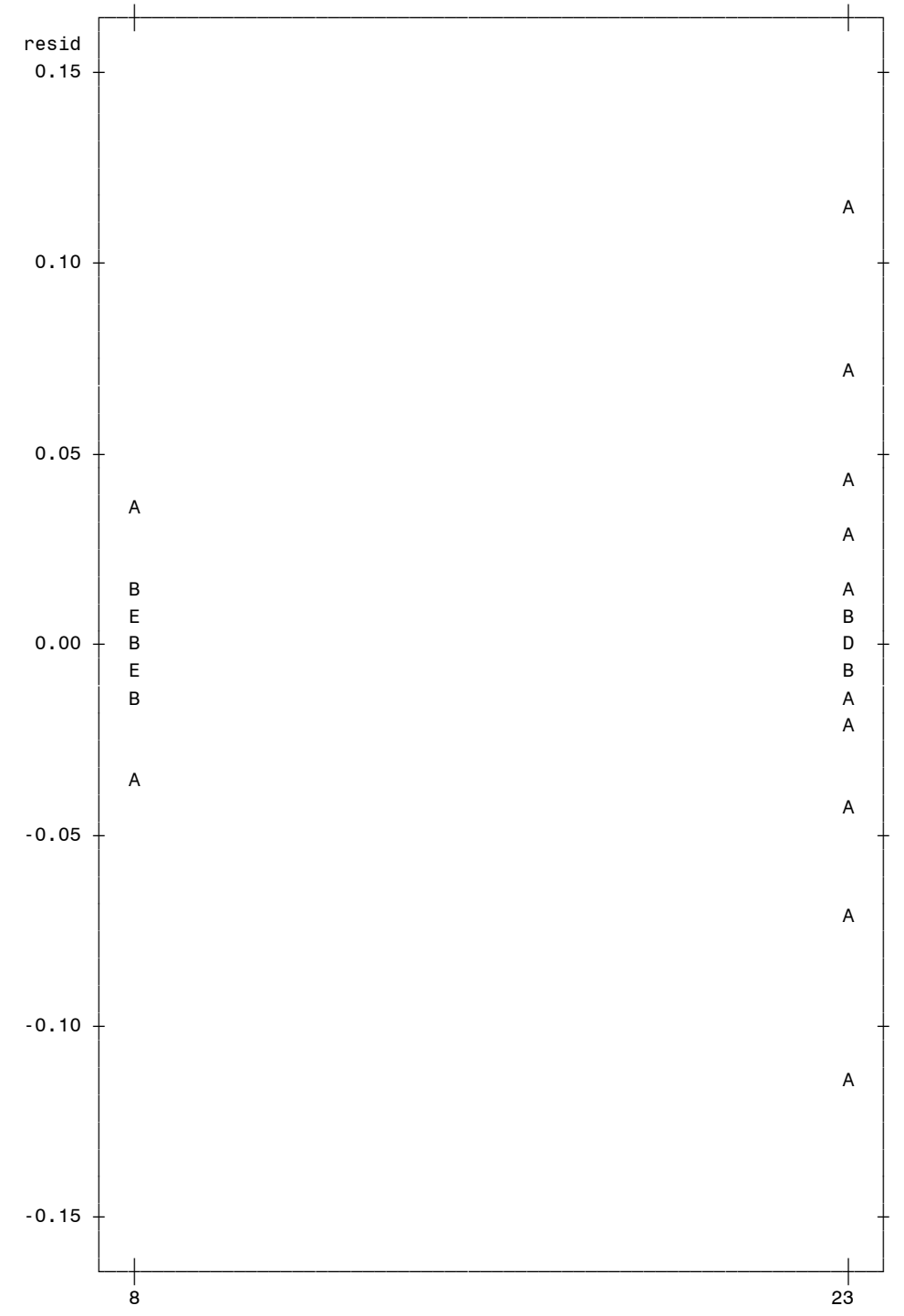

Dissertation 15:48 Wednesday, December 5, 2007 14

Plot of resid*workpiece. Legend: A = 1 obs, B = 2 obs, etc.

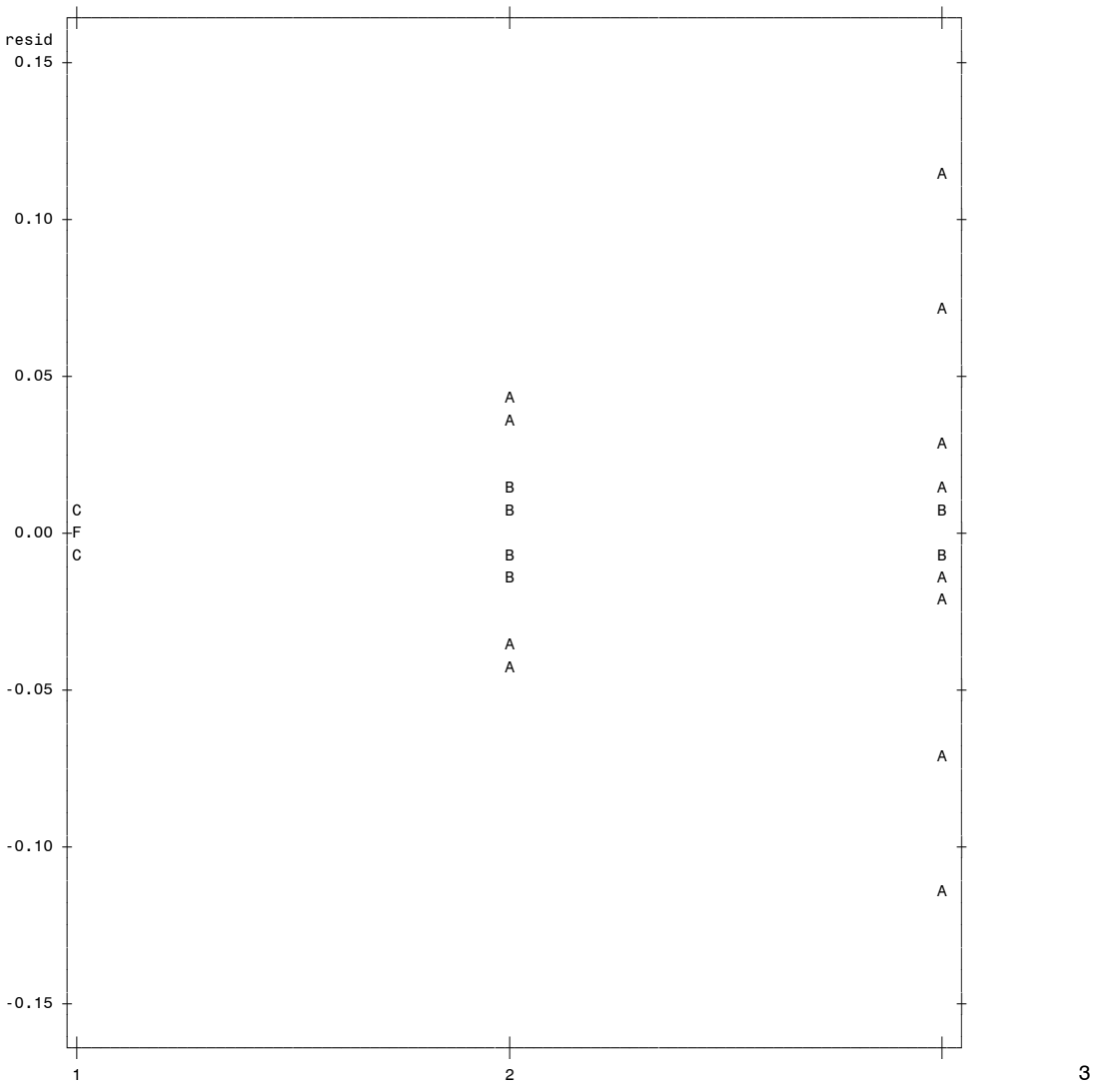

workpiece

The UNIVARIATE Procedure
Variable: resid

Moments

N	36	Sum Weights	36
Mean	0	Sum Observations	0
Std Deviation	0.03631214	Variance	0.00131857
Skewness	0	Kurtosis	4.72669691
Uncorrected SS	0.04615	Corrected SS	0.04615
Coeff Variation	.	Std Error Mean	0.00605202

Basic Statistical Measures

Location		Variability	
Mean	0.00000	Std Deviation	0.03631
Median	0.00000	Variance	0.00132
Mode	-0.01000	Range	0.23000
		Interquartile Range	0.02000

NOTE: The mode displayed is the smallest of 6 modes with a count of 2.

Tests for Location: Mu0=0

Test	-Statistic-		-----p Value------	
Student's t	t	0	Pr > |t|	1.0000
Sign	M	0	Pr >= |M|	1.0000
Signed Rank	S	-4.5	Pr >= |S|	0.9400

Tests for Normality

Test	--Statistic---		-----p Value------	
Shapiro-Wilk	W	0.864121	Pr < W	0.0004
Kolmogorov-Smirnov	D	0.200883	Pr > D	<0.0100
Cramer-von Mises	W-Sq	0.378814	Pr > W-Sq	<0.0050
Anderson-Darling	A-Sq	1.991752	Pr > A-Sq	<0.0050

Quantiles (Definition 5)

Quantile	Estimate
100% Max	0.115
99%	0.115
95%	0.070
90%	0.035
75% Q3	0.010
50% Median	0.000

The UNIVARIATE Procedure
Variable: resid

Quantiles (Definition 5)

Quantile	Estimate
25% Q1	-0.010
10%	-0.035
5%	-0.070
1%	-0.115
0% Min	-0.115

Extreme Observations

-----Lowest----		----Highest----	
Value	Obs	Value	Obs
-0.115	22	0.025	10
-0.070	34	0.035	32
-0.045	29	0.045	30
-0.035	31	0.070	33
-0.025	9	0.115	21

```
Stem Leaf                     #             Boxplot
  10 5                        1                *
   8
   6 0                        1                0
   4 5                        1                0
   2 55                       2                |
   0 0000005555000555        16             +--+--+
  -0 5550005555              10             +-----+
  -2 55                       2                |
  -4 5                        1                0
  -6 0                        1                *
  -8
 -10 5                        1                *
     ----+----+----+----+
 Multiply Stem.Leaf by 10**-2
```


The UNIVARIATE Procedure
Variable: resid

Normal Probability Plot

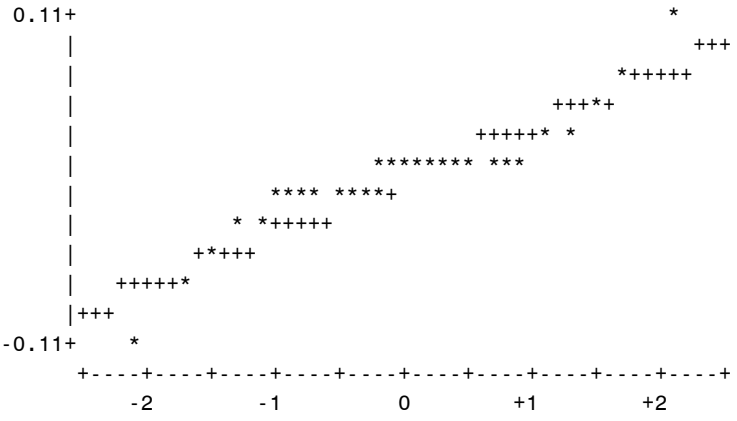

APPENDIX G

Types of Velocity

Velocity can be classified into six categories: angular, circumferential, linear, rotational, sliding, and tangential velocity. In a lapping operation, three types of velocity that are observed include: circumferential velocity, rolling velocity, and sliding velocity.

(i) Angular Velocity or Rolling Velocity

The angular velocity, ω, is derivative of angular position as a function of time, that is, $\omega = \frac{d\theta}{dt}$. Also, in magnitude, the angular velocity is given as linear velocity divided by radius of rotation, that is, $\omega = \frac{v}{r}$. It is the speed at which an object rotates. The SI unit of angular velocity is radians per second, but revolution per minute is also a common unit.

(ii) Circumferential Speed or Cutting Speed (πD N). It is the speed of the workpiece.

(iii) Linear Velocity (distance/time)

(iv) Rotational Velocity (2πN). It is the speed of the spindle.

(v) Skidding or Sliding or Slip Velocity

(vi) Tangential Velocity (ds/dt)

Tangential velocity represents the linear velocity of a point on a rotating rigid body at a given distance. It is the differential of the circumferential speed.

APPENDIX H

CONNECTION OF AMP METER (STRASBAUGH, 1999)

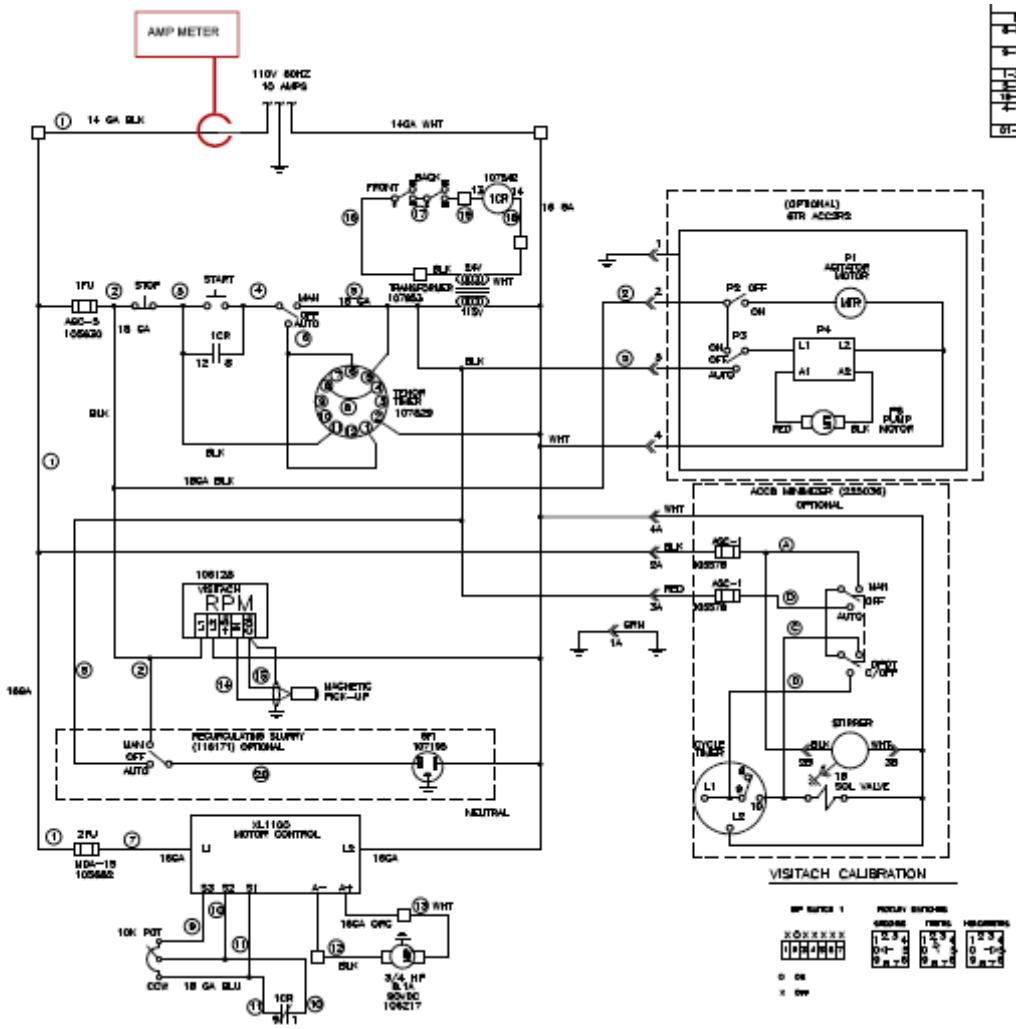

APPENDIX I

FRICTIONAL TORQUE DATA - Al 2024 + GARNET

K = 3.375, N = 85	Frictional Torque, Dry Run	Time	K = 3.375, N = 85	Frictional Torque, Wet Run	Δ frictional torque
Current, i (amp)	(lbf)	Al, # 1_2	Current, i (amp)	(lbf)	Wet run - Dry run
Dry run	K*i	(sec)	Wet Run	K*i	(lbf)
1.9335	6.5254	1	2.1776	7.3494	0.8240
1.9309	6.5166	2	2.1712	7.3278	0.8112
1.9345	6.5288	3	2.1712	7.3278	0.7990
1.9298	6.5131	4	2.1873	7.3821	0.8691
1.9307	6.5159	5	2.1834	7.3690	0.8530
1.9263	6.5013	6	2.1955	7.4098	0.9086
1.9314	6.5183	7	2.1800	7.3575	0.8392
1.9293	6.5112	8	2.1768	7.3467	0.8355
1.9293	6.5112	9	2.1685	7.3187	0.8075
1.9344	6.5286	10	2.1690	7.3204	0.7918
1.9365	6.5355	11	2.1713	7.3281	0.7926
1.9337	6.5261	12	2.1867	7.3801	0.8540
1.9350	6.5306	13	2.1753	7.3416	0.8110
1.9340	6.5273	14	2.1769	7.3470	0.8198
1.9385	6.5424	15	2.1920	7.3980	0.8556
1.9312	6.5176	16	2.1907	7.3936	0.8760
1.9394	6.5455	17	2.1810	7.3609	0.8154
1.9342	6.5278	18	2.1703	7.3248	0.7970
1.9399	6.5470	19	2.1807	7.3599	0.8129
1.9351	6.5308	20	2.1766	7.3460	0.8152
1.9371	6.5377	21	2.1778	7.3501	0.8124
1.9335	6.5256	22	2.1973	7.4159	0.8903
1.9362	6.5347	23	2.1888	7.3872	0.8525
1.9301	6.5141	24	2.1908	7.3940	0.8799
1.9367	6.5364	25	2.1832	7.3683	0.8319
1.9306	6.5158	26	2.1749	7.3403	0.8245
1.9368	6.5367	27	2.1833	7.3686	0.8319
1.9306	6.5158	28	2.1648	7.3062	0.7904
.	.	.	.	.	.
.	.	.	.	.	.
1.8714	6.3160	1199	2.2360	7.5463	1.2304
1.8737	6.3236	1200	2.2499	7.5934	1.2698

FRICTIONAL TORQUE DATA - 304 Stainless + SiC

K = 3.375, N = 85	Frictional Torque, Dry Run	Time	K = 3.375, N = 85	Frictional Torque, Wet Run	Δ Frictional Torque
Current, i (amp)	(lbf)	Stainless, # 3_4	Current, i (amp)	(lbf)	Wet Run - Dry Run
Dry Run	K*i	(sec)	Wet Run	K*i	(lbf)
1.9216	6.4854	1	2.26035	7.6287	1.1433
1.9198	6.4793	2	2.25415	7.6078	1.1284
1.9280	6.5070	3	2.2578	7.6201	1.1131
1.9224	6.4881	4	2.2578	7.6199	1.1318
1.9196	6.4785	5	2.2612	7.6316	1.1531
1.9223	6.4878	6	2.2541	7.6074	1.1197
1.9115	6.4513	7	2.2605	7.6290	1.1777
1.9172	6.4706	8	2.2538	7.6064	1.1359
1.9263	6.5013	9	2.2606	7.6294	1.1281
1.9212	6.4839	10	2.2578	7.6201	1.1362
1.9182	6.4738	11	2.2601	7.6278	1.1541
1.9184	6.4746	12	2.2595	7.6258	1.1512
1.9213	6.4844	13	2.2544	7.6086	1.1242
1.9259	6.4997	14	2.2559	7.6137	1.1139
1.9315	6.5188	15	2.2557	7.6130	1.0942
1.9127	6.4552	16	2.2600	7.6275	1.1723
1.9299	6.5134	17	2.2564	7.6152	1.1018
1.9190	6.4766	18	2.2562	7.6147	1.1381
1.9186	6.4753	19	2.2559	7.6137	1.1384
1.9150	6.4630	20	2.2592	7.6246	1.1617
1.9187	6.4754	21	2.2556	7.6125	1.1370
1.9112	6.4503	22	2.2585	7.6223	1.1720
1.9176	6.4719	23	2.2579	7.6202	1.1483
1.9193	6.4776	24	2.2621	7.6344	1.1568
1.9210	6.4834	25	2.2573	7.6184	1.1350
1.9149	6.4628	26	2.2587	7.6229	1.1602
1.9218	6.4861	27	2.2617	7.6332	1.1472
1.9208	6.4825	28	2.2642	7.6415	1.1590
.	.	.	.	.	.
.	.	.	.	.	.
1.9063	6.4338	1199	2.2532	7.6044	1.1706
1.9046	6.4280	1200	2.2605	7.6290	1.2010

FRICTIONAL TORQUE DATA - 1018 Steel + White Al_2O_3

K = 3.375, N = 85	Frictional Torque, Dry Run	Time	K = 3.375, N = 85	*Frictional Torque, Wet Run*	Δ *Frictional Torque*
Current, i (amp)	(lbf)	Steel, # 5_6	Current, i (amp)	(lbf)	Wet Run - Dry Run
Dry Run	K*i	(sec)	Wet Run	K*i	(lbf)
1.9236	6.4922	1	2.2680	7.6543	1.1622
1.9217	6.4857	2	2.2696	7.6597	1.1740
1.9246	6.4955	3	2.2724	7.6694	1.1738
1.9238	6.4928	4	2.2700	7.6611	1.1683
1.9231	6.4905	5	2.2718	7.6672	1.1767
1.9237	6.4925	6	2.2688	7.6572	1.1647
1.9277	6.5060	7	2.2710	7.6645	1.1585
1.9234	6.4913	8	2.2677	7.6533	1.1620
1.9246	6.4955	9	2.2697	7.6601	1.1645
1.9227	6.4891	10	2.2710	7.6646	1.1755
1.9276	6.5057	11	2.2607	7.6297	1.1240
1.9199	6.4797	12	2.2658	7.6469	1.1672
1.9301	6.5141	13	2.2638	7.6403	1.1262
1.9215	6.4849	14	2.2608	7.6302	1.1453
1.9272	6.5043	15	2.2648	7.6435	1.1392
1.9214	6.4847	16	2.2591	7.6243	1.1396
1.9258	6.4996	17	2.2537	7.6061	1.1065
1.9202	6.4807	18	2.2643	7.6420	1.1613
1.9243	6.4945	19	2.2657	7.6467	1.1522
1.9257	6.4992	20	2.2667	7.6499	1.1507
1.9276	6.5057	21	2.2707	7.6636	1.1580
1.9269	6.5033	22	2.2740	7.6748	1.1715
1.9202	6.4805	23	2.2724	7.6692	1.1887
1.9266	6.5021	24	2.2535	7.6056	1.1035
1.9266	6.5023	25	2.2716	7.6665	1.1643
1.9295	6.5121	26	2.2623	7.6353	1.1232
1.9216	6.4854	27	2.2694	7.6592	1.1738
1.9273	6.5046	28	2.2679	7.6542	1.1495
.	.	.	.	.	.
.	.	.	.	.	.
1.9013	6.4169	1199	2.2436	7.5722	1.1553
1.9087	6.4419	1200	2.2675	7.6528	1.2110

APPENDIX J

FEA RESULTS

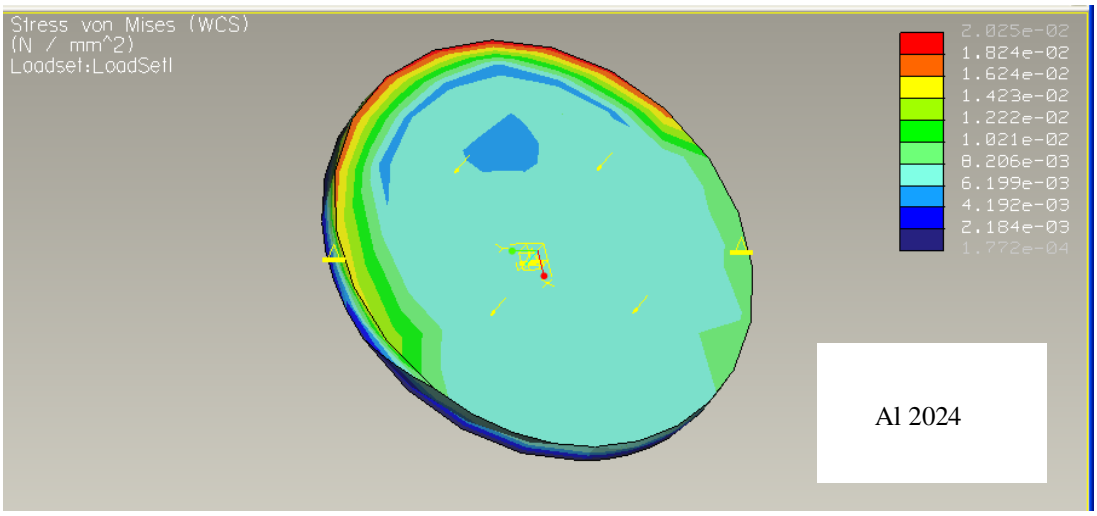

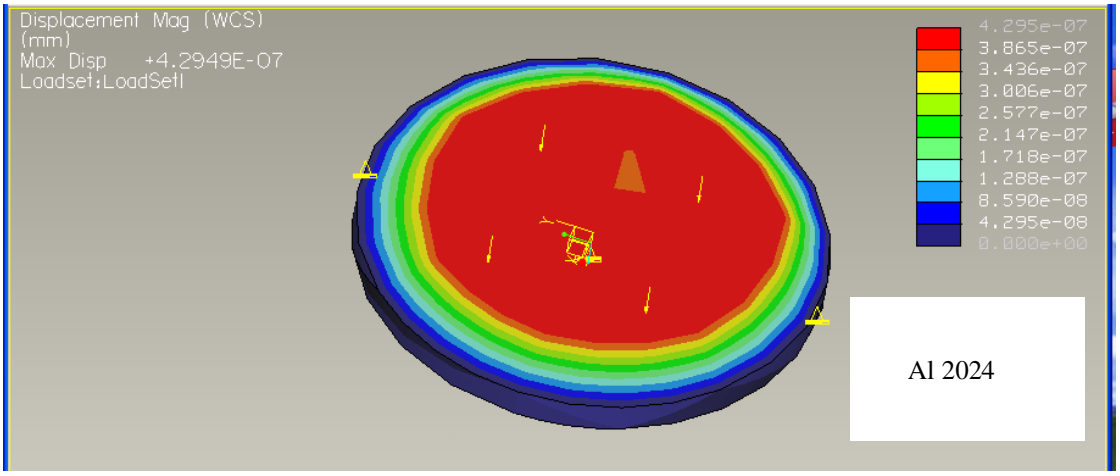

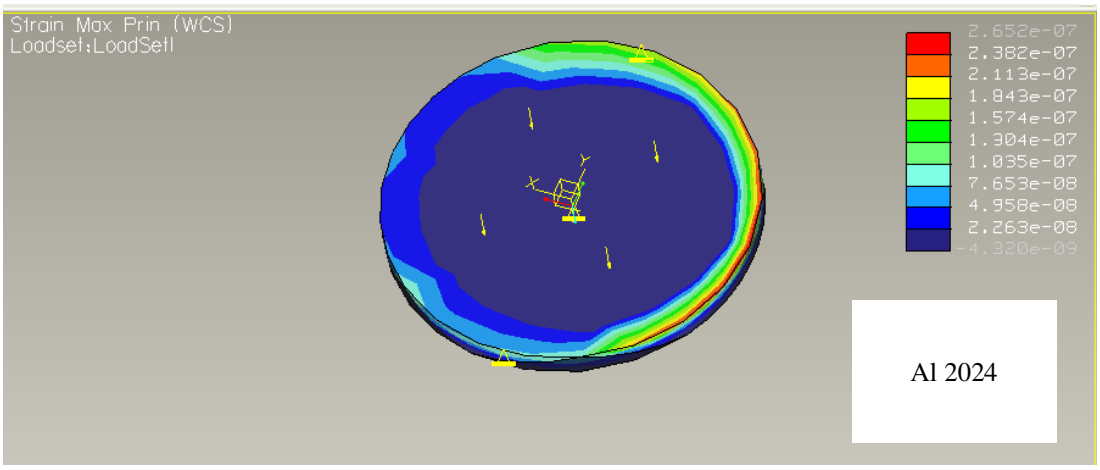
Strain Max Prin (WCS)
Loadset:LoadSet1
2.652e-07
2.382e-07
2.113e-07
1.843e-07
1.574e-07
1.304e-07
1.035e-07
7.653e-08
4.958e-08
2.263e-08
-4.320e-09
Al 2024

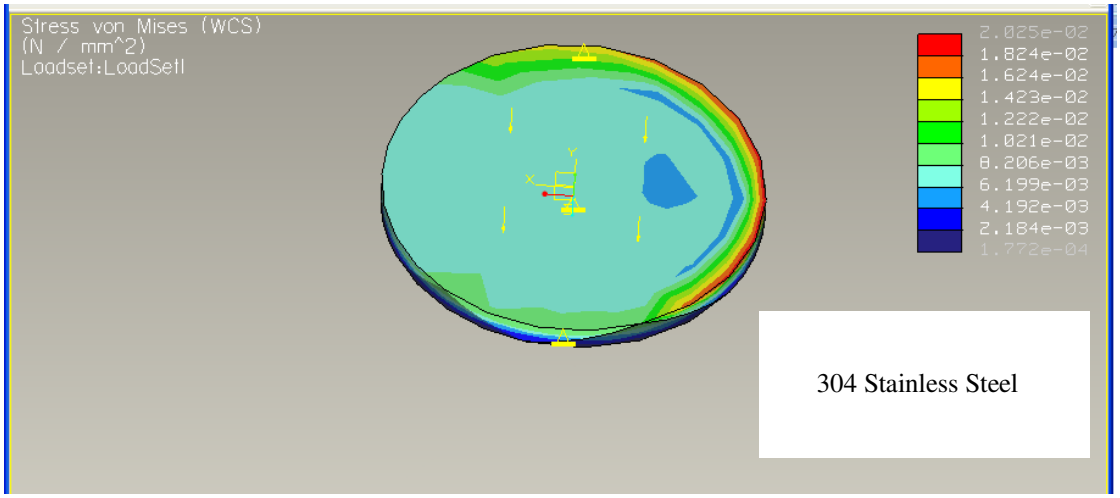
Stress von Mises (WCS)
(N / mm^2)
Loadset:LoadSet1
2.025e-02
1.824e-02
1.624e-02
1.423e-02
1.222e-02
1.021e-02
8.206e-03
6.199e-03
4.192e-03
2.184e-03
1.772e-04
304 Stainless Steel

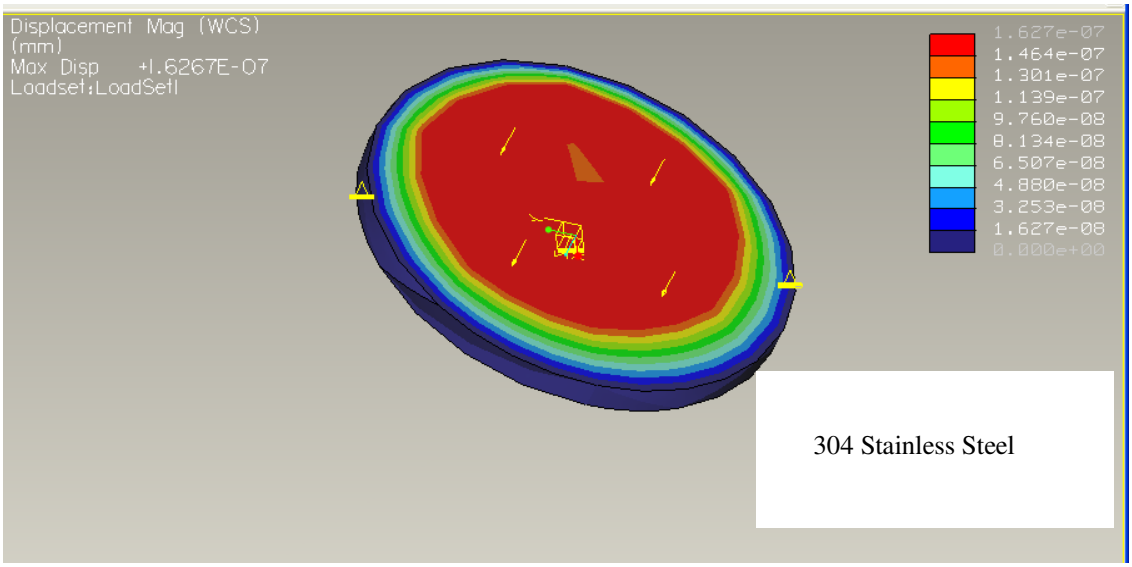
Displacement Mag (WCS)
(mm)
Max Disp +1.6267E-07
Loadset:LoadSet1
1.627e-07
1.464e-07
1.301e-07
1.139e-07
9.760e-08
8.134e-08
6.507e-08
4.880e-08
3.253e-08
1.627e-08
0.000e+00
304 Stainless Steel

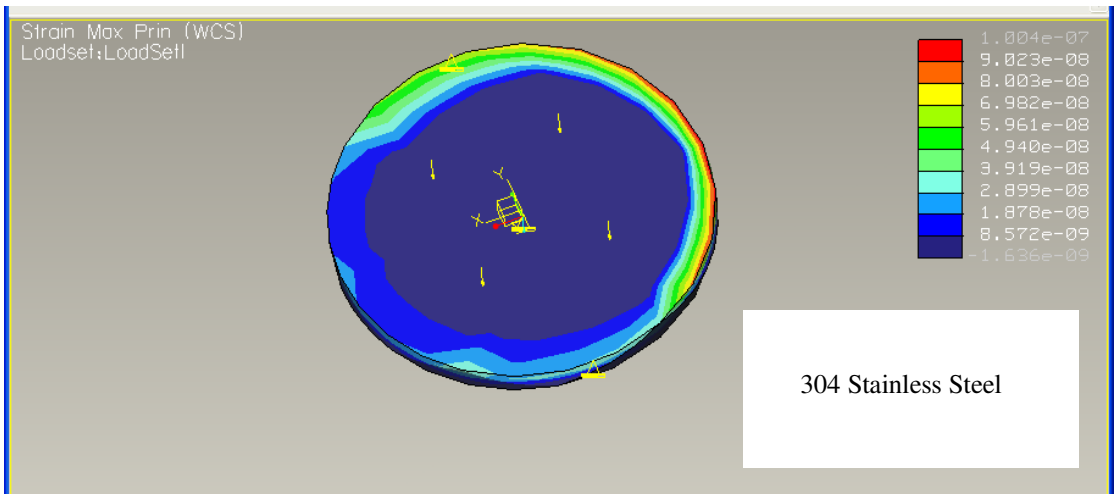
Strain Max Prin (WCS)
Loadset:LoadSet1
1.004e-07
9.023e-08
8.003e-08
6.982e-08
5.961e-08
4.940e-08
3.919e-08
2.899e-08
1.878e-08
8.572e-09
1.636e-09
304 Stainless Steel

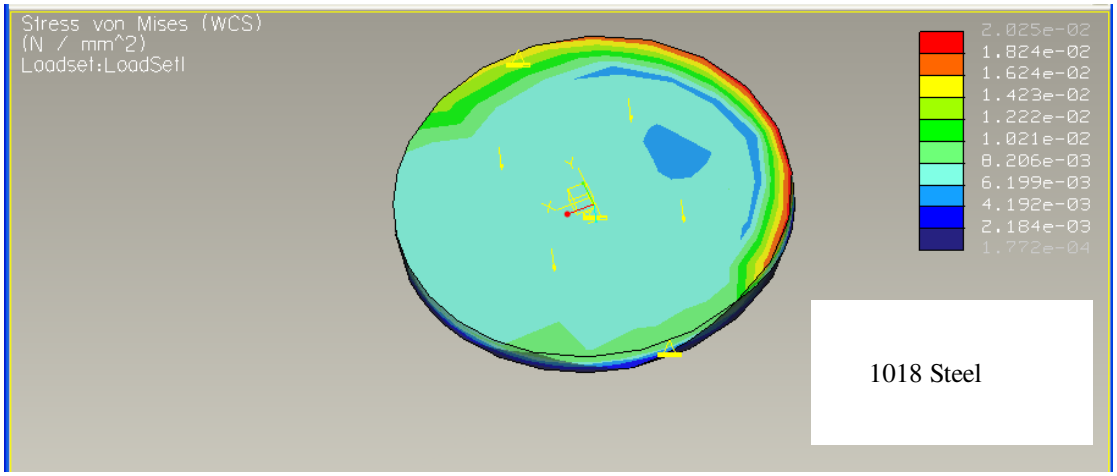
Stress von Mises (WCS)
(N / mm^2)
Loadset:LoadSet1
2.025e-02
1.824e-02
1.624e-02
1.423e-02
1.222e-02
1.021e-02
8.206e-03
6.199e-03
4.192e-03
2.184e-03
1.772e-04
1018 Steel

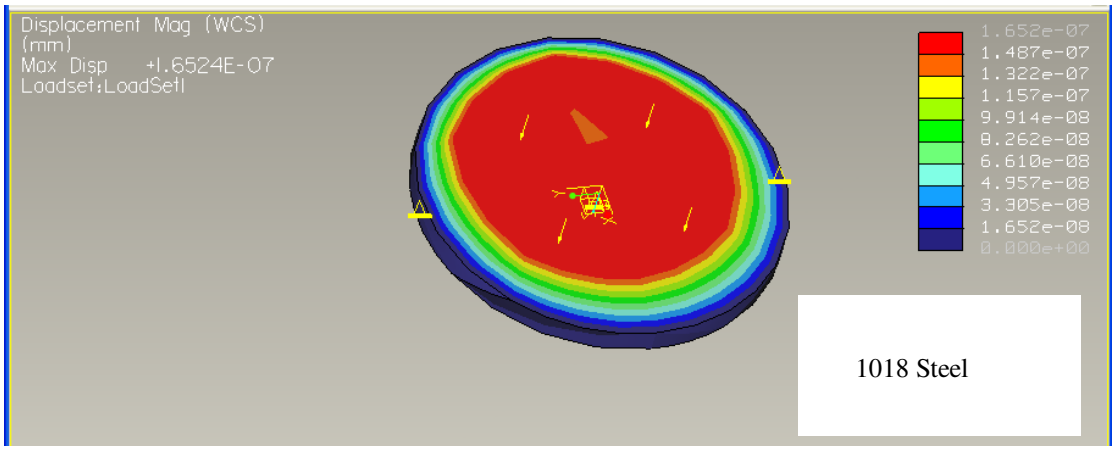
Displacement Mag (WCS)
(mm)
Max Disp +1.6524E-07
Loadset:LoadSet1
1.652e-07
1.487e-07
1.322e-07
1.157e-07
9.914e-08
8.262e-08
6.610e-08
4.957e-08
3.305e-08
1.652e-08
0.000e+00
1018 Steel

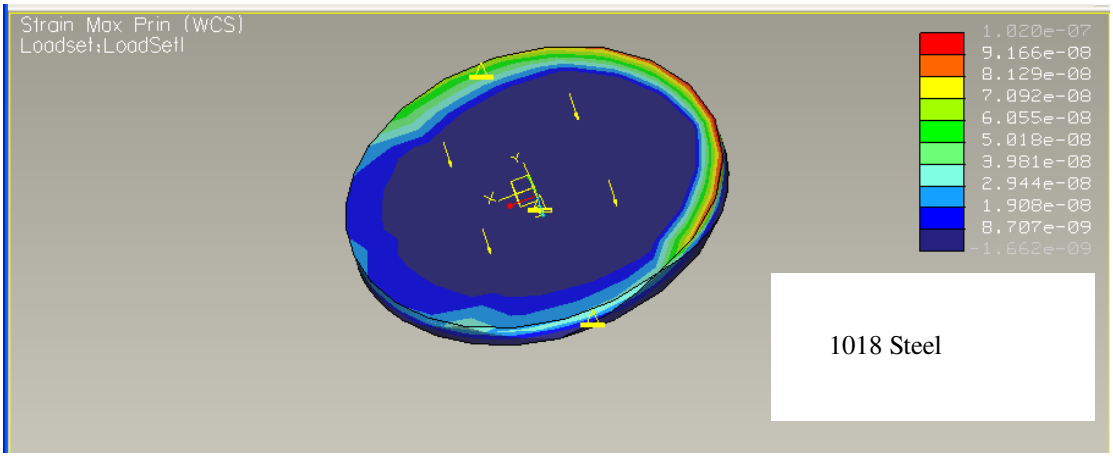
Strain Max Prin (WCS)
Loadset:LoadSet1
1.020e-07
9.166e-08
8.129e-08
7.092e-08
6.055e-08
5.018e-08
3.981e-08
2.944e-08
1.908e-08
8.707e-09
1.662e-09
1018 Steel